DYNAMICS OF HELICAL FLOW STRUCTURES

A Description of Vortex Formation in Turbulent Fluids

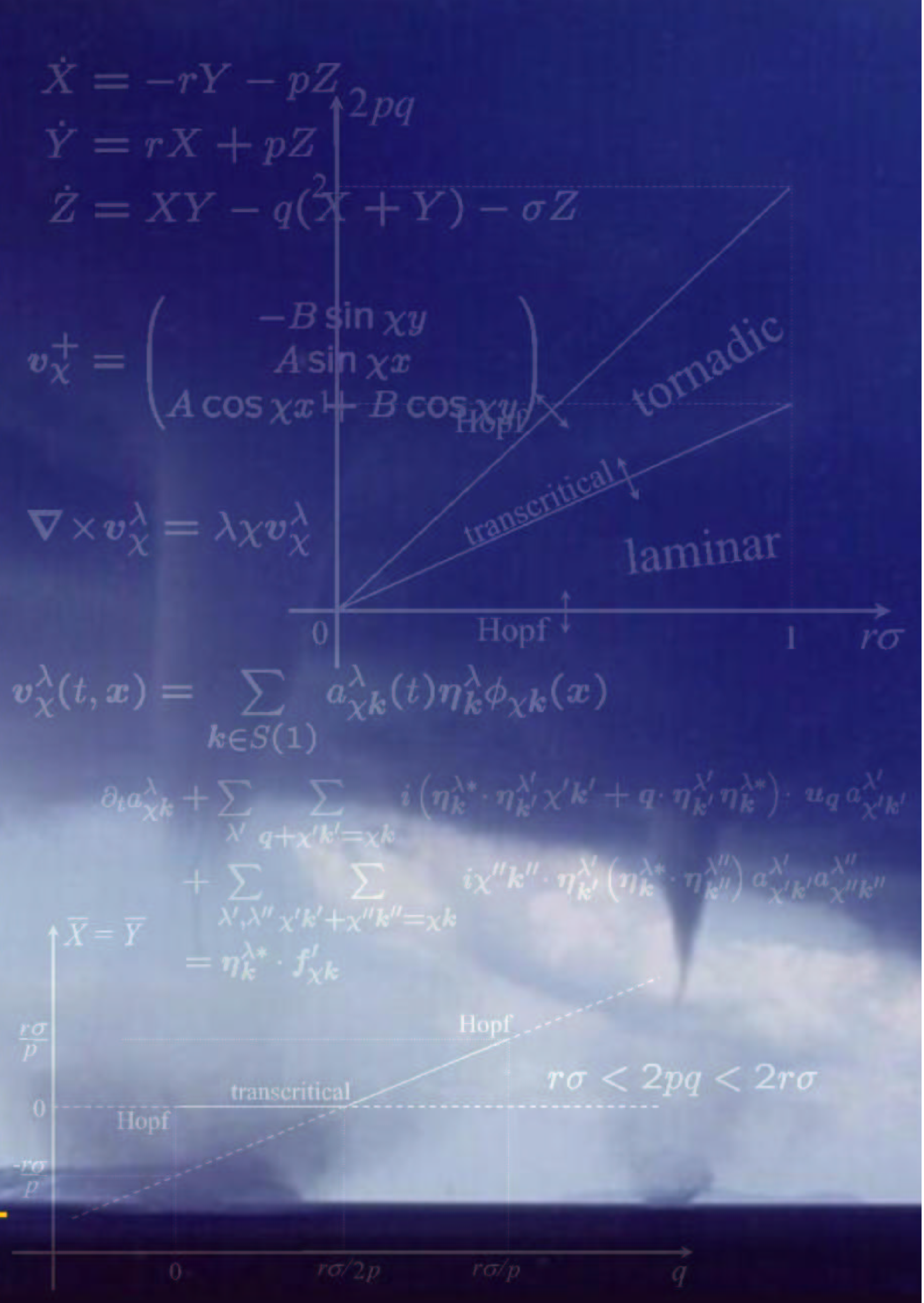

Nikolaj Nawri

Dynamics of Helical Flow Structures

A Description of Vortex Formation in Turbulent Fluids

by
Nikolaj Nawri

Dissertation submitted to the
Faculty of the Graduate School of the University of Maryland at College Park
in partial fulfillment of the requirements for the degree of
Doctor of Philosophy, 2003.

Nikolaj Nawri
Department of Meteorology
University of Maryland at College Park
Maryland, United States.

Street address:

Department of Meteorology
Computer and Space Sciences Building
University of Maryland
College Park, MD 20742
United States

Electronic mail: nnawri@atmos.umd.edu

This research was funded by an
Earth System Science Fellowship from the
National Aeronautics and Space Administration
of the United States under the programme
Mission to Planet Earth.

Abstract

Helicity, as a combined measure of the intensity and persistence of turbulent eddies, is likely to be the most important kinematical characteristic of tornadolike vortices. It is shown that in simplified form a maximally helical vortex can be described by two Fourier waves with the same sign of helicity and a fixed amplitude and phase relationship.

Tornadolike vortices tend to occur in the vicinity of strong horizontal gradients of velocity. It is therefore assumed that they are generated primarily by instabilities of these intense shear zones of the storm system. Consequently significant variability of the storm flow is on the scale of the embedded vortex rather than on the scale of the storm circulation itself.

The velocity field is separated into a slowly evolving part representing the storm flow, and a rapidly evolving part representing the tornadolike vortex. A three-dimensional dynamical system is then obtained from the equations of motion for the vortex flow by Fourier transformation and truncation, restricting the fast flow to the two vortex waves and a non-helical catalyst wave. The two equilibria of the dynamical system are the phase space origin, referred to as the ground state, and a nonvanishing vortex state. The system parameters depend on the expansion coefficients of the slow background flow. The stability of the equilibria can therefore be analysed as a function of the background flow state. With a stable ground state perturbations of the fast velocity field are damped out. As the ground state loses stability in a transcritical bifurcation the vortex state simultaneously gains stability and weak vortical perturbations are intensified, approaching a steady state as long as the vortex equilibrium is maintained by the background flow.

In the simple model the most relevant changes in the background flow affecting vortex stability are changes in the horizontal shear of horizontal velocity. It is shown that for a given background updraft strength a certain minimum amount of horizontal shear is necessary to spin up an intense vortex. However, as the horizontal shear increases relative to the updraft strength, at a certain point the coherent vortex is destroyed.

Contents

List of Figures

1 Introduction

The scientific complexity of vortex formation in a turbulent fluid, in addition to operational difficulties, makes the study of tornadoes one of the great frontiers of dynamic meteorology.

Globally the social relevance of tornadoes is negligible compared with other severe weather phenomena such as hail and lightning, causing more damage or fatalities than tornadoes, respectively. However, locally tornadoes can make the difference between minor and complete destruction. The vast majority of severe supercell thunderstorms is not tornadic. The sporadic nature of tornadoes, especially of the most intense tornadoes, together with the short time frame in which tornadogenesis takes place, make reliable tornado forecasting, without significant overwarning, a very difficult task. Moreover and, aside from the operational difficulties, even the theoretical understanding of the mechanisms involved in the process is incomplete.

Traditionally, tornado and severe storm research follow an essentially empirical approach, focussing on the analysis of large-scale severe storm features and their possible connection to the formation of tornadoes. Turbulence theory on the other hand holds the opposite point of view, trying to identify properties of the small-scale flow that are independent of the specific large-scale forcing.

Tornadoes and tornadic waterspouts, by definition, are associated with severe thunderstorms, as opposed to typically smaller and less intense atmospheric vortices such as landspouts and dust devils, or larger vortices such as hurricanes that are storm systems by themselves. The association of the tornado vortex to the larger-scale circulation of the storm system leads to a strong coupling of a wide range of spatial and temporal scales. The complete description of tornadogenesis therefore requires a comprehensive theory of fluid flow including both the intrinsic, universal properties of small scales and a consideration of the energy input on large scales by specific forcing.

Due to the seemingly stochastic nature of turbulence there are legitimate concerns about the practical predictability of tornadoes. However, despite significant synoptic-scale differences from one tornado occurrence to another, the visually recognisable qualitative similarity in the appearance of supercell thunderstorms and tornadoes, and the similarity of the formation and decay cycle at different times of the year and in different geographical locations suggests that, at least at a smaller scale, there exists a unique forcing mechanism responsible for tornadogenesis under all these circumstances. In that case tornadoes really are manifestations of one type of vortex phenomena rather than unrelated realisations of unlimited possible scenarios in a strongly turbulent fluid with an infinite number of degrees of freedom. Only then can a unified theoretical treatment and eventually forecasting be successful.

However, before one is able to answer the question about how a tornado forms, one must answer the question about what a tornado really is.

Verbally a tornado is usually defined as a violently rotating column of air extending from the base of a rotating swelling cumulus or cumulonimbus cloud down to the ground. While that is certainly true it is not a very useful definition for theoretical investigations of tornadogenesis. Since it simply is a translation from the visual appearance of a tornado

Figure 1.1: *Waterspouts over the Mediterranean Sea near the coast of Italy.*

into words, this statement contains no more information than looking at a photograph of a tornado. In particular, as a description of the *status quo*, it does not say anything about the specific details leading to the formation of this 'violently rotating column of air.'

On the elementary level of this investigation, as in the verbal definition, no distinction will be made between tornadoes and tornadic waterspouts. The arguments presented generally refer to a *tornadolike* vortex, i.e., any atmospheric vortex with a diameter of a few hundred metres associated with a storm system or otherwise driven by larger-scale flow features such as fronts or squall lines. More specifically, a tornadolike vortex is defined as a vortical instability of intense shear zones associated with mesoscale weather systems, possibly intensified by convection. Although, compared with the more general definition, this *physical* definition may limit the type of atmospheric vortices that can be described under the heading of 'tornadolike vortices,' it is based on possible generating mechanisms and therefore offers a starting point for the investigation of their formation. Eventually, however, mathematics is needed to make precise statements about the current and future state of the flow. For the simple models considered here, *mathematically* a tornadolike vortex is defined as a helical eddy or flow structure with a particular phase and amplitude relationship between certain Fourier expansion coefficients.

Despite the turbulent behaviour of a weakly dissipative fluid such as the atmosphere it is usually assumed that the time evolution at least of appropriately averaged properties of the flow is governed by deterministic equations of motion. Although the existence and uniqueness of solutions for three-dimensional compressible flow has not been proven, the time evolution of fluid flow is normally described by some form of the Navier-Stokes equations, given by

Figure 1.2: *Waterspouts over the Adriatic Sea near the coast of Italy.*

a system of nonlinear partial differential equations. Due to the lack of even approximate analytical solutions in most cases the equations of motion must be solved numerically as a specific initial value problem to obtain the time evolution of the flow. However, due to the mathematical complexity of the fluid mechanical equations, even numerical integration is very difficult. Numerical simulations of tornadogenesis additionally suffer from the fact that currently an adequate integration of the equations of motion, together with the time required for data acquisition and initialisation, takes far too long to be of use to real forecasts. The main question therefore is how the mathematical complexity of the equations of motion can be reduced for a particular application without loosing important aspects of the dynamics.

The two complicating characteristics of the fluid mechanical equations are the four independent variables of time and space and nonlinearity. For solving initial value problems it must be assumed that the initial state, i.e., the spatial dependence of all dynamically relevant variables at the initial time, is given by observations. The degrees of freedom of the equations of motion can be reduced by projecting the discrete observational fields onto some basis functions in space. An analytical approximation of the spatial dependence of all variables is then obtained by a series expansion in these basis functions, where the time-dependence of the expansion coefficients is given by the projection of the full equations of motion onto the same basis functions. That way the system of partial differential equations is reduced to a system of ordinary differential equations. However, nonlinearity usually persists. Without nonlinearity qualitative changes are limited to oscillatory motion and exponential growth and decay. Since the qualitative motion of the atmosphere is clearly more complicated than that, some form of nonlinearity must be retained, generally precluding analytical solutions even for the simplified models. Still, if the knowledge of the qualitative behaviour of the nonlinear system is sufficient for predictions, there exist alternative methods to the explicit integration of the dynamical equations.

One possibility would be to *a priori* integrate the equations of motion for a large number of initial and boundary conditions, thereby creating a 'climatology of motion.' However, due to the infinite number of initial conditions, and the sensitive dependence of a nonlinear system on initial conditions, this procedure is not practicable. A similar approach, employed in observational tornado research, is to calculate certain forecast parameters from data of the storm system (obtained prior to tornadogenesis) and to compare their values between tornadic and nontornadic cases. That way the derived statistics are based on physically relevant initial states of the system and the 'integration of the equations of motion' is performed in exact form by Nature itself. However, even assuming that the observations are dense and accurate enough, it appears as if the currently employed parameters are not adequate for reliable predictions of tornadogenesis. The question therefore is how forecast parameters can be found that uniquely characterise the storm system with regard to its potential to spawn tornadolike vortices or not.

The approach taken here is strictly mathematical. It is based on the bifurcation analysis of low-dimensional dynamical systems derived from the equations of motion via Fourier transformation and subsequent truncation of spectral components.

Based on the problems with the large-scale forecast parameters, together with the fact that tornadoes tend to occur in the vicinity of strong velocity gradients, it is hypothesised that, although tornadolike vortices are primarily forced by a relatively slowly evolving storm system, the relevant spatial variability of the coherent large-scale system is on the scale of the smaller vortex. To simplify the analysis and to reduce the amount of information that is required to specify the initial state it is therefore assumed that tornadolike vortices are not significantly affected directly by turbulent and thermodynamic forcing varying on the same timescale. Instead they are directly forced only through kinematical instabilities of the larger-scale flow. Since these instabilities are assumed to be associated with spatial variability of the storm system on the vortex scale, a separation of the flow into large and small wavenumber components is not possible. The velocity field is therefore separated into a slowly evolving 'background' flow representing the storm motion, and a rapidly evolving perturbation flow representing the tornadolike vortex. In the dynamical system for the rapidly evolving expansion coefficients various combinations of the slowly evolving expansion coefficients, over short periods of time, are considered to be constant parameters. For the simple mathematical models these parameters determine if and under what circumstances a tornadolike vortex develops or not, where the 'tornadic' and 'nontornadic' parameter regions and the corresponding background flow states follow from a bifurcation analysis. Given a certain background flow an explicit solution of the nonlinear equations of motion is therefore not necessary to determine the qualitative evolution of the fast flow. Since it is based on criteria for the stability of the final state, the identification of relevant states of the background flow through bifurcation analysis essentially is an inverse process of a large number of numerical simulations from arbitrarily chosen initial conditions. In a more realistic setting, as the number of qualitatively different dynamical possibilities, or the number of the degrees of freedom, increases it gets progressively more complicated to explicitly perform this bifurcation analysis. However, in principle the same method can be extended to any complexity.

The dynamically derived parameters are very abstract and unlike the currently employed forecast parameters cannot easily be interpreted in terms of physical concepts such as 'static instability' or 'vertically veering wind profile.' The basic idea therefore is to use the empirical insight into the problem to simplify the dynamical equations and then to let the theory decide what the dynamically relevant variables are and what one should try to observe.

The text is grouped into two main chapters concerning flow in physical and phase space, respectively.

Chapter 2 introduces the fundamental concepts and definitions of fluid mechanics relevant for the investigation of tornadolike vortices. The various kinematical scalar variables associated with the velocity field, such as kinetic energy and helicity, are defined and their meaning for the evolution of the flow is investigated. Elementary physical properties of the flow, such as large and small spatial scale, or slow and fast timescale are discussed. The mathematical formalism for the spectral and helical decomposition of the velocity field is then introduced, and the scaled equations of motion for the slowly and rapidly evolving flow components are derived.

In Chapter 3 the evolution of the Fourier expansion coefficients is investigated. Stationary solutions of the low-dimensional dynamical system, or definite observable states of the flow, and their linear stability as a function of the various system parameters are determined. It is shown that the qualitative behaviour in phase space is determined by an exchange of stability between the ground state representing vanishing perturbation flow and the vortex state. The parameter values associated with a stable vortex state are then interpreted in terms of slow background flows.

Implications of the results from the low-dimensional analysis for predictions of tornadogenesis are discussed in Section 4, and a general summary of the main results is given in Section 5.

Unless necessary for the immediate understanding of the discussion in the main text, the more elaborate derivations are collected in Appendix A. For easy reference, a glossary of some of the special terms used in the discussion is given in Appendix B, and abbreviations and mathematical symbols used are listed in Appendices C and D, respectively.

2 Flow in Physical Space

You don't seriously believe that a theory must restrict itself to observables? Perhaps I did use this sort of philosophy, but it's nonsense. Only the theory decides what one can observe.

Albert Einstein to Werner Heisenberg (1926)

2.1 Flow Properties

This section briefly summarises the basic concepts of fluid dynamics. It introduces the fundamental kinematical variables, terminology, and notation used in later sections.

2.1.1 Description of Motion

The description of the motion of a fluid by a continuous velocity field allows the use of the mathematical formalism of vector analysis. However, the actual motion of the fluid as a continuum does not exist. Theoretically the smallest scale at which the *continuum hypothesis* holds must be larger than the mean free path of fluid molecules. In practice, however, the smallest resolvable scale depends on the quality and resolution of measurements and, in liquids and the lower[1] atmosphere, is much larger than the mean free path. Still, the continuous velocity field is a purely mathematical construct in the sense that it only represents statistical or bulk properties of the actual motion of matter. Flow on the observable scale can only be described as the result of the collective motion on a smaller scale. Denoting the velocity field on the smallest resolvable scale by $\boldsymbol{v}_S$,

$$\boldsymbol{v} = \boldsymbol{v}_S + \boldsymbol{v}' \; , \tag{2.1.1}$$

where $\boldsymbol{v}'$ are the unobservable perturbations of the elusive 'true' velocity field $\boldsymbol{v}$ relative to $\boldsymbol{v}_S$. Just as a Fourier series in the spatial variables is a representation of the velocity field as a superposition of plane waves with different wavelengths, the velocity field can be written as a superposition of flow on different physical scales. By defining the average over the smallest observable scale, $\boldsymbol{v}_L \stackrel{\text{def}}{=} \langle \boldsymbol{v}_S \rangle$, where averages over a fixed volume in space are denoted by brackets, this process can be continued to larger and larger scales by writing

$$\boldsymbol{v}_S = \boldsymbol{v}_L + \boldsymbol{v}'_S \tag{2.1.2}$$

and

$$\boldsymbol{v} = \boldsymbol{v}_L + \boldsymbol{v}'_S + \boldsymbol{v}' \tag{2.1.3}$$

where $\boldsymbol{v}'_S$ are perturbations of $\boldsymbol{v}_S$ relative to the mean flow $\boldsymbol{v}_L$. On all scales, averages and perturbations are always determined based on the continuous approximation with a higher

[1]The mean free path in the troposphere is on the order of 10^{-7} m.

resolution. In applications the velocity field derived from the observational data on the smallest resolved scale must be treated as the true *material velocity field* and for simplicity is denoted by $\boldsymbol{v}$.

For any given averaged flow, or *macrostate*, in general, there is a large number of compatible flows with a higher resolution, or *microstates*.[2] In that sense any continuous velocity field must be regarded as a macrostate of the actual motion of matter on a much smaller scale. The fact that different microstates of the same ensemble are usually not dynamically equivalent introduces an uncertainty in the time evolution of the macrostate. The lack of uniqueness of microstates for a given macrostate can be interpreted as the independence of small spatial scales from the observable large scale and the forces acting on it. It will be seen in Section 2.3.1, that this is in fact one of the fundamental assumptions in turbulence theory.

The same decomposition of the velocity field into mean and perturbation field can of course also be defined with respect to time.

For all computational purposes, the velocity field and the equations of motion will be written in a *stationary* (inertial), right-handed Cartesian frame of reference with spatial coordinates $\{x, y, z\}$, corresponding unit vectors $\{\boldsymbol{e}_x, \boldsymbol{e}_y, \boldsymbol{e}_z\}$, and position vector $\boldsymbol{x} \stackrel{\text{def}}{=} (x, y, z)^T$. This representation of the flow in which position coordinates are independent of time parameter t is called *Eulerian description*. The time rate of change of flow properties at each point is given by *partial derivatives* with respect to time.

In some cases, however, a better conceptional understanding of fluid dynamical processes can be gained with the *Lagrangian description* of the flow. Under the continuum hypothesis, instead of as a collection of molecules, the fluid can be described as a continuous ensemble of infinitesimally small *fluid elements*. As the flow evolves each fluid element may change its size and shape such that, by definition, it contains the same molecules at all times. A collection of fluid elements of finite size is called *Lagrangian volume* and its bounding surface is called a *Lagrangian surface*. Contrary to the Eulerian description, vector fields in the Lagrangian description of the flow are written in a *continuous field of reference frames* each one of which follows the motion of a fluid element. In these noninertial frames of reference the time rate of change of properties of a fluid element not only includes changes measured locally in an Eulerian frame but also changes due to the displacement of the fluid element. For variables such as the velocity components that are only functions of time and space the time rate of change following the motion is given by the total or *Lagrangian time derivative*

$$\begin{aligned} d_t &\stackrel{\text{def}}{=} \partial_t + \partial_{\boldsymbol{v}} \\ &= d_t x\, \partial_x + d_t y\, \partial_y + d_t z\, \partial_z \end{aligned} \tag{2.1.4}$$

where $\partial_{\boldsymbol{v}} \stackrel{\text{def}}{=} \boldsymbol{v} \cdot \boldsymbol{\nabla}$ is the directional derivative along the trajectory of the fluid element.

2.1.2 Forms of Energy

The vector variable of velocity contains all information about the kinematical state of the fluid. However, for the description of instantaneous flow properties it is convenient to intro-

[2] In statistical physics, this number is taken as a measure of the probability or entropy of the macrostate.

duce certain scalar variables.

Neglecting their deformation as they move with the flow, fluid elements to some extent can be treated as solid particles. Then with each of their degrees of freedom there is associated a particular form of energy. As for any solid body, two three-dimensional vectors are necessary to describe all degrees of freedom and to completely specify the kinematical state. These are the velocity $\boldsymbol{u}$ of the centre of mass, and a spin vector $\boldsymbol{s}$ describing rotation about it. Consequently, associated with the motion of the centre of mass is the translational kinetic energy per unit mass $\boldsymbol{u} \cdot \boldsymbol{u}$, and associated with the spin vector is the rotational kinetic energy per unit moment of inertia $\boldsymbol{s} \cdot \boldsymbol{s}$. The spin vector is defined through the relationship $\boldsymbol{v} = \boldsymbol{s} \times \boldsymbol{x}$, where $\boldsymbol{v}$ is the velocity at a point $\boldsymbol{x}$ inside the fluid element. Assuming that in the infinitesimal volume the fluid element is in solid body rotation $\boldsymbol{s}$ is constant for each fluid element.

By making the transition from point to continuums mechanics, the rotational properties of fluid elements become encoded in the spatial dependence of the velocity field. Then the *vorticity vector*,

$$\boldsymbol{\omega} \stackrel{\text{def}}{=} \boldsymbol{\nabla} \times \boldsymbol{v} \ , \tag{2.1.5}$$

for a fluid element in solid body rotation is equal to twice the spin vector,

$$\begin{aligned} \boldsymbol{\omega} &= \boldsymbol{\nabla} \times (\boldsymbol{s} \times \boldsymbol{x}) \\ &= \boldsymbol{s}\, \boldsymbol{\nabla} \cdot \boldsymbol{x} - (\boldsymbol{s} \cdot \boldsymbol{\nabla})\, \boldsymbol{x} \\ &= 2\boldsymbol{s} \ . \end{aligned} \tag{2.1.6}$$

In analogy with the particle picture the *kinetic energy density* is defined as

$$\kappa \stackrel{\text{def}}{=} \boldsymbol{v} \cdot \boldsymbol{v} \ , \tag{2.1.7}$$

and the *rotational kinetic energy density* or *enstrophy density* is defined as

$$\varepsilon \stackrel{\text{def}}{=} \boldsymbol{\omega} \cdot \boldsymbol{\omega} \ . \tag{2.1.8}$$

The *intensity* of the flow,

$$\sigma \stackrel{\text{def}}{=} \sqrt{\kappa \varepsilon} \ , \tag{2.1.9}$$

is defined as a combined measure of the densities of kinetic energy and enstrophy.

The spatial averages of kinetic energy and enstrophy are denoted by

$$K \stackrel{\text{def}}{=} \langle \kappa \rangle \tag{2.1.10}$$

and

$$E \stackrel{\text{def}}{=} \langle \varepsilon \rangle \ , \tag{2.1.11}$$

respectively. For simplicity, the densities and averaged quantities will both be referred to as kinetic energy or enstrophy, specifying if local or averaged values are meant only if there is a chance for confusion.

Taking into account deformation of fluid elements another form of energy becomes important. Compression and expansion of fluid elements changes the density of the fluid and therefore its thermodynamic properties. Shearing deformation and viscosity lead to an irreversible dissipation of kinetic energy. In both cases thermal energy of the fluid is changed. As seen in Section 2.2, changes in the fluid density are related to the divergence $\boldsymbol{\nabla} \cdot \boldsymbol{v}$ of the velocity field, and for a Newtonian fluid with constant viscosity the dissipation of kinetic energy is described by a forcing term proportional to $\boldsymbol{\nabla}^2\boldsymbol{v} + \frac{1}{3}\boldsymbol{\nabla}(\boldsymbol{\nabla} \cdot \boldsymbol{v})$ [*Batchelor*, 1999]. The field vector $\boldsymbol{v}$ therefore contains not only all information about the translational and rotational properties of the flow, but also some information about thermal processes.

If, as usual, the fluid is in an external gravitational field, then potential energy also has to be taken into account. More complicated forcing due to water in the atmosphere and its phase changes, or absorbtion and emission of radiative energy can only be described in approximate, parameterised form and will therefore be neglected.

2.1.3 Order and Disorder

At a high resolution both the velocity and vorticity fields of a weakly dissipative and strongly forced fluid such as the atmosphere, independently or relative to each other, are very irregular. When interested in an apparently regular flow such as a tornado vortex embedded in an otherwise irregular flow associated with a convective storm system the first idea could be to suspect that velocity and vorticity, at least in a limited domain, have to be regular relative to each other. Since vorticity is related to the spatial dependence of the velocity field this seems to be reasonable and, as seen in Section 2.3.2, the relative regularity of velocity and vorticity is indeed related to the absolute regularity of the velocity field.

To describe the relative orientation of velocity and vorticity the scalar field of *alignment* is defined as

$$\alpha \overset{\text{def}}{=} \cos\phi \ , \tag{2.1.12}$$

where at each point in space ϕ is the shortest planar angle between the velocity and vorticity vectors. Related to alignment is *helicity density* defined as

$$\begin{aligned} \eta &\overset{\text{def}}{=} \boldsymbol{v} \cdot \boldsymbol{\omega} \\ &= \sqrt{\kappa\varepsilon}\cos\phi \ . \end{aligned} \tag{2.1.13}$$

Helicity is therefore a combined measure of intensity and alignment. The averaged value of helicity is denoted by

$$H \overset{\text{def}}{=} \langle \eta \rangle \ . \tag{2.1.14}$$

From (2.1.13) it follows that

$$\kappa\varepsilon - \eta^2 \geq 0 \ , \tag{2.1.15}$$

where the equality holds if and only if the velocity and vorticity vectors are parallel or antiparallel. If this is true throughout a domain $\mathcal{B}$, then there exists a relationship between velocity and vorticity such that in $\mathcal{B}$

$$\boldsymbol{\omega} = \chi \boldsymbol{v} \tag{2.1.16}$$

with a suitable pseudo-scalar function $\chi(t, \boldsymbol{x})$. This ideal situation is known as *Beltrami flow*. Scalar multiplying (2.1.16) by $\boldsymbol{v}$, χ is found to be given by the ratio of the densities of helicity and kinetic energy and will be called *chirality*.

As shown in Appendix A.1, from Schwarz's inequality for continuous vector fields it follows that

$$KE - H^2 \geq 0 \ . \tag{2.1.17}$$

Volume averages of helicity as well as the local values are therefore limited by the given distribution of kinetic energy and enstrophy, and, by (2.1.15), Beltrami flows *locally* extremise helicity with respect to kinetic energy and enstrophy. However, the defining equation (2.1.16) permits chirality to be a function of space and time, in particular it can have positive and negative values in the same domain. With $\chi^2 = \varepsilon\kappa^{-1}$, the local values of kinetic energy and enstrophy only determine the magnitude of chirality. Averaged helicity of a Beltrami flow in that domain can therefore attain arbitrary values depending on chirality given kinetic energy and enstrophy. For Beltrami flows it follows from (2.1.17) that

$$\langle \chi\kappa \rangle^2 = \langle \kappa \rangle \langle \chi^2 \varepsilon \rangle \ . \tag{2.1.18}$$

For a given distribution of kinetic energy, this condition must be satisfied by chirality for averaged helicity to be extremised. One solution of (2.1.18) is $\chi \equiv \bar{\chi}$, where $\bar{\chi}$ is not a function of the spatial variables. Considering perturbations χ' of χ about that solution, $\chi = \bar{\chi} + \chi'$, with $\bar{\chi} \stackrel{\text{def}}{=} \langle \chi \rangle$, and writing $\kappa = K + \kappa'$, condition (2.1.18) becomes

$$K^2 \langle \chi'^2 \rangle + K \langle \chi'^2 \kappa' \rangle - \langle \chi' \kappa' \rangle^2 = 0 \ . \tag{2.1.19}$$

For this to be satisfied for arbitrary values of averaged kinetic energy K, the linearly independent terms must each vanish. In particular, the variance of χ, $\langle \chi'^2 \rangle = \langle (\chi - \bar{\chi})^2 \rangle$, must be zero and $\chi \equiv \bar{\chi}$ in fact is the only solution to (2.1.18). Therefore, Beltrami flows, in a finite volume, only extremise helicity for given kinetic energy (and enstrophy) if chirality is constant throughout that domain. In that case the velocity field is nondivergent and helicity, kinetic energy and enstrophy are proportional to each other. In the following, a Beltrami flow with constant value of chirality will be referred to as a *B-flow*. Since B-flows satisfy

$$\boldsymbol{\nabla} \times \boldsymbol{v} = \chi \boldsymbol{v} \ , \tag{2.1.20}$$

with a constant eigenvalue χ, they can be regarded as the eigenvectors of the curl operator. In Section 2.5.2 this property will be used to construct an orthonormal system for the helical decomposition of velocity.

There is a fundamental difference between velocity and vorticity regarding their behaviour under certain coordinate transformations. While velocity as a *true vector* is the same in all frames of reference at rest with respect to each other, the calculation of vorticity as a *pseudo-vector* depends on the handedness of the frame of reference. As a result kinetic energy, enstrophy, and intensity are *true scalars* whereas helicity and related quantities such as chirality and alignment are *pseudo-scalars*. Although helicity changes sign under a *parity transformation*, i.e., a change of handedness of the frame of reference, the equations of motion are invariant. The sign of overall helicity of a flow therefore cannot be dynamically relevant. The concept of parity is discussed in greater detail in Appendix A.6.

2.1.4 Velocity Perturbations

Interesting flow properties in some sense are always deviations from the 'normal' state of the flow. However, there are several possibilities to define the normal flow state, and consequently the perturbations therefrom.

The average of a vector field over the entire domain is specified by the average amount and average direction of the vectors at each point. In complex flow however the global average is usually not representative and 'perturbations' from that normal state are generally not small.

To include some variability, the normal flow state can be defined as a spatially varying mean by pointwise averaging or smoothing over some limited domain around each point. Then perturbations of extent less than the volume of averaging are 'filtered out.' The spatial extent and intensity of deviations from that mean state then depend on the size of the averaging domain. This procedure leads to the velocity decomposition (2.1.1) introduced in Section 2.1.1.

In Fourier series representation the global averages of the Cartesian components of velocity are given by the zero-wave vector component. More generally the normal flow state can be defined as the velocity field resulting from the waves with wavenumber below a certain cutoff value. The spatial extent and intensity of deviations from that normal state then depend on the energy spectrum and the wavenumber cutoff. As shown in Section 2.6.1, the results of pointwise averaging in space, even for the velocity field given by a Fourier series, and spectral truncation are not identical.

Regardless of how the normal flow state is defined, an *eddy* is defined here as a spatially limited positive perturbation of kinetic energy from the normal flow state. Then, based on the kinematical properties introduced in the previous sections, *intense eddies* are defined as localised positive perturbations in intensity, i.e., positively correlated positive perturbations in kinetic energy and enstrophy, and *helical eddies* are defined as localised, positively correlated positive perturbations in intensity and alignment. Since tornadoes are intense, vortical velocity and vorticity perturbations from the normal flow state they can be considered to be special helical eddies.

2.2 Conservation Laws

Depending on the hydrodynamic model there may be a whole range of 'conserved quantities,' i.e., mathematical expressions that in some sense are invariant, usually under some transformations associated with the motion of the fluid. These conserved quantities can broadly be separated into two classes: *local* and *integral invariants*.

Tur and Yanovsky [1993] showed that all local invariants can be represented by *differential forms* in the calculus of differential geometry.

Invariant zero-forms are associated with *Lagrange invariants* I defined by

$$d_t I \equiv 0 \tag{2.2.1}$$

and characterised by surfaces $I = const.$ that are 'frozen into the fluid,' meaning that they move with or are advected by the flow field $\boldsymbol{v}$. The velocity components in inertial flow are examples of Lagrange invariants.

An invariant one-form represents a partial differential equation for a vector field $\boldsymbol{S}$ that, in tensor notation, is given by

$$\partial_t S_j + v^k \partial_k S_j + S_k \partial_j v^k \equiv 0 \ , \tag{2.2.2}$$

where

$$\partial_j \stackrel{\text{def}}{=} \partial_{x^j} \tag{2.2.3}$$

and summation over a pair of covariant and contravariant indices is implied. The planes $\boldsymbol{S} \cdot d\boldsymbol{x} = 0$ perpendicular to $\boldsymbol{S}$ are frozen-in if and only if $\boldsymbol{S}$ satisfies the *Frobenius condition* $\boldsymbol{S} \cdot \boldsymbol{\nabla} \times \boldsymbol{S} = 0$, i.e., if and only if $\boldsymbol{S}$ is nonhelical.

Invariant two-forms in coordinate representation lead to the differential equation

$$\partial_t \boldsymbol{J} + \mathcal{L}_{\boldsymbol{v}} \boldsymbol{J} \equiv 0 \tag{2.2.4}$$

which is satisfied for a vector field $\boldsymbol{J}$ whose vector lines are frozen into the flow. Here the *Lie-derivative*

$$\mathcal{L}_{\boldsymbol{v}} \boldsymbol{J} \stackrel{\text{def}}{=} \partial_{\boldsymbol{v}} \boldsymbol{J} - \partial_{\boldsymbol{J}} \boldsymbol{v} \tag{2.2.5}$$

in Cartesian coordinates represents advection of the vector lines of $\boldsymbol{J}$ along streamlines of the vector field $\boldsymbol{v}$. Vortex lines in incompressible flow or vector lines of *potential vorticity*

$$\boldsymbol{\omega}_p \stackrel{\text{def}}{=} \frac{\boldsymbol{\omega}}{\rho} \tag{2.2.6}$$

with mass density ρ in barotropic flow are frozen-in.

An invariant three-form is a coordinate independent representation of the differential equation

$$\partial_t \rho + \boldsymbol{\nabla} \cdot (\rho \boldsymbol{v}) \equiv 0 \tag{2.2.7}$$

in Cartesian coordinates for any *conserved density* ρ. In fluid dynamics the most important conserved density is mass density.

The connection between different local invariants allows the derivation of new invariants from known invariants of a different type. For any Lagrange invariant I, $\boldsymbol{S} = \boldsymbol{\nabla} I$ has frozen-in surfaces $I = const.$ perpendicular to $\boldsymbol{S}$. Alternatively, for any vector field $\boldsymbol{S}$ with frozen-in planes $\boldsymbol{S}\cdot d\boldsymbol{x}=0$, and any frozen-in vector field $\boldsymbol{J}$, $I=\boldsymbol{J}\cdot\boldsymbol{S}$ is a Lagrange invariant. In isentropic (adiabatic and reversible) flow for example potential temperature θ is a Lagrange invariant. As seen before, under barotropic conditions potential vorticity is frozen-in. Therefore, under isentropic and barotropic conditions, *Ertel's potential vorticity* $\boldsymbol{\omega}_p\cdot\boldsymbol{\nabla}\theta$ is a Lagrange invariant. Since for an ideal gas potential temperature is a function of any *two* (e.g., pressure p and density ρ) of the three basic thermodynamic variables, $\boldsymbol{\nabla}\theta\cdot(\boldsymbol{\nabla}\rho\times\boldsymbol{\nabla}p)\equiv 0$. In that case the potential vorticity equation of a Lagrangian fluid element reads

$$d_t\boldsymbol{\omega}_p=\partial_{\boldsymbol{\omega}_p}\boldsymbol{v}+\rho^{-3}\boldsymbol{\nabla}\rho\times\boldsymbol{\nabla}p\ . \tag{2.2.8}$$

Invariance of Ertel's potential vorticity then follows from the fact that

$$\begin{aligned} d_t(\partial_{\boldsymbol{\omega}_p}\theta) &= \partial_{\partial_{\boldsymbol{\omega}_p}\boldsymbol{v}}\theta+\boldsymbol{\omega}_p\cdot d_t\boldsymbol{\nabla}\theta \\ &= \partial_{\boldsymbol{\omega}_p}d_t\theta\ , \end{aligned} \tag{2.2.9}$$

and $d_t\theta\equiv 0$ in isentropic flow [cf. *Dutton*, 1995; pp. 381–383]. Here the general product rule of partial differentiation

$$\partial_{\boldsymbol{\omega}}\partial_{\boldsymbol{v}}\theta=\partial_{\partial_{\boldsymbol{\omega}}\boldsymbol{v}}\theta+\boldsymbol{\omega}\cdot(\partial_{\boldsymbol{v}}\boldsymbol{\nabla}\theta) \tag{2.2.10}$$

was used which holds for any two vectors $\boldsymbol{v}$ and $\boldsymbol{\omega}$ and any scalar θ. For an ideal gas the Lagrange invariance of Ertel's potential vorticity can therefore be extended to baroclinic, isentropic and therefore inviscid flow.

Integral invariants are obtained from local invariants through integration. The integral over an invariant one-form is interpreted in coordinate representation as the conservation of circulation of the vector field $\boldsymbol{S}$ along any closed contour frozen into the fluid. The integral over an invariant two-form represents the constant flux of a frozen-in vector field $\boldsymbol{J}$ across any closed Lagrangian surface, and the integral of a three-form or the volume integral of a conserved density over a volume moving with the flow is constant. An example is the conservation of mass in any Lagrangian volume since mass density satisfies (2.2.7) independently of the forcing.[3]

For special forcing other integral conservation laws can be derived. In the presence of conservative forces only, conservation of kinetic energy holds in any Lagrangian volume. Conservative forces exclude compressibility and molecular viscosity since the energy transfer from kinetic to thermal energy during compression and dissipation is irreversible. Conservation of kinetic energy therefore only applies to an ideal fluid. However, a transformation of the equations of motion to a rotating frame by the inclusion of Coriolis and centrifugal forces does not change the result since pseudo-forces by definition cannot do work. With constant mass density ρ_0 the equation of motion of an ideal fluid, or *Euler equation*, in a frame of reference at rest with the Earth's surface is given by

$$\frac{\partial\boldsymbol{v}}{\partial t}=\boldsymbol{v}\times(\boldsymbol{\omega}+2\boldsymbol{\Omega})-\boldsymbol{\nabla}\left(\frac{1}{2}\boldsymbol{v}^2+\frac{p}{\rho_0}+\Phi\right) \tag{2.2.11}$$

[3] As mentioned before, mass conservation is in fact the defining property of Lagrangian volumes.

where $\mathbf{\Omega}$ is the spin vector of the Earth and Φ is the effective gravitational potential taking into account centrifugal forces. Then

$$\begin{aligned}\partial_t \kappa &= -\boldsymbol{v} \cdot \boldsymbol{\nabla} \left(\kappa + 2\rho_0^{-1} p + 2\Phi\right) \\ &= -\boldsymbol{\nabla} \cdot \left[\left(\kappa + 2\rho_0^{-1} p + 2\Phi\right) \boldsymbol{v}\right] \ ,\end{aligned} \tag{2.2.12}$$

where the second equality holds since for an incompressible fluid $\boldsymbol{\nabla} \cdot \boldsymbol{v} \equiv 0$. The time rate of change of total kinetic energy is derived by the use of Gauß' law of integration,

$$\begin{aligned}d_t K &= \int_{\mathcal{V}_L} \partial_t \kappa \, dV \\ &= -\oint_{\mathcal{S}(\mathcal{V}_L)} \left(\kappa + 2p\rho_0^{-1} + 2\Phi\right) \boldsymbol{v} \cdot \boldsymbol{n} \, dS \ ,\end{aligned} \tag{2.2.13}$$

where the integral over the closed surface $\mathcal{S}(\mathcal{V}_L)$ of $\mathcal{V}_L$ with outward directed unit normal vector $\boldsymbol{n}$ vanishes since by definition any flux across the boundary of a Lagrangian volume is zero. This proves the invariance of the total kinetic energy of a fixed portion of mass of an ideal fluid.

Under slightly more general forcing but for more special boundary conditions integrated helicity is also conserved. For a barotropic fluid the density $\rho = \rho(p)$ is a function of pressure only and

$$\begin{aligned}\boldsymbol{\nabla} \int_{p_0}^{p(\boldsymbol{x})} \frac{dp}{\rho(p)} &= \boldsymbol{\nabla} \left[F_{\rho^{-1}}(p(\boldsymbol{x})) - F_{\rho^{-1}}(p_0)\right] \\ &= \partial_{p(\boldsymbol{x})} F_{\rho^{-1}}(p(\boldsymbol{x})) \boldsymbol{\nabla} p(\boldsymbol{x}) \\ &= \rho^{-1} \boldsymbol{\nabla} p \ ,\end{aligned} \tag{2.2.14}$$

where

$$F_{\rho^{-1}} \stackrel{\text{def}}{=} \int \frac{dp}{\rho(p)} \tag{2.2.15}$$

is the undeterminate integral of ρ^{-1} over pressure, and p_0 is a constant reference pressure. The equation of motion of a barotropic fluid is given by

$$d_t \boldsymbol{v} = -\boldsymbol{\nabla} \left(\int \frac{dp}{\rho(p)} + \Phi\right) \tag{2.2.16}$$

from which, with mass conservation (2.2.7), the equation of motion

$$d_t \boldsymbol{\omega}_p = \partial_{\boldsymbol{\omega}_p} \boldsymbol{v} \tag{2.2.17}$$

of potential vorticity can be derived. The total Lagrangian volume $\mathcal{V}_L$ is divided into fluid elements $dm = \rho dV$ that are infinitesimally Lagrangian volumes themselves. Therefore

$$d_t(dm) = 0 \tag{2.2.18}$$

and

$$
\begin{aligned}
d_t H &= \int_{\mathcal{V}_L} d_t(\boldsymbol{v}\cdot\boldsymbol{\omega}_p\,\rho dV) \\
&= \int_{\mathcal{V}_L} d_t(\boldsymbol{v}\cdot\boldsymbol{\omega}_p)\rho dV \\
&= \int_{\mathcal{V}_L} \left[-\boldsymbol{\omega}_p\cdot\boldsymbol{\nabla}\left(\int\frac{dp}{\rho(p)}+\Phi\right)+\boldsymbol{v}\cdot\partial_{\boldsymbol{\omega}_p}\boldsymbol{v}\right]\rho dV \\
&= \int_{\mathcal{V}_L} \boldsymbol{\nabla}\cdot\left[\left(\frac{1}{2}\boldsymbol{v}^2-\int\frac{dp}{\rho(p)}-\Phi\right)\boldsymbol{\omega}\right]dV \\
&= \oint_{\mathcal{S}(\mathcal{V}_L)}\left(\frac{1}{2}\boldsymbol{v}^2-\int\frac{dp}{\rho(p)}-\Phi\right)\boldsymbol{\omega}\cdot\boldsymbol{n}\,dS\ .
\end{aligned}
\tag{2.2.19}
$$

In the fourth equality the product rule $\partial_{\boldsymbol{\omega}_p}\frac{1}{2}\boldsymbol{v}^2=\boldsymbol{v}\cdot\partial_{\boldsymbol{\omega}_p}\boldsymbol{v}$ was used together with the fact that the vorticity field is nondivergent. A sufficient condition for the invariance of the total helicity of a barotropic fluid in a Lagrangian volume is that the flux of vorticity out of the volume vanishes everywhere. This may be due to the fact that vorticity is zero on or parallel to the bounding surface.

Moffatt [1969] demonstrated that for closed, isolated vortex filaments in a barotropic fluid helicity is related to the oriented winding number of any pair of linked vortex filaments, or to the self-winding number of a single vortex filament. In both cases helicity can be interpreted as a measure of the topological complexity or 'knottedness' of an ensemble of closed, isolated vortex lines. For such a discrete vorticity field in a barotropic fluid there exists at least one Lagrangian volume in which helicity is conserved. It contains only complete, closed vortex lines. Conservation of helicity in that case has a simple topological explanation as the conservation of the oriented linking number since in the absence of viscosity vortex line reconnection is impossible. However, in a fluid with a continuous vorticity field, single vortex lines and vortex filaments are generally not closed. A closed vortex line corresponds to a periodic solution of a generally nonlinear ordinary differential equation $d_t\boldsymbol{\xi}(t,\boldsymbol{\xi}_0)=\boldsymbol{\omega}(t,\boldsymbol{\xi}(t,\boldsymbol{\xi}_0))$, where $\boldsymbol{\xi}$ is the position vector along the vortex line. Initial conditions $\boldsymbol{\xi}(0,\boldsymbol{\xi}_0)=\boldsymbol{\xi}_0$ that belong to periodic solutions generally lie on a possibly fractal set of very small Lebesgue measure. In that case even for an ideal fluid the topological interpretation of helicity does not hold.

In fact, as shown above, the invariance of helicity only holds under very special boundary conditions that generally cannot be satisfied in a bounded barotropic fluid. It is therefore much more instructive to use the conservation laws as a starting point for the discussion of mechanisms responsible for *nonconservation* of kinetic energy and helicity in realistic flow situations. For that a kinematical instead of topological interpretation of helicity will be developed in the following sections.

2.3 Flow Instability and Stability

In Section 2.1.3 the regularity of the vorticity field relative to the velocity field was discussed. Helicity was introduced as a measure for the relative regularity of velocity and vorticity. In this section the role of helicity in the regularity of the velocity field itself is established.

2.3.1 Onset of Turbulence

One of the fundamental questions in fluid mechanics is when and under what circumstances a regular flow becomes irregular.

A regular or *laminar flow* is characterised in space by smooth streamlines that show a similar pattern in nearby flow regions. Significant qualitative changes occur slowly and continuously. The spectral characteristics include a narrow range at small wave numbers containing most of the kinetic energy. A special type of laminar flow is a *potential flow* that by definition is irrotational. More generally, laminar flows are simple rotational flows that can be approximated well by analytical functions in space and time, at least in a piecewise fashion.

An irregular or *turbulent flow* is simply defined as one that is not laminar. It has qualitatively very different streamline patterns in neighbouring flow regions and shows significant qualitative changes over short time intervals interrupted by periods of little change. This unsteady behaviour is called *temporal intermittency* and is one of the hallmarks of turbulence. Turbulent flows are inherently rotational and as seen in the next section are likely to have values of integrated helicity close to zero. They have a broad spectral range of kinetic energy and other kinematical scalar variables.

The transition from laminar to turbulent flow is referred to as *flow instability* . However to quantify exactly when a laminar flow becomes turbulent is highly subjective. Qualitatively the onset of turbulence occurs when the forcing mechanisms dominate over the damping mechanisms.

For the atmosphere the most important damping mechanisms on the large scale are negative buoyancy or a stable density stratification, the Coriolis force due to the Earth's rapid rotation, and boundary layer effects at the Earth's solid surface. Excitations of waves with very large wavenumbers are also damped out efficiently by internal viscosity and molecular diffusion of momentum. These short waves are usually, although not necessarily, associated primarily with kinetic energy perturbations of small spatial extent.

The forcing mechanisms in the atmosphere are a lot more complex than the damping mechanisms. In a coffee cup turbulence can be created simply by random external stirring. In engineering flow turbulence is created by forcing the fluid through a system of pipes or by objects moving through the fluid (turbine blades, airplanes, cars). In all cases the shape of the mechanical object is well defined and within the pipes or in the vicinity of the moving object imposes a certain flow on the fluid. It is then possible to calculate at which values of the scale invariant parameters such as Reynolds and Prandtl number the streamlines separate from the imposed boundary which is then defined as the onset of turbulence. Mechanical stirring by moving objects including ocean waves exists in the atmosphere as well but is insignificant for the generation of turbulence in the free atmosphere where storm formation takes place.

All important forcing mechanisms can eventually be traced back to radiative energy input from the sun. Differences in the material properties of the atmosphere and the Earth's surface lead to spatially varying amounts of energy absorbed and to varying changes in temperature, pressure, and density of the absorbing material (essentially air and water). These thermodynamic differences do not create turbulence by themselves, only indirectly through their influences on the velocity field. Generally fluid motion is described by the system of nonlinear partial differential equations

$$\begin{aligned} \partial_t \boldsymbol{v} &= -\partial_{\boldsymbol{v}} \boldsymbol{v} + \boldsymbol{f} \\ &= \boldsymbol{v} \times \boldsymbol{\omega} - \boldsymbol{\nabla} \frac{1}{2} \boldsymbol{v}^2 + \boldsymbol{f} \ , \end{aligned} \tag{2.3.1}$$

where $\boldsymbol{f}$ denotes the acceleration due to the sum of all forces acting on fluid elements. The gradient of kinetic energy $-\boldsymbol{\nabla}\frac{1}{2}\boldsymbol{v}^2$ can be included in the gradient of potential energy due to gravity and pressure forces (weighted by density), $-\boldsymbol{\nabla}\left(\int \frac{dp}{\rho} + \Phi\right)$, that is part of the forcing term $\boldsymbol{f}$. The term $\boldsymbol{v} \times \boldsymbol{\omega}$ is responsible for basically all interesting kinematical phenomena in fluid dynamics, in particular for the generation of turbulent velocity perturbations and energy transfer between spectral components of the velocity field. It is called inertial forcing term because even in the absence of the redefined forcing term in Eulerian coordinates it creates local changes in the velocity and vorticity field with time such that

$$\partial_t \boldsymbol{v} - \boldsymbol{v} \times \boldsymbol{\omega} \equiv \boldsymbol{0} \ . \tag{2.3.2}$$

There are essentially two different ways of describing the onset of turbulence in a laminar fluid.

In space the flow is only actively turbulent in regions where $\boldsymbol{v} \times \boldsymbol{\omega}$ exceeds the sum of all damping forces. There the effect of the inertial forcing term is to generate turbulent velocity perturbations or eddies from intense shear zones of the laminar flow and to mix the turbulent kinetic energy away from the shear zone and into the laminar part of the fluid, thereby spreading the region of turbulence. First instabilities typically occur over a small spatial extent on a scale where viscosity is the dominant damping mechanism, and the route to turbulence proceeds through continued forcing and repeated interactions of turbulent eddies.

In addition to creating shear instabilities the inertial forcing term is also responsible for cross-spectral energy transfer, statistically from spectral regions of high kinetic energy to spectral regions with low kinetic energy. As mentioned before a laminar flow has a narrow spectral peak at small wavenumbers. This peak must be due to external forcing. From that initial state a net transfer of kinetic energy by inertial forcing takes place to larger wave numbers while the main spectral peak is maintained if external forcing persists. Transport of kinetic energy usually proceeds through *local* spectral interactions, i.e., interactions between wave components with similar wavenumbers, in many small steps across the spectrum and is therefore referred to as a cascade of kinetic energy; more precisely a *direct cascade* in the usual case of energy transport from small to large wavenumbers or an *inverse cascade* in the opposite case. In addition to the cascading process cross-spectral energy transfer can also occur through *nonlocal* interactions whereby waves with very different wavenumbers interact, or a wave is excited through the local interaction of two other waves with very different wavenumbers. If the kinetic energy 'reaches' large enough wavenumbers for which molecular diffusion becomes important it is dissipated. Through these processes often a stationary state is reached where kinetic energy transferred from small wavenumbers into the spectral range between the forced and damped wavenumbers is equal to the kinetic energy removed at large wavenumbers. The intermediate spectral region that is neither significantly forced externally nor significantly damped by internal viscosity and only influenced by inertial forcing is referred to as *inertial range*.

A continuously forced weakly dissipative fluid such as the atmosphere is almost always and everywhere fully turbulent, and eddies of many different sizes exist and interact. The fluid is in a state where statistically the generation of turbulence by the inertial force is balanced by the dissipation of turbulence by damping forces.

The mathematical description of turbulence is still considered to be one of the most challenging problems in science. The greatest difficulties arise due to the apparent randomness that seems to be incompatible with the usual deterministic laws of classical mechanics. Starting with the work by *Taylor* [1935, 1936, 1938] and *von Kármán* [1937] many scientists have therefore contributed to the formulation of a *statistical* theory of turbulence. Even Werner Heisenberg after establishing the foundation of modern quantum theory and during the final years of World War II felt compelled to return to the topic of his dissertation [*Heisenberg*, 1924] and, in collaboration with von Weizsäcker during their internment at Farm Hall in 1945, independently from *Kolmogorov* [1941a, 1941b] and *Onsager* [1945], derived scaling laws for the kinetic energy spectrum and velocity correlation functions of isotropic turbulence [*Heisenberg*, 1948]. The starting point for a statistical description is an assumption about the existence of a *universal equilibrium* for motion on scales small enough to be essentially decoupled from the relatively slow evolution of the large scales yet too large for dissipation due to internal viscosity to be effective. While large-scale fluid dynamical problems must be solved for specific forces and boundary conditions this assumption asserts that motion, corresponding essentially to kinetic energy in the inertial range, reaches an asymptotic state that to some degree is independent of the large-scale forcing and the structure of the viscous boundary layer.

Turbulence theory strongly focusses on the discrete or continuous Fourier representation of the flow and the associated kinetic energy spectra. For that reason most works on turbulence define eddies as flow components associated with a single wavenumber k, and the inverse $L \sim k^{-1}$ of that wavenumber as their typical length scale. The interaction timescale T of small scales is then defined to be of order $L/v(k)$ where $v(k)$ is the amount of the Fourier transform of the eddy flow component [e.g., *Chorin*, 1994; Chap. 3]. According to *Kolmogorov* [1941a], kinetic energy in the inertial range has a power law dependence $E(k) \sim k^{-\frac{5}{3}}$. Then $v(k) \sim k^{-\frac{5}{6}}$ and the interaction timescale $T \sim (k\,v(k))^{-1} \sim k^{-\frac{1}{6}}$ decreases with increasing wavenumber. However, this is plausible only if the main energy of individual wavenumbers is associated with velocity perturbations of roughly the same physical extent. If this criterion is not satisfied a meaningful spatial scale and interaction timescale cannot be assigned to individual wave components. Therefore, in turbulence theory the statistical interpretation of flow properties starts with the definition of eddies. The Fourier expansion coefficients for wave vectors on a spherical shell $S(k)$ with radius (wavenumber) k are interpreted as being representative for the typical energy of eddies of spatial scale k^{-1}. The interaction between these Fourier components with those on a shell $S(q)$ is then interpreted statistically as the interaction (i.e., an exchange of energy) between eddies on the corresponding scale. Generally, the interpretation of energy of a certain wavenumber as being representative of flow features of a certain physical size is not possible and a clear separation must be made between spatial and spectral scales. Therefore, an alternative definition of the scale of eddies based on spectral properties is given in Section 2.6.1.

With the usual definition in turbulence of eddies as individual wave components eddies are not recognisable flow features in the sense of localised velocity perturbations of a particular spatial extent as defined in Section 2.1.4. A Fourier series expansion is therefore an abstract mathematical representation of the flow, where unlike the three velocity components the new variables given by the expansion coefficients are not directly observable. However, in Section 3.2 a highly truncated model is derived, where an individual vortex is represented by two waves. In that simple case changes in the corresponding Fourier components are uniquely associated with the evolution of a particular recognisable flow structure. In that sense the expansion coefficients become 'physical' variables or 'observables.'

2.3.2 Flow Structures

Once velocity perturbations are formed at small scales by shear instabilities induced by the inertial force, they interact and start to grow by entrainment of the kinetic energy of the shear zone. However, if the nonlinear forcing persists after their formation kinetic energy in physical space is mixed away from an initially coherent eddy, and in wavenumber space kinetic energy is efficiently 'transported' from large to small spectral scales and eventually dissipated. While the inertial forcing and shear instabilities are responsible for the onset and maintenance of turbulence, these mechanisms are damaging for an increase in the intensity of large eddies. To prevent the diffusion of kinetic energy after the formation of eddies, inertial forcing must be minimised. To survive longer as a coherent kinetic energy perturbation, an eddy must acquire kinematical properties that minimise the very forcing term that created the initial disturbance in the normal flow from which it grew.

With the definitions of Section 2.1.3,

$$|\boldsymbol{v}\times\boldsymbol{\omega}| = \sigma \sin\phi \;, \tag{2.3.3}$$

and locally inertial forcing vanishes with perfect alignment between velocity and vorticity. It can therefore be assumed that intense velocity perturbations with strong alignment are more persistent than velocity perturbations with weak alignment. Since dynamically significant eddies are intense, under that hypothesis, the meaning of helicity for eddies and the flow in general can loosely be expressed as

$$\begin{aligned} \text{helicity} &= \;\;\text{intensity} \;\;\times \text{alignment} \\ &= \text{significance} \times \text{persistence} \;. \end{aligned}$$

If this is true, then helical eddies dominate the present flow state through their intensity, and are likely to dominate the future flow state through their persistence. Intense and persistent eddies that preserve their qualitative kinematical properties over sufficiently long periods of time to be able to interact with each other are also referred to as *flow structures*.

There is a qualitative similarity between helical flow structures and elementary particles. Like quantum mechanical particles they do not have solid or well defined boundaries and therefore their size, shape, position, and other space related parameters cannot be defined precisely. However, their limited spatial extent and their persistence, over some period of time, allow to describe flow structures as entities or 'fluid particles.'

However, the validity of the assumption about the persistence of helical velocity perturbations, particularly vortices, under various circumstances is a topic of much debate.

The idea of the role of alignment in creating low-dimensional coherent structures, or *spatial intermittency*, embedded in a turbulent flow is almost as old as turbulence theory itself. Making the inertial forcing responsible for the generation of turbulence [*Reynolds*, 1883] it is an immediate logical consequence. In a series of papers, based on the above arguments, Levich and coworkers established a theoretical explanation for the existence of large intense and coherent vortices and storms, such as tornadoes and hurricanes, in an otherwise turbulent flow.

Levich and Tsinober [1983a, 1983b] showed that in addition to helicity also the helicity correlation function is invariant in homogeneous turbulence of an ideal fluid and cascades to small wavenumbers. With increasing anisotropy due to large-scale damping mechanisms an increasing fraction of kinetic energy cascades to small wavenumbers together with the helicity correlation function. The authors note that helical eddies are quasistationary and the turbulent cascade proceeds effectively in weakly helical subregions generated as a result of shear instabilities. These sheets of active turbulence are typically fractal with Hausdorf dimension between two and three.

The fact that coherent structures are quasistationary means that they are zeros of the transfer term in the Fourier transformation of the Navier-Stokes equation or singularities of the renormalised Green's function [*Levich and Tsinober*, 1983b]. The presence of coherent structures therefore leads to divergent perturbation series. Helical structures through stirring on the one hand and eddy viscosity on the other contribute significantly to the energy cascade to large wavenumbers. If these effects are subtracted from the dynamical equations the renormalised nonlinear transfer is reduced effectively to the (fractal) turbulent subsets free of helical eddies where reduced mode coupling can be calculated perturbatively.

Levich and Tzvetkov [1984, 1985] argued that turbulent stirring of the cloud field can transfer thermal to kinetic energy with an efficiency of $\sim 2-3\%$. They showed that in nonhelical shear layers strong, short-lived convective perturbations most likely generate pairs of vortices with helicity roughly equal in magnitude and opposite in sign. This turbulisation of the mean flow occurs on a scale much smaller than a tornado or an organised storm system. The formation of larger vortex structures from excitation of random motion on small scales is explained by the inverse cascade of the helicity correlation function. This increases the correlation length or the coherence scale of large-scale velocity fluctuations.

Lilly [1986] reviewed the role of helicity as a stabilising factor for severe convective storms. He confirmed that small wavenumber perturbations are likely to be characterised by high helicity and tend to dominate the flow statistics whereas most dissipation in the same range of wavenumber occurs in regions of low helicity. Moreover for a given kinetic energy, strongly helical flow dissipates only at 1/4 the rate of nonhelical turbulent flow.

Based on perturbation theory, *Belian et al.* [1998] found that the effective turbulent viscosity in helical turbulence is less than for the nonhelical case, resulting in a slow-down of the energy transfer along the spectrum from small to large wavenumbers. These effects are noticeable for Gaußian turbulence in second order of the perturbation velocity field, and in third and higher order for non-Gaußian turbulence.

However, it was shown by *Wallace and Balint* [1990] in wind tunnel experiments on scales of a few centimetres to metres that helicity density is not a necessary property of coherent vortices. They found that in turbulent boundary layers, mixing layers, and in grid flow the relative orientation of velocity and vorticity inside the vortex depends on the orientation of the vortex axis relative to the mean flow. They also found little connection between the energy dissipation rate and helicity density.

Ditlevsen and Giuliani [2001] and *Chen et al.* [2003] found that statistically helicity often vanishes at laboratory scales and for most engineering applications. The hypothesis brought forward by *Levich and Tsinober* [1983] that organised, large-scale coherent motions are a universal and intrinsic property of all turbulent flows, stabilised by large values of helicity and not necessarily related to shear instabilities, is therefore not justified.

On the other hand, *Moffatt and Tsinober* [1992] state that nonzero mean values of helicity occur naturally in a wide variety of geophysical flows, in which cases it is likely to play an important role in the evolution and stability of these laminar or turbulent flows. As specific examples they note that helicity density of the rotating updraft of thunderstorms (mesocyclone) is on the order of $0.1\,\mathrm{ms}^{-1}$, and of the tornado vortex $10\,\mathrm{ms}^{-1}$.

There obviously is a large difference between laboratory and geophysical flows concerning the role of helicity in the formation of coherent flow structures and spatial and temporal intermittency in a turbulent fluid. The importance of helicity specifically for the formation of updraft rotation in thunderstorms and for the formation of smaller, embedded vortices is discussed in greater detail in the following section.

2.4 Tornado Phenomenology

Observational tornado research focusses on visually striking storm features and their possible connection to tornadogenesis. As such it focusses on large-scale persistent structures associated with all or at least the majority of tornadic thunderstorms. Among the main characteristics of tornadic thunderstorms are the *mesocyclone*, i.e., the main rotating updraft with a diameter on the order of 10 km, the *hook echo*, a hook-shaped precipitation region to the right rear of the updraft facing downstream with the horizontal mean flow, and the *rear-flank downdraft*. Just prior to tornadogenesis, the mesocyclone often contains a smaller vortex with a diameter of about 1 km called *tornado cyclone*.

Although the phenomenological approach in many ways is opposite to the approach taken by turbulence theory, the two scientific branches have the same fundamental goal in that they are trying to establish the common *statistical* relationships between events. While turbulence theory focusses on the forcing independent universal properties of turbulent small-scale motion in the inertial range, tornado research identifies forcing mechanisms associated with the common features of large, well organised severe storm complexes that may be responsible for the formation of a coherent smaller-scale vortex.

The most intense tornadoes tend to occur between mesocyclone and rear-flank downdraft. Since the mesocyclone is a cyclonically rotating updraft and the rear-flank downdraft an anticyclonically rotating downdraft, tornadoes therefore tend to form near the most intense positively helical shear zone, and in this region are typically found to rotate cyclonically.[4] In addition, the large-scale horizontal mean flow is typically veering over the lowest few kilometres. The severe storm system and the embedding larger-scale mean flow are therefore an overall positively helical flow environment.

The explanation of how an intense rotating updraft can form from an essentially horizontally homogeneous, vertically sheared horizontal flow is well established. Starting point is the vorticity equation

$$d_t\boldsymbol{\omega} = \partial_{\boldsymbol{\omega}}\boldsymbol{v} - \boldsymbol{\omega}\,\boldsymbol{\nabla}\cdot\boldsymbol{v} + \boldsymbol{\nabla}\times\boldsymbol{f} \tag{2.4.1}$$

where again $\boldsymbol{f}$ represents the sum of all forcing terms. The role of the various terms in the generation of a vertical vortex is best investigated by separating vorticity into horizontal, $\boldsymbol{\omega}_h$, and vertical, ζ, components. Neglecting the forcing terms, the time evolution of these vorticity components is determined by

$$d_t\boldsymbol{\omega}_h = \underbrace{\boldsymbol{\omega}_h\cdot\boldsymbol{\nabla}\boldsymbol{v}_h}_{A}\underbrace{+\zeta\partial_z\boldsymbol{v}_h}_{B}\underbrace{-\boldsymbol{\omega}_h\boldsymbol{\nabla}\cdot\boldsymbol{v}}_{C}+\cdots \tag{2.4.2}$$

and

$$d_t\zeta = \underbrace{\boldsymbol{\omega}_h\cdot\boldsymbol{\nabla}w}_{A}\underbrace{+\zeta\partial_z w}_{B}\underbrace{-\zeta\boldsymbol{\nabla}\cdot\boldsymbol{v}}_{C}+\cdots\ , \tag{2.4.3}$$

where $\boldsymbol{v}_h$ denotes horizontal velocity. Term A in (2.4.3) is positive if horizontal vorticity has a component along the horizontal gradient of vertical velocity. If horizontal flow with vorticity along the direction of motion (positive helicity) enters a region where vertical velocity is increasing (an updraft region), fluid elements will be deflected upward from their horizontal trajectories. At the same time, through term A, they acquire positive vertical vorticity. Their helicity therefore remains positive. If horizontal flow with positive helicity encounters a downdraft region (negative horizontal gradient of vertical velocity), fluid elements will be deflected downward while gaining negative vertical vorticity and thus remaining positively helical. Similarly negatively helical flow acquires anticyclonic vorticity in an updraft region and cyclonic vorticity in a downdraft region, again maintaining its sign of helicity. The effects of terms A and B in (2.4.2) are complimentary to those in (2.4.3). For *helical* flow their combined effect is to 'tilt' vortex lines with or against the curvature of streamlines depending on whether the flow is positively or negatively helical. The term $\partial_{\boldsymbol{\omega}}\boldsymbol{v}$ in (2.4.1) is therefore called *tilting term*. Given a (thermally direct) circulation cell of positively helical motion the effect of the inertial forcing term is to produce a 'tilting cycle' with cyclonic updraft and anticyclonic downdraft. It is important to note that for nonhelical horizontal and horizontally homogeneous flow entering an updraft or downdraft region no vertical vorticity is generated through the tilting term. Term B in (2.4.3) implies that (positive) vertical vorticity increases

[4] There may be a weaker anticyclonically rotating tornado along the leading edge of the storm.

if vertical velocity increases with height. This term is therefore referred to as *stretching term*.

The terms C in (2.4.2) and (2.4.3) are straightforward to interpret. In a region of convergent flow they lead to a higher concentration of positive or negative vorticity depending on the momentary sign of the respective vorticity component and to a lower concentration in a region of divergent flow. They are therefore called *convergence terms*. For an irrotational flow they do not generate vorticity.

As shown in Section 2.2 local changes in helicity must be such that the total helicity in a Lagrangian volume is conserved for barotropic, inviscid flow in an inertial frame of reference, and therefore also for inertial motion. Tilting and convergence on the average only transfer helicity between different modes of motion such as from a horizontal, vertically veering shear flow to a cyclonically rotating updraft.

For inertial flow with $d_t\boldsymbol{v} \equiv \boldsymbol{0}$ it follows that the time rate of change of helicity density following the motion of a fluid element is given by

$$d_t\eta = \boldsymbol{\omega} \cdot \boldsymbol{\nabla}\frac{1}{2}\boldsymbol{v}^2 - \eta\boldsymbol{\nabla} \cdot \boldsymbol{v} \ . \tag{2.4.4}$$

Neglecting convergence, helicity increases if vorticity has a component along the gradient of kinetic energy. If the fluid element momentarily has perfect alignment the increase in helicity is maximised if the motion is along the direction of largest increase in kinetic energy. Since alignment is already maximised the increase in helicity is only due to an increase in intensity (definitely due to an increase in kinetic energy and possibly also due to an increase in enstrophy). Conversely for a momentarily nonhelical fluid element the increase in helicity is maximised if the motion is along an isosurface of kinetic energy. The increase in helicity is then primarily due to an increase in alignment and possibly enstrophy.

Davies-Jones [1984] investigated the linearised, inviscid, isentropic, shallow, and dry equations of motion where the mean flow state was assumed to be steady, horizontal, only a function of height, and in hydrostatic balance. Due to large vertical shear the Coriolis force was neglected. Basically the same results were found as for inertial motion. Tilting of horizontal vorticity by an updraft produces a counterrotating pair of vertical vortices. While for 'streamwise' vorticity in a vertically veering horizontal flow (with positive helicity) there is a spatial correlation between vertical velocity and vorticity (both vortices, cyclonically rotating updraft and anticyclonically rotating downdraft, are positively helical) no correlation is found for 'crosswise' vorticity in a horizontal mean flow with pure vertical speed shear (zero helicity). However the reason for that is different to that in the case of inertial motion.

It was shown in Section 2.2 that Ertel's potential vorticity is a Lagrange invariant of isentropic flow. Then, if the initial conditions of the horizontal mean flow are such that isentropic surfaces and vorticity are horizontal, Ertel's potential vorticity is identically zero following the motion. This can only be true if vortex lines remain in isentropic surfaces. For these special initial conditions effectively the variable $\boldsymbol{\omega}\cdot\boldsymbol{\nabla}\theta$ is a Lagrange invariant although density may fluctuate along trajectories. If the buoyant updraft shows up as an isolated peak on the isentropic surfaces this explains the tilting of vortex lines and the formation of the counterrotating pair of vortices.

Tilting and convergence processes are both purely kinematical mechanisms in that they do not directly involve external forcing. An investigation of inertial motion allows inferences about the general, forcing independent behaviour of the flow and an identification of the basic mechanisms of vortex formation. Again this procedure is similar in principal to turbulence theory, where the investigation of inertial forcing focusses on different scales and phenomena, using a spectral rather than a spatial representation of the flow.

For more general forcing the previous arguments about the Lagrange invariance of Ertel's potential vorticity do not hold and mechanisms other than tilting and convergence must be considered. The most important question that needs to be addressed is how helicity necessary for the generation of a vertical vortex through vortex line tilting can be generated in the first place. Generally this can be achieved by any mechanism that had to be excluded in Section 2.2 in deriving the helicity conservation law for a barotropic fluid in a Lagrangian volume. These are baroclinic processes and Coriolis force affecting the main body of the fluid, and molecular viscosity acting mainly on the solid boundaries. Fluxes of vorticity across the open boundaries also lead to helicity changes inside a Lagrangian volume. The importance of veering wind shear for high helicity in the storm inflow region was already mentioned. The typical existence of this vertical wind profile in the lowest kilometre of the atmosphere is explained in the Ekman theory by the adjustment of the boundary layer flow to the geostrophic wind aloft, i.e., by the combined action of Coriolis and pressure gradient force together with surface friction. In the northern hemisphere, by the thermal wind relationship, a veering wind profile can also be the result of warm advection by the geostrophic wind.[5] Along outflow boundaries and other fronts helicity can be generated by baroclinic processes. The potential relevance of these mechanisms specifically for tornadogenesis was confirmed in numerical simulations by *Walko* [1993] for veering wind shear and by *Klemp and Rotunno* [1983] for baroclinicity.

Given initial helicity several conceptual models were proposed to explain the formation of tornadoes in severe storm systems. They are essentially all combinations of three basic mechanisms:

(i) tilting of horizontal streamwise vorticity by an updraft or downdraft, i.e., transfer of helicity from a horizontal shear flow to a rotating updraft,

(ii) spin-up or vortex line stretching in zones of convergent flow with accelerating vertical motion and preexisting vertical vorticity, and

(iii) solenoidal production of horizontal streamwise vorticity in baroclinic zones and subsequent tilting and stretching.

Davies-Jones and Brooks [1993] described a mechanism similar to the tilting cycle described above that keeps helicity concentrated in the storm system and may therefore promote tornadogenesis. It includes deflection of the horizontal, helical storm outflow by the downdraft at the inversion layer, and transport of helicity close to surface where it is deflected again and recycled back into the updraft. Since helicity of the storm is maintained, as the thermal circulation is intensified so is updraft and downdraft rotation.

In addition to a buoyant updraft also forced lifting along outflow boundaries may be responsible for strong tilting close to the ground. Convergence at air mass boundaries and

[5]In the southern hemisphere warm advection leads to a backing wind profile, negative helicity, and therefore again, as expected, to cyclonic updraft rotation (negative vertical vorticity) through tilting.

in the inflow region of the storm updraft contributes further to the intensification of vertical vorticity. In fact *Wakimoto and Atkins* [1996] suggested that convergence may in some cases dominate tornadogenesis. In that scenario a tornado is spun up by stretching of vertical vorticity if an intense mesocyclone moves over a layer of vertical circulation that exists independently of the storm system in a horizontal shear zone. This is essentially the same mechanism that is responsible for the formation of nonsupercell tornadoes or landspouts [*Wakimoto and Wilson*, 1989].

Several other mechanism were proposed to explain the formation of tornadolike vortices independently of severe storm systems. *Barcilon and Drazin* [1972] for example suggested that dust devils may form from horizontal shearing instabilities along gust fronts when vertical vortex sheets roll up into vortices. In the landspout or dust devil scenario the role of the storm system if any is to intensify 'foreign' circulation through stretching by the storm updraft and the own circulation simply serves to stabilise the storm system. Normally these relatively weak non-storm-related vortices are spun up by convergence along shear zones and air mass boundaries from which they derive their circulation. However in the presence of an intense updraft the same mechanisms may be responsible for the formation of an intense tornado.

All these conceptual models suggest that the main characteristics of the larger-scale storm environment for the generation of mesoscale circulation are veering wind shear, together with intense neighbouring regions of positive and negative buoyancy. In a large climatological study, *Rasmussen and Blanchard* [1998] indeed confirmed that combined measures of buoyancy and vertically turning wind shear are able *statistically* to discriminate between supercell and ordinary thunderstorms, while measures of shear and buoyancy alone only weakly differentiate between the two types of storms.[6]

Part of the problem may be that shear parameters such as boundary layer to 6 km shear and mean shear[7] contain both effects due to speed and directional shear, while speed shear only in connection with strong directional shear contributes to helicity in a storm environment and therefore to rotating updrafts through tilting. Consequently these parameters separate only weakly between rotating and ordinary thunderstorms. Storm-relative helicity[8] takes into account primarily changes in the horizontal mean flow perpendicular to the mean flow at a given level and therefore separates well between supercell and ordinary thunderstorms. As a result a combined measure of shear and buoyancy such as the energy-helicity-index performs better than the Bulk-Richardson-Number in predicting supercell thunderstorms.

However, the differences between tornadic and nontornadic severe thunderstorms seen in forecast parameters are not sufficiently significant to allow for reliable tornado forecasting without high false alarm rates. The severe weather parameters mentioned above were defined to characterise the potential of a large-scale, horizontal mean flow to produce a ro-

[6]For a short description of the distinguishing characteristics of ordinary and supercell thunderstorms see Appendix B.

[7]For a definition of operational forecasting parameters see *Rasmussen and Blanchard* [1998].

[8]This parameter is equal to helicity only for a purely turning vertical profile of a horizontally homogeneous horizontal velocity field. For the maximally helical Beltrami vortex flow discussed in Section 2.6.1, for example, storm-relative helicity is zero.

tating updraft in a positively buoyant storm system. As such they serve as predictors of mesocyclone or supercell formation. However, they are not intended to be forecast parameters for tornadogenesis. Apparently, a certain rotational potential of the storm system is not sufficient to determine the formation of a smaller-scale vortex. Therefore, the question is how the rotational energy can be transferred to the smaller scale, or how the rotation of the thunderstorm interacts with the environmental mean flow to produce conditions conducive to tornadogenesis.

Although currently observational data is probably neither accurate nor dense enough to dismiss or validate any theory, based on the wide range of scales of motion involved in thunderstorm dynamics it can be speculated that the specification of the storm and larger-scale environment alone is not sufficient to uniquely classify the state of the atmosphere with regard to the formation of tornadolike vortices. It is now generally acknowledged that, while the large-scale vertical distributions of temperature, moisture and wind shear determine the type of the forming thunderstorm, it are details of the dynamical structure in the storm system that determine tornadogenesis.

As briefly outlined above, tornadolike vortices are usually formed in regions of strong *horizontal* velocity gradients such as between main updraft and downdraft, or on or near flow discontinuities such as gust fronts, more organised squall lines, other outflow boundaries, or at the leading edge of a thunderstorm. Consequently relevant spatial variability of the storm flow may be in the horizontal rather than in the vertical, and on the scale of the smaller, embedded vortex rather than on the scale of the storm circulation itself. With parameters derived from a single vertical profile (sounding) the horizontal variability of the flow on any scale is not characterised at all. The immediate environment of the tornado inside the storm cloud, dominated by horizontal shear zones, can only be determined from (horizontal) wind velocity data obtained by Doppler radar measurements.

It is likely that there are fundamental differences in the dynamical mechanisms leading to mesoscale storm rotation and to the rotation of an embedded tornado-scale vortex. It is therefore hypothesised for the investigation here that tornadolike vortices can be modelled as instabilities of flow discontinuities and shear zones, intensified by vertical motion, in principle similar to the conceptual landspout model. In addition it is discussed in Section 2.7 that there are important differences in the external forcing of the two vortex phenomena.

The idea of having criteria for tornadogenesis based on parameters that can be evaluated from observations of the storm flow prior to tornadogenesis, without the need for time-consuming numerical simulations, is very appealing from a forecasters perspective. Ideally, in principle similar to the parameter charts derived from observations by *Rasmussen and Blanchard* [1998; particularly Figures 9, 11, and 13], one would like to find new parameters for which a clear separation between tornadic and nontornadic storms is possible. For the investigation of the dynamics of idealised tornadolike vortices governed by an autonomous dynamical system of first-order ordinary differential equations in time these parameters are derived in Chapter 3 and 'tornadic' and 'nontornadic' states of the embedding flow, based on these parameters, are given by bifurcation charts.

2.5 Space-Dependence of the Velocity Field

To investigate the process of vortex formation the velocity field must somehow be expressed mathematically. Based on observations a discrete pointwise representation of the flow at a particular time is obtained. While this is adequate for numerical simulations, for theoretical investigations of the time-dependence of the velocity field the analysis is simplified significantly if an approximate analytical representation of the spatial dependence of the velocity field can be obtained. An example for the spatial dependence of a vortex flow is given by a *potential vortex*. In cylinder coordinates the radial and vertical velocity components are set identical zero and the tangential component is inversely proportional to the radial coordinate. The velocity field is then irrotational and has a singularity at the vortex centre. Another example is a *solid body vortex*, $\boldsymbol{v} = \boldsymbol{s} \times \boldsymbol{x}$, with a constant rotation vector $\boldsymbol{s}$ parallel to the vortex centre. Since the vorticity $\boldsymbol{\omega} = 2\boldsymbol{s}$ is perpendicular to the velocity field the helicity of solid body flow is zero. Both simple vortex models are not adequate for the description of helical, tornadolike vortices.

As discussed in the previous sections, at least in a geophysical context (particularly in supercell thunderstorms), helicity plays an important role for the persistence of eddies (particularly vortical velocity perturbations) in a turbulent larger-scale flow. As shown in Section 2.1.3, for a given distribution of intensity helicity in a finite volume is extremised by B-flows. The question now is, if these maximally helical flows also represent vortices. If this is the case, a special class of B-flows can be used as an idealised model for the spatial dependence of tornadolike vortices. The description of vortex flow used in this study is therefore based on solutions of the Beltrami condition with constant chirality. Three B-flow solutions to (2.1.20) are found by Fourier series expansion, i.e., by a spectral representation of the spatial dependence of the velocity field. It is then shown that superpositions of these three solutions are complete representations of general, spatially periodic velocity fields, and that in particular tornadolike vortices can be represented by a special superposition of helical waves.

2.5.1 Spectral Decomposition

For the relatively small-scale flows of severe thunderstorms without a particular symmetry a Cartesian coordinate system is most convenient. In this coordinate system the *Fourier series* in the variables $\boldsymbol{x}$ of function $f(t, \boldsymbol{x})$ is defined by

$$S_f \stackrel{\text{def}}{=} \sum_{j,k,l=-\infty}^{\infty} a_{jkl}(t) \exp i\chi_0(jx + ky + lz) \ , \tag{2.5.1}$$

where the smallest nonzero wavenumber χ_0 determines the fundamental wavelength, and $i \stackrel{\text{def}}{=} \sqrt{-1}$ is the imaginary unit. However, for the discussion of kinetic energy spectra and curl eigenstates in the following sections it is more convenient to rewrite the *Fourier basis functions*

$$\phi_{jkl}(\boldsymbol{x}) \stackrel{\text{def}}{=} \exp i\chi_0(jx + ky + lz) \ , \tag{2.5.2}$$

and to define them as

$$\begin{aligned}\phi_{\chi\boldsymbol{k}}(\boldsymbol{x}) &\stackrel{\text{def}}{=} \exp i\chi\boldsymbol{k}\cdot\boldsymbol{x}\\ &= \exp i\chi_0\boldsymbol{q}\cdot\boldsymbol{x}\ ,\end{aligned} \tag{2.5.3}$$

where $\boldsymbol{q} \stackrel{\text{def}}{=} (j,k,l)^T$ and the unit wave vectors $\boldsymbol{k}$ are defined as $\boldsymbol{q}/q$, with the amount $q \stackrel{\text{def}}{=} \sqrt{j^2+k^2+l^2}$ of $\boldsymbol{q}$. Relabelling the expansion coefficients

$$a_{jkl} \rightarrow a_{\chi\boldsymbol{k}} \tag{2.5.4}$$

the Fourier series (2.5.1) can also be written as

$$S_f = \sum_{\chi\in\Gamma}\sum_{\boldsymbol{k}\in S(1)} a_{\chi\boldsymbol{k}}(t)\exp i\chi\boldsymbol{k}\cdot\boldsymbol{x}\ , \tag{2.5.5}$$

where the set Γ is defined as

$$\Gamma \stackrel{\text{def}}{=} \{\chi \mid \chi = q\chi_0,\ q=\sqrt{j^2+k^2+l^2},\ j,k,l\in\mathbb{Z},\ \chi_0\in\mathbb{R}\}\ , \tag{2.5.6}$$

and the set $S(1)$ contains all three-dimensional unit vectors $\boldsymbol{k}$ and their negatives.

If $f(t,\boldsymbol{x})$ is periodic in the variables $\boldsymbol{x}$ with period $2\pi/\chi_0$, only has a finite number of point discontinuities and extrema over one period, and if

$$\int_0^{\frac{2\pi}{\chi_0}} |f(t,\boldsymbol{x})|d^3x \tag{2.5.7}$$

is finite in an interval T of t, the Fourier series converges to $f(t,\boldsymbol{x})$ in T if $\boldsymbol{x}$ is not a point of discontinuity [e.g., *Cohen*, 1992; pp. 175–176]. The *Fourier expansion coefficients* of the discrete spectral superposition are obtained through the transformation

$$a_{\chi\boldsymbol{k}}(t) \stackrel{\text{def}}{=} \langle f(t,\boldsymbol{x})\exp -i\chi\boldsymbol{k}\cdot\boldsymbol{x}\rangle_{\mathcal{P}^3}\ , \tag{2.5.8}$$

where the averaging operator over the three-dimensional periodic domain $\mathcal{P}^3$ is defined as

$$\langle(\quad)\rangle_{\mathcal{P}^3} \stackrel{\text{def}}{=} \left(\frac{\chi_0}{2\pi}\right)^3 \int_0^{\frac{2\pi}{\chi_0}} (\quad)\, d^3x\ . \tag{2.5.9}$$

The validity of this transformation can easily be verified by using the *orthonormality relationship*

$$\left\langle \phi_{\chi\boldsymbol{k}}(\boldsymbol{x})\phi^*_{\chi\boldsymbol{k}'}(\boldsymbol{x})\right\rangle_{\mathcal{P}^3} = \delta_{\boldsymbol{k}',\boldsymbol{k}} \tag{2.5.10}$$

of the system of basis functions $\phi_{\chi\boldsymbol{k}}$, and substituting the Fourier series (2.5.5) for f in (2.5.8). Here * denotes the complex conjugate of a variable and $\delta_{\boldsymbol{k}',\boldsymbol{k}}$ denotes the three-dimensional Kronecker symbol. Conversely, consistency of the Fourier transformation with the series expansion (or inverse transformation) can be checked by substituting the definition (2.5.8) of the expansion coefficients into (2.5.5) and making use of the *completeness relationship*

$$\left(\frac{\chi_0}{2\pi}\right)^3 \sum_{\chi\in\Gamma} \sum_{\boldsymbol{k}\in S(1)} \phi_{\chi\boldsymbol{k}}(\boldsymbol{x}')\phi^*_{\chi\boldsymbol{k}}(\boldsymbol{x}) = \delta(\boldsymbol{x}'-\boldsymbol{x}) \tag{2.5.11}$$

of the system of basis functions, where $\delta(\boldsymbol{x}'-\boldsymbol{x})$ is the three-dimensional Dirac distribution.

To be able to represent *aperiodic* functions via spectral decomposition a *continuous* superposition of plane waves is required. It is shown in elementary texts on mathematics that for any function $f(t,\boldsymbol{x})$ for which

$$\int_{-\infty}^{\infty} |f(t,\boldsymbol{x})| d^3x \tag{2.5.12}$$

is finite the *Fourier transform*

$$F(t,\boldsymbol{q}) \stackrel{\text{def}}{=} (2\pi)^{-\frac{3}{2}} \int_{-\infty}^{\infty} f(t,\boldsymbol{x})\phi^*(\boldsymbol{x},\boldsymbol{q}) d^3x \tag{2.5.13}$$

exists for all continuous wave vectors $\boldsymbol{q}$ and is bounded and steady over the real numbers. If in addition $f(t,\boldsymbol{x})$ is steady and in each finite interval piecewise differentiable, the Fourier transform is invertible and unique. In that case f is given by the *inverse transformation*

$$f(t,\boldsymbol{x}) = (2\pi)^{-\frac{3}{2}} \int_{-\infty}^{\infty} F(t,\boldsymbol{q})\phi(\boldsymbol{x},\boldsymbol{q}) d^3q \ , \tag{2.5.14}$$

where the basis functions

$$\phi(\boldsymbol{x},\boldsymbol{q}) \stackrel{\text{def}}{=} \exp i\boldsymbol{q}\cdot\boldsymbol{x} \tag{2.5.15}$$

now satisfy the orthogonality and completeness relations

$$(2\pi)^{-3} \int_{-\infty}^{\infty} \phi(\boldsymbol{x},\boldsymbol{q})\phi^*(\boldsymbol{x},\boldsymbol{q}') d^3x = \delta(\boldsymbol{q}'-\boldsymbol{q}) \tag{2.5.16}$$

and

$$(2\pi)^{-3} \int_{-\infty}^{\infty} \phi(\boldsymbol{x},\boldsymbol{q})\phi^*(\boldsymbol{x}',\boldsymbol{q}) d^3q = \delta(\boldsymbol{x}'-\boldsymbol{x}) \ , \tag{2.5.17}$$

respectively. It is then easy to verify that

$$\int_{-\infty}^{\infty} |f(t,\boldsymbol{x})|^2 d^3x = \int_{-\infty}^{\infty} |F(t,\boldsymbol{q})|^2 d^3q \ . \tag{2.5.18}$$

Occasionally, this equality is also referred to as the completeness relation.

The Fourier transformation equation (2.5.13) is obtained from the transformation equation (2.5.8) for the discrete spectral expansion if the boundaries are pushed further and further away to infinity. The periodic boundary conditions are then replaced by integrability (boundedness) conditions. As the periodic domain increases the basic period, i.e., the longest wavelength increases and therefore the difference between neighbouring discrete wavenumbers decreases. In applications the Fourier transformation is invariably calculated for a discrete spectrum over a finite domain in which the observational data is given. The smaller this domain the poorer the spectral resolution. The boundaries of the 'data volume' must therefore be sufficiently far enough away such that flow in the interior of the domain can be well resolved.

2.5.2 Helical Decomposition

It is possible to redefine the six independent real variables associated with each three-dimensional complex Fourier expansion coefficient by decomposing the Fourier transform of the velocity field into the eigenstates of the curl operator. For many purposes, such as the representation of specific types of flows, this change of variables has the advantage that the new expansion coefficients can physically be interpreted more easily.

The curl eigenvector equation (2.1.20) allows for three qualitatively different solutions $\boldsymbol{v}_\chi^\lambda$ that satisfy

$$\boldsymbol{\nabla}\times\boldsymbol{v}_\chi^\lambda = \lambda\chi\boldsymbol{v}_\chi^\lambda \ , \tag{2.5.19}$$

where the constants $\lambda\chi$ with $\chi > 0$ and $\lambda = 0, \pm 1$ are the chiralities of the eigenvectors $\boldsymbol{v}_\chi^\lambda$. Assuming spatial periodicity in a domain $\mathcal{P}^3$, as shown in Appendix A.2, these solutions are given by

$$\boldsymbol{v}_\chi^\lambda(t,\boldsymbol{x}) = \sum_{\boldsymbol{k}\in S(1)} a_{\chi\boldsymbol{k}}^\lambda(t)\boldsymbol{\eta}_{\boldsymbol{k}}^\lambda\phi_{\chi\boldsymbol{k}}(\boldsymbol{x}) \ . \tag{2.5.20}$$

The spatial basis functions $\phi_{\chi\boldsymbol{k}}(\boldsymbol{x})$ satisfy the orthonormality and completeness conditions (2.5.10) and (2.5.11) introduced in the previous section. In addition, as shown in Appendix A.3, the $\boldsymbol{\eta}_{\boldsymbol{k}}^\lambda$ form a complete set of orthonormal spectral basis vectors[9] in wavenumber space. They are defined by

$$\begin{aligned} \boldsymbol{\eta}_{\boldsymbol{k}}^\pm &\stackrel{\text{def}}{=} \frac{1}{\sqrt{2}}(\boldsymbol{k}\times\boldsymbol{n} \mp i\boldsymbol{n}) \\ \boldsymbol{\eta}_{\boldsymbol{k}}^0 &\stackrel{\text{def}}{=} -i\boldsymbol{k} \ , \end{aligned} \tag{2.5.21}$$

and will be referred to as *helical basis vectors.* Each unit vector $\boldsymbol{n}$ is orthogonal to the corresponding unit wave vector $\boldsymbol{k}$, and the normal vector corresponding to $-\boldsymbol{k}$ is defined to be $-\boldsymbol{n}$. The Fourier expansion coefficients are defined by

$$a_{\chi\boldsymbol{k}}^\lambda(t) \stackrel{\text{def}}{=} \left\langle \left(\boldsymbol{\eta}_{\boldsymbol{k}}^\lambda\phi_{\chi\boldsymbol{k}}(\boldsymbol{x})\right)^\dagger \boldsymbol{v}(t,\boldsymbol{x})\right\rangle_{\mathcal{P}^3} \ , \tag{2.5.22}$$

[9]The two helical eigenvectors $\boldsymbol{\eta}_{\boldsymbol{k}}^\pm$ are identical with those of *Waleffe* [1992], however, other choices are possible [e.g., *Moses*, 1971].

where † denotes the Hermitean transpose, $\boldsymbol{a}^\dagger \stackrel{\text{def}}{=} (\boldsymbol{a}^T)^* \equiv (\boldsymbol{a}^*)^T$. As shown in Appendix A.6 for the $\boldsymbol{v}_\chi^\lambda$ to be real, the Fourier amplitudes have to satisfy $a_{-\chi\boldsymbol{k}}^\lambda = a_{\chi\boldsymbol{k}}^{\lambda *}$.

The vector functions $\boldsymbol{\eta}_{\boldsymbol{k}}^\lambda \phi_{\chi\boldsymbol{k}}$ individually satisfy (2.5.19) and will therefore be called *curl eigenvectors*. The flows (2.5.20), as a superposition of curl eigenvectors with the same chirality, are perfectly positively or negatively helical, or irrotational for each nonzero wavenumber χ and will be called *curl eigenstates*. In Appendix A.4 it is shown that the helicity of these eigenstates and therefore the decomposition of the velocity field is invariant under spatial rotations.

It is shown in Appendix A.5 that the curl operator is Hermitean for vector fields that satisfy periodic boundary conditions in a finite domain, such as the curl eigenstates. As a result its eigenvalues (chirality) are real and its eigenvectors form a complete orthonormal basis system. This is explicitly shown in Appendix A.3. Due to the orthonormality of the curl eigenvectors,

$$\begin{aligned} \left\langle (\boldsymbol{\eta}_{\boldsymbol{k}}^\lambda \phi_{\chi\boldsymbol{k}})^\dagger \boldsymbol{\eta}_{\boldsymbol{k}'}^{\lambda'} \phi_{\chi'\boldsymbol{k}'} \right\rangle_{\mathcal{P}^3} &= \boldsymbol{\eta}_{\boldsymbol{k}}^{\lambda\dagger} \boldsymbol{\eta}_{\boldsymbol{k}'}^{\lambda'} \left\langle \phi_{\chi\boldsymbol{k}}^* \phi_{\chi'\boldsymbol{k}'} \right\rangle_{\mathcal{P}^3} \\ &= \delta_{\lambda\lambda'} \delta_{\chi\chi'} \delta_{\boldsymbol{k},\boldsymbol{k}'} \end{aligned} \tag{2.5.23}$$

the curl eigenstates themselves are orthogonal to each other,

$$\left\langle \boldsymbol{v}_\chi^\lambda \cdot \boldsymbol{v}_\chi^{\lambda'} \right\rangle_{\mathcal{P}^3} = \delta_{\lambda\lambda'} \sum_{\boldsymbol{k}\in S(1)} a_{\chi\boldsymbol{k}}^{\lambda *} a_{\chi\boldsymbol{k}}^{\lambda'} , \tag{2.5.24}$$

and due to the completeness of the helical basis vectors any *monochromatic*, periodic, and analytic velocity field with wavenumber χ can be written as

$$\begin{aligned} \boldsymbol{v}_\chi &= \sum_{\lambda=0,\pm 1} \boldsymbol{v}_\chi^\lambda \\ &= \sum_{\lambda=0,\pm 1} \sum_{\boldsymbol{k}\in S(1)} a_{\chi\boldsymbol{k}}^\lambda \boldsymbol{\eta}_{\boldsymbol{k}}^\lambda \phi_{\chi\boldsymbol{k}}(\boldsymbol{x}) , \end{aligned} \tag{2.5.25}$$

from which it follows that the vorticity of $\boldsymbol{v}_\chi$ is given by

$$\boldsymbol{\omega}_\chi = \chi \sum_{\lambda=0,\pm 1} \lambda \boldsymbol{v}_\chi^\lambda . \tag{2.5.26}$$

Defining

$$\kappa^\lambda \stackrel{\text{def}}{=} \sum_{\boldsymbol{k}\in S(1)} \left| a_{\chi\boldsymbol{k}}^\lambda \right|^2 , \tag{2.5.27}$$

it can be shown with (2.5.25) and (2.5.26) that

$$\begin{aligned} K &= \kappa^+ + \kappa^- + \kappa^0 , \\ \chi^{-2} E &= \kappa^+ + \kappa^- , \\ \chi^{-1} H &= \kappa^+ - \kappa^- . \end{aligned} \tag{2.5.28}$$

Therefore, the irrotational term does not affect the helicity and enstrophy averages in a periodic domain. Since in general η, κ, and ε are not proportional to each other $H^2 = KE$ is satisfied if and only if $\kappa^+\kappa^- = 0$ and $\kappa^0 = 0$. From a sub-maximally helical state with positively and negatively helical as well as divergent flow components present, the flow can evolve into a purely helical state only if all but one of the curl eigenstates vanish with time within a given (necessarily limited) region of space.

Finally, due the orthonormality and completeness of the curl eigenvectors any periodic and analytic velocity field can be written as

$$\begin{aligned} \boldsymbol{v} &= \sum_{\chi\in\Gamma} \boldsymbol{v}_\chi \\ &= \sum_{\lambda=0,\pm1} \sum_{\chi\in\Gamma} \sum_{\boldsymbol{k}\in S(1)} a^\lambda_{\chi\boldsymbol{k}} \boldsymbol{\eta}^\lambda_{\boldsymbol{k}} \phi_{\chi\boldsymbol{k}} \ , \end{aligned} \tag{2.5.29}$$

which is identical to the regular Fourier series of $\boldsymbol{v}$.

2.6 Scales of Motion

Regardless as to whether a tornado is thought of originating from a breakdown of the larger-scale storm circulation, from the organisation of smaller-scale turbulent eddies, or both, the vortex is forming on a scale at which previously no intense circulation was present. In one way or the other, the formation of tornadoes involves the interaction between different scales of motion or the interaction between eddies of different sizes.

In a turbulent fluid, at any resolution there may be dominant flow features, or eddies, of different spatial extent. Just how exactly to define eddies and their size is not obvious.

2.6.1 Large and Small

To reduce the complexity of fluid flow an attempt is often made to focus on phenomena of a particular spatial scale. However, the definition of scale or size of flow phenomena is often very subjective and case dependent, and the different definitions lead to very different values and meanings of scale.

Levich and Tsinober [1983a] define a 'natural' scale L through the invariants of homogeneous turbulence of an ideal fluid. The ensemble average, indicated here by brackets, of average kinetic energy in domain $\mathcal{V}$ of volume V is defined as

$$\langle K \rangle = \left\langle \frac{1}{V} \int_{\mathcal{V}} \boldsymbol{v}^2 \, d^3x \right\rangle \ , \tag{2.6.1}$$

and the ensemble average of the spatial helicity correlation function is defined as

$$I = \left\langle \frac{1}{V} \int_{\mathcal{V}} \eta(\boldsymbol{x})\eta(\boldsymbol{x}+\boldsymbol{r}) \, d^3x \right\rangle \ , \tag{2.6.2}$$

which, by the homogeneity assumption, is constant in space (not a function of $\boldsymbol{r}$). Spatial scale L is then defined by[10]

$$L = \frac{\langle K \rangle}{\sqrt{|I|}} \tag{2.6.3}$$

which, as the authors point out, is intrinsic in the sense that it is not related to any external parameters and defined only by the flow properties. However, simply because a parameter such as L, or K/H for that matter, has units of length does not mean that it also has the meaning of a physically or dynamically relevant scale or size.

As mentioned already in Section 2.3.1, in turbulence theory eddies are often defined as the flow associated with the Fourier components of the same wavenumber k, whose scale is then defined as k^{-1}. Similarly, the scale L of the most dominant eddies can be defined such that

$$L = k_{\max}^{-1} , \tag{2.6.4}$$

where the kinetic energy spectrum peaks at the wavenumber $k_{\max}$. However, since continuous and discrete spectral components are defined globally this definition of scale does not imply any spatial localisation of eddies. The definition of scale based on individual wavelengths of spectral components is not representative of the physical size of eddies. The representation of the flow as a superposition of waves with large and small wavelengths is fundamentally different to a superposition of actual physical scales as in (2.1.1). Similarly there is a fundamental difference between the interaction[11] of spatially unlimited spectral components, or eddies as defined above, and the interaction between spatially limited velocity perturbations, or eddies as defined in Section 2.1.4. Based on the wave definition, interactions between eddies of different scales are interactions between different spectral components that do not have to correspond to recognisable kinematical flow features of any size. As mentioned in Section 2.3.1 it is commonly assumed in turbulence theory that interactions in wavenumber space are local. However, since all eddies are spread over the entire volume, eddy interactions occur globally in physical space. Contrary to that, interactions between eddies defined based on spatial characteristics are local in physical space. However, as shown below, since spatially limited velocity perturbations are associated with a continuum of spectral components, interactions between these eddies is nonlocal in wavenumber space.

The fundamental difference between spatial and spectral scale can easily be seen from a simple one-dimensional example. Consider a periodic function $f(x)$ given by its Fourier series,

$$f(x) = \sum_{k=-\infty}^{\infty} a_k \exp \frac{2\pi i k x}{L} , \tag{2.6.5}$$

[10] Strictly speaking the authors define $\langle K \rangle = \left\langle \int_{\mathcal{V}} \frac{1}{2} \boldsymbol{v}^2 \, d^3x \right\rangle$, $I = \int_{\mathcal{V}} \langle \eta(\boldsymbol{x}) \eta(\boldsymbol{x} + \boldsymbol{r}) \rangle \, d^3x$, and $L = \frac{I}{\langle K \rangle^2}$, which has units of length^{-5}, but the idea is the same.

[11] Generally interaction is defined here as any form of energy transfer.

where

$$a_k \stackrel{\text{def}}{=} \frac{1}{L}\int_{x=-\frac{1}{2}L}^{\frac{1}{2}L} f(x)\exp\frac{-2\pi ikx}{L}\,dx\ . \tag{2.6.6}$$

If this function is pointwise averaged (smoothed) over an interval L/n with $n \in \mathbb{N}\setminus\{0\}$,

$$\begin{aligned}\langle f(x)\rangle &= \sum_{k=-\infty}^{\infty} a_k \frac{n}{L}\int_{x=-\frac{L}{2n}}^{\frac{L}{2n}} \exp\frac{2\pi ikx}{L}\,dx \\ &= a_0 + \sum_{k\neq 0} a_k \frac{n}{\pi k}\sin\frac{\pi k}{n}\ ,\end{aligned} \tag{2.6.7}$$

waves with wavenumbers k positive or negative integer multiples of n drop out of the Fourier series. However for any $n > 1$ some waves with wavelengths shorter than L/n remain, where the generally nonvanishing range between spectral gaps created by pointwise averaging is equal to n. Similarly, for an aperiodic function

$$f(x) = \frac{1}{\sqrt{2\pi}}\int_{k=-\infty}^{\infty} f(k)\exp ikx\,dk \tag{2.6.8}$$

with a continuous spectrum

$$f(k) = \frac{1}{\sqrt{2\pi}}\int_{x=-\infty}^{\infty} f(x)\exp -ikx\,dx \tag{2.6.9}$$

the pointwise averaged function[12]

$$\begin{aligned}\langle f(x)\rangle &= \frac{1}{L}\int_{x=-\frac{1}{2}L}^{\frac{1}{2}L}\frac{1}{\sqrt{2\pi}}\int_{k=-\infty}^{\infty} f(k)\exp ikx\,dk\,dx \\ &= \frac{1}{\sqrt{2\pi}}\int_{k=-\infty}^{\infty} f(k)\frac{1}{L}\int_{x=-\frac{1}{2}L}^{\frac{1}{2}L}\exp ikx\,dx\,dk\end{aligned} \tag{2.6.10}$$

has spectral gaps where k is equal to a positive or negative integer multiple of $2\pi L^{-1}$. Although spatial pointwise averaging of the flow field will remove perturbations on a scale smaller than the averaging domain, this ‘large-scale’ flow generally has still contributions from the large wavenumbers of the original flow field. A clear association of physical properties such as large and small with spectral properties is therefore not possible.

The fundamental difference between spatially periodic and aperiodic flows is that they have discrete or continuous spectra, respectively. In periodic flows the speed of propagation of interaction has to be infinite since independent changes between distant spatial regions are impossible. This violates the principle of relativity and true spatial periodicity in reality cannot be sustained. Since the speed of propagation of interaction between different flow regions in real fluids is finite, independent changes of remote flow regions have to occur, naturally leading to aperiodicity and a continuous spectrum. Each local change in the

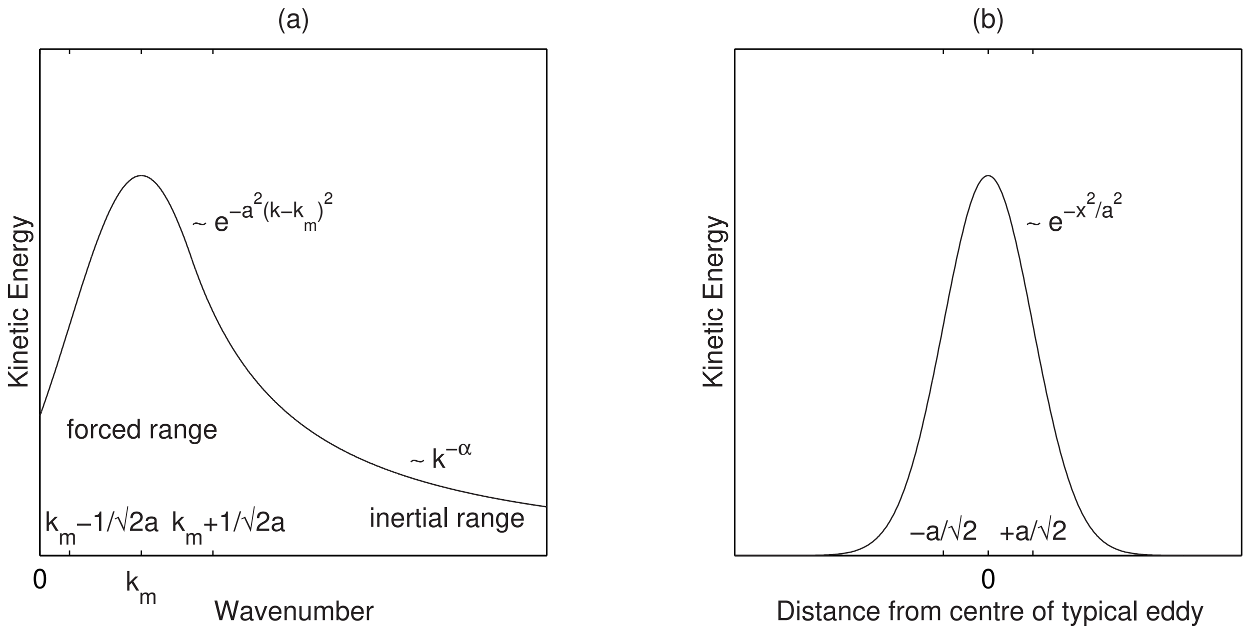

Figure 2.1: *Hypothetical distributions of kinetic energy over (a) wavenumber and (b) across the most intense eddies in space.*

velocity field affects the continuous spectrum. The same local flow properties are therefore described by varying spectra depending on the other flow regions.

Given a set of initial data, in practice it is only possible to calculate a discrete spectrum for which the inverse transformation is a Fourier series expansion representing a spatially periodic velocity field. All ‘eddies’ associated with individual waves are spread over the entire space. However, by calculating a continuous approximation of the discrete kinetic energy spectrum an estimate of the spatial extent of the most intense eddies can be obtained via (continuous) inverse Fourier transformation.

A discrete *isotropic* spectrum contains for each wavenumber contributions from all spectral terms $|a^{\lambda}_{\chi\boldsymbol{k}}|^2$ with the same wavenumber χ. Due to the orthonormality (2.5.23) of the curl eigenvectors the energy terms for each wavenumber are additive, and the isotropic kinetic energy spectrum of a Fourier series is given by

$$|a_\chi|^2 \stackrel{\mathrm{def}}{=} \sum_{\lambda=0,\pm1} \sum_{\boldsymbol{k}\in S(1)} \left|a^{\lambda}_{\chi\boldsymbol{k}}\right|^2 \ . \tag{2.6.11}$$

For simplicity assume that the energy spectrum consists of essentially two bands: a forced range at small wavenumbers close to a Gaußian distribution, and an inertial range at large wavenumbers close to a power law distribution. This hypothetical energy spectrum is shown in Figure 2.1. Most energy is contained in the forced band and the Fourier components in that range of wavenumbers dominate the instantaneous flow characteristics. The discrete

[12]To be able to exchange the order of integration it must be assumed that $f(k)$ is bounded and steady for k in $(-\infty, \infty)$.

spectrum calculated from the observational data in the forced range can then be interpolated by a Gaußian envelope function

$$|a(k)|^2 \stackrel{\text{def}}{=} a^2|A|^2 \exp -a^2(k-k_{\text{max}})^2 \ , \tag{2.6.12}$$

where the real constant a determines the spectral width of the main peak around the wavenumber k_{max} with the highest energy, and the complex amplitude A determines the overall intensity. Both parameters can be calculated by minimising the mean-square error of $|a(k)|^2$ with the discrete spectrum $|a_\chi|^2$ in the forced range. Only the real quantity $|A|^2$ can be determined from observations, the amplitude A is therefore determined only up to an arbitrary phase factor. The continuous spectral function $a(k)$ is then given by

$$\begin{aligned} a(k) &= aA \exp -\frac{a^2}{2}(k-k_{\text{max}})^2 \\ &= \frac{1}{\sqrt{2\pi}} \int_{-\infty}^{\infty} \psi(x) e^{-ikx} dx \ , \end{aligned} \tag{2.6.13}$$

from which the inverse Fourier transform $\psi(x)$ can be explicitly calculated [e.g., *Greiner*, 2001; pp. 60–62]

$$\begin{aligned} \psi(x) &\stackrel{\text{def}}{=} \frac{1}{\sqrt{2\pi}} \int_{-\infty}^{\infty} a(k) e^{ikx} dk \\ &= A \exp -\frac{x^2}{2a^2} + ik_{\text{max}} x \ . \end{aligned} \tag{2.6.14}$$

It represents a one-dimensional wave packet with dominant wavenumber k_{max}, where coordinate x denotes the distance from the main peak along any direction in space. The total kinetic energy is obtained by integrating over the whole spectrum

$$\begin{aligned} \bar{K} &\stackrel{\text{def}}{=} \int_{-\infty}^{\infty} |a(k)|^2 \, dk \\ &= \int_{x=-\infty}^{\infty} \int_{x'=-\infty}^{\infty} \psi(x)\psi^*(x') \frac{1}{2\pi} \int_{k=-\infty}^{\infty} e^{ik(x'-x)} dk \, dx' dx \\ &= \int_{-\infty}^{\infty} |\psi(x)|^2 \, dx \ , \end{aligned} \tag{2.6.15}$$

where the completeness of the one-dimensional Fourier basis functions,

$$\frac{1}{2\pi} \int_{-\infty}^{\infty} e^{ik(x'-x)} dk = \delta(x'-x) \ , \tag{2.6.16}$$

was used. Since the discrete spectrum $|a_\chi|^2$ and the continuous approximation $|a(k)|^2$ have units of energy, $\bar{K}$ has units of energy over length. From (2.6.15) it is apparent that $|a(k)|^2$ is the spectral kinetic energy distribution function, and

$$|\psi(x)|^2 = |A|^2 \exp -\frac{x^2}{a^2} \tag{2.6.17}$$

is the spatial kinetic energy distribution function. The typical extent of the most intense eddies, i.e., the most intense kinetic energy perturbations, is determined by the width of the spatial distribution function. The slope of $|\psi(x)|^2$ decreases from the maximum towards larger wavenumbers until $k_{\max} + 1/\sqrt{2}a$ where it reaches its minimum and then starts to increase again towards zero at infinity. Similarly, the slope increases from the maximum towards smaller wavenumbers and reaches a maximum at $k_{\max} - 1/\sqrt{2}a$ from where it decreases again towards zero at minus infinity. The spectral width Δk of kinetic energy can therefore be defined as the distance $\sqrt{2}/a$ between the two extrema of the slope of the envelope function. Following the same argument, the width Δx of the spatial energy distribution is defined as $\sqrt{2}a$. The product $\Delta x \Delta k \equiv 2$ is independent of a and therefore the same for all Gaußian curves and their Fourier transforms. If instead the spatial and spectral intervals are defined based on the half-widths of the Gaußian functions, $\Delta k = \sqrt{\ln 2}/a$, $\Delta x = \sqrt{\ln 2}a$, and $\Delta x \Delta k = \ln 2$, which is less than one. Generally the widths of the spatial and spectral kinetic energy distribution functions satisfy

$$\Delta x \Delta k \sim 1 \; . \tag{2.6.18}$$

In quantum mechanics this relationship is known as the *uncertainty principle* and is valid for very general kinetic energy distributions. If eddies are defined as localised kinetic energy perturbations,

$$\Delta x \sim (\Delta k)^{-1} \tag{2.6.19}$$

can be taken as a measure of their typical size. Qualitatively a more precise localisation in space requires a wider range of wavenumbers, whereas a single wavenumber, as for a B-flow, represents a completely unlocalised infinite wave train. Consequently, small eddies must be associated with excitations of waves over a large continuous range of wavenumbers rather than a single large wavenumber. If the interaction between eddies is defined as energy transfer between the corresponding velocity perturbations, the range of interaction of the most intense eddies is also related to the width of the spatial energy distribution function.

Under anisotropic conditions this definition of the spatial extent of eddies can be refined by calculating spectra for individual directions in space.

In a vertically stratified fluid with essentially horizontal solid lower boundary there are important differences between the horizontal and vertical statistics, and isotropy is not a good assumption. In that case the isotropic spectrum is split up into horizontal and vertical components

$$|a_{\chi\mathrm{hor}}|^2 \stackrel{\mathrm{def}}{=} \sum_{\lambda=0,\pm 1} \sum_{\boldsymbol{k} \in S_{xy}(1)} \left| a^{\lambda}_{\chi\boldsymbol{k}} \right|^2 \tag{2.6.20}$$

and

$$|a_{\chi\mathrm{vert}}|^2 \stackrel{\mathrm{def}}{=} \sum_{\lambda=0,\pm 1} \sum_{\boldsymbol{k} \in S_{z}(1)} \left| a^{\lambda}_{\chi\boldsymbol{k}} \right|^2 \; , \tag{2.6.21}$$

respectively, where $S_{xy}(1) = \{\pm \boldsymbol{e}_x, \pm \boldsymbol{e}_y\}$ is the set of horizontal, and $S_z(1) = \{\pm \boldsymbol{e}_z\}$ is the set of vertical unit wave vectors. Assuming that for each spectrum the same qualitative energy distribution in forced and inertial band exists as for the isotropic spectrum, the forced ranges as before are approximated by Gaußian distribution functions

$$\begin{aligned} a_{\text{hor}}(k_h) &\stackrel{\text{def}}{=} aA \exp -\frac{a^2}{2}(k_h - k_{h\text{max}})^2 \\ a_{\text{vert}}(k_z) &\stackrel{\text{def}}{=} bB \exp -\frac{b^2}{2}(k_z - k_{z\text{max}})^2 \ , \end{aligned} \tag{2.6.22}$$

where $k_h \stackrel{\text{def}}{=} \sqrt{k_x^2 + k_y^2}$ is the horizontal wave vector, and the $\{k_x, k_y, k_z\}$ are now continuous components of the unnormalised wave vector. The corresponding spatial distribution functions are then given by

$$\begin{aligned} \psi_{\text{hor}}(x_h) &\stackrel{\text{def}}{=} A \exp -\frac{r_h^2}{2a^2} + ik_{h\text{max}} r_h \\ \psi_{\text{vert}}(z) &\stackrel{\text{def}}{=} B \exp -\frac{z^2}{2b^2} + ik_{z\text{max}} z \ , \end{aligned} \tag{2.6.23}$$

where $r_h \stackrel{\text{def}}{=} \sqrt{x^2 + y^2}$ is the horizontal position vector.

In some cases it may be instructive to look at spectra of individual helical components of the velocity field. For that the horizontal and vertical spectra are split up into contributions from each curl eigenstate,

$$\begin{aligned} |a^\lambda_{\chi\text{hor}}|^2 &\stackrel{\text{def}}{=} \sum_{\boldsymbol{k} \in S_{xy}(1)} \left|a^\lambda_{\chi\boldsymbol{k}}\right|^2 \\ |a^\lambda_{\chi\text{vert}}|^2 &\stackrel{\text{def}}{=} \sum_{\boldsymbol{k} \in S_z(1)} \left|a^\lambda_{\chi\boldsymbol{k}}\right|^2 \ . \end{aligned} \tag{2.6.24}$$

The continuous spectral distribution functions $a^\lambda_{\text{hor}}(k_h)$ and $a^\lambda_{\text{vert}}(k_z)$, and the corresponding spatial distribution functions $\psi^\lambda_{\text{hor}}(x_h)$ and $\psi^\lambda_{\text{vert}}(z)$ are then defined analogously to (2.6.22) and (2.6.23).

In the presence of dominant horizontal density gradients and shear flows, the horizontal spectrum can also be split up into components parallel and perpendicular to the air mass boundary.

An infinite, single plane wave train such as

$$a^\lambda_{\boldsymbol{k}} \exp i\boldsymbol{k} \cdot \boldsymbol{x} \tag{2.6.25}$$

has constant intensity $|a^\lambda_{\boldsymbol{k}}|$ throughout the entire space and therefore carries an unlocalised property labelled by λ. For the signal to have meaningful information about that property a wave pulse must be generated by amplitude modulation of the carrier wave. By a continuous superposition of plane waves a compact wave packet can be generated. If λ is the helical state of the wave, this wave packet describes a localised perturbation of helicity, i.e., a helical eddy.

To illustrate that point consider the positively helical curl eigenstates

$$\boldsymbol{v}^+_\chi = \frac{1}{\sqrt{2}} \sum_{\boldsymbol{k} \in S(1)} a^+_{\chi\boldsymbol{k}} (\boldsymbol{k} \times \boldsymbol{n} - i\boldsymbol{n}) \exp i\chi\boldsymbol{k} \cdot \boldsymbol{x} \ , \tag{2.6.26}$$

as given by (2.5.20) with $\lambda = +1$. To simplify the analysis assume that all Fourier amplitudes $a^+_{\chi\boldsymbol{k}} \equiv \sqrt{2}$ and restrict the set of wave vectors to

$$S^+_{xy} \overset{\text{def}}{=} \left\{ \begin{pmatrix} 1 \\ 0 \\ 0 \end{pmatrix}, \begin{pmatrix} 0 \\ 1 \\ 0 \end{pmatrix} \right\} . \tag{2.6.27}$$

Then the curl eigenstates are Beltrami vortex flows

$$\boldsymbol{v}^+_\chi = \sum_{\boldsymbol{k} \in S^+_{xy}} \boldsymbol{n} \cos \chi \boldsymbol{k} \cdot \boldsymbol{x} + \boldsymbol{n} \times \boldsymbol{k} \sin \chi \boldsymbol{k} \cdot \boldsymbol{x} . \tag{2.6.28}$$

As shown in Figure 2.2 (a) for $\chi = 1$ they are a periodic pattern of counterrotating updrafts and downdrafts.

In simplified form helical vortices can therefore be described by two entangled waves with a fixed amplitude and phase relationship. In that sense coherent vortices can very literally be called flow structures. As they intensify or weaken the amplitude and phase relationship between the vortex waves is maintained. The corresponding expansion coefficients therefore must have a very similar time-dependence. If this entanglement is destroyed the vortex disintegrates.[13]

To calculate a continuous superposition of these vortex flows the discrete wave vectors $\chi\boldsymbol{k}$ of the Fourier series are replaced by the continuous wave vector $\boldsymbol{q} = (j, k, l)^T$, and the constraint of $|\boldsymbol{q}| \equiv 1$ is relaxed. The spatially periodic vortex flow (2.6.28) is then integrated over the wavenumbers j, k, and l in the intervals $[j_0 - \Delta j, j_0 + \Delta j]$, $[k_0 - \Delta k, k_0 + \Delta k]$, and $[l_0 - \Delta l, l_0 + \Delta l]$, respectively. For the explicit calculations see Appendix A.7. For $j_0 = k_0$, $\Delta j = \Delta k$, and $\Delta l = 0$ the resulting velocity fields are shown in Figure 2.2 for different values of the parameter $\delta \overset{\text{def}}{=} \Delta j / j_0 = \Delta k / k_0$ with fixed wavenumbers j_0 and k_0. As δ increases towards one a single vortex emerges from the periodic vortex pattern at $\delta = 0$. Since the central wavenumbers j_0 and k_0 are fixed the increase in δ and the decrease in the range of nonzero kinetic energy are due to an increase in the spectral interval. As the spectral intervals increase kinetic energy averaged over the spectral volume and space steadily decreases, while the maximum kinetic energy in the vortex centre remains constant.

It should be noted that in this simple example where all superposed waves have the same intensity, the diameter of the vortex, for a given spectral interval also depends inversely on the central wavenumber. However, for a given spectral distribution of kinetic energy such as (2.6.12) the vortex diameter is influenced primarily by the width of the spectral interval.

Unlike for classical mechanics of macroscopic solid bodies the scale of fluid motion is an elusive property. All approaches discussed in this section in one way or the other require subjective definitions. However, in a given application a ‘visual’ classification of scales is often straightforward. In the case of severe storms horizontal scales can be classified as follows. The large scale is defined as the size of the storm (supercell or mesoscale convective

[13] For comparison, in quantum mechanics entanglement refers to a situation in which two particles are described by the same wave function that cannot be factorised in single particle wave functions. The two particles, regardless how far apart they are, therefore have the same time evolution. They have no individual characteristics and only their combined properties are observable.

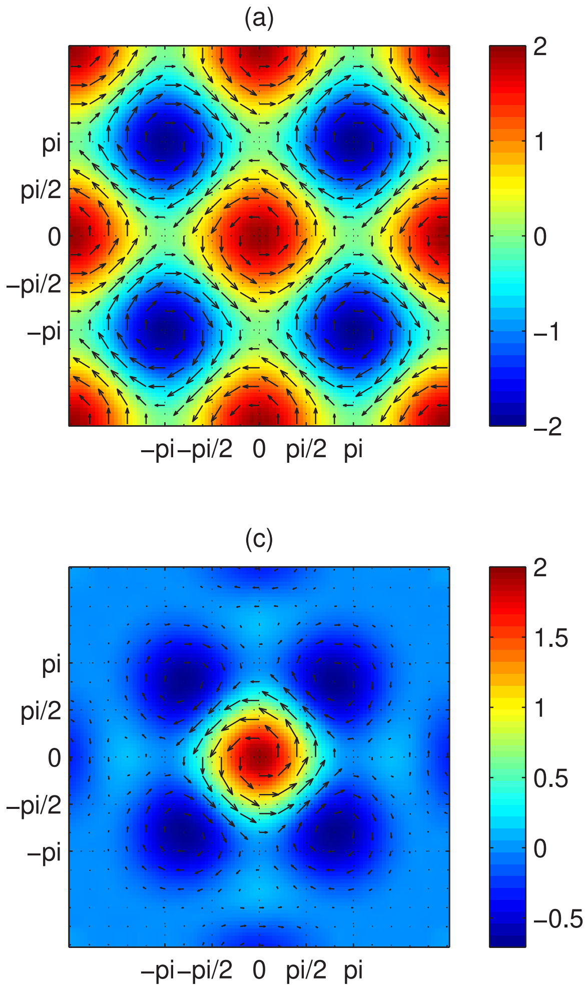

Figure 2.2: *Continuous superposition of Beltrami vortex flows with* $\chi = 1$ *and (a)* $\delta = 0$*, a spatially periodic Beltrami vortex flow pattern as given by Equation 2.6.28, (b)* $\delta = 0.3$*, (c)* $\delta = 0.6$*, and (d)* $\delta = 1$*. The vectors represent the horizontal components of the velocity field, and the colour shading denotes vertical velocity.*

complex) which is typically on the order of $10^4 - 10^5$ m. The intermediate scale ranges from the diameter of a tornado cyclone of $1 - 5$ km to the diameter of the tornado of roughly $10^2 - 10^3$ m. The small scales on the order of $1 - 10$ m cover the inertial range. The essentially laminar micro scale on which dissipation due to internal viscosity becomes dominant is usually excluded from the analysis of atmospheric motion above the planetary boundary layer by truncating large wavenumbers and neglecting dissipative terms in the equations of motion for the remaining larger scales. Of course, the visual classification is not without problems as well. The diameter of the condensation funnel of a tornado is determined by the radial pressure gradient and relative humidity. For a dust devil the diameter of the funnel depends on the updraft strength and rotational speed but also on the type of surface material. In both cases the visible size of the vortex may not be consistent with any definition of scale discussed above. It may also not be dynamically relevant, i.e., if the equations of motion were Reynolds averaged over the visible scale they may not represent the relevant forcing. However, given actual wind velocity data of the tornado circulation the width of the funnel can simply be defined kinematically as the diameter of the maximum tangential speed.

2.6.2 Slow and Fast

Spatial and temporal scales of flow phenomena are often related, where phenomena on a small spatial scale tend to have shorter timescales than larger-scale phenomena. Given the complications with the definition of spatial scale the question is now how to define a meaningful timescale.

How fast a variable $x(t)$ is changing *momentarily* is given by the time-rate of change $\dot{x}$. For a continuous process of growth or decay in which the time-rate of change itself does not change much, $\dot{x}$ and derived parameters such as half-life can be taken as a measure of the timescale of the process. For more complicated processes $\dot{x}$ and higher order derivatives themselves depend on time. In general, the time-dependence of an analytic function $x(t)$ is given by its Taylor series

$$x(t) = x(0) + \dot{x}|_{t=0}\, t + \frac{1}{2}\, \ddot{x}|_{t=0}\, t^2 + \mathcal{O}(t^3) \ . \tag{2.6.29}$$

To second order ($\ddot{x} \approx const.$) the variable x follows an increase and decay cycle or vice versa, depending on the sign of $\ddot{x}$. For cyclic phenomena, such as the formation and dissipation of tornadolike vortices, a typical magnitude of the second time-derivative of the velocity field, or the timescale of the forcing field, therefore is a better indicator for the timescale of the flow phenomenon than the magnitude of the forcing field itself.

To be able to develop a model for the investigation of the development of tornadolike vortices based on characteristics of the storm flow, it is necessary to mathematically separate the two flow phenomena. As seen in the previous subsection it is impossible to associate specific local flow phenomena of any spatial extent with any particular wave or Fourier basis function. Since eddies are forced as an entity in real space, all waves involved in the local representation of the eddy have the same causal connection to the forcing, regardless of their wavelength relative to the spatial extent of the flow perturbation. A separation of a small vortex from a large storm system based on spectral characteristics is therefore not possible.

It was briefly discussed in Section 2.3.1 that timescale separation between large and small-scale motion is a common assumption in turbulence theory. With the approximate spatial scales given in the previous subsection, there is an order of $10 - 100$ difference between the length-scales of the main storm circulation and the tornado vortex. Furthermore, since the storm system evolves over a period of several tens of minutes to hours, while the tornado forms and dissipates in usually less than 15 minutes, there is a difference of order 10 between the timescales of storm and tornado.

In the following, the storm flow is therefore considered to be a slowly evolving, or simply 'slow' flow, and the tornado vortex is referred to as a rapidly evolving or 'fast' flow.[14] Since

[14]The classification in slow and fast is incidental to the fact that tangential and updraft speeds in the

the main interest is in the evolution of the fast perturbation flow, the slow flow will also be referred to as 'background' flow.

As mentioned in Section 2.4, tornadolike vortices usually form on or near intense shear zones, such as the region of intense gradients in vertical velocity between main updraft and rear and forward-flank downdraft. Since this shear zone is maintained by the two forced intense, larger-scale counterrotating vortices it has a component that is varying on the same slow timescale. There is a fundamental difference in the small-scale variability of the slowly evolving quasistationary shear zones of the externally forced storm system, and the spatial variability of rapidly evolving small-scale motion. In the following sections, the formation of tornadolike vortices is therefore modelled as a rapidly evolving instability of stationary shear zones of the background flow.

2.7 Time-Dependence of the Velocity Field

For the derivation of a simple dynamical system describing vortex formation it is necessary to uniquely associated the vortex flow with particular values of some expansion coefficients. In a large-scale flow the formation of a smaller vortex changes the kinetic energy spectrum (i.e., the Fourier expansion coefficients). However, the spectral difference depends on the large-scale flow and the relative position of the vortex. For the formation of identical vortices under different flow situations there can therefore be no unique spectral 'vortex signature.' A solution to that problem is the separation of the total velocity field, $\tilde{\boldsymbol{v}}$, into a slowly evolving background flow, $\boldsymbol{u}$, and a rapidly evolving eddy flow, $\boldsymbol{v}$,

$$\tilde{\boldsymbol{v}}(t,\boldsymbol{x}) = \boldsymbol{u}(\tau,\boldsymbol{x}) + \boldsymbol{v}(t,\boldsymbol{x}) \ , \tag{2.7.1}$$

where τ and t symbolically represent variation on the slow and fast timescale, respectively.[15] Choosing the spatial and temporal scales such that the main variability of $\boldsymbol{v}$ is on the scale of a typical tornado vortex, and assuming that in the thunderstorm on that scale the tornado, if it occurs, is the dominant vortical perturbation, (2.7.1) can schematically be expressed as

$$\text{total flow} = \text{storm} + \text{tornado} \ , \tag{2.7.2}$$

where fast perturbations smaller than the tornado are neglected. Before deriving the equations of motion for the slow and fast flow it is necessary to get an idea about the relative magnitude of the expansion coefficients of the two velocity fields. Consider the case where the storm velocity data is given in a three-dimensional domain $\mathcal{D}$, the 'storm volume.' From (2.7.1) it follows that the expansion coefficients for the total flow are given by

$$\begin{aligned} \tilde{\boldsymbol{v}}_{\boldsymbol{q}}(t) &\stackrel{\text{def}}{=} \left\langle \tilde{\boldsymbol{v}}(t,\boldsymbol{x})\phi^*_{\boldsymbol{q}}(\boldsymbol{x}) \right\rangle_{\mathcal{D}} \\ &= \boldsymbol{u}_{\boldsymbol{q}}(\tau) + \boldsymbol{v}_{\boldsymbol{q}}(t) \ , \end{aligned} \tag{2.7.3}$$

vortex of an intense tornado exceed those in the rest of the storm system and in fact any weather related flow phenomena in the troposphere of our planet.

[15] The total velocity field $\tilde{\boldsymbol{v}}(t,\boldsymbol{x})$ can of course have strong fluctuations on the slow timescale. However, the primary timescale of a variable is determined by the fastest (measurable) fluctuations.

where the expansion coefficients of the slow and fast flow,

$$\boldsymbol{u}_{\boldsymbol{q}}(\tau) \stackrel{\text{def}}{=} \left\langle \boldsymbol{u}(\tau,\boldsymbol{x})\phi^*_{\boldsymbol{q}}(\boldsymbol{x})\right\rangle_{\mathcal{D}} \tag{2.7.4}$$

and

$$\boldsymbol{v}_{\boldsymbol{q}}(t) \stackrel{\text{def}}{=} \left\langle \boldsymbol{v}(t,\boldsymbol{x})\phi^*_{\boldsymbol{q}}(\boldsymbol{x})\right\rangle_{\mathcal{D}} \ , \tag{2.7.5}$$

respectively, are also calculated over domain $\mathcal{D}$. However, the fast flow, under the assumption that it describes the tornado vortex, is significantly nonvanishing only in a small, horizontally limited domain $\mathcal{V}$ of the size of the tornado, the 'tornado volume'. For a typical tornado $\mathcal{V}$ has a horizontal extent on the order of $0.1\times 0.1 - 1\times 1\,\mathrm{km}$ with the same height as the storm volume. Similarly, the mesocyclone is contained in a three-dimensional domain $\mathcal{M}$ of horizontal extent of order $10\times 10\,\mathrm{km}$. For scaling purposes assume that the slow (storm) expansion coefficients are dominated by the mesocyclone. As discussed in Section 2.6.1, to be able to describe spatially limited vortices such as mesocyclone and tornado a superposition of a large number of waves with increasingly larger wavenumbers is necessary. Each wave contributes to the total velocity within the respective vortex volume. With a maximum rotational speed of $100\,\mathrm{ms}^{-1}$ in the tornado vortex, and storm motion on the tornado scale (prior to tornadogenesis) on the order of $10\,\mathrm{ms}^{-1}$, the speed associated with the tornado locally and within a short period of time exceeds the magnitude of mesocyclone circulation on a comparable scale by roughly a factor of 10. However, since the expansion coefficients for slow and fast flow are calculated (averaged) over the whole storm volume, the spectra hypothetically calculated locally for mesocyclone and tornado are scaled by the factors $V(\mathcal{M})/V(\mathcal{D})$ and $V(\mathcal{V})/V(\mathcal{D})$, respectively, where $V(\mathcal{D})$ denotes the size of domain $\mathcal{D}$, and similarly for the other domains.[16] As a result, since $V(\mathcal{V}) \sim 10^{-4} - 10^{-2}V(\mathcal{M})$, there is at least an order of magnitude difference between expansion coefficients of the slow and fast motion for the same wave vectors. Despite the local intensity of a tornadolike vortex, due to its transient character and small spatial extent, the fast expansion coefficients associated with this short, localised event are relatively small perturbations on the expansion coefficients of the 'normal' flow state given by the storm motion.

Substituting the decomposition of the velocity field (2.7.1) into the equation of motion (2.3.1), and expanding also the forcing term $\tilde{\boldsymbol{f}}$ into slow, $\boldsymbol{f}(\tau,\boldsymbol{x})$, and fast, $\boldsymbol{f}'(t,\boldsymbol{x})$, components leads to

$$\partial_\tau \boldsymbol{u} + \partial_t \boldsymbol{v} + (\boldsymbol{u}\cdot\boldsymbol{\nabla})\boldsymbol{u} + (\boldsymbol{u}\cdot\boldsymbol{\nabla})\boldsymbol{v} + (\boldsymbol{v}\cdot\boldsymbol{\nabla})\boldsymbol{u} + (\boldsymbol{v}\cdot\boldsymbol{\nabla})\boldsymbol{v} = \boldsymbol{f} + \boldsymbol{f}' \ . \tag{2.7.6}$$

To obtain a dynamical system of ordinary differential equations, the slow and fast velocity fields are expanded in Fourier series. For computational purposes, calculation of expansion coefficients of the slow velocity field from observational data and for high-order numerical simulations, the compact notation of slow expansion coefficients without helical decomposition is used. However, for truncation of the fast flow and interpretation of the simple

[16] In reality of course the slow expansion coefficients are effectively calculated over the entire storm volume, and are not associated with any particular local excitation of any spatial extent and intensity.

examples discussed below, the helical decomposition of the expansion coefficients as introduced in Section 2.5.2 is more convenient. The slow and fast velocity fields are then given by

$$\boldsymbol{u}(\tau, \boldsymbol{x}) = \sum_{\boldsymbol{q}} \boldsymbol{u}_{\boldsymbol{q}}(\tau)\phi_{\boldsymbol{q}}(\boldsymbol{x}) \tag{2.7.7}$$

and

$$\boldsymbol{v}(t, \boldsymbol{x}) = \sum_{\lambda,\chi,\boldsymbol{k}} a^{\lambda}_{\chi\boldsymbol{k}}(t)\boldsymbol{\eta}^{\lambda}_{\boldsymbol{k}}\phi_{\chi\boldsymbol{k}}(\boldsymbol{x}) \ , \tag{2.7.8}$$

respectively. Fourier transformation with projection onto the helical basis vectors (2.5.22) of (2.7.6) then leads to

$$\begin{aligned}\partial_\tau \left(\boldsymbol{\eta}^{\lambda*}_{\boldsymbol{k}} \cdot \boldsymbol{u}_{\chi\boldsymbol{k}}\right) + \partial_t a^{\lambda}_{\chi\boldsymbol{k}} + &\sum_{\boldsymbol{q}+\boldsymbol{q}'=\chi\boldsymbol{k}} i\boldsymbol{q}' \cdot \boldsymbol{u}_{\boldsymbol{q}} \left(\boldsymbol{\eta}^{\lambda*}_{\boldsymbol{k}} \cdot \boldsymbol{u}_{\boldsymbol{q}'}\right) \\ &+ \sum_{\lambda'} \sum_{\boldsymbol{q}+\chi'\boldsymbol{k}'=\chi\boldsymbol{k}} i\left(\boldsymbol{\eta}^{\lambda*}_{\boldsymbol{k}} \cdot \boldsymbol{\eta}^{\lambda'}_{\boldsymbol{k}'}\, \chi'\boldsymbol{k}' + \boldsymbol{q} \cdot \boldsymbol{\eta}^{\lambda'}_{\boldsymbol{k}'}\, \boldsymbol{\eta}^{\lambda*}_{\boldsymbol{k}}\right) \cdot\, \boldsymbol{u}_{\boldsymbol{q}}\, a^{\lambda'}_{\chi'\boldsymbol{k}'} \\ &+ \sum_{\lambda',\lambda''} \sum_{\chi'\boldsymbol{k}'+\chi''\boldsymbol{k}''=\chi\boldsymbol{k}} i\chi''\boldsymbol{k}'' \cdot \boldsymbol{\eta}^{\lambda'}_{\boldsymbol{k}'} \left(\boldsymbol{\eta}^{\lambda*}_{\boldsymbol{k}} \cdot \boldsymbol{\eta}^{\lambda''}_{\boldsymbol{k}''}\right) a^{\lambda'}_{\chi'\boldsymbol{k}'} a^{\lambda''}_{\chi''\boldsymbol{k}''} \\ &= \boldsymbol{\eta}^{\lambda*}_{\boldsymbol{k}} \cdot \left(\boldsymbol{f}_{\chi\boldsymbol{k}} + \boldsymbol{f}'_{\chi\boldsymbol{k}}\right) \ .\end{aligned} \tag{2.7.9}$$

Since $\boldsymbol{u}$ and $\boldsymbol{v}$ vary on two different timescales, and since the expansion coefficients $a^{\lambda}_{\chi\boldsymbol{k}}$ of the fast flow are small compared with the magnitude of the Fourier transforms of the slow flow $|\boldsymbol{u}_{\chi\boldsymbol{k}}|$, it is reasonable to assume that the zeroth-order terms in the perturbations $a^{\lambda}_{\chi\boldsymbol{k}}$ in (2.7.9) are approximately balanced,

$$\partial_\tau \boldsymbol{u}_{\boldsymbol{q}} + \sum_{\boldsymbol{q}'+\boldsymbol{q}''=\boldsymbol{q}} i\left(\boldsymbol{q}'' \cdot \boldsymbol{u}_{\boldsymbol{q}'}\right)\boldsymbol{u}_{\boldsymbol{q}''} = \boldsymbol{f}_{\boldsymbol{q}} \ . \tag{2.7.10}$$

Subtracting this *slow balance equation* from the original transformed equations of motion (2.7.9) then leads to an approximate balance equation for the fast expansion coefficients

$$\begin{aligned}\partial_t a^{\lambda}_{\chi\boldsymbol{k}} &+ \sum_{\lambda'} \sum_{\boldsymbol{q}+\chi'\boldsymbol{k}'=\chi\boldsymbol{k}} i\left(\boldsymbol{\eta}^{\lambda*}_{\boldsymbol{k}} \cdot \boldsymbol{\eta}^{\lambda'}_{\boldsymbol{k}'}\, \chi'\boldsymbol{k}' + \boldsymbol{q} \cdot \boldsymbol{\eta}^{\lambda'}_{\boldsymbol{k}'}\, \boldsymbol{\eta}^{\lambda*}_{\boldsymbol{k}}\right) \cdot\, \boldsymbol{u}_{\boldsymbol{q}}\, a^{\lambda'}_{\chi'\boldsymbol{k}'} \\ &+ \sum_{\lambda',\lambda''} \sum_{\chi'\boldsymbol{k}'+\chi''\boldsymbol{k}''=\chi\boldsymbol{k}} i\chi''\boldsymbol{k}'' \cdot \boldsymbol{\eta}^{\lambda'}_{\boldsymbol{k}'} \left(\boldsymbol{\eta}^{\lambda*}_{\boldsymbol{k}} \cdot \boldsymbol{\eta}^{\lambda''}_{\boldsymbol{k}''}\right) a^{\lambda'}_{\chi'\boldsymbol{k}'} a^{\lambda''}_{\chi''\boldsymbol{k}''} \\ &= \boldsymbol{\eta}^{\lambda*}_{\boldsymbol{k}} \cdot \boldsymbol{f}'_{\chi\boldsymbol{k}} \ .\end{aligned} \tag{2.7.11}$$

In this derivation (2.7.10) is obtained based on order-of-magnitude and time-scaling arguments. The same set of equations (2.7.11) could have been obtained in 'exact' form by simply defining the slow background flow to satisfy (2.7.10), and then to define the fast perturbation flow such that it satisfies the equations of motion (2.7.6) with a particular forcing term $\boldsymbol{f}'$.

However, the motivation and ultimately justification for these definitions would have been based on the arguments given in the 'phenomenological' derivation above. A mathematically rigorous scaling method such as time-averaging in this particular case is not applicable since this would require the fast velocity field to have a zero time-mean over a particular period of time. With the fast velocity field representing a particular vortex and the period of averaging taken as its formation and decay cycle this would not be satisfied. However, as discussed in Appendix A.8, the results obtained by time-averaging are identical with the phenomenological approach if terms quadratic in the fast perturbations in (2.7.10) are neglected. Instead of defining the fast flow through $\boldsymbol{v} \stackrel{\text{def}}{=} \tilde{\boldsymbol{v}} - \boldsymbol{u}$, where $\boldsymbol{u}$ is defined as a certain time-mean of $\tilde{\boldsymbol{v}}$*at all times*, as in Reynolds theory, the fast flow here is defined *dynamically* through $\partial_t \boldsymbol{v} \stackrel{\text{def}}{=} \partial_t \tilde{\boldsymbol{v}} - \partial_\tau \boldsymbol{u}$, where $\boldsymbol{u}$ is defined to satisfy the slow balance equation (2.7.10). In that case only the initial values for $\boldsymbol{u}$ and $\boldsymbol{f}$ are obtained from observational time-series through averaging or frequency filtering. Since the slow balance equation does not depend on time-averaged quantities, the system (2.7.10) and (2.7.11) can be solved explicitly without further closure assumptions, and the fast perturbations $a^\lambda_{\chi\boldsymbol{k}}$ have no impact on the slow expansion coefficients $\boldsymbol{u}_{\boldsymbol{q}}$. The set of equations (2.7.10) and (2.7.11) therefore only describes situations in which the fast flow is driven without feedback by a slow background flow. For the onset of tornadogenesis that is a reasonable assumption as in this case initially the fast flow vanishes. As the tornado reaches maximum intensity it may affect the surrounding storm motion. However, for the investigation of the initialisation of vortex formation this is irrelevant. In fact, in the decomposition into slow storm flow and fast vortex flow changes in the expansion coefficients due to the formation and evolution of the tornado by definition are associated with the fast velocity field while other rapidly evolving flow perturbations are neglected.

Aside from the phenomenological arguments given in the previous section, the mixing of temporal and spatial scales over a range of spectral scales also follows from the fact that (2.7.10) and (2.7.11) are nonlinear partial differential equations for persistent and transient motion. As a result generally a full spectrum develops on both timescales. Starting with the excitation of primarily long waves by large-scale external forcing shorter waves are excited by nonlinear (triad) interactions. It was argued in Section 2.6.2 that for formation and decay phenomena such as tornadoes the timescale of the flow is determined by the timescale of the forcing. If there were waves with very different timescales, each forcing term and the corresponding expansion coefficient would change on the timescale of the fastest evolving expansion coefficient involved in the particular expression. In the time-evolution equations for the Fourier expansion coefficients, except for very special truncations, all waves are somehow coupled. They must therefore all vary on roughly the same timescale.

Next to gravity the most dominant forcing of geophysical flow is due to pressure gradients $-\rho^{-1}\boldsymbol{\nabla} p$. This term introduces two independent thermodynamic variables into the dynamical equations. For density the time evolution equation independent of the forcing follows from mass conservation and is given by the continuity equation (2.2.7). Even assuming the atmosphere to be an ideal gas that still leaves one thermodynamic variable unexplained. To close the dynamical system of equations an 'energy equation' is needed [e.g., *Dutton*, 1995; pp. 238–247]. This in turn requires the introduction of additional variables and flux equations describing water in the atmosphere and its phase changes as well as radiative energy transfer. All these processes have to be parameterised since, except for very special cases, forcing of fluid flow is too complex for an exact mathematical formulation.

Without equations for the forcing terms $\boldsymbol{f}$ and $\boldsymbol{f}'$, (2.7.10) and (2.7.11) are not a closed system of equations. Based on the arguments given in Section 2.6.2 about the connection of the timescale of the forcing and the timescale of a cyclic growth and decay process it can be assumed that the most relevant thermodynamic processes for tornadogenesis vary on the fast timescale of the vortex flow and therefore differ from the slow thermodynamic forcing involved in storm formation and evolution. If, however, as suggested in Section 2.4, tornadogenesis is investigated as a flow instability of intense shear zones and fronts of the storm flow, it can be assumed that rapid changes in the thermodynamic variables do not contribute directly to vortex formation and can be neglected altogether. Effects of the Earth's rotation are noticeable only on space and timescales larger than those of tornadogenesis and can safely be neglected for forcing on the fast timescale. Stationary forcing such as gravity and effects due solid boundaries (and other imposed stationary boundary conditions) are only included in the slow forcing term $\boldsymbol{f}$. To derive a kinematical system of equations for the rapidly evolving velocity field it can therefore be assumed that the fast forcing term $\boldsymbol{f}'$ is negligible for vortex formation. The total time-rate of change of the velocity field of thunderstorm and tornado vortex is therefore due to two qualitatively different processes: the externally forced slow evolution of the storm flow and a rapidly evolving small-scale vortex instability of that large-scale velocity field which is not directly affected by thermodynamic and external forces. Tornadogenesis tends to occur during the most intense state of the thunderstorm or mesocyclone. At this stage the storm is fully developed and approximately stationary over the period of the formation and decay of the tornado. Assuming that the slow expansion coefficients are approximately constant during tornadogenesis, (2.7.11) with $\partial_\tau \boldsymbol{u} = \boldsymbol{f}' \equiv \boldsymbol{0}$ is a closed dynamical system for the fast expansion coefficients, in which the slow expansion coefficients are constant parameters.[17] If the slow forcing term $\boldsymbol{f}$ is known at a particular time, equations (2.7.10) *and* (2.7.11) are a closed dynamical system of a *diagnostic* equation for the constant background flow and a *prognostic* equation for the fast perturbation flow. Since under the assumptions made above the slow balance equation does not depend on the time-averaged fast advection term (or the time-averaged stress tensor in the case of incompressible fast flow) as it would be the case for the Reynolds averaged equations, a change in the fast flow is not inconsistent with a constant steering background flow. The system of equations (2.7.11) with $\boldsymbol{f}$ undetermined to investigate the effects of the background flow on the perturbation flow as in the next chapter, or the system of equations (2.7.10) and (2.7.11) with $\boldsymbol{f}$ given by observations are therefore not only mathematically complete but also dynamically consistent.

Under these assumptions the interpretation of the slow flow as a 'background' flow can be taken very literally. Since it is assumed to be constant over the short period of the vortex formation and decay cycle, it only sets the stage for the evolution of the fast flow. However, the perturbation flow, although it evolves significantly faster than the externally forced large-scale flow, is still strongly coupled to and forced by that background flow. The vortex phenomenon described by the fast flow is therefore on a scale just above the inertial range.

[17] Here the identical vanishing of a vector field is used to indicate the vanishing of all expansion coefficients independently.

3 Flow in Phase Space

The Fourier transformation of the equations of motion introduced in the previous section transforms a system of three partial differential equations for the velocity components into an infinite-dimensional system of ordinary differential equations for their expansion coefficients. To be able to solve that system a reduction of the degrees of freedom is required. This is done through spectral and helical truncation.

3.1 Truncation

The first step in the spectral truncation was already done by the discretisation of the spatial spectrum, i.e., by replacing the continuous Fourier transform by Fourier series. To further reduce the number of variables in the dynamical system (2.7.11) for the fast expansion coefficients, all but a few of the most dominant waves will be neglected. Since the special interest here is in a particular vortex instability of the slow flow, the few waves chosen to represent the fast flow must, at least with a certain amplitude and phase relationship, describe a cyclonically rotating, radially converging updraft.

As mentioned in Section 2.6.1, for the representation of an isolated vortex a continuous spectrum is required. This continuum of waves adds up to generate a locally intense vortex. However, as shown in Section 2.6.1 and Appendix A.7 a simple periodic Beltrami vortex field can be represented by two positively helical 'vortex waves' corresponding to the wave vectors

$$\boldsymbol{k}_x \stackrel{\text{def}}{=} \begin{pmatrix} 1 \\ 0 \\ 0 \end{pmatrix} \tag{3.1.1}$$

and

$$\boldsymbol{k}_y \stackrel{\text{def}}{=} \begin{pmatrix} 0 \\ 1 \\ 0 \end{pmatrix} \quad , \tag{3.1.2}$$

and by setting either the real or imaginary parts of the expansion coefficients zero and the other parts of the complex numbers equal. As mentioned before, this eliminates the varying phase relationship between the two vortex waves leading to phase locking. However, to be able to describe vortex formation and decay a varying amplitude relationship is retained. Finally, the negatively helical and irrotational waves associated with the same wave vectors are neglected.

The question is now about the maximum simplification of the system (2.7.11) such that it still represents the most important aspects of vortex formation. Neglecting all but the two vortex waves leads to two uncoupled, linear equations that cannot be expected to faithfully represent the qualitative behaviour of the full system, in particular with respect to the formation of a symmetrical vortex flow. To retain the coupled, nonlinear character of the original equations the consideration of *triad interactions*, i.e., the interaction of the vortex waves with a third 'catalyst' wave, is required such that

$$\boldsymbol{k}_x \pm \boldsymbol{k}_y = \boldsymbol{q}, \tag{3.1.3}$$

where $\boldsymbol{q}$ is the wave vector of the catalyst wave.

3.2 Basic Interactions

For the equations of motion for the total flow the investigation of single triad interactions [*Kraichnan*, 1973; *Waleffe*, 1992] has shown that local spectral interactions between two waves of the same sign of helicity only excite a third wave with the opposite sign of helicity, whereas in local interactions between three nonvanishing waves of which one has the opposite sign of helicity of the others, only the equal helicity modes interact significantly. These interactions result in a net direct cascade of energy from large to small scales or from small to large wave numbers. However, due to the coupling of the fast flow to the slow background flow through the linear terms (in the fast expansion coefficients) in (2.7.11), these results are generally not true for the triad interactions of fast vortex waves.

As discussed in Section 2.6.1, for the particular case of vortex formation the expansion coefficients of the two vortex waves must have a very similar time-dependence. There are only two expansion coefficients that couple the two amplitudes corresponding to the wave vectors $\boldsymbol{k}_x$ and $\boldsymbol{k}_y$ of the simple vortex flow (2.6.28) directly. These belong to the wave vectors

$$\boldsymbol{k}_{x,y} \stackrel{\text{def}}{=} \frac{1}{\sqrt{2}} \begin{pmatrix} 1 \\ 1 \\ 0 \end{pmatrix} \tag{3.2.1}$$

and

$$\boldsymbol{k}_{x,-y} \stackrel{\text{def}}{=} \frac{1}{\sqrt{2}} \begin{pmatrix} 1 \\ -1 \\ 0 \end{pmatrix} , \tag{3.2.2}$$

with the triads

$$\boldsymbol{k}_x + \boldsymbol{k}_y = \sqrt{2}\boldsymbol{k}_{x,y} \tag{3.2.3}$$

and

$$\boldsymbol{k}_x - \boldsymbol{k}_y = \sqrt{2}\boldsymbol{k}_{x,-y} . \tag{3.2.4}$$

To determine conditions under which the two vortex waves are forced simultaneously it is reasonable to assume that these two triads represent the dominant *spectral interactions* for vortex formation. It is then instructive to investigate the low-dimensional dynamical systems for single triad interactions. Since both catalyst wave vectors for the vortex waves also lie in the horizontal plane, the fast perturbation flow represented by a single wave vector triad only has horizontal spatial variability.

Furthermore, under the high truncation the fast system is coupled to the slow background flow only through wave vectors of roughly the same magnitude and larger. As a result, vortex formation is controlled by quasistationary shear zones on roughly the same scale as the vortex, while large-scale variability of the slow flow is only of indirect importance through cascading of energy towards short waves. This is consistent with tornado phenomenology as discussed in Section 2.4 in that tornadoes invariably occur near fronts or in regions of strong velocity gradients. On the other hand storms with very different large-scale structure are associated with tornadoes and, vice versa, of two storms with a very similar large-scale structure only one may spawn a tornado.

Each of the three waves that are coupled in a triad interaction can be in three different helical states. There can then be $3^3 = 27$ different interactions for a single wave vector triad. In the particular case of the 'vortex triads' (3.2.3) and (3.2.4), in the following referred to as triads T1 and T2, respectively, two of the waves have the same positive sign of helicity. That reduces the number of different *helical interactions* for each of the two spectral interactions to three, one for each helical state of the catalyst wave vector (3.2.1) or (3.2.2). There is therefore a total of six basic *vortex interactions*.

Setting either the real or imaginary parts of the expansion coefficients zero leads to a real three-dimensional dynamical system for each vortex triad. For a positively or negatively helical catalyst wave the four resulting dynamical systems are all conservative, i.e., divergence of the flow in phase space vanishes. As a result there can be no attractors, and in particular there can be no asymptotically stable equilibria. The only hyperbolic fixed points are saddle points. Without asymptotically stable equilibria there can be no transition between definite (observable) states of the system for generic perturbations from one of the equilibria. While the basin of attraction of saddle or possibly nonhyperbolic fixed points is nonvanishing, the probability that an arbitrary perturbation from another fixed point lies within the basin of attraction of these equilibria is generally smaller than for an asymptotically stable fixed point. Moreover, the representation of the qualitative behaviour of the nonlinear system by the linearised system about the stationary solution requires a hyperbolic fixed point with empty centre manifold.

Generally, a meaningful definition of 'state of a system' requires at least some degree of persistence. In the following, 'state' will therefore always be referring to an equilibrium of the system. Otherwise the transition probability between states, together with the states themselves, is time-dependent. Without asymptotically stable equilibria there can only be transient fluctuations and the momentary development of a vortex flow would not be a convincing argument for the formation of tornadolike vortices in a turbulent fluid.

The existence of stable equilibria for the rapidly evolving velocity field may seem counterintuitive. It is important to remember, however, that the simple dynamical systems are derived to model the initial instability leading to the transition to the vortex state, not the long-term behaviour of the flow. The constancy of the slow expansion coefficients during this initial transition period is an idealisation of the temporal evolution of the full system. Eventually the background flow changes and 'moves out' of the 'tornadic' parameter region, causing a qualitative change in the dynamics of the fast system. This leads to the concept of dynamic bifurcations discussed in Section 4.1.

For the existence of a stable vortex equilibrium a nonhelical, divergent catalyst mode is required. Physically this can be expected for two reasons. As discussed in Section 2.3, while the *persistence* of vortices is likely to increase with their helicity, the *generation* of turbulent eddies requires inertial forcing and therefore a nonhelical flow component. Furthermore, due to vortex line stretching and concentration of vertical vorticity, one would expect that a radially converging vortex is more stable than a nondiverging or even diverging vortex. As seen below, the only stationary vortex states are indeed converging cyclonically rotating updrafts or anticyclonically rotating downdrafts.

To be able to explicitly derive real dynamical systems from (2.7.11) for particular sets of waves, the expansion coefficients must be decomposed into their real and imaginary parts. The slow expansion coefficients are therefore written as

$$\boldsymbol{u}_{\boldsymbol{q}} = \boldsymbol{\alpha}_{\boldsymbol{q}} + i\boldsymbol{a}_{\boldsymbol{q}} \ , \tag{3.2.5}$$

where

$$\boldsymbol{\alpha}_{\boldsymbol{q}} \stackrel{\text{def}}{=} \begin{pmatrix} \alpha_{\boldsymbol{q}} \\ \beta_{\boldsymbol{q}} \\ \gamma_{\boldsymbol{q}} \end{pmatrix} \tag{3.2.6}$$

and

$$\boldsymbol{a}_{\boldsymbol{q}} \stackrel{\text{def}}{=} \begin{pmatrix} a_{\boldsymbol{q}} \\ b_{\boldsymbol{q}} \\ c_{\boldsymbol{q}} \end{pmatrix} \ , \tag{3.2.7}$$

and the fast expansion coefficients are written as

$$a^{\lambda}_{\chi\boldsymbol{k}} = \alpha^{\lambda}_{\chi\boldsymbol{k}} + i\beta^{\lambda}_{\chi\boldsymbol{k}} \ , \tag{3.2.8}$$

with real numbers $\alpha^{\lambda}_{\chi\boldsymbol{k}}$, $\beta^{\lambda}_{\chi\boldsymbol{k}}$, $\alpha_{\boldsymbol{q}}$, $a_{\boldsymbol{q}}$, etc.. Since for the truncated systems wave vectors are restricted to the horizontal plane, $\boldsymbol{q} = \chi(j,k,0)^T$, with integers j and k, a simplified index notation

$$\boldsymbol{u}_{\boldsymbol{q}} \longrightarrow \boldsymbol{u}_{j,k} \qquad \text{etc.} \tag{3.2.9}$$

for the slow expansion coefficients can be introduced. For triad T1 with positively helical vortex waves and nonhelical catalyst wave, setting $\alpha^{+}_{\chi\boldsymbol{k}_x} = \alpha^{+}_{\chi\boldsymbol{k}_y} = \beta^{0}_{\chi\boldsymbol{k}_{x,y}} \equiv 0$, the complex dynamical system (2.7.11) then reduces to the three-dimensional real system

$$\begin{aligned}
\dot\beta^{+}_{\chi\boldsymbol{k}_x} &= -\frac{\chi}{2}\left(\gamma_{1,1} - \gamma_{1,-1}\right)\beta^{+}_{\chi\boldsymbol{k}_y} + \frac{\chi}{2}\left(-a_{0,1} + \gamma_{0,1} + a_{2,1} - 2b_{2,1} + 3\gamma_{2,1}\right)\alpha^{0}_{\chi\boldsymbol{k}_{x,y}} \\
\dot\beta^{+}_{\chi\boldsymbol{k}_y} &= \frac{\chi}{2}\left(\gamma_{1,1} - \gamma_{1,-1}\right)\beta^{+}_{\chi\boldsymbol{k}_x} + \frac{\chi}{2}\left(b_{1,0} + \gamma_{1,0} + 2a_{1,2} - b_{1,2} + 3\gamma_{1,2}\right)\alpha^{0}_{\chi\boldsymbol{k}_{x,y}} \\
\dot\alpha^{0}_{\chi\boldsymbol{k}_{x,y}} &= \frac{\chi}{\sqrt{2}}\beta^{+}_{\chi\boldsymbol{k}_x}\beta^{+}_{\chi\boldsymbol{k}_y} + \frac{\chi}{2}\left(2a_{0,1} + b_{0,1} + b_{2,1}\right)\beta^{+}_{\chi\boldsymbol{k}_x} - \frac{\chi}{2}\left(2b_{1,0} + a_{1,0} - a_{1,2}\right)\beta^{+}_{\chi\boldsymbol{k}_y} \\
&\quad - \chi\left(a_{2,2} + b_{2,2}\right)\alpha^{0}_{\chi\boldsymbol{k}_{x,y}} \ ,
\end{aligned} \tag{3.2.10}$$

where the dot over a variable denotes total differentiation with respect to time. Defining the new variables

$$X \stackrel{\text{def}}{=} \sqrt{2}\beta^{+}_{\chi\boldsymbol{k}_x} \tag{3.2.11}$$

$$Y \stackrel{\text{def}}{=} \sqrt{2}\beta^{+}_{\chi\boldsymbol{k}_y} \tag{3.2.12}$$

$$Z \stackrel{\text{def}}{=} \frac{2\sqrt{2}}{\chi}\alpha^{0}_{\chi\boldsymbol{k}_{x,y}} \ , \tag{3.2.13}$$

and the new parameters

$$r \stackrel{\text{def}}{=} \frac{\chi}{2}\left(\gamma_{1,1} - \gamma_{1,-1}\right) \tag{3.2.14}$$

$$r_1 \stackrel{\text{def}}{=} \frac{\chi^2}{4}\left(-a_{0,1} + \gamma_{0,1} + a_{2,1} - 2b_{2,1} + 3\gamma_{2,1}\right) \tag{3.2.15}$$

$$r_2 \stackrel{\text{def}}{=} \frac{\chi^2}{4}\left(b_{1,0} + \gamma_{1,0} + 2a_{1,2} - b_{1,2} + 3\gamma_{1,2}\right) \tag{3.2.16}$$

$$r_3 \stackrel{\text{def}}{=} 2a_{0,1} + b_{0,1} + b_{2,1} \tag{3.2.17}$$

$$r_4 \stackrel{\text{def}}{=} 2b_{1,0} + a_{1,0} - a_{1,2} \tag{3.2.18}$$

$$\sigma \stackrel{\text{def}}{=} \chi\left(a_{2,2} + b_{2,2}\right) \ , \tag{3.2.19}$$

the notation of system (3.2.10) simplifies to

$$\begin{aligned} \dot{X} &= -rY + r_1 Z \\ \dot{Y} &= rX + r_2 Z \\ \dot{Z} &= XY + r_3 X - r_4 Y - \sigma Z \ . \end{aligned} \tag{3.2.20}$$

The same dynamical system is obtained for triad T2 if

$$Z \stackrel{\text{def}}{=} \frac{2\sqrt{2}}{\chi}\alpha^{0}_{\chi\boldsymbol{k}_{x,-y}} \ , \tag{3.2.21}$$

and the parameters $\{r_1, \ldots, r_4, \sigma\}$ are defined as

$$r_1 \stackrel{\text{def}}{=} \frac{\chi^2}{4}\left(-a_{0,1} + \gamma_{0,1} - a_{2,-1} - 2b_{2,-1} + 3\gamma_{2,-1}\right) \tag{3.2.22}$$

$$r_2 \stackrel{\text{def}}{=} \frac{\chi^2}{4}\left(b_{1,0} + \gamma_{1,0} - 2a_{1,-2} - b_{1,-2} + 3\gamma_{1,-2}\right) \tag{3.2.23}$$

$$r_3 \stackrel{\text{def}}{=} 2a_{0,1} - b_{0,1} - b_{2,-1} \tag{3.2.24}$$

$$r_4 \stackrel{\text{def}}{=} 2b_{1,0} - a_{1,0} + a_{1,-2} \tag{3.2.25}$$

$$\sigma \stackrel{\text{def}}{=} \chi\left(a_{2,-2} - b_{2,-2}\right) \ , \tag{3.2.26}$$

For particular initial and boundary conditions the time-evolution of both systems can easily be determined to arbitrary accuracy through numerically integration. However, the *qualitative* behaviour of the systems over a larger volume of initial conditions in phase space and boundary conditions in parameter space can be obtained through essentially analytical methods. The discussion in the following two sections of the equilibria of system (3.2.20), their stability, and transitions between equilibria equally applies to the dynamical systems for both vortex triads. Distinctions only have to be made in Section 3.5 for the interpretation of the system parameters in terms of background flows. To simplify the analysis it is assumed in the following that

$$\boldsymbol{u}_{2,1} = \boldsymbol{u}_{1,2} = \boldsymbol{u}_{2,-1} = \boldsymbol{u}_{1,-2} \equiv \boldsymbol{0} \ . \tag{3.2.27}$$

Then parameters r_1 and r_2 for both triads are identical.

3.3 Equilibria and Their Stability

The divergence of the flow $\dot{\boldsymbol{X}}$ in phase space with $\boldsymbol{X} \overset{\text{def}}{=} (X, Y, Z)$ is given by

$$\partial_X \dot{X} + \partial_Y \dot{Y} + \partial_Z \dot{Z} = -\sigma \ . \tag{3.3.1}$$

For the existence of attractors and stable equilibria it is therefore necessary that $\sigma > 0$.

The two stationary solutions of (3.2.20) are $\boldsymbol{X}_0 \overset{\text{def}}{=} (0, 0, 0)$, which exists for all parameter values, and $\bar{\boldsymbol{X}} \overset{\text{def}}{=} (\bar{X}, \bar{Y}, \bar{Z})$, where

$$\bar{X} \overset{\text{def}}{=} \frac{r_1 r_4 + r_2 r_3 + r\sigma}{r_1} \tag{3.3.2}$$

$$\bar{Y} \overset{\text{def}}{=} -\frac{r_1 r_4 + r_2 r_3 + r\sigma}{r_2} \tag{3.3.3}$$

$$\bar{Z} \overset{\text{def}}{=} -\frac{r(r_1 r_4 + r_2 r_3 + r\sigma)}{r_1 r_2} \ . \tag{3.3.4}$$

For $\bar{\boldsymbol{X}}$ to represent a symmetrical vortex it is required that $|\bar{X}| = |\bar{Y}|$, or $|r_1| = |r_2|$. For $\bar{X} \mapsto -\bar{X}$ the periodic vortex pattern is shifted by $\pi\chi^{-1}$ along the x-axis, while for $\bar{Y} \mapsto -\bar{Y}$ the vortex pattern is shifted by $\pi\chi^{-1}$ along the y-axis. There are therefore essentially two possibilities for vortex equilibria in which cases $p \overset{\text{def}}{=} r_2 = \pm r_1$.

Under the simplification (3.2.27) parameter p can be interpreted by assuming that the slow background flow is given by the positively helical Beltrami vortex (A.7.8). With (A.7.6) and (A.7.7) the slow expansion coefficients are given by

$$\begin{aligned} \boldsymbol{u}_{1,0} &= \frac{iA}{\sqrt{2}} \frac{1}{\sqrt{2}} \begin{pmatrix} 0 \\ -1 \\ -i \end{pmatrix} \\ &= \frac{A}{2} \begin{pmatrix} 0 \\ -i \\ 1 \end{pmatrix} \end{aligned} \tag{3.3.5}$$

and

$$\boldsymbol{u}_{0,1} = \frac{B}{2} \begin{pmatrix} i \\ 0 \\ 1 \end{pmatrix} \ . \tag{3.3.6}$$

Then

$$b_{1,0} = -\gamma_{1,0} \ , \tag{3.3.7}$$
$$a_{0,1} = \gamma_{0,1} \ , \tag{3.3.8}$$

and therefore $p \equiv 0$ for all $A, B \in \mathbb{R}$ and arbitrary phase shifts of the vortex centre. On the other hand for a negatively helical Beltrami vortex the slow expansion coefficients are given by

$$\boldsymbol{u}_{1,0} = \frac{A}{2}\begin{pmatrix} 0 \\ -i \\ -1 \end{pmatrix} \tag{3.3.9}$$

and

$$\boldsymbol{u}_{0,1} = \frac{B}{2}\begin{pmatrix} i \\ 0 \\ -1 \end{pmatrix} \ , \tag{3.3.10}$$

in which case

$$b_{1,0} = \gamma_{1,0} \ , \tag{3.3.11}$$
$$-a_{0,1} = \gamma_{0,1} \ , \tag{3.3.12}$$

and $p = 2b_{1,0} = 2\gamma_{1,0} = 2a_{0,1} = -2\gamma_{0,1}$. For generality consider now the function $p = a + b$ with real numbers a and b. For a given value c^2 of the 'kinetic energy' $a^2 + b^2$, $p^2 = 2ab + c^2$ and therefore $|p|$ are extremised for $a^2 = b^2$, where for $a = -b$, $|p|_{\min} = 0$ and for $a = b$, $|p|_{\max} = 2|a| = 2|b|$.[1] For a given value of $b_{1,0}^2 + \gamma_{1,0}^2$ and $a_{0,1}^2 + \gamma_{0,1}^2$, the magnitude of p is therefore minimised (zero) for a positively helical Beltrami vortex and maximised for a negatively helical Beltrami vortex. In as much as the negatively helical vortex can be considered to be the 'opposite' of the positively helical vortex, parameter p can be interpreted as the deviation of the background flow from a positively helical Beltrami vortex.

Consider first the case $p = r_2 = -r_1$ which results in a vortex centred over the origin in the horizontal plane. Then

$$\bar{X} = \bar{Y} = -\frac{p}{r}\bar{Z} = r_4 - r_3 - \frac{r\sigma}{p} \ . \tag{3.3.13}$$

The corresponding flow in physical space is given by

$$\boldsymbol{v} = \begin{pmatrix} -\bar{Y}\sin\chi y + \frac{\chi}{2}\bar{Z}\sin\chi(x+y) \\ \bar{X}\sin\chi x + \frac{\chi}{2}\bar{Z}\sin\chi(x+y) \\ \bar{X}\cos\chi x + \bar{Y}\cos\chi y \end{pmatrix} \tag{3.3.14}$$

[1] Since $c^2 = a^2 + b^2$ is required to be constant $p^2 = 2ab + c^2$ is extremised for the same values of a and b as ab. With $a, b > 0$ the example given above has a simple geometrical analogue in that for a given circumference $2(a + b)$ of a rectangle its volume ab is maximised by a square $a = b$.

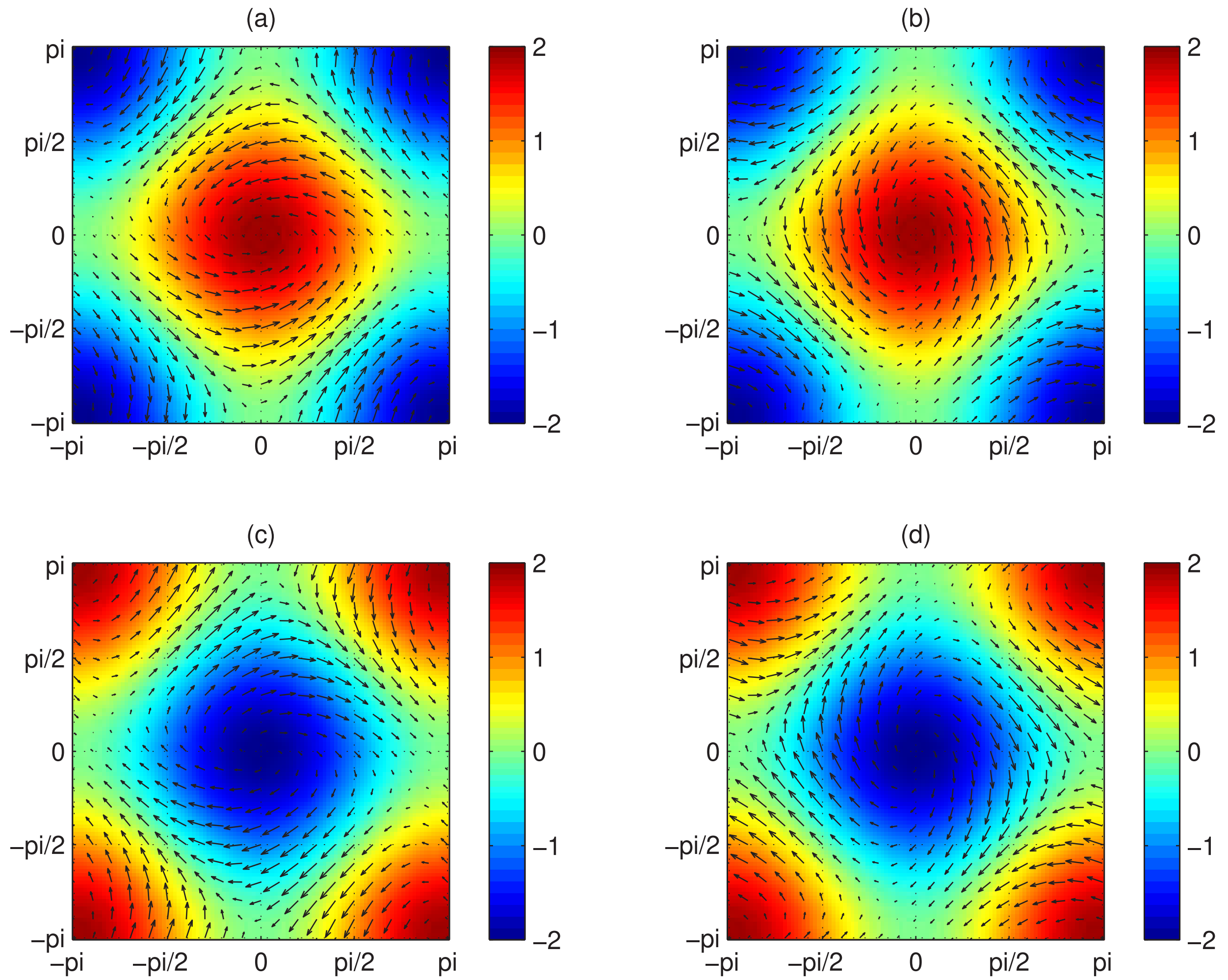

Figure 3.1: *Flow in physical space around the origin corresponding to vortex equilibria in phase space for triad T1 (left column) and triad T2 (right column), with* $\bar{X} = \bar{Y} = -\bar{Z} > 0$ *(converging cyclonically rotating updrafts) in the first row and* $\bar{X} = \bar{Y} = -\bar{Z} < 0$ *(diverging anticyclonically rotating downdrafts) in the second row. The vectors represent the horizontal components of the velocity field, and the colour shading denotes vertical velocity.*

for triad T1, and

$$\boldsymbol{v} = \begin{pmatrix} -\bar{Y}\sin\chi y + \frac{\chi}{2}\bar{Z}\sin\chi(x-y) \\ \bar{X}\sin\chi x - \frac{\chi}{2}\bar{Z}\sin\chi(x-y) \\ \bar{X}\cos\chi x + \bar{Y}\cos\chi y \end{pmatrix} \tag{3.3.15}$$

for triad T2. These vector fields are shown in Figure 3.1 for $\chi = 1$ and different values of the equilibrium expansion coefficients. It is apparent that the vortex states for both triads, just as the corresponding catalyst wave vectors, are simply rotated relative to each other by 90° about the vertical axis. Consequently, as seen in Section 3.5, for every tornadic background flow for the T1 vortex state there is a corresponding tornadic background flow for the T2 vortex state which is rotated counterclockwise by 90° relative to the T1 background flow, and vice versa.

The linear stability of the two equilibria of each system is analysed by calculating the eigenvalues of the Jacobian matrix

$$\begin{aligned} J(\boldsymbol{X}) &\stackrel{\text{def}}{=} \begin{pmatrix} \partial_X \dot{X} & \partial_Y \dot{X} & \partial_Z \dot{X} \\ \partial_X \dot{Y} & \partial_Y \dot{Y} & \partial_Z \dot{Y} \\ \partial_X \dot{Z} & \partial_Y \dot{Z} & \partial_Z \dot{Z} \end{pmatrix} \\ &= \begin{pmatrix} 0 & -r & r_1 \\ r & 0 & r_2 \\ (\bar{Y} + r_3) & (\bar{X} - r_4) & -\sigma \end{pmatrix} \end{aligned} \tag{3.3.16}$$

evaluated at the stationary solutions $\boldsymbol{X}_0$ and $\bar{\boldsymbol{X}}$

$$J(\boldsymbol{X}_0) = \begin{pmatrix} 0 & -r & -p \\ r & 0 & p \\ r_3 & -r_4 & -\sigma \end{pmatrix} \tag{3.3.17}$$

and

$$J(\bar{\boldsymbol{X}}) = \begin{pmatrix} 0 & -r & -p \\ r & 0 & p \\ (r_4 - \frac{r\sigma}{p}) & -(r_3 + \frac{r\sigma}{p}) & -\sigma \end{pmatrix} . \tag{3.3.18}$$

The characteristic equations for eigenvalues λ are given by

$$\lambda^3 + \sigma\lambda^2 + \left[p(r_4 + r_3) + r^2\right]\lambda \mp r\left[p(r_4 - r_3) - r\sigma\right] = 0 , \tag{3.3.19}$$

where the upper sign of the term $r\left[p(r_4 - r_3) - r\sigma\right]$ corresponds to the phase space origin and the lower sign corresponds to the vortex equilibrium. Since the coefficients in the characteristic equations are real it follows from the fundamental law of algebra that for each complex solution the complex conjugate also is a solution. For an algebraic equation with an uneven order this implies that at least one solution of (3.3.19) must be real for all parameter values.

To simplify the analysis consider the two cases $q \stackrel{\text{def}}{=} r_4 = \pm r_3$. Then for $q = r_4 = r_3$

$$\bar{X} = \bar{Y} = -\frac{p}{r}\bar{Z} = -\frac{r\sigma}{p} \tag{3.3.20}$$

and

$$\lambda^3 + \sigma\lambda^2 + \left(2pq + r^2\right)\lambda \pm r^2\sigma = 0 , \tag{3.3.21}$$

and for $q = r_4 = -r_3$

$$\bar{X} = \bar{Y} = -\frac{p}{r}\bar{Z} = 2q - \frac{r\sigma}{p} \tag{3.3.22}$$

and

$$\lambda^3 + \sigma\lambda^2 + r^2\lambda \mp r\,(2pq - r\sigma) = 0\ . \tag{3.3.23}$$

In both characteristic equations parameters p and q effectively only appear as one parameter in the combination pq. Through the definition of the parameters p and q the number of independent parameters in the stability analysis is therefore reduced from six to three.

The linear stability of the system near any of the fixed points depends on the sign of the real parts of the three eigenvalues λ_i. For asymptotic stability $\mathrm{Re}\,[\lambda_i] \overset{!}{<} 0$ for all $i = 1, 2, 3$. Conversely, for instability $\mathrm{Re}\,[\lambda_i] \overset{!}{>} 0$ for at least one eigenvalue. Since for $\sigma > 0$ the system (3.2.20) is dissipative there must always be at least one stable direction. To characterise the combined instability or stability of all three eigendirections of the linearised flow around any equilibrium $\bar{\boldsymbol{X}}$, the *repellor strength* of $\bar{\boldsymbol{X}}$ is defined as the magnitude of the vector containing all its unstable eigenvalues,

$$R(\bar{\boldsymbol{X}}) \overset{\mathrm{def}}{=} \left(\sum_{\mathrm{Re}[\lambda_i]>0} \mathrm{Re}\left[\lambda_i(\bar{\boldsymbol{X}})\right]^2 \right)^{\frac{1}{2}}\ , \tag{3.3.24}$$

while the *attractor strength* of $\bar{\boldsymbol{X}}$ is defined as

$$A(\bar{\boldsymbol{X}}) \overset{\mathrm{def}}{=} \left(\sum_{i=1}^{3} \mathrm{Re}\left[\lambda_i(\bar{\boldsymbol{X}})\right]^2 \right)^{\frac{1}{2}}\ , \tag{3.3.25}$$

for all $\mathrm{Re}\,[\lambda_i]$ negative, else $A(\bar{\boldsymbol{X}}) \overset{\mathrm{def}}{=} 0$.

Since the term $r^2\sigma$ in (3.3.21) is greater than zero for all values of r and $\sigma > 0$, as shown in Figure 3.2, for $q = r_4 = r_3$ the ground state is stable over the entire parameter space, while, as shown in Figure 3.3, the vortex state has unstable directions for all parameter values. However, as shown in Figures 3.4 and 3.5, for $q = r_4 = -r_3$ both equilibria have nonoverlapping parameter regions of stability. In all figures attractor and repellor strengths are shown only for positive values of pq, r and σ. However, there is a mirror symmetry in pq and r with respect to the origin in parameter space.

Consider now the case $p = r_2 = r_1$. Then, for $q = r_4 = r_3$

$$\bar{X} = -\bar{Y} = -\frac{p}{r}\bar{Z} = 2q + \frac{r\sigma}{p} \tag{3.3.26}$$

and

$$\lambda^3 + \sigma\lambda^2 + r^2\lambda \pm r\,(2pq + r\sigma) = 0\ , \tag{3.3.27}$$

while for $q = r_4 = -r_3$

$$\bar{X} = -\bar{Y} = -\frac{p}{r}\bar{Z} = \frac{r\sigma}{p} \tag{3.3.28}$$

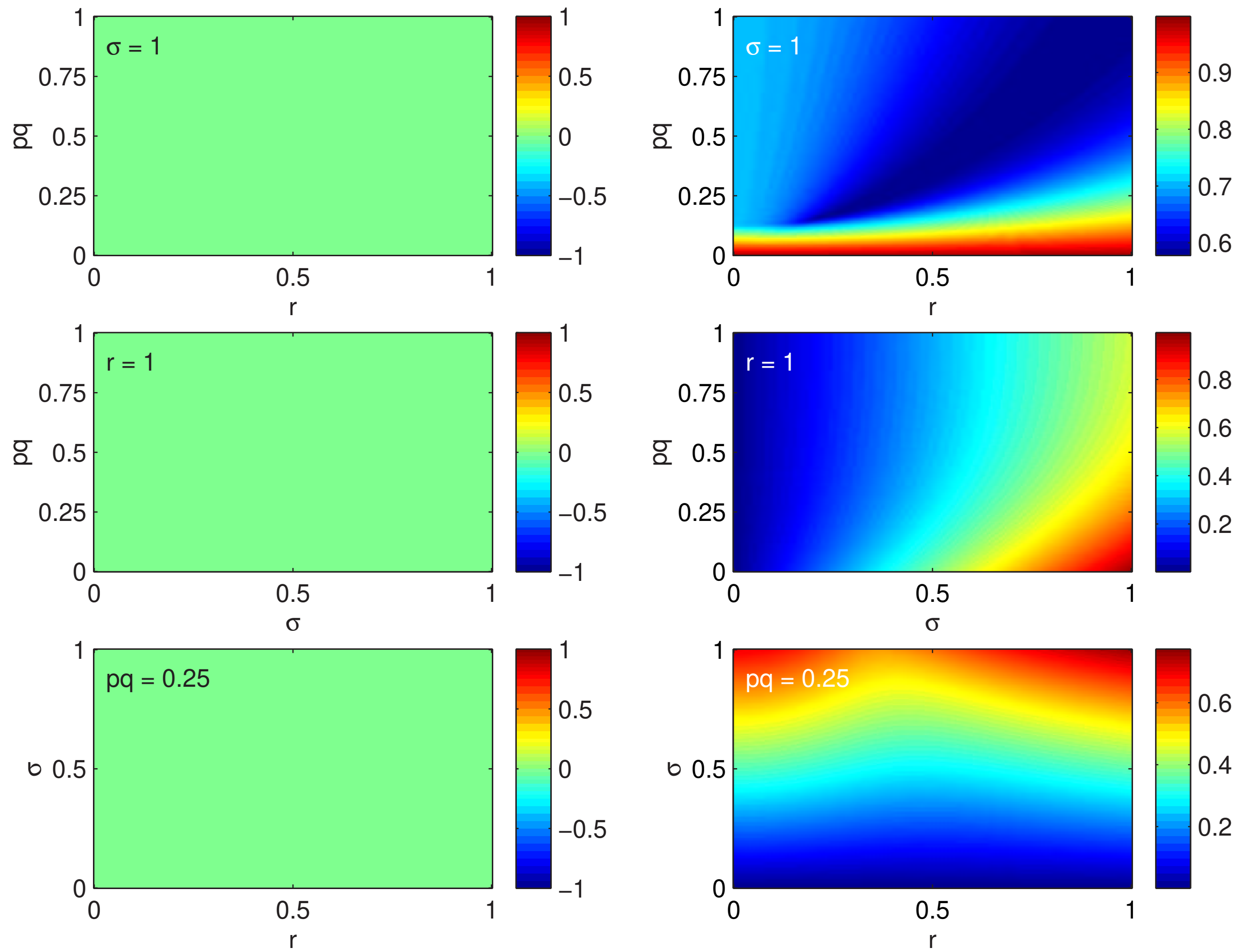

Figure 3.2: *Ground state repellor strength (left column) and attractor strength (right column) for $p = r_2 = -r_1$ and $q = r_4 = r_3$.*

and

$$\lambda^3 + \sigma\lambda^2 + \left(2pq + r^2\right)\lambda \pm r^2\sigma = 0\ . \tag{3.3.29}$$

As before, the upper sign corresponds to the phase space origin and the lower sign to the vortex equilibrium. As shown in Figures 3.6 and 3.7, for $q = r_4 = r_3$ neither the ground nor the vortex state are stable for any combination of parameters. The characteristic equation (3.3.29) is identical with (3.3.21). For $q = r_4 = -r_3$ the vortex state is therefore unstable for all parameter values.

For a perfectly helical background vortex with $p = r_2 = \pm r_1 = 0$ the vortex equilibrium of the fast flow does not exist for nonvanishing r and σ. For $q = r_4 = \pm r_3 = 0$ and $p = r_2 = \pm r_1 \neq 0$ identical characteristic equations

$$\lambda^3 + \sigma\lambda^2 + r^2\lambda \pm r^2\sigma = 0 \tag{3.3.30}$$

are obtained. It can be seen from the previous figures that in those cases the vortex state is

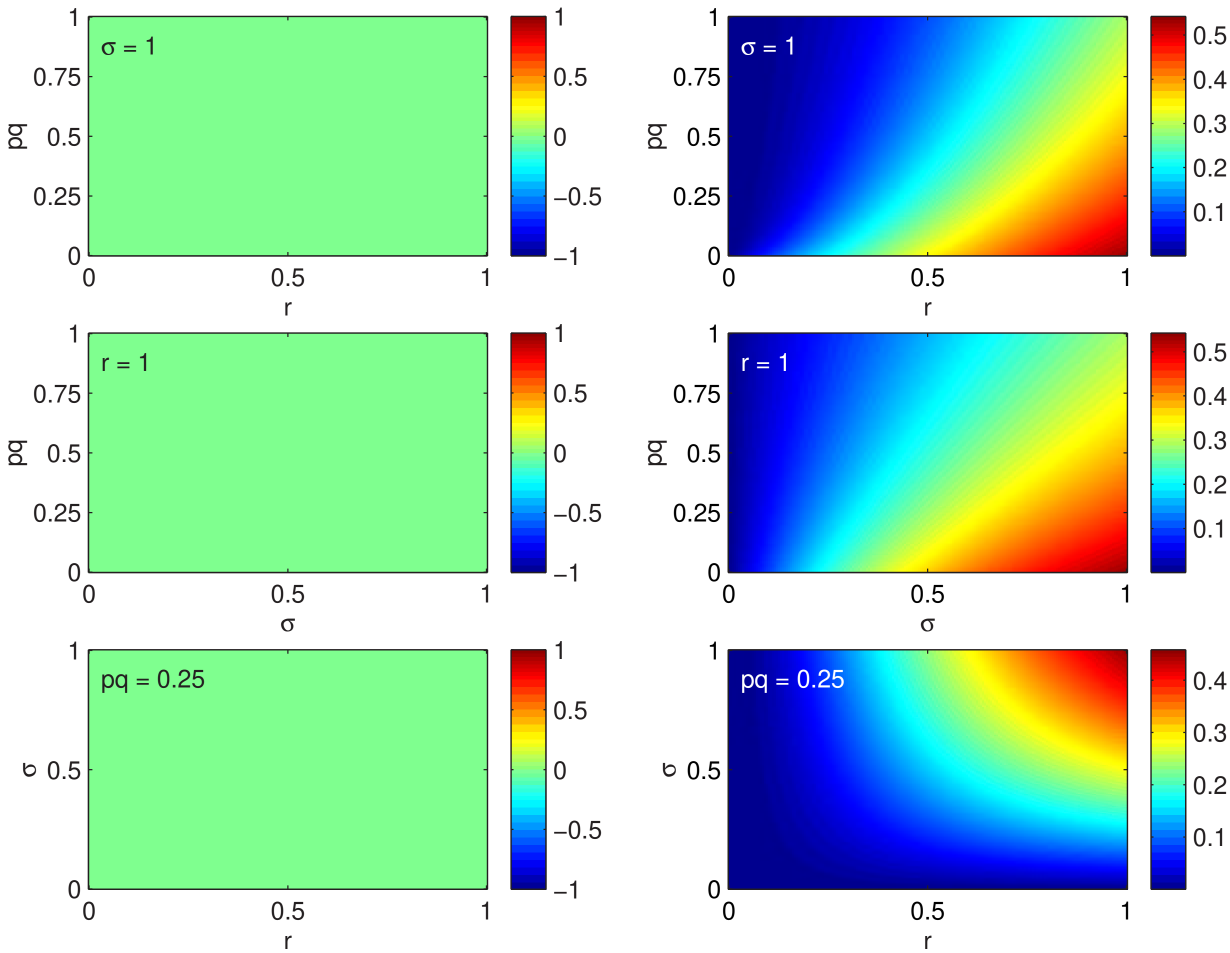

Figure 3.3: *Vortex state attractor strength (left column) and repellor strength (right column) for $p = r_2 = -r_1$ and $q = r_4 = r_3$.*

unstable for all values of p, r and σ. Finally, for $r = 0$ or $\sigma = 0$ there exist only nonhyperbolic equilibria.

3.4 Conditions for Vortex Formation

In practice, for the purpose of tornado forecasting, the slow velocity field is calculated from observations of the storm system prior to tornadogenesis. Relevant initial conditions for phase space trajectories are therefore small perturbations from the phase space origin. Since stable (or unstable) manifolds of two distinct hyperbolic fixed points cannot intersect, a point arbitrarily close to the origin, which lies within the basin of attraction of the vortex fixed point, must necessarily also lie on the unstable manifold of the origin. Then vortex formation from small initial perturbations, i.e., a transition from a state close to the origin to the vortex equilibrium, takes place. Stated differently, if both fixed points are simultaneously asymptotically stable, arbitrarily small perturbations from the origin cannot lie within the basin of attraction of the vortex equilibrium and a transition from perturbations of the

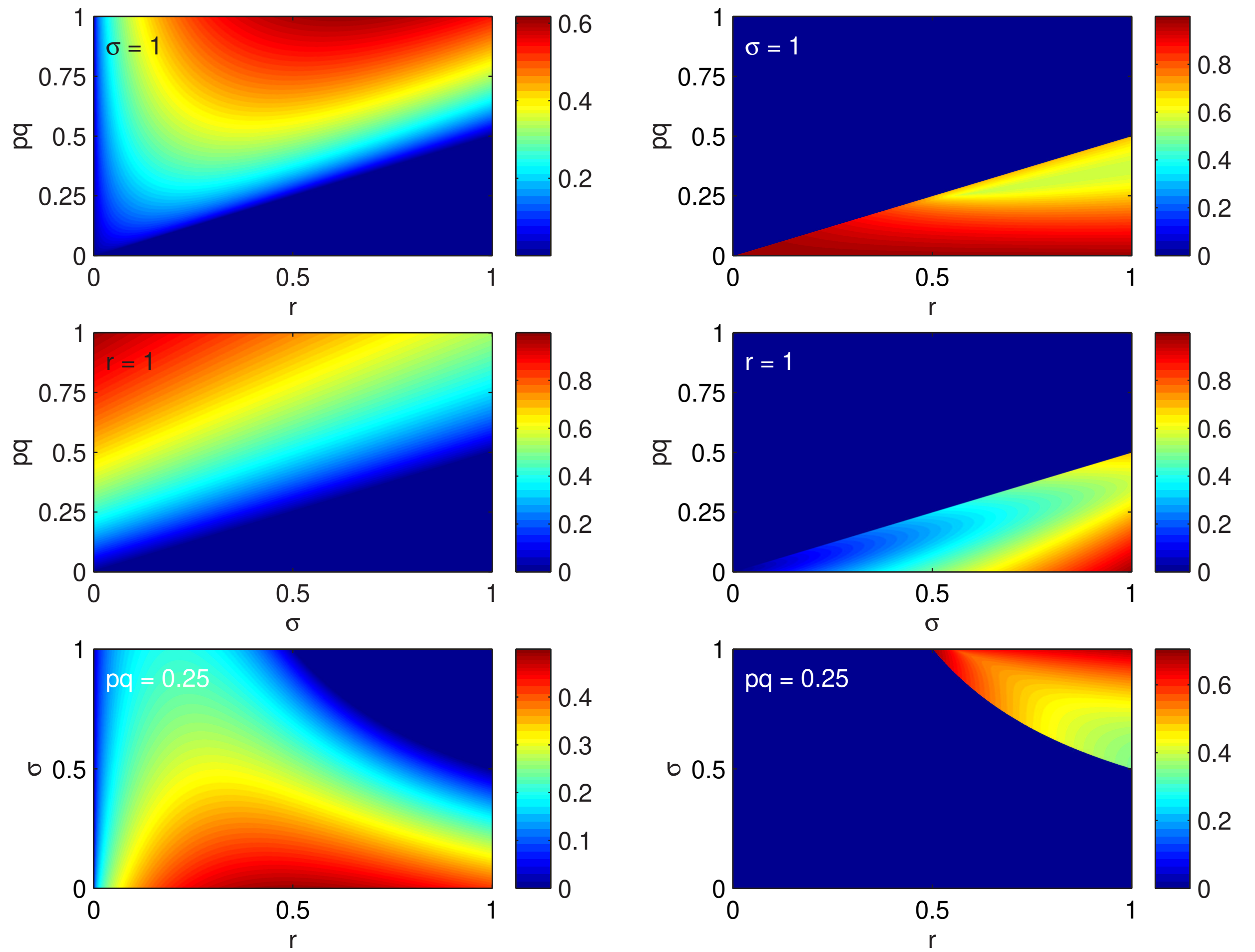

Figure 3.4: *Ground state repellor strength (left column) and attractor strength (right column) for* $p = r_2 = -r_1$ *and* $q = r_4 = -r_3$*.*

'ground state' to the vortex state cannot take place. Moreover, as discussed in Section 3.2, the transition probability for arbitrary perturbations from the origin to a saddle or nonhyperbolic fixed point is generally very small.

The isolated stability or instability[2] of fixed points is therefore not a sufficient criterion for a transition between equilibria. To characterise the transition probability between states of the system, a combined measure of the instability of the initial state and the stability of the final state must be introduced. Based on the definition of repellor and attractor strength, (3.3.24) and (3.3.25), respectively, it is straightforward to define the *transition probability* from equilibrium state $\bar{\boldsymbol{X}}_1$ to equilibrium state $\bar{\boldsymbol{X}}_2$ as the product of the repellor strength of the initial state with the attractor strength of the final state,

$$\mathrm{TP}\left[\bar{\boldsymbol{X}}_1 \rightarrow \bar{\boldsymbol{X}}_2\right] \stackrel{\text{def}}{=} R(\bar{\boldsymbol{X}}_1)A(\bar{\boldsymbol{X}}_2) \ . \tag{3.4.1}$$

Since generally not all perturbations from the initial state lie within the basin of attraction

[2]In the following stability is always referring to asymptotic stability of the linearised system, while instability is referring to the absence of asymptotic stability.

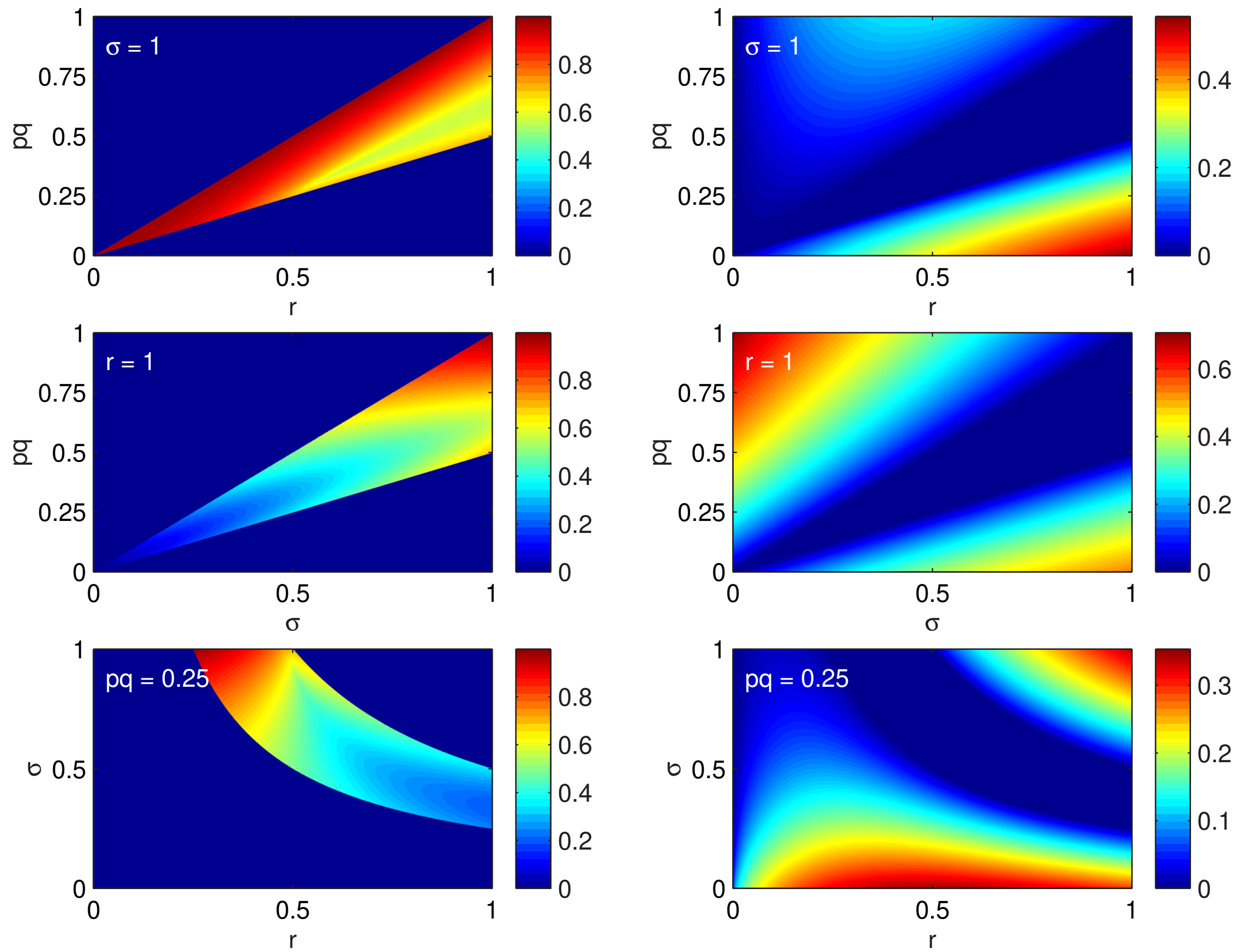

Figure 3.5: *Vortex state attractor strength (left column) and repellor strength (right column) for* $p = r_2 = -r_1$ *and* $q = r_4 = -r_3$.

of the final state, nonvanishing transition probability, as the name suggests, only is a statistical measure and not a sufficient criterion for the transition to take place. Unlike the case in quantum mechanics transition probability here is unnormalised. Since the magnitudes of the eigenvalues of the linearised system in phase space are dynamically relevant, unnormalised transition probabilities allow comparisons of transitions between equilibria for two velocity fields that are scaled in the same way. However, since the dynamical system is autonomous the transition probability is constant in time and is therefore a meaningful statistical measure.

The transition probabilities for the four cases $p = r_2 = \pm r_1$ and $q = r_4 = \pm r_3$ discussed in the previous section are shown in Figures 3.8, 3.9, and 3.10. It can be seen that for $p = r_2 = r_1$ and $q = r_4 = \pm r_3$, and for $p = r_2 = -r_1$ and $q = r_4 = r_3$ transitions from the ground to the vortex state are extremely unlikely. For these special parameter values the only likely contribution to vortex formation comes from the case when $p = r_2 = -r_1$ and $q = r_4 = -r_3$. The following discussion will therefore focus on these parameter values.

The information in the previous figures can then be summarised by four inequalities. The

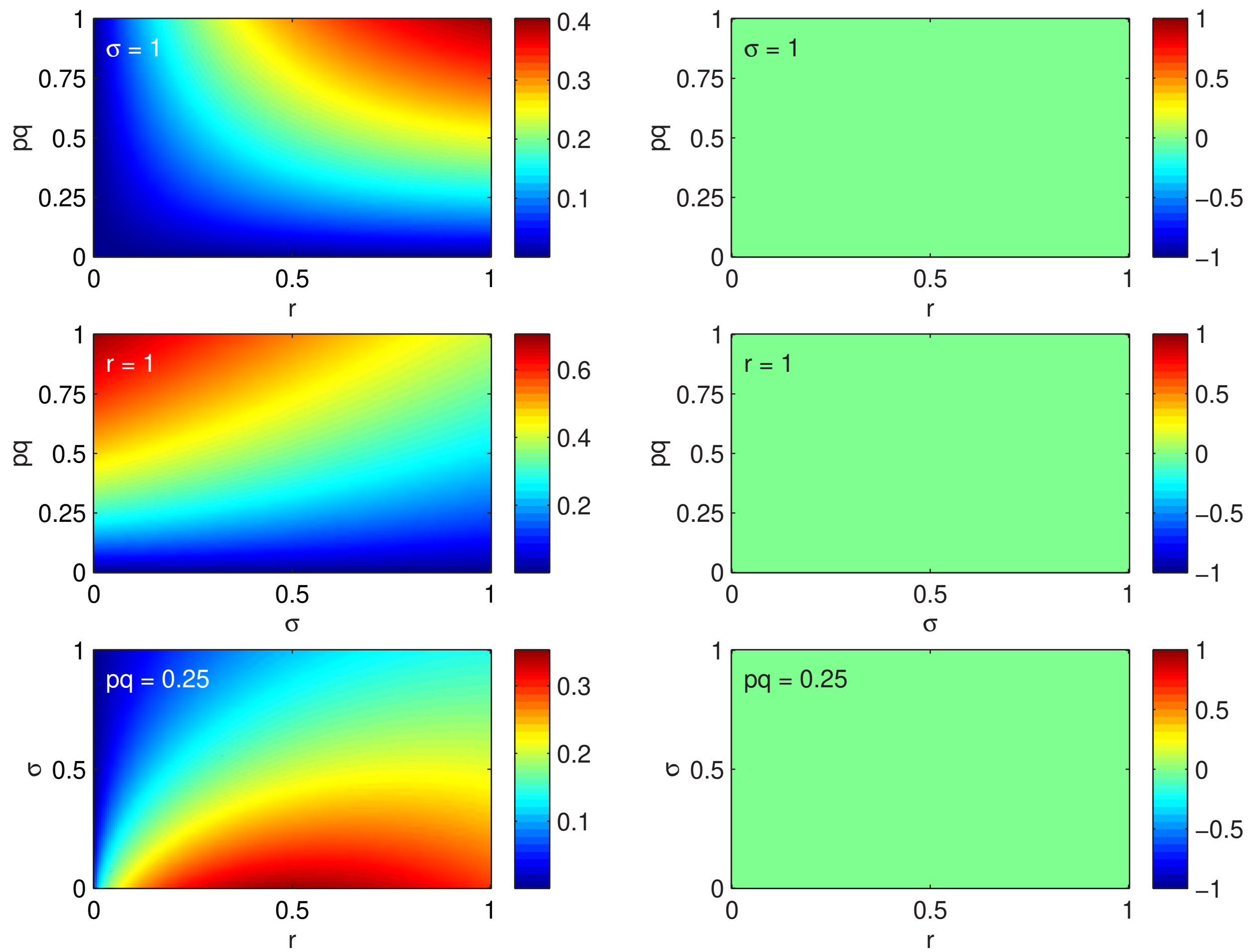

Figure 3.6: *Ground state repellor strength (left column) and attractor strength (right column) for* $p = r_2 = r_1$ *and* $q = r_4 = r_3$.

ground state is stable for parameter values satisfying

$$0 < pq < \frac{r\sigma}{2} \tag{3.4.2}$$

for $r > 0$, and for parameter values satisfying

$$\frac{r\sigma}{2} < pq < 0 \tag{3.4.3}$$

for $r < 0$. Since in those cases arbitrary, small perturbations of the fast flow are damped out, the part of parameter space satisfying (3.4.2) and (3.4.3) is referred to as the 'laminar' region. Similarly, the part of parameter space satisfying

$$\frac{r\sigma}{2} < pq < r\sigma \tag{3.4.4}$$

for $r > 0$, and

$$r\sigma < pq < \frac{r\sigma}{2} \tag{3.4.5}$$

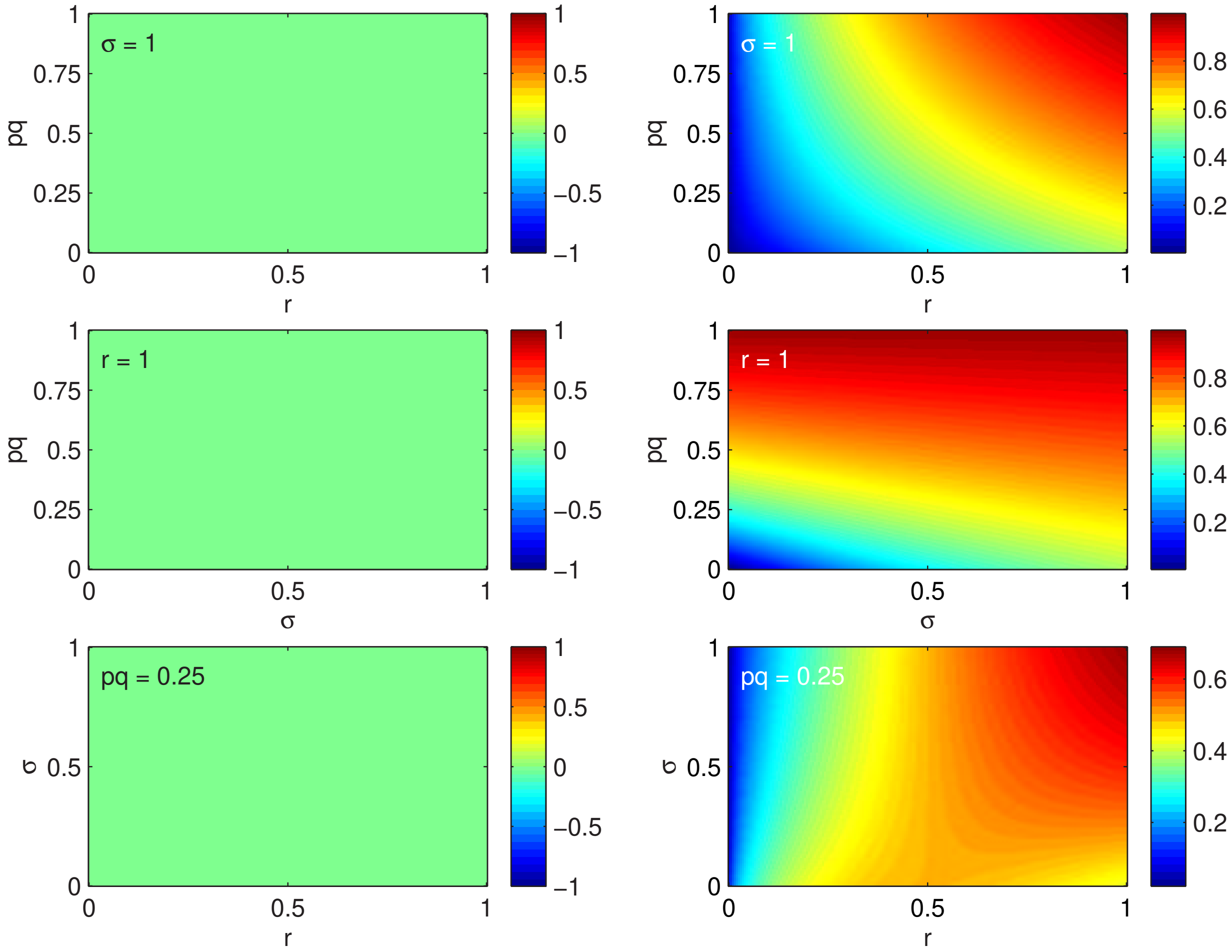

Figure 3.7: *Vortex state attractor strength (left column) and repellor strength (right column) for $p = r_2 = r_1$ and $q = r_4 = r_3$.*

for $r < 0$, in which the vortex state is stable, is referred to as the 'tornadic' region.

A classification of dynamical regimes can be based on the volume of parameter space with nonvanishing transition probability and the magnitude of transition probability in that region. In the domain of positive parameters the dynamical regime for vortex development becomes more significant with increasing parameters r and σ, and the magnitude of transition probability for given parameters r and σ increases towards the upper limit of the tornadic region given by (3.4.4). While a larger tornadic volume of parameter space allows for storm evolution and measurement errors, the magnitude of the transition probability determines the speed at which the vortex state is approached.

By continuity, at the boundaries of the laminar and tornadic regions at least one of the real parts of the corresponding eigenvalues of the linearised system must be zero. At the common boundary $pq = r\sigma/2$ the ground and vortex state coincide (i.e., the fast vortex flow vanishes) and one of the real eigenvalues vanishes.[3] This kind of transition is called

[3]Since for a real dynamical system complex eigenvalues always come in complex conjugate pairs, if the real part vanishes for a single eigenvalue, this eigenvalue must be real.

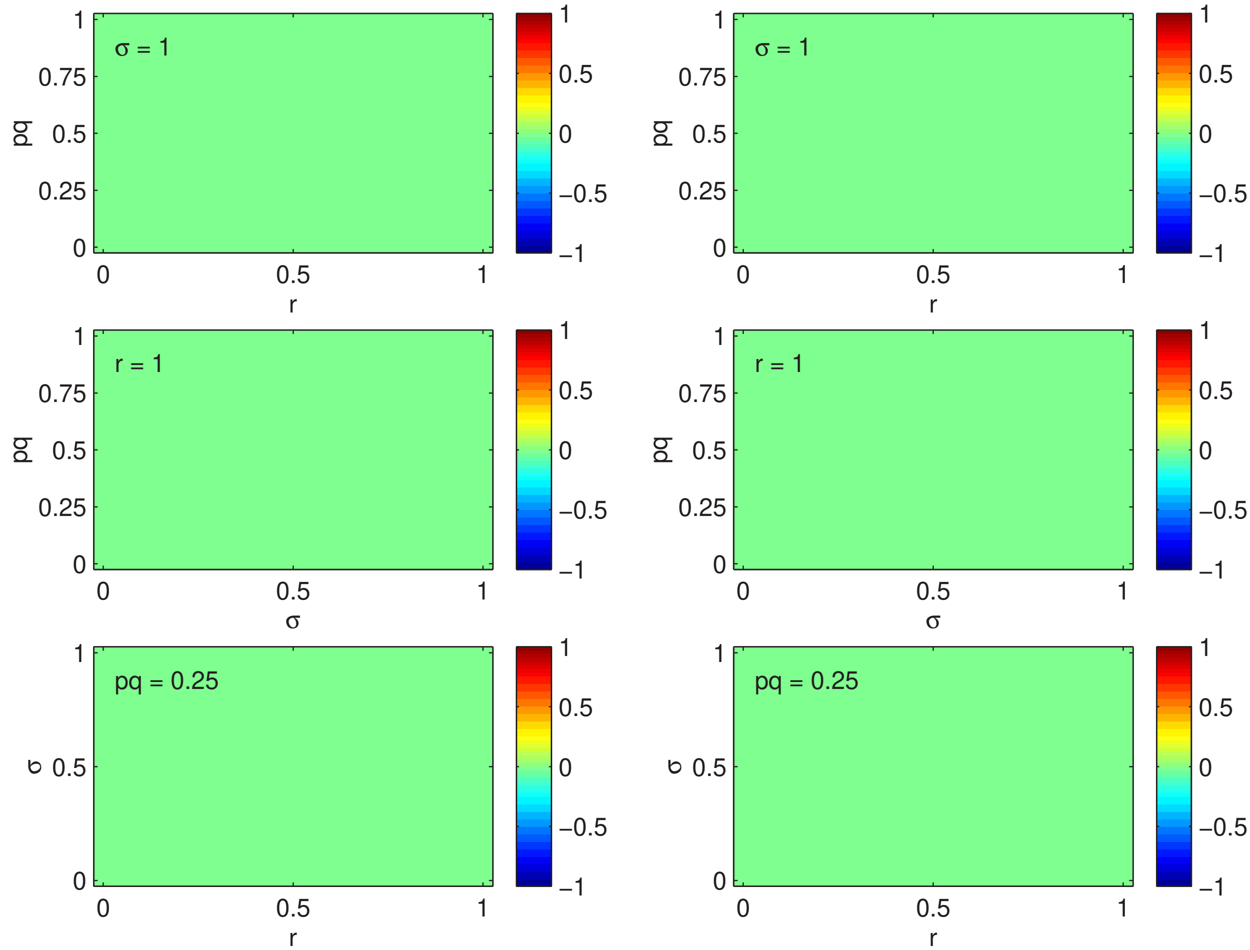

Figure 3.8: *Transition probability from ground to vortex state (left column) and from vortex to ground state (right column) for $p = r_2 = r_1$ and $q = r_4 = r_3$.*

a *steady-state bifurcation*. More specifically, since two equilibria simply exchange stability without being created or destroyed at the bifurcation point, this steady-state bifurcation is a *transcritical bifurcation*. At the outer boundaries of the two dynamical regimes the real parts of a pair of complex conjugate eigenvalues vanishes. These transitions, generally referred to as *Hopf bifurcations*,[4] are associated with the change of stability of only one of the equilibria. At $pq = 0$ the ground state changes stability while the vortex state remains unstable, whereas at $pq = r\sigma$ the vortex state changes stability while the origin remains unstable. The two dynamical regimes with transition boundaries (bifurcation points) are schematically shown on a *bifurcation chart* in Figure 3.11.

In a multiparameter problem such as (3.2.20) there are several different possibilities for any of the transitions to take place. However, by keeping all but one of the parameters constant the simple normal-form dynamics of one-parameter problems derived via centre-

[4]The Hopf bifurcations here differ from those typically encountered in 1-parameter systems in that the stationary solution gaining stability is not created (nor is a stable stationary solution destroyed) at the bifurcation point.

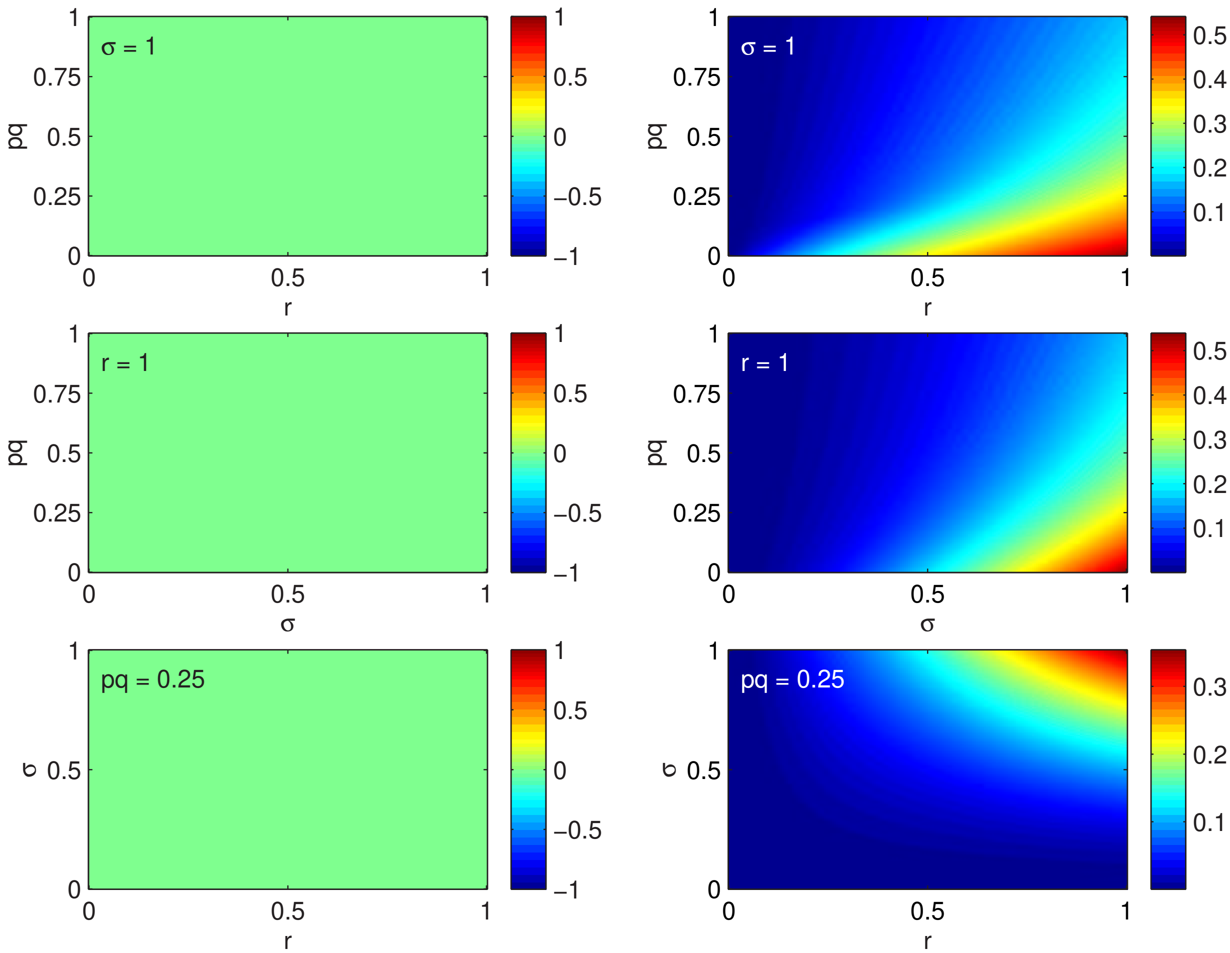

Figure 3.9: *Transition probability from ground to vortex state (left column) and from vortex to ground state (right column) for* $p = r_2 = \pm r_1$ *and* $q = r_4 = \mp r_3$.

manifold reduction can be recovered. For the transcritical bifurcation between the laminar and tornadic regions this is briefly outlined in Appendix A.9. For simplicity consider two one-parameter bifurcation sequences.

In the first case, shown in Figure 3.12, $p, q, \sigma > 0$ are fixed. For $0 < r < pq\sigma^{-1}$ both the ground and vortex state are unstable. With $\bar{X} = \bar{Y} > 0$ and $\bar{Z} < 0$ the vortex is a converging, cyclonically rotating updraft whose intensity (kinetic energy) is continuously decreasing as r approaches $2pq\sigma^{-1}$. As r increases above $pq\sigma^{-1}$ the vortex becomes stable in a Hopf bifurcation and remains stable in the interval $pq\sigma^{-1} < r < 2pq\sigma^{-1}$, while the origin is unstable. At $r = 2pq\sigma^{-1}$ the two equilibria coincide. As r increases above that critical value there is an exchange of stability from the vortex to the ground state. Since $\bar{X} = \bar{Y} < 0$ and $\bar{Z} > 0$ the unstable vortex now is a diverging, anticyclonically rotating downdraft whose intensity continuously increases with r.

Similarly the case where $p, r, \sigma > 0$ are fixed and q varies can be analysed. This situation is shown on the second bifurcation diagram in Figure 3.13. For $q < 0$ both equilibria are unstable. The vortex is a diverging, anticyclonically rotating downdraft whose intensity is

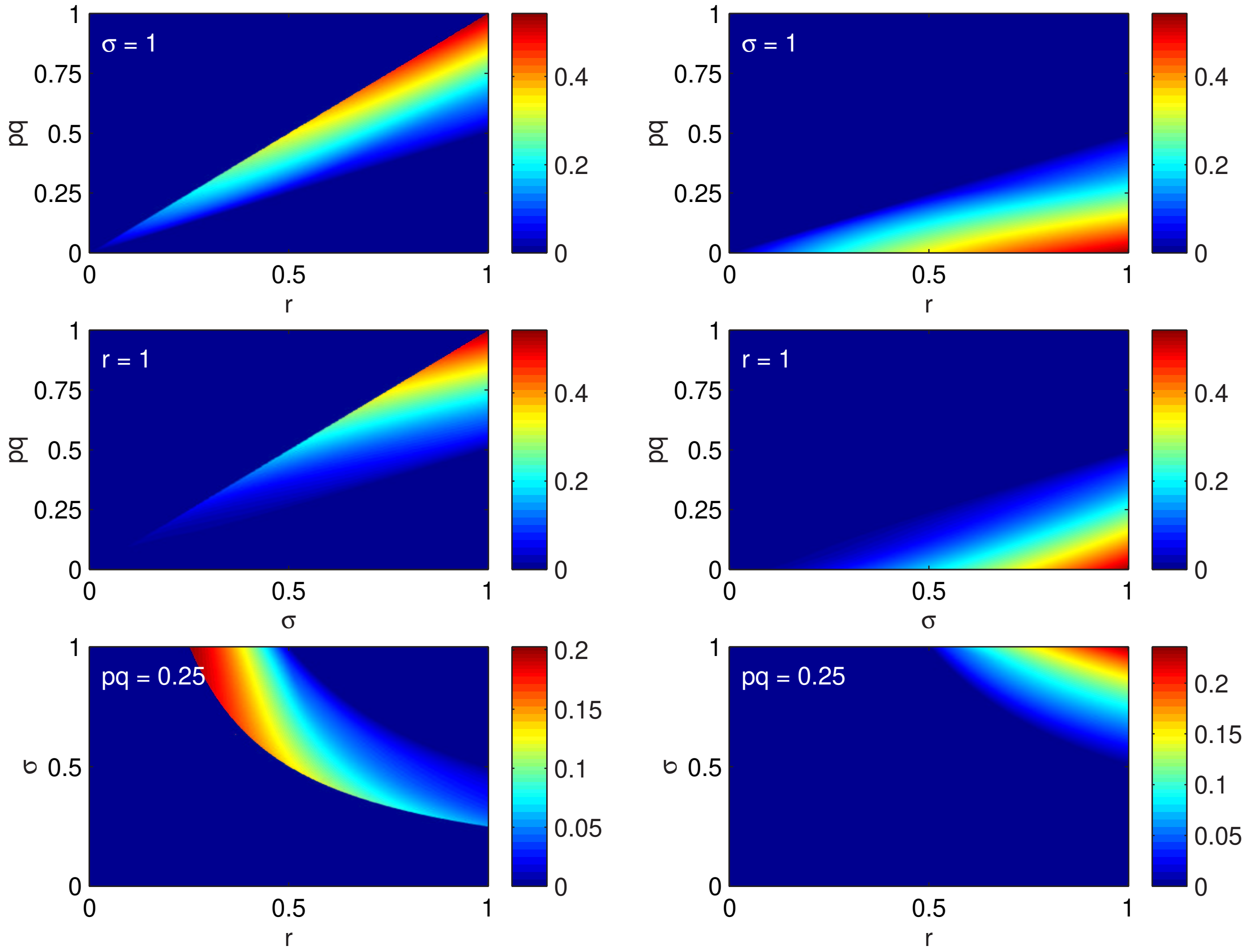

Figure 3.10: *Transition probability from ground to vortex state (left column) and from vortex to ground state (right column) for $p = r_2 = -r_1$ and $q = r_4 = -r_3$.*

continuously decreasing as q approaches $r\sigma/2p$. As q increases above zero the ground state gains stability in a Hopf bifurcation and remains stable until q reaches $r\sigma/2p$, where it loses stability in a transcritical bifurcation to the vortex state. At the bifurcation point the vortex flow vanishes and increases in intensity as a converging, cyclonically rotating updraft as q increases above its critical value. The vortex state remains stable until q reaches $r\sigma p^{-1}$, where it loses stability again in a second Hopf bifurcation.

Due to the reflectional symmetry with respect to the parameter space origin the same bifurcations occur with $r < 0$ if the stability criteria (3.4.2) and (3.4.4) are replaced by (3.4.3) and (3.4.5).

The question now is if these bifurcations are *generic*, i.e., if they are robust in the sense that they also occur in a slightly perturbed system. It is easy to verify that by adding arbitrary small terms linear or quadratic in any of the phase space variables to any of the equations in (3.2.20) the bifurcations persist. The nontrivial stationary solution and the bifurcation points are simply shifted by a small amount depending on the perturbation of the system. Since the bifurcations are generic with respect to six parameters they are

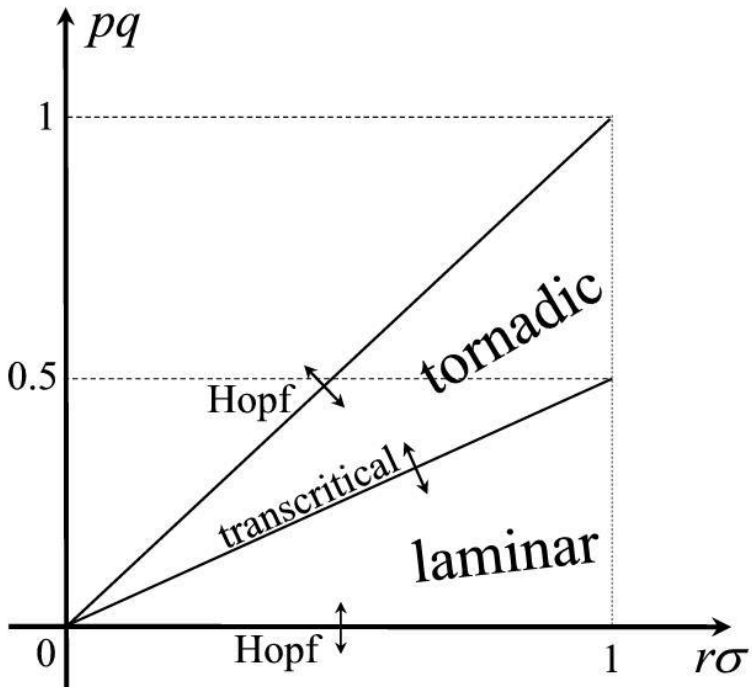

Figure 3.11: *Bifurcation chart showing dynamical regimes and transition boundaries in the positive parameter plane.*

codimension-six bifurcations, i.e., the codimension of system (3.2.20) is six. The system (3.2.20) itself is generic in the sense that it is neither symmetric in any of the phase space variables nor Hamiltonian.

With $p = r_2 = -r_1$ and $q = r_4 = -r_3$ the dynamical system (3.2.20) becomes

$$\begin{aligned} \dot{X} &= -rY - pZ \\ \dot{Y} &= rX + pZ \\ \dot{Z} &= XY - q(X + Y) - \sigma Z \ , \end{aligned} \tag{3.4.6}$$

with stationary solutions

$$\bar{X} = \bar{Y} = -\frac{p}{r}\bar{Z} = 2q - \frac{r\sigma}{p} \ , \tag{3.4.7}$$

and a critical value $q_c = r\sigma/2p$ of q at the transcritical bifurcation. With $\sigma > 0$ it follows from the criteria (3.4.4) and (3.4.5) for stable vortex states[5] that the sign of the stationary solutions $\bar{X} = \bar{Y}$ only depends on the sign of the product pr, while $\bar{Z} < 0$ for all parameter values within the tornadic range. The stable vortex states may therefore represent

[5] As it can be seen from Figure 3.5, since ground and vortex state have nonoverlapping regions of stability, the criteria for stable vortex states are identical with those for a nonvanishing transition probability from the ground state.

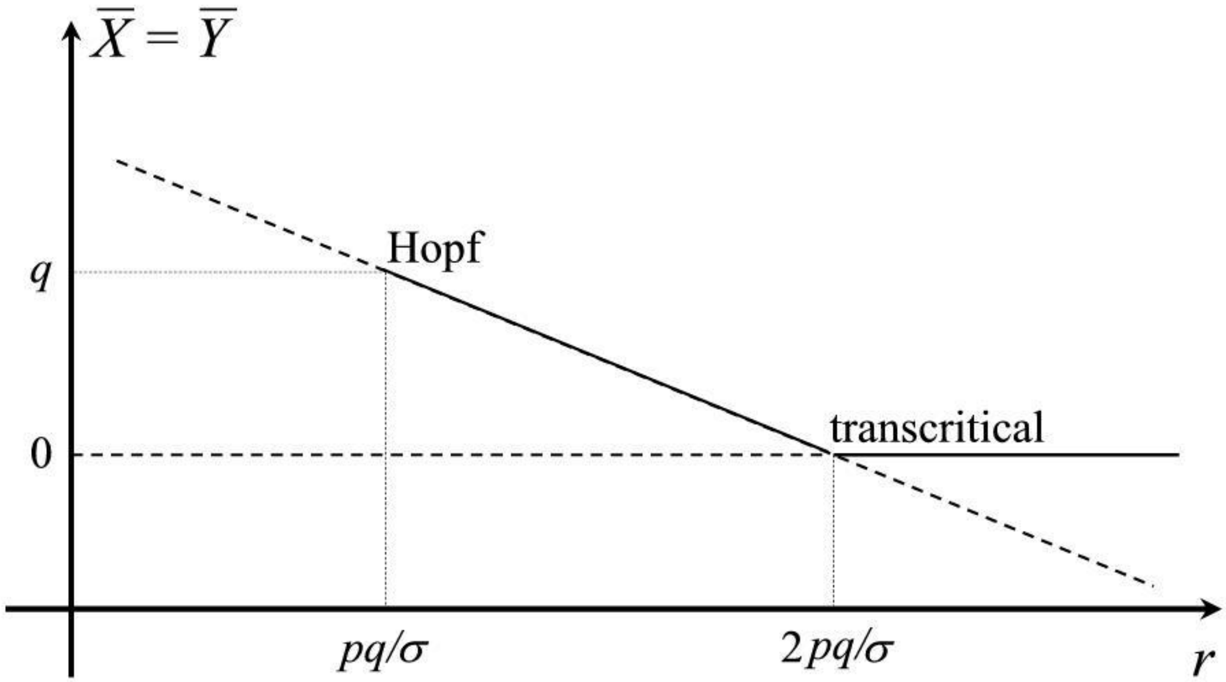

Figure 3.12: *Bifurcation diagram with respect to parameter r. The positions of the stable equilibria are shown by solid lines, while the positions of the unstable equilibria are shown by dashed lines.*

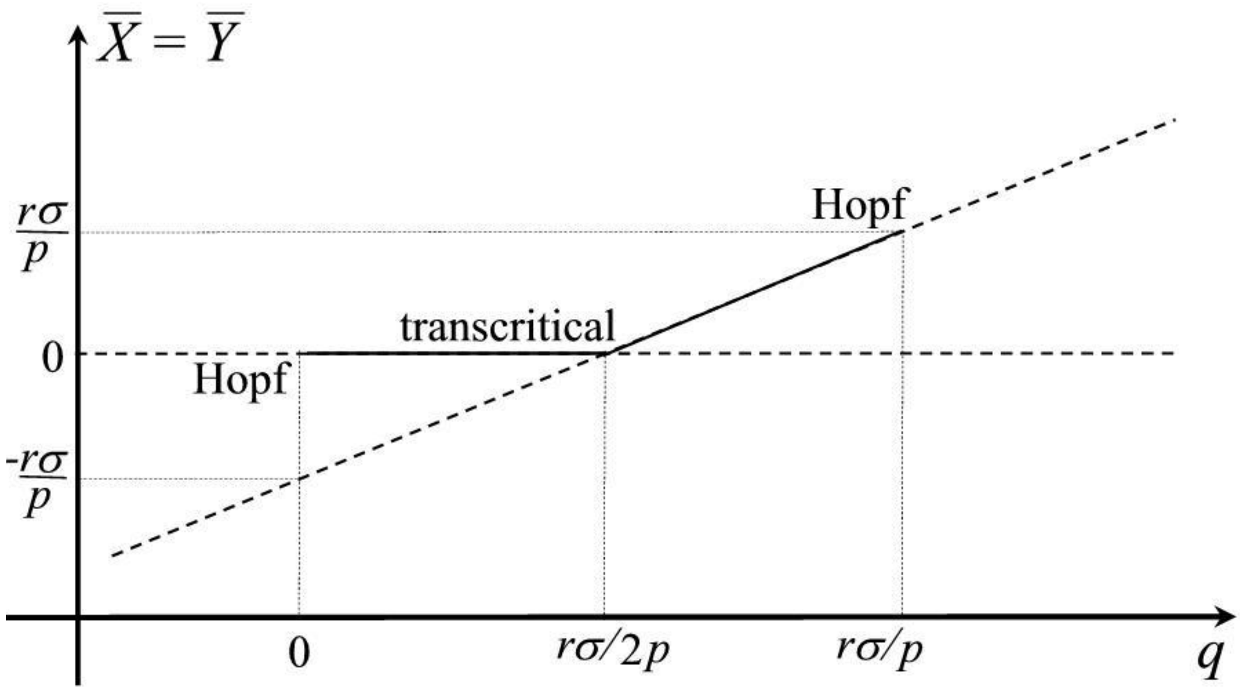

Figure 3.13: *As in Figure 3.12 but for bifurcations with respect to parameter q.*

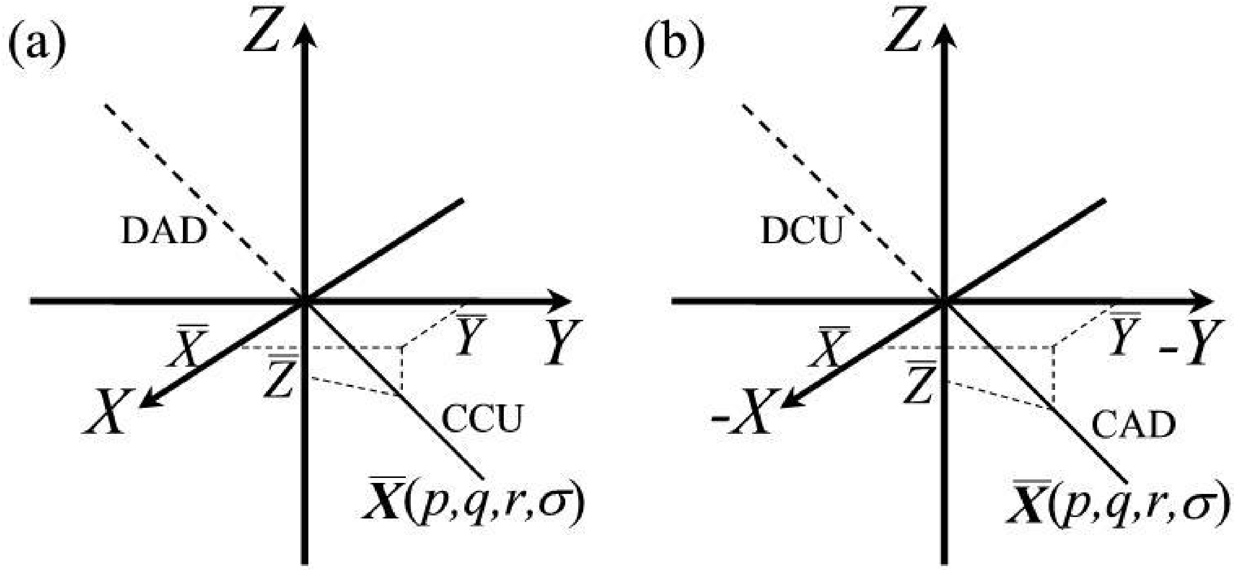

Figure 3.14: *Locations of vortex equilibria in phase space and their stability. The solid lines indicate stable equilibria and the dashed lines unstable equilibria. (a)* $\operatorname{sig} p = \operatorname{sig} r$*, the stable equilibria are CCUs, and the unstable equilibria are divergent anticyclonically rotating downdrafts (DADs); (b)* $\operatorname{sig} p = -\operatorname{sig} r$*, the stable equilibria are CADs, and the unstable equilibria are divergent cyclonically rotating updrafts (DCUs).*

convergent cyclonically rotating updrafts (CCUs) with $\operatorname{sig} p = \operatorname{sig} r$, or anticyclonically rotating downdrafts (CADs) with $\operatorname{sig} p = -\operatorname{sig} r$.[6] The locations in phase space of the vortex equilibria and their stability for $\operatorname{sig} p = \operatorname{sig} r$ and $\operatorname{sig} p = -\operatorname{sig} r$ are shown in Figure 3.14.

To get an idea about the qualitative flow in phase space it is best to separate the system into smaller components. Considering only the linear terms in X and Y in the $\dot{X}$ and $\dot{X}$ equations gives the system

$$\begin{aligned} \dot{X} &= -rY \\ \dot{Y} &= rX \\ \dot{Z} &= 0 \ , \end{aligned} \tag{3.4.8}$$

which is simply a cyclonically ($r > 0$) or anticyclonically ($r < 0$) rotating, nondiverging vortex over the origin in the horizontal plane with vanishing vertical velocity, where the continuous string of stationary solutions $(0, 0, Z)$ with arbitrary Z lies along the vortex axis. Under the coordinate transformation

$$\begin{pmatrix} X \\ Y \end{pmatrix} \mapsto \begin{pmatrix} X \\ Y \end{pmatrix} + \frac{p}{r} Z \begin{pmatrix} 1 \\ 1 \end{pmatrix} \ , \tag{3.4.9}$$

with

$$\begin{pmatrix} \dot{X} \\ \dot{Y} \end{pmatrix} \mapsto \begin{pmatrix} \dot{X} \\ \dot{Y} \end{pmatrix} \ , \tag{3.4.10}$$

[6] Anticyclonically rotating updrafts or cyclonically rotating downdrafts have negative helicity in a right-handed frame of reference and are therefore not represented by the positively helical vortex waves.

the system (3.4.8) becomes

$$\begin{aligned}\dot{X} &= -rY - pZ\\ \dot{Y} &= rX + pZ\\ \dot{Z} &= 0\ .\end{aligned} \tag{3.4.11}$$

On a horizontal plane $Z = const.$ the vortex centre is shifted to $-pZ/r$. The steady solutions $\bar{X} = \bar{Y} = -pZ/r$ therefore lie along the axis $(p/r, p/r, -1)$ of a slanted vortex. With $\dot{Z} = XY - q(X+Y) - \sigma Z$, as in the actual system (3.4.6), the horizontal flow in each plane $Z = const.$ remains unchanged but the continuous line of stationary solutions in the vortex centre now reduces to the two discrete stationary solutions $(0,0,0)$ and (3.4.7).

To determine if for parameters in the tornadic region small perturbations from the origin really lie within the basin of attraction of the vortex equilibrium, phase space trajectories have to be explicitly calculated. For $\operatorname{sig} p = \operatorname{sig} r$, the case of a cyclonically rotating updraft over the origin in physical space, Figures 3.15, 3.16, and 3.17 show ensembles of trajectories starting from near the phase space origin for values of q on or near the transcritical bifurcation points between the laminar and tornadic regions. To be able to compare the speed of the transition between equilibria *supercriticality* s is defined as a measure of the bifurcation parameter relative to its critical value, e.g. q/q_c.[7] The integration time is 40 nondimensional time units (NTU). Scaled to physical variables as in Section 3.5 this corresponds to a period of 2 min. The trajectories were calculated with a forth-order Runge-Kutta scheme and a time-step of 0.01 NTU.

For supercritical parameter values there exist trajectories that leave the origin and are attracted by the stable vortex equilibrium. These trajectories rapidly approach the line $(p/r, p/r, -1)$ leading straight into the fixed point, indicating that the linearised flow around the vortex equilibrium only has real negative eigenvalues. As a result the two Beltrami vortex amplitudes proportional to X and Y increase proportionally sufficiently far enough away from the origin. Therefore the vortex really is generated as a flow structure. After a short transition period the two vortex amplitudes become practically identical forming a symmetric vortex which intensifies as the phase space trajectory approaches the stable fixed point.

As usual for weakly nonlinear and weakly dissipative systems such as (3.4.6), as the origin becomes unstable there also exist unbounded trajectories, i.e., initial conditions leading to an essentially exponential growth in time of some of the phase space variables. Some of these trajectories are shown in Figure 3.18. Unlike for the bounded trajectories there lies no stable stationary state 'in the way' of the unbounded trajectories leading away from the origin. The line towards which they are all attracted approaches a tangent vector of $\left(\dot{X}, \dot{Y}, \dot{Z}\right) \propto (-1, 0, 1)$ as $Z \to \infty$. Clearly, in the case of fluid flow these trajectories have no physical interpretation. The question therefore is if the initial conditions leading to these unbounded trajectories are physically relevant.

[7] This definition is valid if $q_c \neq 0$. If $q_c = 0$, as at the first Hopf bifurcation, *subcriticality* for q near q_c can be defined as q_c/q. The prefixes 'sub' and 'super' are relative of course, and in this case refer to the ground to vortex state transition.

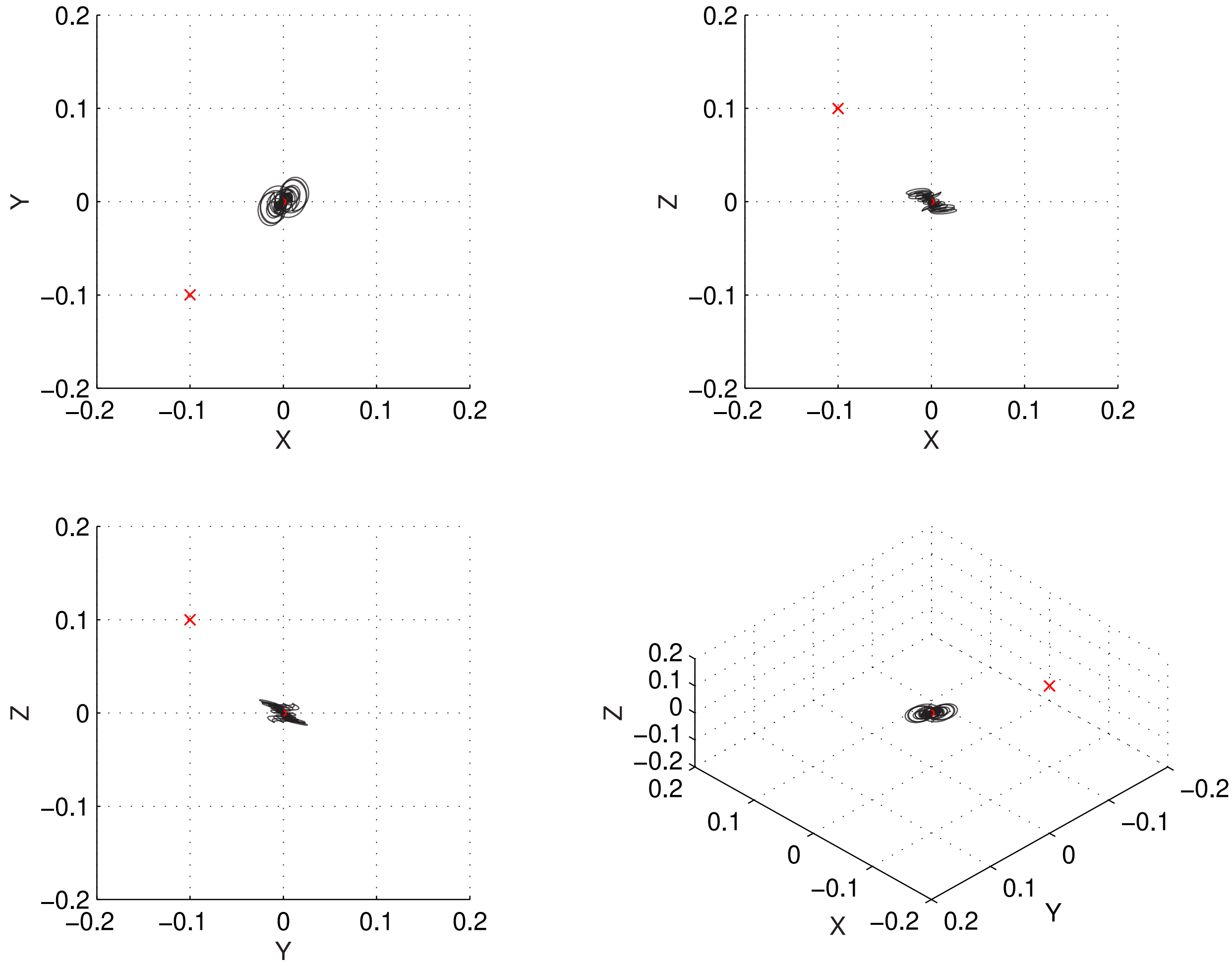

Figure 3.15: *Phase space trajectories for a supercriticality of $s = 0.8$. The ground state is stable and small initial perturbations are damped out. The ground state is marked by symbol $\circ$, and the vortex state is marked by symbol $\times$.*

For all parameter values within the tornadic region all trajectories with initial perturbations from the origin such that $Z < 0$ are attracted towards the fixed point, while for initial perturbations with $Z > 0$ trajectories are unbounded. For $\operatorname{sig} p = \operatorname{sig} r$, analysing the trajectories for initial perturbations in the horizontal plane $Z = 0$, the corresponding initial flows in physical space fall into two categories. For

$$(X(0), Y(0), Z(0)) \in \{(\pm\varepsilon, 0, 0); (0, \pm\varepsilon, 0) |\ \varepsilon > 0\} \tag{3.4.12}$$

the velocity fields are the straight-line shear flows shown in Figure 3.19. They only differ from each other by a shift of $\pm\pi\chi^{-1}$ along any of the horizontal directions or by a 90-degree rotation. Depending on where within the vortex around the origin in phase space the perturbations fall, their trajectories are either swept inside the vortex centre and towards the stable fixed point or in the opposite direction in which case they follow the unbounded

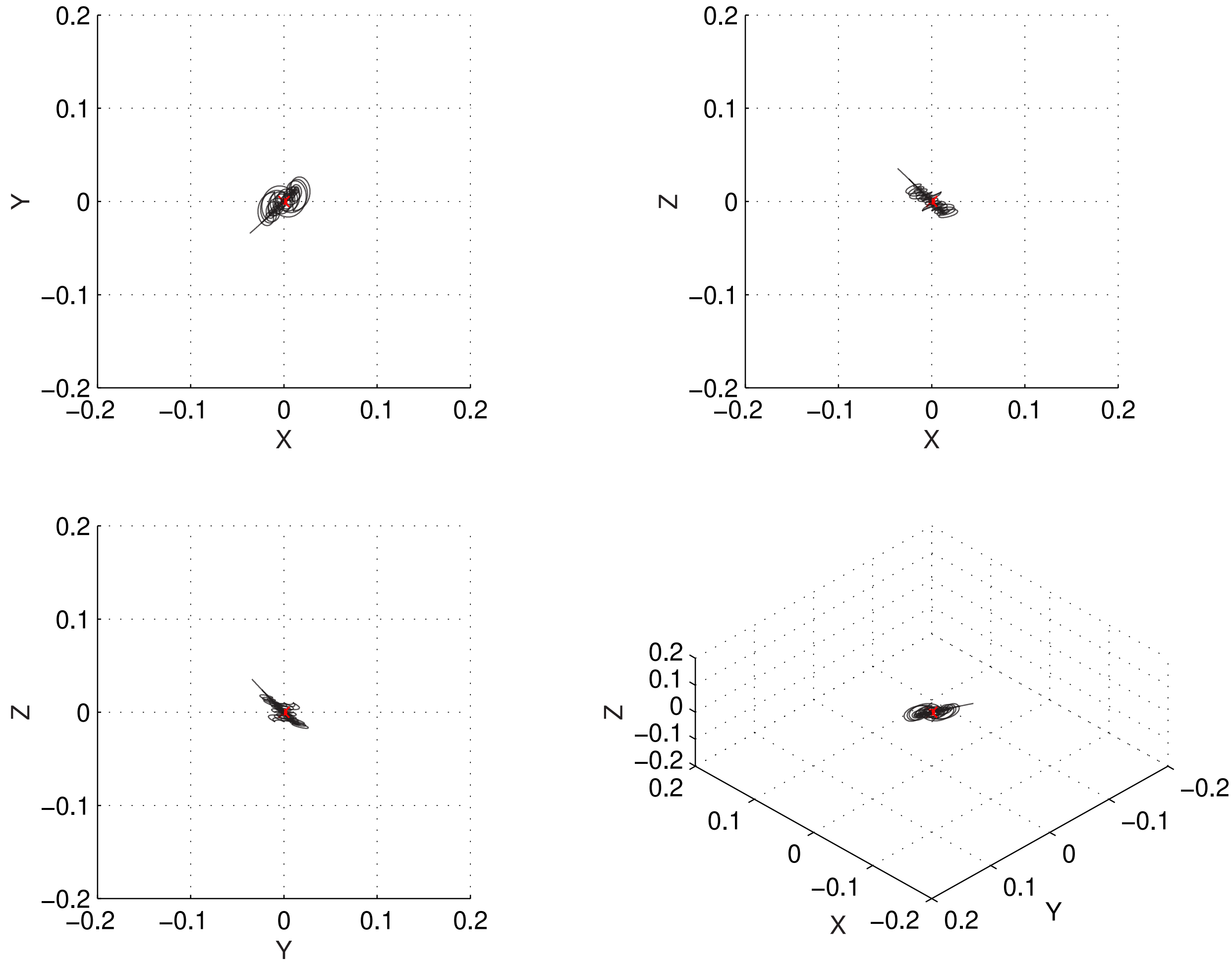

Figure 3.16: *Phase space trajectories at criticality ($s = 1$).*

line attractor towards infinity. For

$$(X(0), Y(0), Z(0)) \in \{(\pm\varepsilon, \pm\varepsilon, 0); (\pm\varepsilon, \mp\varepsilon, 0) | \, \varepsilon > 0\} \tag{3.4.13}$$

the velocity fields are shown in Figures 3.20. They are a periodic pattern of counterrotating updrafts and downdrafts that only differ from each other by a shift of $\pm\pi\chi^{-1}$ along the horizontal directions. Dynamically however, as for the initial perturbations satisfying (3.4.12), they are very different. For $(X(0), Y(0), Z(0)) = (\varepsilon, \pm\varepsilon, 0)$ the phase space trajectories tend towards the fixed point, whereas for $(X(0), Y(0), Z(0)) = (-\varepsilon, \pm\varepsilon, 0)$ the phase space trajectories are unbounded.

Velocity fields represented by Fourier series are always periodic in space. As discussed in Section 2.5.1 they are calculated over a given finite domain and for aperiodic velocity fields are valid approximations only in the interior of that domain. Moreover, the fast expansion coefficients are associated with a flow phenomenon of much smaller extent than

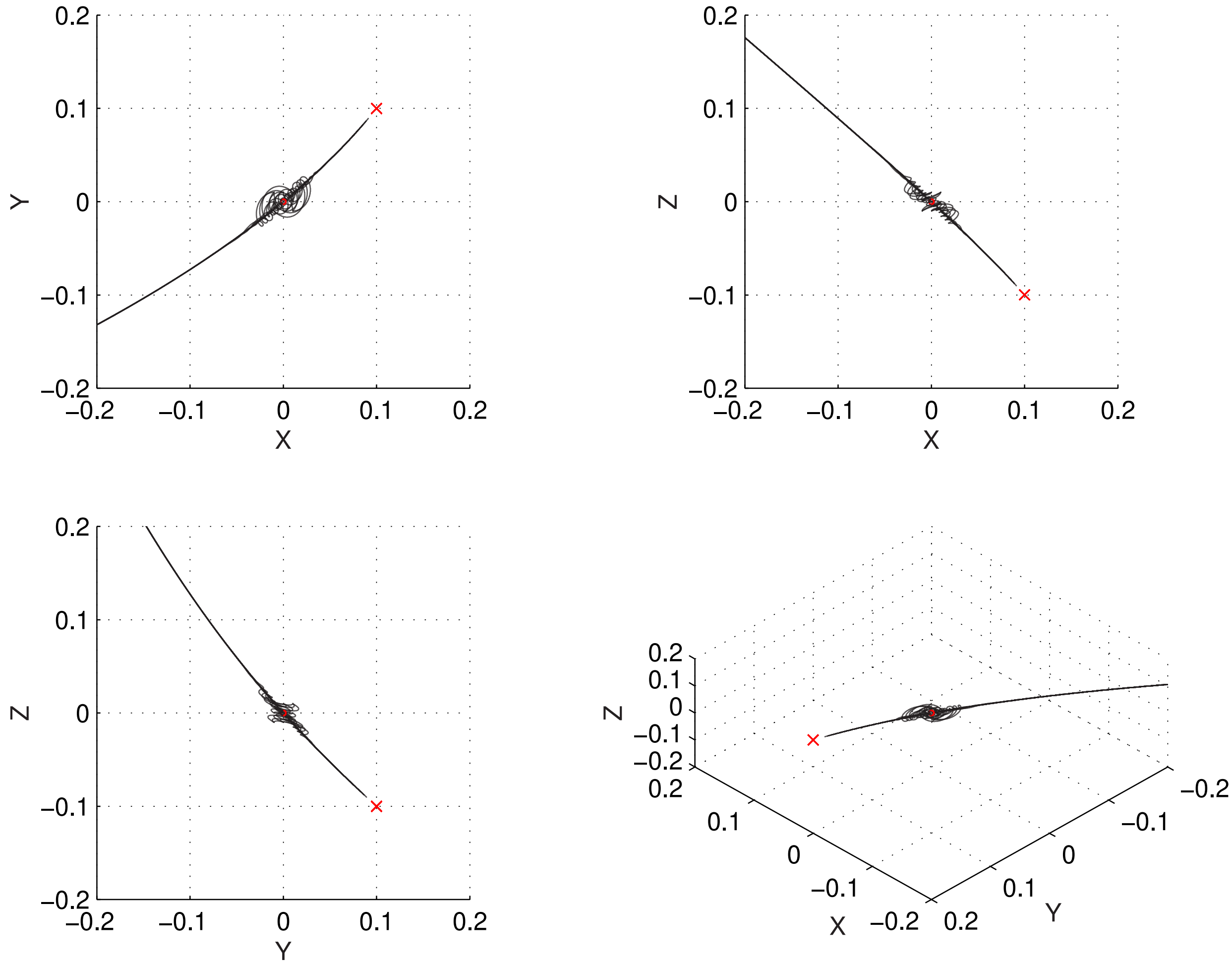

Figure 3.17: *Phase space trajectories for $s = 1.2$. The vortex state is stable and some initial perturbations from the ground state are attracted towards it.*

the total domain over which the expansion coefficients are calculated. Based on the discussion in Section 2.6.1 the fast expansion coefficients are therefore part of a continuous spectrum associated with a fluid volume of small extent in which all waves add up to generate a locally intense vortex while cancelling each other out away from that domain. For an equilibrium state representing a vortex over the origin in physical space the velocity fields corresponding to the various initial states must therefore be interpreted in a horizontal domain $\{(x, y)|\ x \in [-\pi\chi^{-1}, \pi\chi^{-1}];\ y \in [-\pi\chi^{-1}, \pi\chi^{-1}]\}$. Since the real parts of the fast expansion coefficients of the vortex waves are set equal to zero there can be no phase changes and therefore no continuous shifts of the vortex centres. In the highly truncated system it is therefore not possible that vortices move into the domain of the final vortex state.

The flows around the origin in physical space for the different cases of initial perturbations from the origin in phase space discussed above for $\operatorname{sig} p = \operatorname{sig} r$ are schematically shown in Figure 3.21. Initial perturbations corresponding to straight-line or hyperbolic shear flows around the origin in physical space may either lead to bounded or unbounded phase space

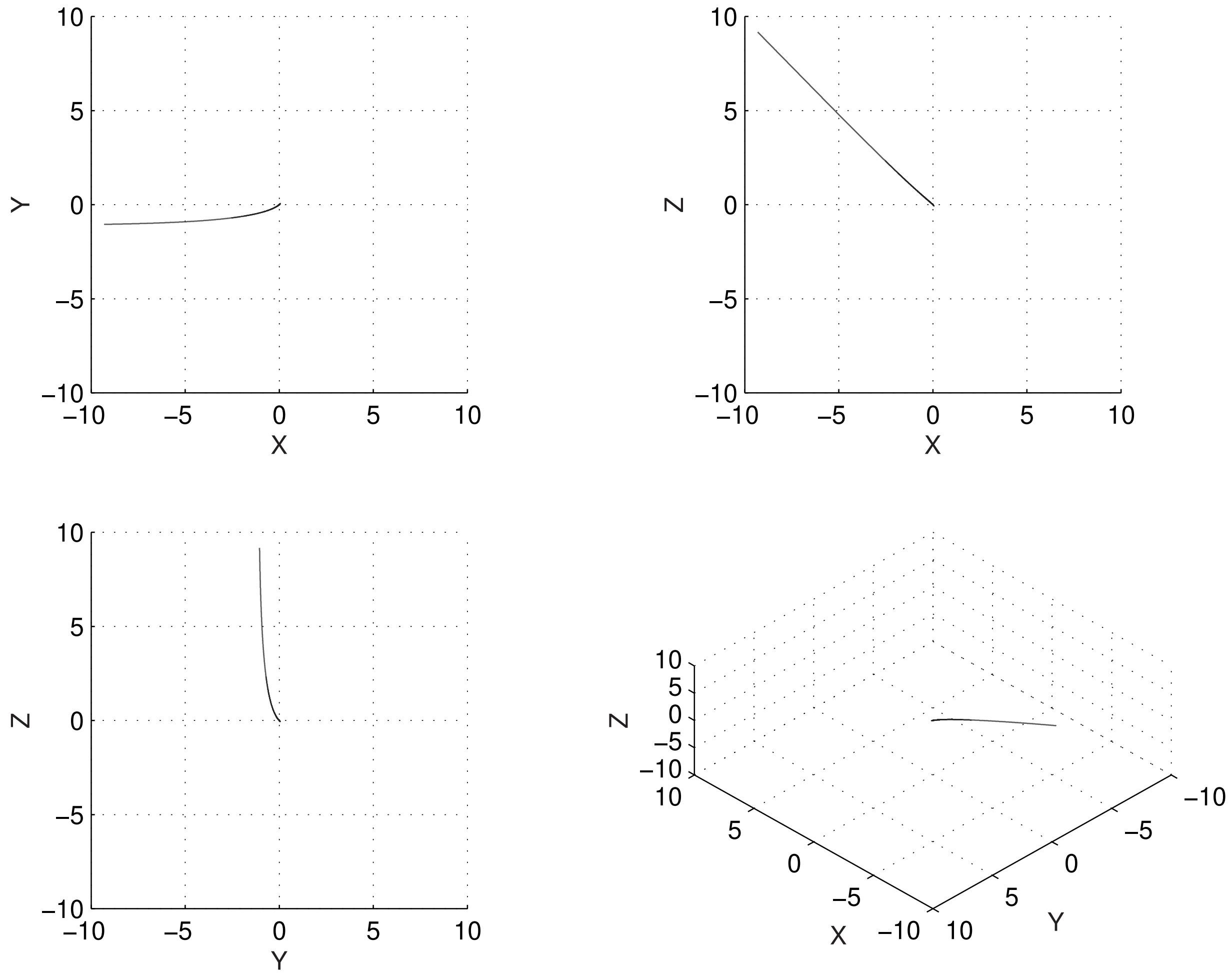

Figure 3.18: *The same trajectories as in Figure 3.17 shown over a larger phase-space region and calculated only over a period of 27 NTU. Due to the larger numbers involved the time-step was reduced to 0.001 NTU.*

trajectories. An initially weak cyclonically rotating updraft steadily intensifies and reaches a stationary state, while an anticyclonically rotating downdraft develops into approximately exponentially intensifying countermoving and meandering jets with strong shear zones about the origin, i.e., into an unphysical state with unbounded phase space trajectory. Similarly, the initial perturbation $(X(0), Y(0), Z(0)) = (0, 0, -\varepsilon)$, associated with a converging flow around the origin develops into a vortex state, while a diverging flow corresponding to the initial perturbation $(X(0), Y(0), Z(0)) = (0, 0, \varepsilon)$ becomes unbounded. In simplified form it can be said that converging and/or cyclonically rotating updraft perturbations develop into a more intense vortex given the right background flow, whereas diverging and/or anticyclonically rotating downdraft perturbations belong to a set of initial conditions for which the highly truncated system (3.4.6) has unphysical solutions. Therefore, if the various initial states are correctly interpreted in physical space relative to the evolving final vortex state it is apparent that initial conditions that are likely to be found in the thunderstorm on the scale

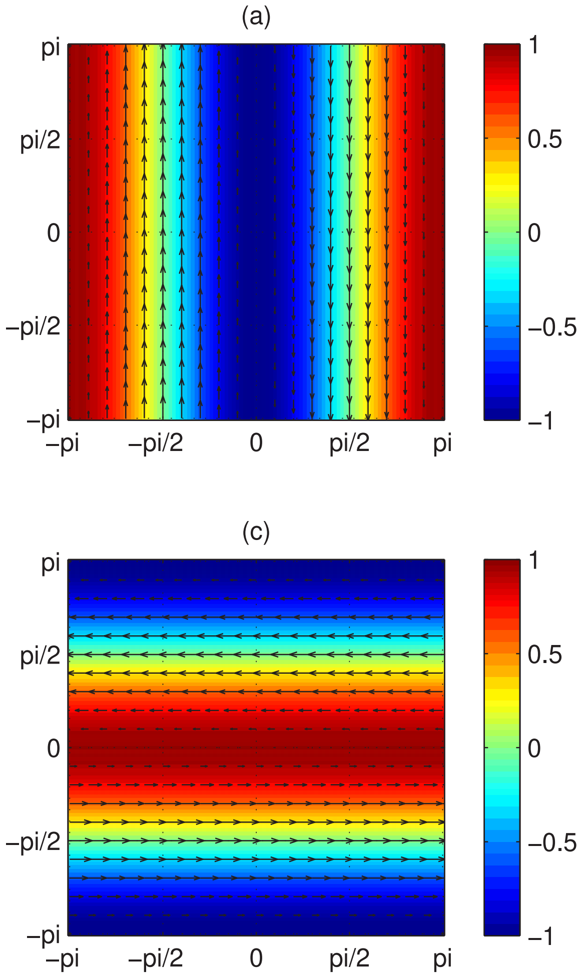

Figure 3.19: *Flows in physical space corresponding to perturbations about the phase space origin with* $\chi = 1$. *Flows in the left column have unbounded trajectories, while flows in the right column develop into a CCU at the origin. In phase space the initial perturbations are (a)* $(-\varepsilon, 0, 0)$, *(b)* $(\varepsilon, 0, 0)$, *(c)* $(0, \varepsilon, 0)$, *and (d)* $(0, -\varepsilon, 0)$.

of a tornado and around the typical locations of tornadogenesis are in fact uniquely associated with a transition from perturbations of the ground state to the vortex state, given the right state of the storm flow. The qualitative analytical results obtained through bifurcation analysis are therefore sufficient to determine if vortex formation from small perturbations takes place or not, and explicit numerical solutions of the low-dimensional dynamical system for specific initial conditions are not required. Moreover, since for an autonomous dynamical system such as (3.2.20) the phase space structure is fixed, the verification of bifurcations by explicit phase space trajectories does not have to be done for every forecast.

There are several unphysical scenarios that are possible in the simple system, whereas several processes that are possible in nature cannot happen. The focus must therefore be on initial and boundary (i.e., background flow) conditions that are physically relevant for tornadogenesis or any vortex phenomenon under consideration. A useful model must then

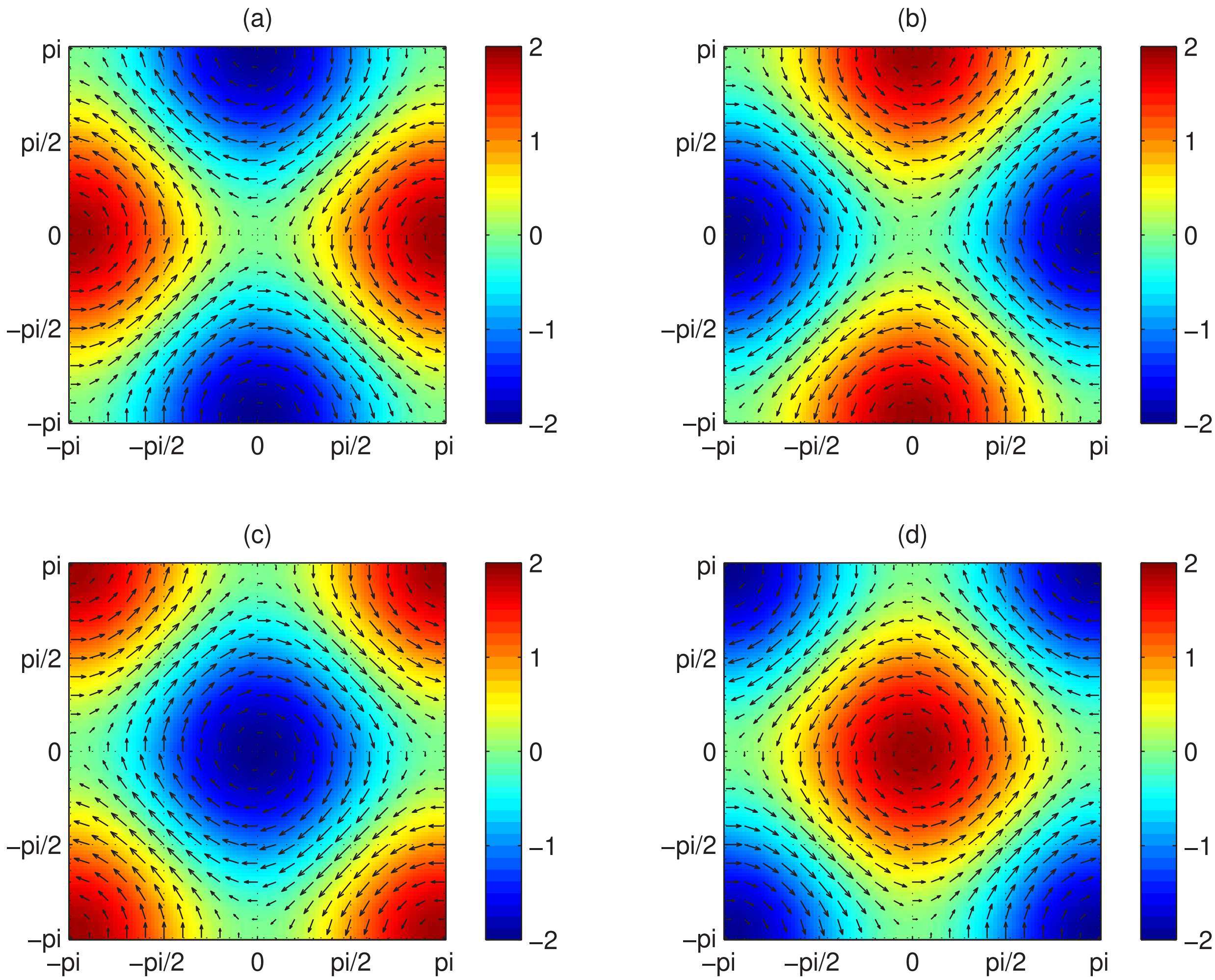

Figure 3.20: *As for Figure 3.19 but for initial phase space perturbations (a)* $(-\varepsilon, \varepsilon, 0)$*, (b)* $(\varepsilon, -\varepsilon, 0)$*, (c)* $(-\varepsilon, -\varepsilon, 0)$*, and (d)* $(\varepsilon, \varepsilon, 0)$*.*

produce physically reasonable results. However, 'physically relevant' initial conditions are determined only relative to the final state. The same results obtained for $\operatorname{sig} p = \operatorname{sig} r$ are also true for $\operatorname{sig} p = -\operatorname{sig} r$ representing an anticyclonically rotating downdraft equilibrium vortex state if 'cyclonically rotating updraft' is replaced with 'anticyclonically rotating downdraft,' and vice versa, in the previous paragraph. In the simple model there is no symmetry breaking mechanism such as buoyancy that favours the formation of either an updraft or downdraft.[8]

In summary, the dynamics in phase space is characterised primarily by the line attractor, on which the two fixed points $(0, 0, 0)$ and $\left(\bar{X}, \bar{Y}, \bar{Z}\right)$ are local disturbances. For bounded, i.e., physically relevant trajectories, significant qualitative changes in the dynamics are due to the exchange of stability between these two equilibrium states.

[8]The favoured formation of cyclonic updraft rotation or anticyclonic downdraft rotation in the simple model is due to the helical truncation of the system and not due to the Coriolis force as in Nature.

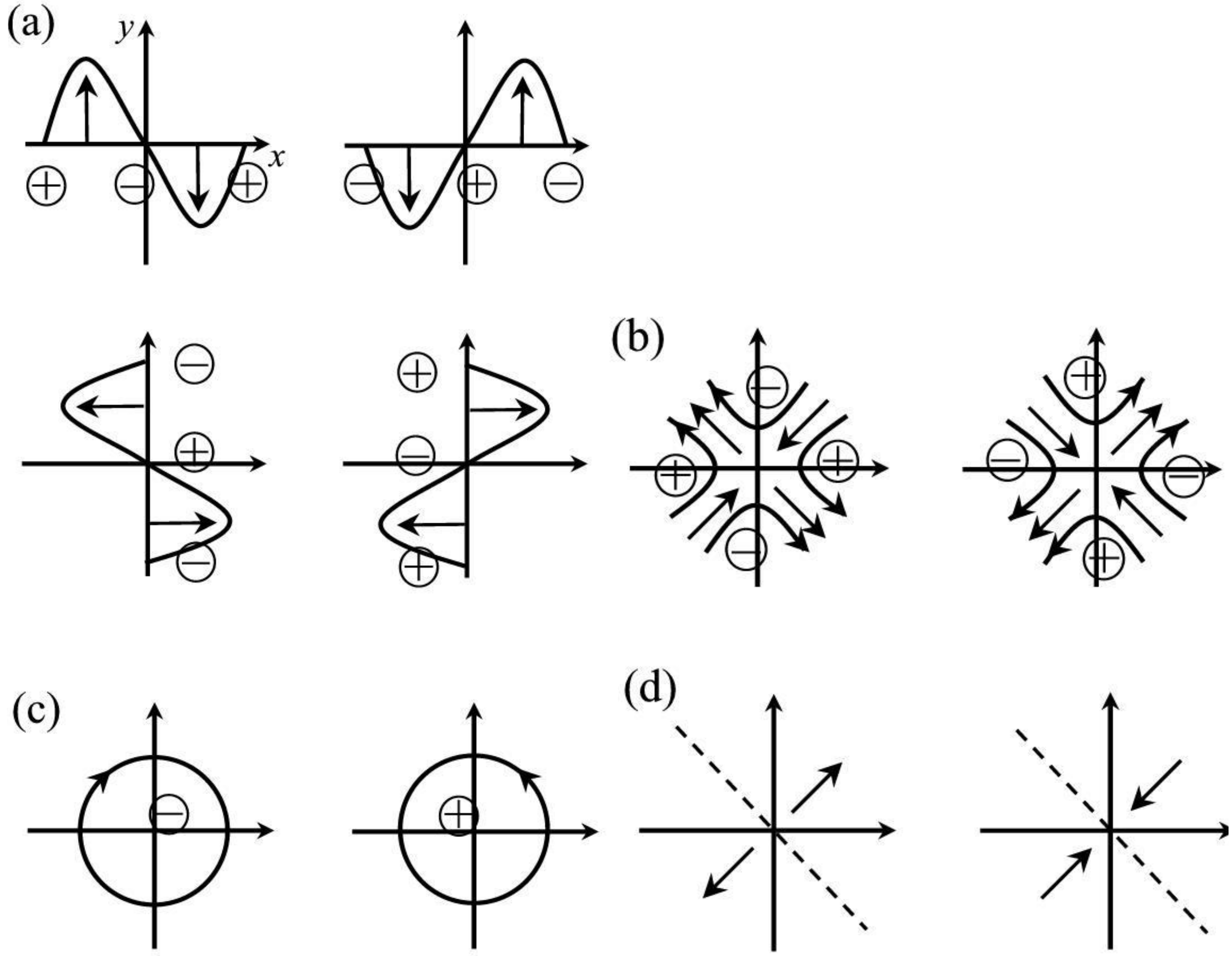

Figure 3.21: *Schematic flow around the origin in physical space corresponding to initial perturbations from the origin in phase space. The symbols* $\oplus$ *and* $\ominus$ *indicate positive or negative vertical velocity, respectively. The initial states on the left of each subfigure have unbounded phase space trajectories, while the flows on the right develop into a stationary CCU at the origin. (a) from top left to bottom right the initial perturbations* $(X(0), Y(0), Z(0))$ *are equal to* $(-\varepsilon, 0, 0)$, $(\varepsilon, 0, 0)$, $(0, \varepsilon, 0)$, *and* $(0, -\varepsilon, 0)$; *(b) initial perturbations* $(-\varepsilon, \varepsilon, 0)$ *and* $(\varepsilon, -\varepsilon, 0)$; *(c) initial perturbations* $(-\varepsilon, -\varepsilon, 0)$ *and* $(\varepsilon, \varepsilon, 0)$; *(d) initial perturbations* $(0, 0, \varepsilon)$ *and* $(0, 0, -\varepsilon)$.

3.5 Environments of Vortex Formation

In the bifurcation scenarios discussed in the previous section vortex formation is described as an instability of the ground state, where the *mathematical* mechanism for the instability is a loss of hyperbolicity of the coinciding equilibria at the critical point of the transcritical bifurcation. To be able to interpret the bifurcation scenario as a real process, *physical* instability mechanisms corresponding to the mathematical instabilities must be identified.

The transcritical bifurcation between laminar and tornadic region taken alone could be interpreted by saying that some forcing, e.g., buoyancy (represented by background updraft strength in the kinematical model) or shear or a combination thereof,[9] must exceed a certain threshold value for the spin-up of an intense vortex. However, as that forcing is increased, at some point a second critical value is reached, in which the vortex state loses stability again in a Hopf bifurcation. If buoyancy or convective instability was the main forcing mechanism it would be hard to imagine that at some point where convection exceeds a certain intensity the vortex is destroyed. As long as convection is maintained there is a convergence into the vortex centre with tilting of horizontal vortex lines close to the surface and stretching of vertical vortex lines in the updraft, and therefore an intensification of the existing circulation. If on the other hand shear instability is the primary mechanism it is conceivable that a certain minimum amount of shear is required for an initial vortex spin-up. However, if the shear zones persist (as it is assumed) a too strong background shear destroys or prevents the formation of an ordered vortex. Therefore it is reasonable to suspect that in the simple model shear rather than convective instability is responsible for vortex formation.

To interpret the different parameter values as certain slow background flows emphasis must then be on the description of shear flows. The separation of slow background flow and fast perturbation flow on the same spatial scale is therefore not only with respect to timescales but also with respect to qualitatively different flow phenomena. While the fast flow is defined to represent a certain vortex instability of the slow background flow and initial shear perturbations are ignored, the slow flow on the scale of the rapidly evolving vortex instability is defined to represent a persistent shear flow, where rotational motion on that scale is ignored. This is consistent with the situation found in typical supercell thunderstorms where prior to tornadogenesis there may be no significant circulation on the tornado scale but intense fronts and shear zones close to the favourite locations of tornadogenesis. Based on this observation it was suggested already in Section 2.4 that tornadoes may be vortical instabilities of these shear zones. In reality of course the initial vortex instability is intensified by convection.

With (2.7.7) and (3.2.5) the slow background flow in explicitly real notation is given by

$$\boldsymbol{u} = 2\sum_{\boldsymbol{q}} \boldsymbol{\alpha}_{\boldsymbol{q}} \cos \boldsymbol{q}\cdot\boldsymbol{x} - \boldsymbol{a}_{\boldsymbol{q}} \sin \boldsymbol{q}\cdot\boldsymbol{x} \tag{3.5.1}$$

where summation is only over linearly independent wave vectors. A particular set of slow expansion coefficients uniquely specifies a set of parameters. The evolution of the slow system is therefore associated with a unique trajectory in parameter space. However, a particular set of parameters does not uniquely specify the background flow. Moreover, only a small

[9] Cf. the discussion of tornado forcing mechanisms in Section 2.4.

number of slow expansion coefficients couple to the few fast expansion coefficients considered in the highly truncated systems. The difference between the slow and fast expansion coefficients is that while most of the slow expansion coefficients are explicitly truncated in the derivation of the dynamical system no assumption is being made about the slow expansion coefficients that are not included in the fast equations of motion. Therefore, in addition to the ununiqueness, the system parameters do not completely specify the background flow. In particular none of the parameters contains both the real and imaginary parts of any of the expansion coefficients. With

$$\boldsymbol{\alpha}_{\boldsymbol{q}} = \boldsymbol{A}_{\boldsymbol{q}} \cos \boldsymbol{q} \cdot \boldsymbol{x}_0 \tag{3.5.2}$$
$$\boldsymbol{a}_{\boldsymbol{q}} = -\boldsymbol{A}_{\boldsymbol{q}} \sin \boldsymbol{q} \cdot \boldsymbol{x}_0 \tag{3.5.3}$$

and $\boldsymbol{A}_{\boldsymbol{q}}$ real, $\boldsymbol{u}$ can be written as

$$\boldsymbol{u} = 2 \sum_{\boldsymbol{q}} \boldsymbol{A}_{\boldsymbol{q}} \cos \boldsymbol{q} \cdot (\boldsymbol{x} - \boldsymbol{x}_0) \ , \tag{3.5.4}$$

where the amplitudes $\boldsymbol{A}_{\boldsymbol{q}}$ and phases $\boldsymbol{q} \cdot \boldsymbol{x}_0$ depend on both $\boldsymbol{\alpha}_{\boldsymbol{q}}$ and $\boldsymbol{a}_{\boldsymbol{q}}$. The phases of the slow background waves are therefore all undetermined.

Not taking into account phase shifts, parameter r,

$$r = \frac{\chi}{2} \left(\gamma_{1,1} - \gamma_{1,-1} \right) \ , \tag{3.2.14}$$

is associated with essentially two types of horizontal shear of vertical velocity: localised neighbouring regions of updrafts and downdrafts or ‘plumes’ for $\gamma_{1,1} = \pm\gamma_{1,-1}$, and straight-line ‘frontal’ shear for $\gamma_{1,1} = 0$ or $\gamma_{1,-1} = 0$. These velocity fields are shown in Figure 3.22. For simplicity, here and in the following it is assumed that the length scale is chose such that $\chi = 1$.

Even under the simplification (3.2.27) the background flows associated with parameter p, for both vortex triads,

$$\begin{aligned} p &= \frac{\chi^2}{4} \left(b_{1,0} + \gamma_{1,0} \right) \\ &= \frac{\chi^2}{4} \left(a_{0,1} - \gamma_{0,1} \right) \ , \end{aligned} \tag{3.5.5}$$

shown in Figure 3.23, are more complex. It was mentioned already in Section 3.3 that $p = 0$ implies a positively helical Beltrami vortex. However, for $p = 0$ nontrivial equilibria do not exist. For $a_{0,1}$ and $b_{1,0}$ nonvanishing the background flow has circulation on the fast vortex scale. For physical reasons, as discussed above, these cases must be excluded. For $a_{0,1} = b_{1,0} = 0$, similar to the cases of $\gamma_{1,1} = \pm\gamma_{1,-1}$, the resulting velocity field has horizontal shear of vertical velocity with localised neighbouring regions of updrafts and downdrafts.

Parameter q,

$$\begin{aligned} q &= 2b_{1,0} + a_{1,0} \\ &= -2a_{0,1} - b_{0,1} \ , \end{aligned} \tag{3.5.6}$$

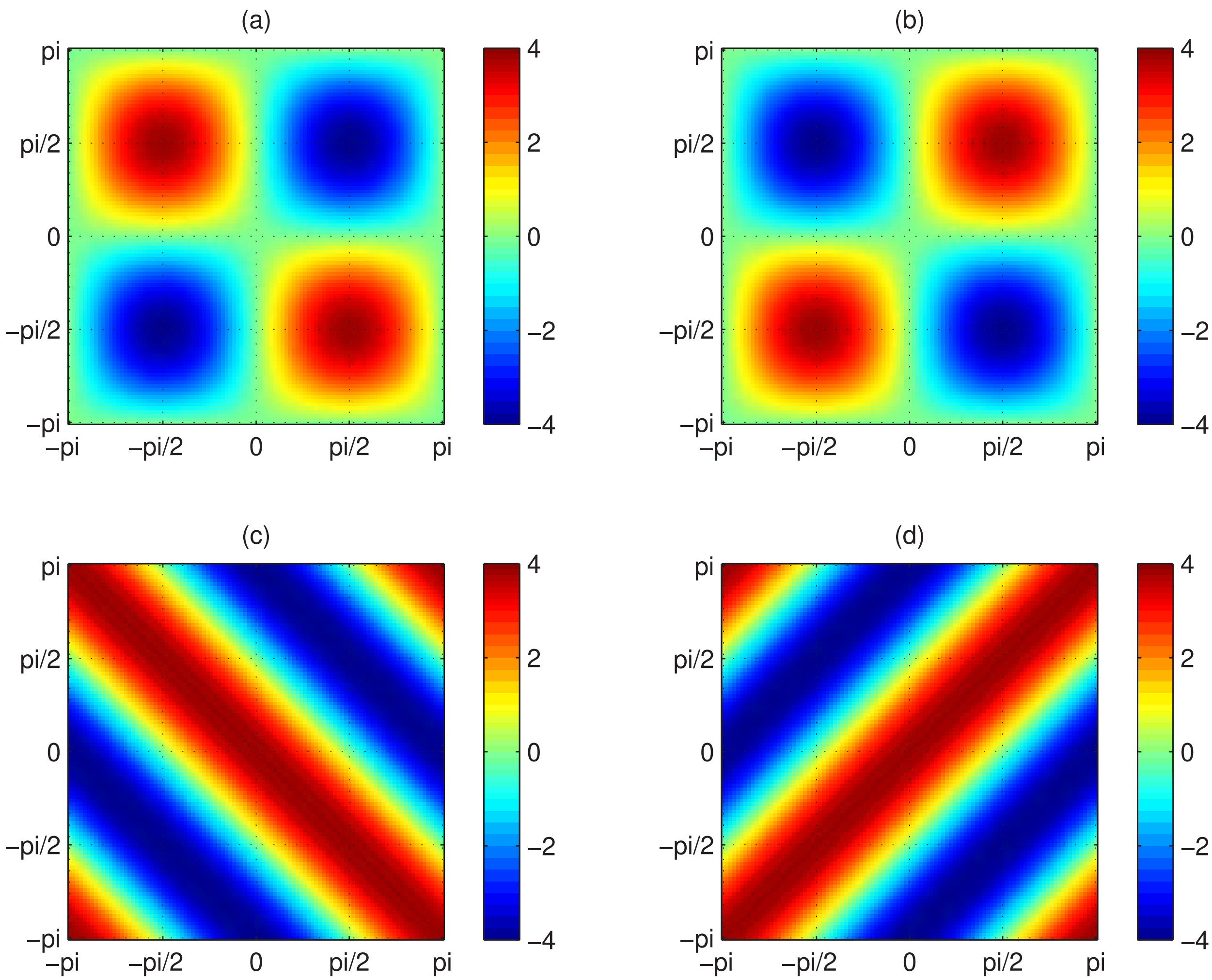

Figure 3.22: *Background flow associated with parameter $r = 1$ (left column) and $r = -1$ (right column): (a) $\gamma_{1,1} = -\gamma_{1,-1} = 1$, (b) $\gamma_{1,1} = -\gamma_{1,-1} = -1$, (c) $\gamma_{1,1} = 2$ and $\gamma_{1,-1} = 0$, (d) $\gamma_{1,1} = 0$ and $\gamma_{1,-1} = 2$.*

for triad T1, and

$$\begin{aligned} q &= 2b_{1,0} - a_{1,0} \\ &= -2a_{0,1} + b_{0,1} \end{aligned} \tag{3.5.7}$$

for triad T2 with $a_{0,1} = b_{1,0} = 0$ is easy to interpret. As shown in Figure 3.24 it creates a horizontal hyperbolic shear flow around the origin. The shear flows for the two vortex triads only differ from each other by a rotation about the vertical axis of 90°. Parameter σ,

$$\sigma = \chi\left(a_{2,2} + b_{2,2}\right) \ , \tag{3.2.19}$$

for triad T1, and

$$\sigma = \chi\left(a_{2,-2} - b_{2,-2}\right) \tag{3.2.26}$$

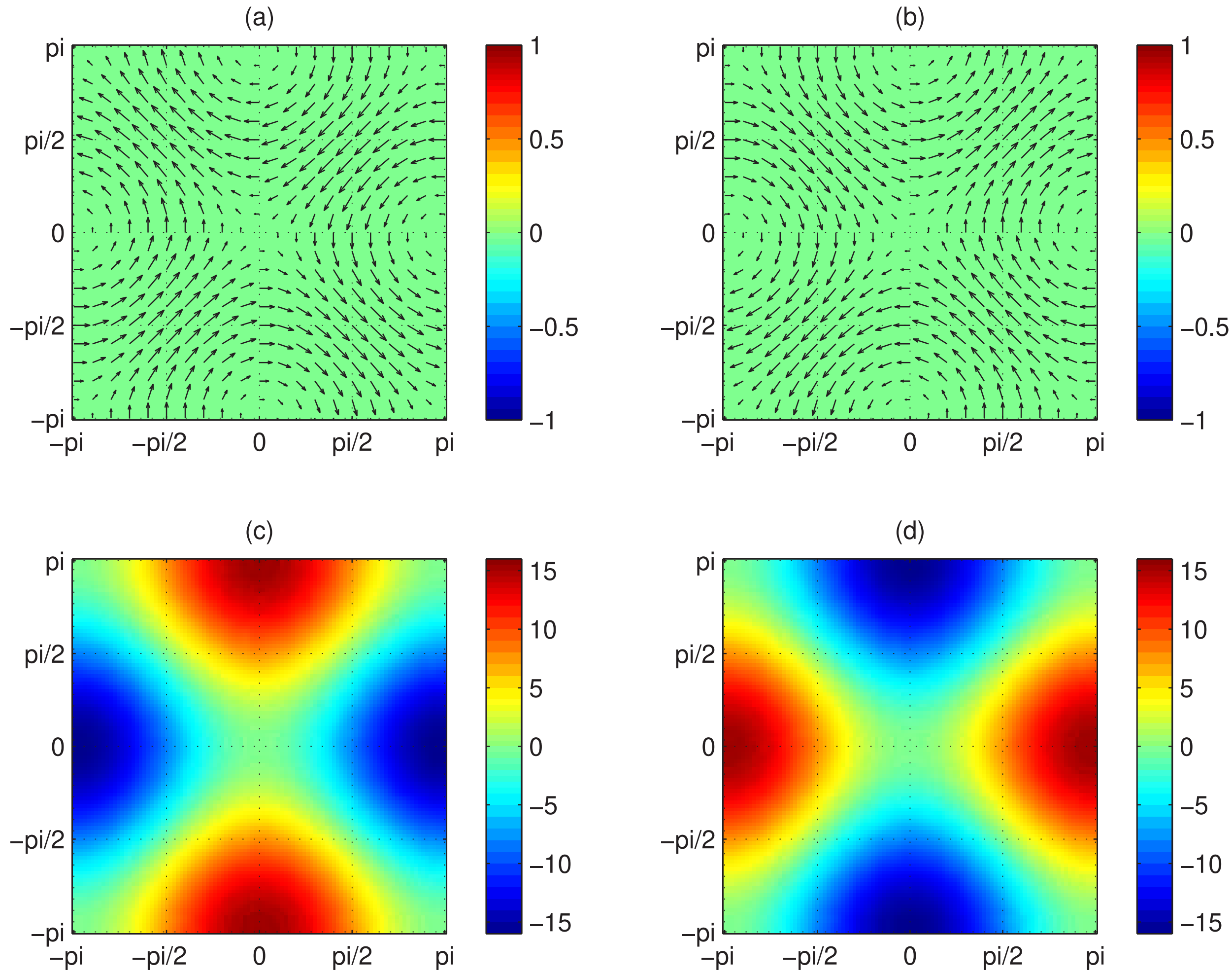

Figure 3.23: *Background flow associated with parameter* $p = 1$ *(left column) and* $p = -1$ *(right column): (a)* $a_{0,1} = b_{1,0} = 4$*, (b)* $a_{0,1} = b_{1,0} = -4$*, (c)* $\gamma_{1,0} = -\gamma_{0,1} = 4$*, (d)* $\gamma_{1,0} = -\gamma_{0,1} = -4$*.*

for triad T2, also does not represent qualitatively different background flows. In both cases it is associated with straight-line convergence near the origin for all $\{a_{2,2}, b_{2,2}\}$ and $\{a_{2,-2}, b_{2,-2}\}$ such that $\sigma > 0$. As for parameter q the two vector fields are simply rotated by $90°$ relative to each other.

With $a_{0,1} = b_{1,0} = 0$ the parameters p and q are decoupled. In that case parameters p and r determine the vertical background velocity field, and parameters q and σ determine the horizontal velocity field.

For triad T1, as an explicit example, consider the case $p = r = 1$ and $\sigma = 0.5$. The critical value of free parameter q at the transcritical bifurcation is then $q_c = 0.25$. For the particular case that $\gamma_{1,1} = 2$, $\gamma_{1,-1} = 0$, and $a_{2,2} = b_{2,2} = 0.25$ the background flow at criticality is shown in Figure 3.25. For the same background flow and triad T2, $q = -0.25$. With $p = r = 1$ T2 therefore does not contribute to vortex formation. For $q < 0$ the stability criteria require

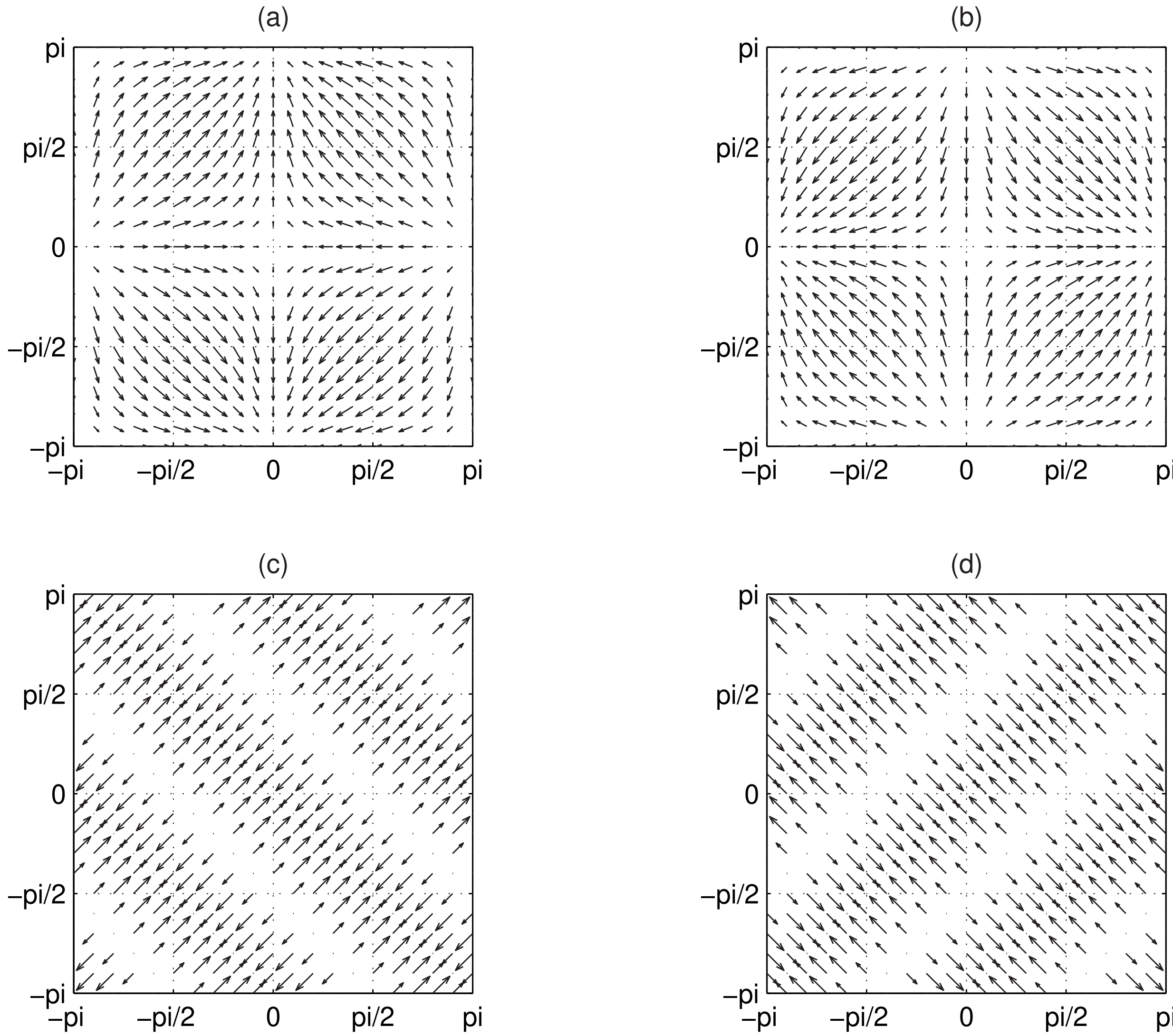

Figure 3.24: *Horizontal background flow for vortex triad T1 (left column) and T2 (right column), associated with parameter q with $a_{0,1} = b_{1,0} = 0$ (first row) and parameter σ (second row): (a) $a_{1,0} = -b_{0,1} = q$, (b) $-a_{1,0} = b_{0,1} = q$, (c) $a_{2,2} = b_{2,2} = \sigma/2$, and (d) $a_{2,-2} = -b_{2,-2} = \sigma/2$.*

that p and r have opposite signs. For $p = -r = 1$ with $\gamma_{1,1} = 0$ and $\gamma_{1,-1} = -2$, the critical background flow for T2 is shown in Figure 3.26. For $q = q_c = \sigma/2 = 0.25$ and $p = r = -1$ the same picture shown in Figure 3.25 for triad T1, rotated by 90°, is obtained for T2. In both cases the centre of the forming vortex is in a positively helical updraft region with strong gradients in vertical velocity and a converging horizontal shear flow. As mentioned before, the system parameters only determine part of the small-scale variability of the background flow, where the phases of all waves are undetermined. The component of the background flow derived from the system parameters does not necessarily represent any recognisable flow features of the actual background flow. A comparison with large-scale

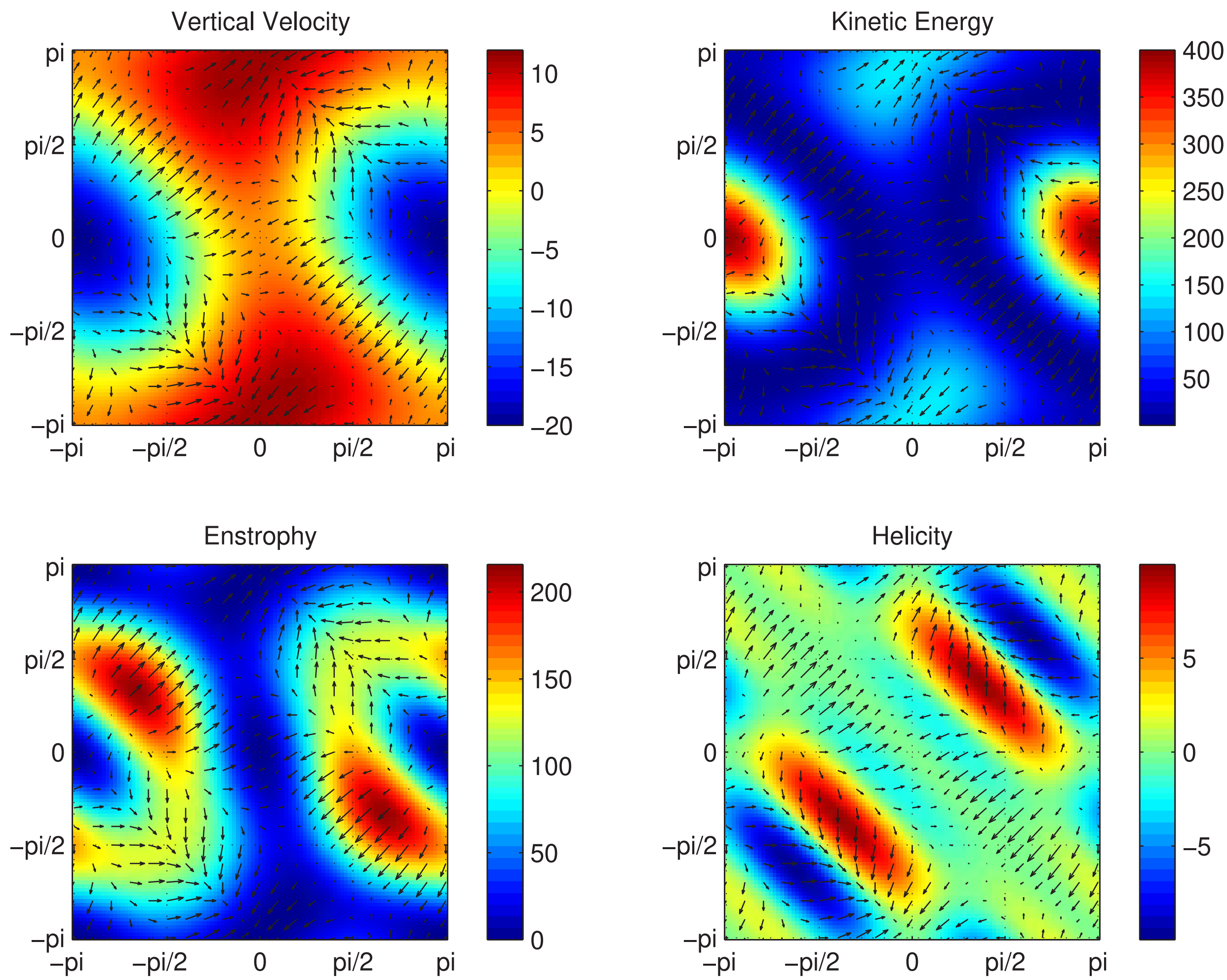

Figure 3.25: *Background flow at criticality of the transcritical bifurcation for triad T1 with* $a_{0,1} = b_{1,0} = 0$*,* $p = \gamma_{1,0}/4 = -\gamma_{0,1}/4 = r = 1$*,* $\gamma_{1,1} = 2$*,* $\gamma_{1,-1} = 0$*, and* $q = a_{1,0} = -b_{0,1} = \sigma/2 = a_{2,2} = b_{2,2} = 0.25$*. Vectors indicate horizontal velocity.*

storm flow characteristics is therefore not possible.

In the bifurcation scenario with respect to parameter q, as shown in Figure 3.13 for triad T1, only the horizontal flow varies. With $a_{2,2} = b_{2,2} = \sigma/2 = q_c$ it is given by

$$u(x, y, q) \stackrel{\text{def}}{=} -q \sin x - q_c \sin 2(x + y) \tag{3.5.8}$$

$$v(x, y, q) \stackrel{\text{def}}{=} q \sin y - q_c \sin 2(x + y) \ . \tag{3.5.9}$$

As shown in Figure 3.27, as q increases towards q_c, the initially converging flow associated with parameter σ more and more develops directional shear at the origin. As this directional shear becomes more intense it creates torques that create the initial perturbation to spin up the vortex. Eventually, as the stress becomes too strong it destroys the ordered vortex. The same pictures rotated by 90° are obtained for T2.

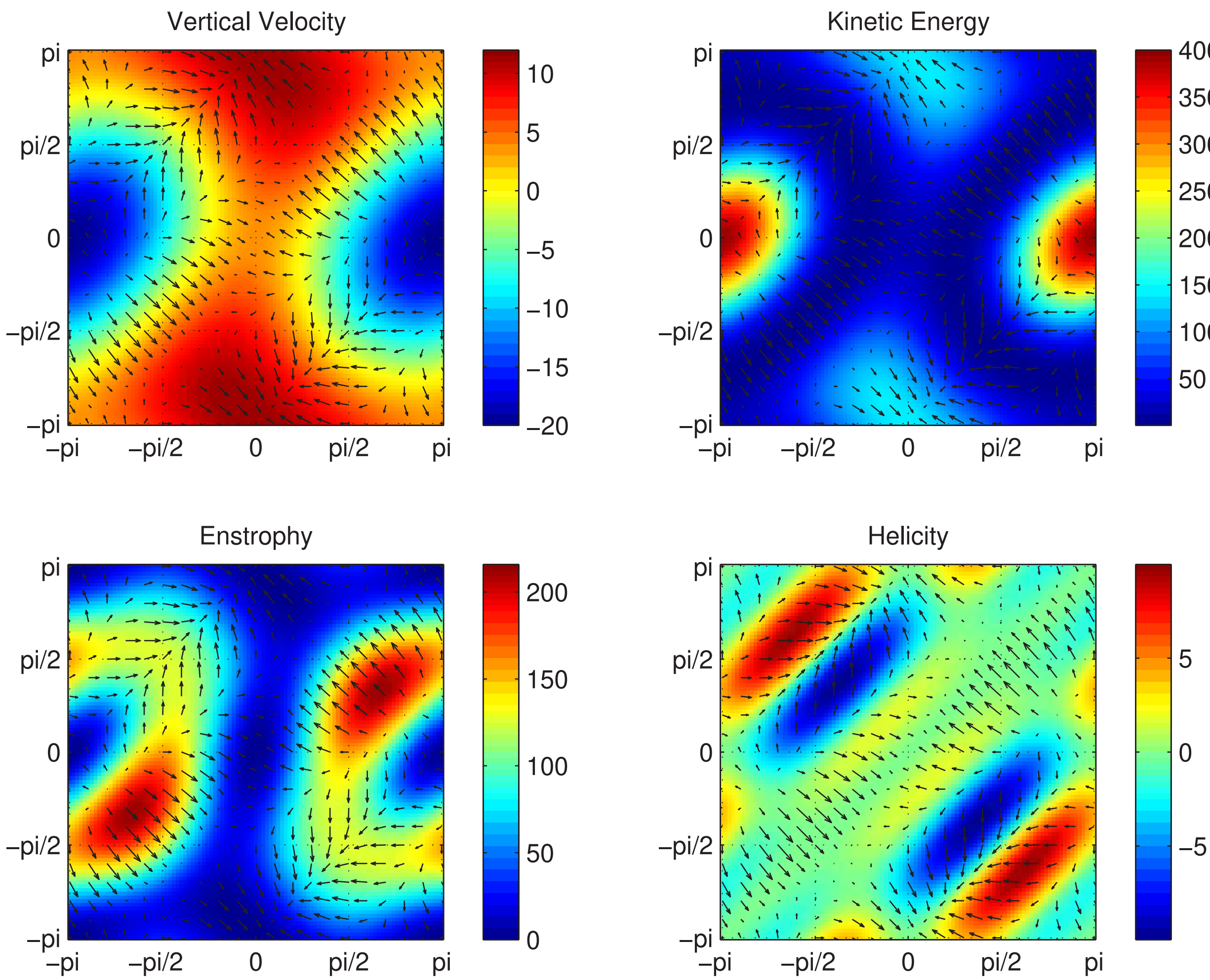

Figure 3.26: *As Figure 3.25 but for triad T2 with* $a_{0,1} = b_{1,0} = 0$, $p = \gamma_{1,0}/4 = -\gamma_{0,1}/4 = -r = 1$, $\gamma_{1,1} = 0$, $\gamma_{1,-1} = 2$, *and* $q = -a_{1,0} = b_{0,1} = -\sigma/2 = -a_{2,-2} = b_{2,-2} = -0.25$.

Parameter r is not uniquely related to the type and intensity of the horizontal shear of vertical velocity, nor to the intensity of vertical motion itself. This can easily be seen by comparing Figure 3.28 with Figure 3.22. However, a large positive or negative value of r means that at least one of the expansion coefficients $\gamma_{1,1}$ and $\gamma_{1,-1}$ is large in magnitude, indicating waves of intense vertical motion in the direction of the corresponding wave vectors. To maintain the qualitative pattern of vertical motion the relative magnitude of all four expansion coefficients $\gamma_{1,0}$, $\gamma_{0,1}$, $\gamma_{1,1}$, and $\gamma_{1,-1}$, and therefore p and r, must remain constant. As shown in Figure 3.29, on the $(r\sigma, pq)$-plane in parameter space the slope of the line of transcritical bifurcation points, i.e., the boundary between the laminar and tornadic regions, is one-half. Increasing or decreasing p and r such that $p = r$ greater or less than zero, the trajectory in parameter space will remain in either the laminar or tornadic region depending on the relative magnitude of q and σ. Consistent with the conjecture above, in the simple model changes in the intensity of vertical background motion representing buoyancy on the

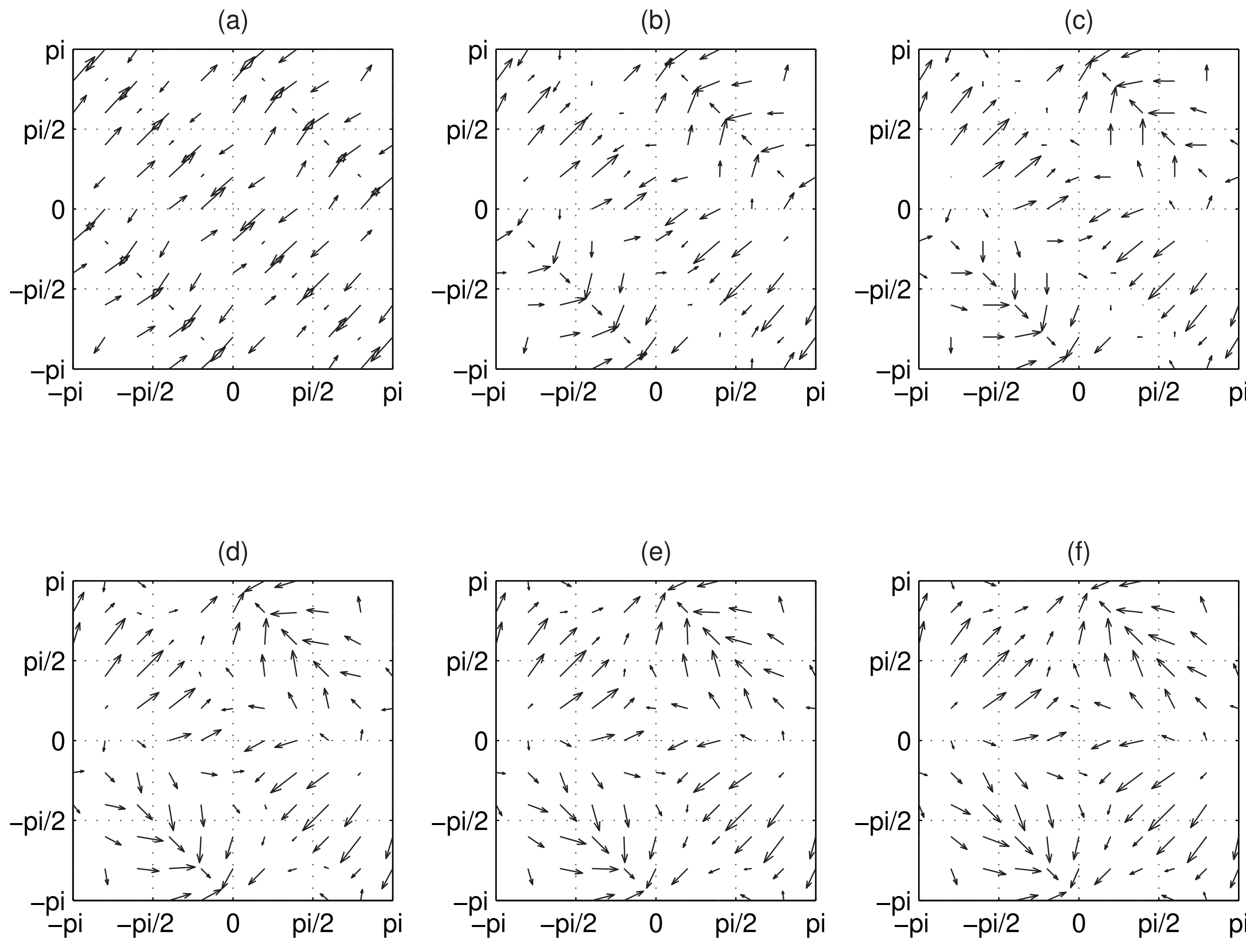

Figure 3.27: *Horizontal background flow for different values of supercriticality s of parameter q with respect to the transcritical bifurcation: (a) $s = .2$, (b) $s = .6$, (c) $s = 1$ (transcritical bifurcation point) , (d) $s = 1.4$, (e) $s = 1.8$, (f) $s = 2.2$ (supercritical with respect to the second Hopf bifurcation).*

tornado scale neither force nor destroy the fast vortex flow.

It is apparent however, that in a multiparameter system such as (3.2.20) there is no unique association of any particular type of shear, either horizontal or vertical, with vortex formation. Only a combination of different types of shear spins up a stable vortex. Although a quantitative change in the vertical background motion may not force or destroy a vortex it is required for vortex formation by a change in the horizontal shear flow.

The interpretation of the system parameters in terms of background flows and background flow variability requires simplifications and associations of the mathematically defined parameters with certain flow properties that may by misleading. Instead of eliminating the 'inconvenient' expansion coefficients for the physical interpretation of the system parameters in terms of simple concepts such as updraft strength or horizontal shear and convergence, the parameters can also be redefined by $p \rightarrow p + \bar{p}$, etc., where p now contains the easily interpretable background flow variability as in the simplified cases discussed above. However,

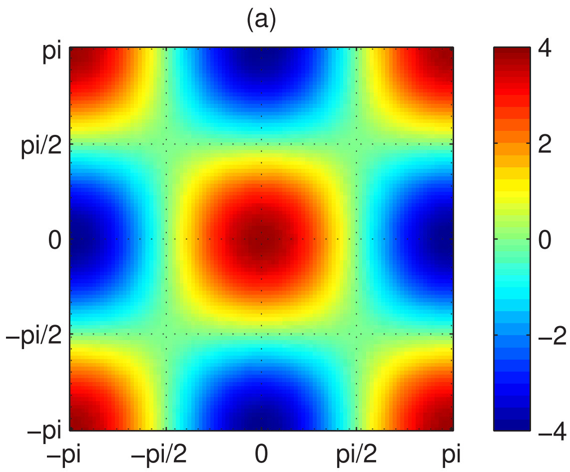

Figure 3.28: *Background flow associated with parameter $r = 0$: (a) $\gamma_{1,1} = \gamma_{1,-1} = 1$, (b) $\gamma_{1,1} = \gamma_{1,-1} = -1$.*

this is probably more useful for completer models that allow better physical interpretations.

Due to the linearity of the forcing equations for the two vortex waves in the dynamical systems (3.2.20), the effects of single triad interactions for the forcing of the vortex waves in a combined system are essentially additive. It is easy to verify that taking into account interactions of four complex waves with wave vectors $\{\boldsymbol{k}_x, \boldsymbol{k}_y, \boldsymbol{k}_{x,y}, \boldsymbol{k}_{x,-y}\}$, the time-dependence of the imaginary parts of the two vortex waves is given by

$$\begin{aligned} \dot{X} &= \left(-\frac{r}{2}Y + r_{11}Z_1\right) + \left(-\frac{r}{2}Y + r_{12}Z_2\right) \\ \dot{Y} &= \left(\frac{r}{2}X + r_{21}Z_1\right) + \left(\frac{r}{2}X + r_{22}Z_2\right) \ , \end{aligned} \tag{3.5.10}$$

where Z_1 and Z_2 denote phase space variable Z for triads T1 and T2, respectively, and the parameters r_{jk} denote the parameters r_j in the dynamical system for single triad Tk. With a rescaled parameter r the combined forcing is therefore just the sum of the individual forcing terms. In terms of sets, contributions to vortex formation in a more complete system can therefore come from the union of tornadic background flows for both single triad systems. As seen above, qualitatively these flows are identical. They only differ by rotations in space about the vertical axis. The unphysical preferred direction of shear for vortex formation that is implied by the individual systems is therefore removed in the combined system.

Consider now the time and length scales involved in the dynamics of the low-dimensional system, and the magnitude of the expansion coefficients in terms of real units. Since there are no physical parameters such as the angular velocity of the Earth or the coefficient of kinematic viscosity, the equations of motion for the fast velocity field (2.7.11) are valid in the same form for dimensional and nondimensionalised variables. They are therefore valid for all spatial and temporal scales. However, the relative magnitudes of speed, length, and duration are coupled. For simplicity the calculations were done in nondimensional coordinates such that $\chi = 1$. As a result the diameter of the vortex with maximum tangential speed is equal to 2π. For a typical tornado vortex with a diameter of about 200 m that would imply a

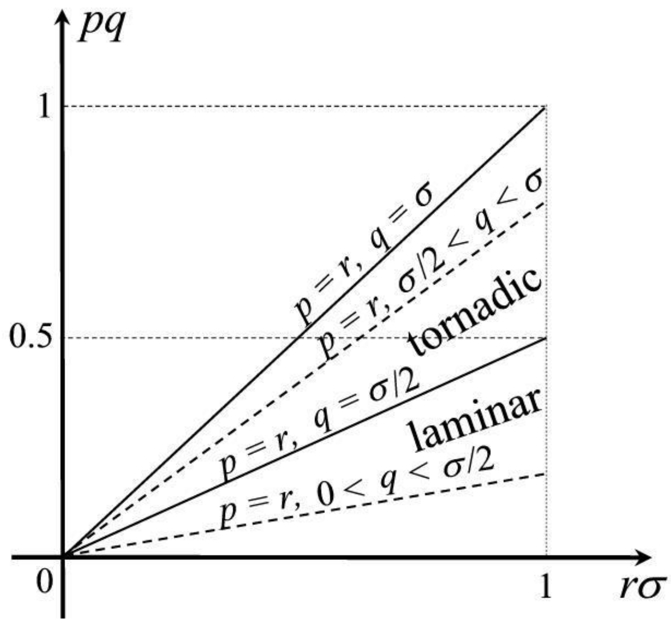

Figure 3.29: *Trajectories in parameter space associated with an increase or decrease of the intensity of the background vertical motion as a function of the horizontal shear.*

length scale $L = 30\,\mathrm{m}$. Depending on the initial perturbation from the origin, the fastest trajectories get to within 50% of the vortex equilibrium after 20 NTU, and to within 90% after 40 NTU for a supercriticality of 1.2. For a vortex development time of about 1–2 min this implies a timescale of $T = 3\,\mathrm{sec}$. Consistent with the discussion in Section 2.7, there is an order of magnitude difference between the slow and fast expansion coefficients. Scaled by the velocity scale $V = L/T = 10\,\mathrm{ms}^{-1}$, individual slow expansion coefficients are of magnitude $10\,\mathrm{ms}^{-1}$, and individual fast expansion coefficients are of magnitude $1\,\mathrm{ms}^{-1}$. As mentioned in Section 2.7, the total speed of the tornado vortex is generated by the superposition of a large number of waves which is necessary to describe an isolated vortex with small horizontal extent.

4 Implications for Tornado Forecasting

Don't worry if your theory doesn't agree with the observations, because they are probably wrong.

Sir Arthur Eddington

4.1 Tornadogenesis

One of the main results of the analysis of the low-dimensional model is that, as suggested in Section 2.4, vortex formation in the simplified setting is determined by horizontal spatial variability of the embedding background flow on approximately the same scale. If transferred to the tornado problem, as discussed in Section 2.6.2, this does not mean that tornadogenesis is dominated by actual small-scale processes such as the rapid interactions of turbulent eddies. If that really is the case, the chances of ever understanding and reliably predicting this phenomenon are very small. Instead the relevant part of the small-scale variability, by definition, is associated with slowly evolving, persistent, intense shear zones of a larger-scale storm system. The key to understanding tornadogenesis, as suggested by the simple model, is therefore through understanding of the structure of these shear zones and the role of mesoscale or even synoptic-scale forcing in their formation.

Another important result of the low-dimensional analysis is that the differences between 'tornadic' and 'nontornadic' background flow states on the vortex scale are very subtle. Considering the qualitative similarity between some tornadic and nontornadic storm systems this is probably also true for real tornadolike vortices.

As mentioned in Section 3.5, the impact of the background flow on the vortex flow is limited only by the truncation of the fast Fourier modes. Other than the fact that the background flow in the region of vortex formation must be reasonably well described by a Fourier series, no simplifying assumptions are being made. For the description of sharp fronts a large number of expansion coefficients are necessary. However, since the background expansion coefficients in the simple model, instead of dynamical variables, are constant parameters, their number does not have to be restricted for numerical simulations of the fast system. One of the primary limiting factors for transferring the results from the simple models to the tornado problem are therefore the spectral truncation of the vortex flow and the omission of the real or imaginary parts of the expansion coefficients. Since positively helical and irrotational (divergent) waves in principle are taken into account, and since tornadoes form in an overall positively helical flow environment, the truncation of the negatively helical waves should not be a problem. Also the omission of vertical variability of the storm flow and consequently of the background flow is consistent with the hypothesis that for the formation of the vortex the most relevant variability of the background flow is in the horizontal. However, the discretisation and reduction of wave vector space and the elimination of varying phase relationships between the waves for each wave vector significantly restricts not only the motion of the fast flow itself but also the coupling to the background flow.

In Section 2.6.1 it was demonstrated that an isolated helical vortex can be described by a continuous spectral superposition of spatially periodic Beltrami vortex flows. The first step towards a more realistic vortex model for the investigation of tornadogenesis is therefore to consider a superposition of the same Fourier waves as for the simple three-dimensional model over some (necessarily discrete) spectral interval. To be representative of the full vortex flow it must be assumed that the wavenumber χ of the vortex waves considered in the previous chapter is at the maximum of the kinetic energy spectrum of the vortex flow, and that the radius of maximum tangential speed is about $2\pi\chi^{-1}$. To maintain that vortex radius, with an approximately symmetrical kinetic energy spectrum around the maximum, the wavenumbers of the superimposed waves must be centred around χ. If the spectral interval is shifted towards smaller or larger wavenumbers, the diameter of the resulting vortex is either larger or smaller, respectively, and a smaller fraction of the kinetic energy of the full vortex flow is captured. Then, since the background flow is coupled to the vortex flow over a wider spectral range, with χ chosen such that $2\pi\chi^{-1}$ corresponds to the radius of maximum tangential speed of a typical tornado vortex, the spectral range of influence of the storm flow is also increased, taking now into account variability on a larger and smaller scale than the vortex diameter.

The other important limiting factor of the simple model is the reduced number of degrees of freedom. As indicated in the introduction, degrees of freedom of a fluid system here are defined as the qualitatively different dynamical possibilities. The dynamical system discussed in the previous chapter for example has three degrees of freedom starting from small perturbations. The perturbations may be damped out, they may develop into a vortex, or into a shear flow whose intensity is increasing indefinitely. The two physically relevant degrees of freedom correspond to the two equilibria or the states of the system as defined in Section 3.2. The number of degrees of freedom is therefore determined by the number of real solutions of the algebraic system of equations $\dot{\boldsymbol{X}}(\bar{\boldsymbol{X}}) \equiv \boldsymbol{0}$. For an autonomous, homogeneous system such as (2.7.11) the ground state $\bar{\boldsymbol{X}} = \boldsymbol{0}$ always is a solution. The number of nontrivial solutions not only depends on the highest order of nonlinearity of the various algebraic equations (at most two in the case of (2.7.11)), but also on the types of nonlinearity. In general it should always be possible to associate at least one of the equilibria with a vortex state. The conditions the system parameters have to satisfy for the *existence* of vortex equilibria (such as $p_1 = \pm p_2 \neq 0$ for the systems discussed in the previous chapter) give criteria the background flow has to satisfy in order to support vortex formation prior to the analysis of their stability. As the number of spectral components and therefore the number of terms in each of the forcing equations is increased, competing nontrivial equilibria may emerge. However, in principle the same bifurcation charts for transitions from the ground state to possibly several vortex states can be derived as in the three-dimensional system.

Although in the dynamical system (3.2.20) for the fast expansion coefficients the slow expansion coefficients were considered to be constant parameters for the purpose of calculating phase space trajectories, the assumption that $\partial_\tau \boldsymbol{u} \equiv \boldsymbol{0}$ is not required in the derivation of (2.7.11). Rather it is based on the fact that there is a scale separation between the magnitude of the expansion coefficients of the background and vortex flow and the timescale of their evolution. It is therefore possible to propose a *dynamic* bifurcation scenario in which the parameters in the fast dynamical system are driven by the equations of motion (2.7.10) for the slow background flow. However, instead of solving the closed system for the expansion coefficients of $\boldsymbol{u}$, $\boldsymbol{v}$, $\boldsymbol{f}$, and $\boldsymbol{f}'$, the response of $\boldsymbol{v}$ on hypothetical *prescribed* variations of $\boldsymbol{u}$ is investigated. The transcritical bifurcation between the laminar and tornadic parameter regions discussed in Section 3.4 can then be interpreted as a simplified description of tornadogenesis. For a storm flow state in the laminar region, (vortical) instabilities of small-scale shear zones are damped out. As the storm system evolves 'into' the tornadic region vortical instabilities are amplified and reach a steady state which persists as long as the storm system remains tornadic. Eventually the storm evolves back into the laminar region and the vortex dissipates.

The dynamic bifurcation scenario involves two timescales. A slow evolution timescale of the system parameters and the position of the equilibria, and fast transitions between equilibria. However, the bifurcation analysis gives no information about the conditions under which the slow storm flow itself behaves in the prescribed way. For the evolution of the storm system thermodynamic and external forcing cannot be neglected. In addition, due to the large range of spatial scales involved in storm dynamics and the complexity of the storm flow a high truncation as for the vortex flow is not possible. In that context also the undetermined background flow expansion coefficients become important. Given the spectral forcing terms $\boldsymbol{f_q}$ they determine the initial values of the expansion coefficients that appear directly in the fast dynamical system and their time-evolution through the slow balance equation (2.7.10). An investigation of the evolution of the storm is therefore significantly more complicated than the study of the formation of an embedded vortex. However, it is a first step towards forecasts of tornadogenesis if predictions can be based on a given storm velocity field. This of course requires the existence of accurate, high resolution data prior to tornadogenesis.

4.2 Storm Data

The completeness of the equations of motion is limited by the knowledge of the mathematical expressions for the (radiative, thermodynamic, dissipative, etc.) forcing terms and by the existence of initial data. The dynamical equations can only be as complete as the knowledge of the initial state of the system. An inaccurate formulation of the equations of motion and an inaccurate specification of the initial state introduce errors in the time-evolution of the system. One source for errors in time for the evolution of the total velocity field is therefore errors in space. For the evolution of the vortex flow errors in the spatial dependence of the background flow translate to errors in the slow expansion coefficients, and therefore to errors in the system parameters. Due to the sensitivity of the qualitative behaviour of the fast dynamical system near the bifurcation points on small changes in the parameter values, the success of the predictions critically depends on the accuracy of the actual measurements of the background flow as well as their analytical representation by Fourier series. For data on a regular grid the shortest wave that can be resolved has a wavelength about four times the gridpoint spacing δx. Hence the Fourier series cutoff must be for wavenumbers exceeding $\chi_{\max} = \pi/2\delta x$.

The airborne and ground-based Doppler radar data obtained over the previous decade during the *Verification of the Origins of Rotation in Tornadoes Experiment* (VORTEX) conducted by the National Severe Storms Laboratory of the United States has a horizontal and vertical gridpoint spacing of 250 m (for a general description of VORTEX prior to the measurement campaigns see *Rasmussen et al.* [1994], and for details of the measurements and data *Straka et al.* [1996]). The shortest resolvable wave therefore has a wavelength of about 1 km, which is larger than the diameter of the maximum tangential speed of most tornadoes. If the spectrum calculated from the storm data down to the smallest wavelength in each direction is sufficiently smooth, it can be fitted (e.g, through least-square polynomial interpolation) by a three-dimensional, analytical spectral function, similarly to the discussion in Section 2.6.1. If from the smallest resolvable scale down the spectrum is qualitatively continuous, an approximation of the energy distribution over the unresolved scales can be obtained by spectral extrapolation. The standard scaling laws of turbulence theory are probably not accurate enough due to the assumptions about isotropy, homgeneity, and locality of spectral interactions.

Tornadoes are resolved by mobile 3 mm-wavelength pulsed Doppler radars, where the resolution at a range of 3 km is less than 10 m in the azimuthal direction and 15 m in the radial direction at all ranges [*Bluestein and Pazmany*, 2000].

The discrete initial velocity and forcing data can be used in two ways. In both cases an analytic approximation of the observational data by means of a Fourier series expansion is obtained.

Based on discrete initial data $\boldsymbol{u}_0(\boldsymbol{r}) = (u_{0,1}(\boldsymbol{r}), u_{0,2}(\boldsymbol{r}), u_{0,3}(\boldsymbol{r}))^T$ on a possibly irregular grid with position vector $\boldsymbol{r}$, the Fourier expansion coefficients of the background flow are obtained by

$$\boldsymbol{u}_{\boldsymbol{q}}(0) = \frac{1}{D} \sum_{\boldsymbol{r}} \boldsymbol{u}_0(\boldsymbol{r}) \phi^*_{\boldsymbol{q}}(\boldsymbol{r}) \ , \tag{4.2.1}$$

for D data points [cf. *Walker*, 1996; Chap. 2], with a similar expression for the expansion coefficients of the forcing term $\boldsymbol{f}$. Then the mean-square error between the Fourier expansion of initial velocity $\boldsymbol{u}(0,\boldsymbol{r}) = (u_1(0,\boldsymbol{r}), u_2(0,\boldsymbol{r}), u_3(0,\boldsymbol{r}))^T$ and observations $\boldsymbol{u}_0(\boldsymbol{r})$ is defined as

$$\Delta^2 \stackrel{\text{def}}{=} \frac{1}{D} \sum_{\boldsymbol{r}} \left(\boldsymbol{u}(0,\boldsymbol{r}) - \boldsymbol{u}_0(\boldsymbol{r})\right)^2 \ . \tag{4.2.2}$$

In the limit of a continuous spectrum of wave numbers from zero to infinity

$$\sum_{\boldsymbol{q}} \exp i\boldsymbol{q} \cdot (\boldsymbol{r} - \boldsymbol{r}') \longrightarrow \delta(\boldsymbol{r} - \boldsymbol{r}') \ , \tag{4.2.3}$$

and for a continuous distribution of data points

$$\frac{1}{D} \sum_{\boldsymbol{r}'} \sum_{\boldsymbol{q}} \boldsymbol{u}_0(\boldsymbol{r}') \exp i\boldsymbol{q} \cdot (\boldsymbol{r} - \boldsymbol{r}') \longrightarrow \int \boldsymbol{u}_0(\boldsymbol{r}') \delta(\boldsymbol{r} - \boldsymbol{r}') d^3 r' = \boldsymbol{u}_0(\boldsymbol{r}) \ . \tag{4.2.4}$$

The mean-square error Δ is therefore due to sparse initial data and a discrete and truncated spectral representation.

Whereas in the case of accurate high resolution data a calculation of Fourier expansion coefficients based on (4.2.1) is easiest, for the typically sparse and irregular (radar, sounding, profiler) data likely to be encountered in meteorological applications, a calculation of the expansion coefficients based on minimisation of the mean-square error might produce better results. The least squares method determines the expansion coefficients $\boldsymbol{u}_{\boldsymbol{q}}(0) = (u_{1,\boldsymbol{q}}(0), u_{2,\boldsymbol{q}}(0), u_{3,\boldsymbol{q}}(0))^T$ from the conditions

$$\partial_{u_{j,\boldsymbol{q}}(0)} \Delta^2 \stackrel{!}{=} 0 \ , \tag{4.2.5}$$

leading to

$$\sum_{\boldsymbol{q}'} \boldsymbol{u}_{\boldsymbol{q}'}(0) \frac{1}{D} \sum_{\boldsymbol{r}} \phi_{\boldsymbol{q}+\boldsymbol{q}'}(\boldsymbol{r}) = \frac{1}{D} \sum_{\boldsymbol{r}} \boldsymbol{u}_0(\boldsymbol{r}) \phi_{\boldsymbol{q}}(\boldsymbol{r}) \ , \tag{4.2.6}$$

with Δ^2 as defined in (4.2.2). In the limit of a continuous distribution of data points in volume $\mathcal{V}$,

$$\frac{1}{D} \sum_{\boldsymbol{r}} \phi_{\boldsymbol{q}+\boldsymbol{q}'}(\boldsymbol{r}) \longrightarrow V(\mathcal{V}) \delta_{\boldsymbol{q}',-\boldsymbol{q}} \ , \tag{4.2.7}$$

and therefore

$$\sum_{\boldsymbol{q}'} \boldsymbol{u}_{\boldsymbol{q}'}(0) \frac{1}{D} \sum_{\boldsymbol{r}} \phi_{\boldsymbol{q}+\boldsymbol{q}'}(\boldsymbol{r}) \longrightarrow \boldsymbol{u}^*_{\boldsymbol{q}} \ . \tag{4.2.8}$$

Since also, in the same limit,

$$\frac{1}{D} \sum_{\boldsymbol{r}} \boldsymbol{u}_0(\boldsymbol{r}) \phi_{\boldsymbol{q}}(\boldsymbol{r}) \longrightarrow \langle \boldsymbol{u}_0(\boldsymbol{r}) \phi_{\boldsymbol{q}}(\boldsymbol{r}) \rangle \ , \tag{4.2.9}$$

the condition (4.2.6) for the minimisation of the mean-square error is identical with the definition of the Fourier expansion coefficients for a continuous initial velocity field. Condition (4.2.6) leads to a linear algebraic system of equations for the expansion coefficients whose solution is given by

$$\boldsymbol{a} = C^{-1} \boldsymbol{b} \ , \tag{4.2.10}$$

where the column vectors $\boldsymbol{a}$ and $\boldsymbol{b}$ are defined as

$$\boldsymbol{a} \stackrel{\text{def}}{=} (\ldots, u_{j,\boldsymbol{q}}(0), \ldots)^T \tag{4.2.11}$$

$$\boldsymbol{b} \stackrel{\text{def}}{=} (\ldots, b_{j,\boldsymbol{q}}(0), \ldots)^T \ , \tag{4.2.12}$$

and

$$b_{j,\boldsymbol{q}}(0) \stackrel{\text{def}}{=} \frac{1}{D} \sum_{\boldsymbol{r}} \boldsymbol{u}_{0,j}(\boldsymbol{r}) \phi_{\boldsymbol{q}}(\boldsymbol{r}) \ . \tag{4.2.13}$$

The coefficient matrix

$$C \stackrel{\text{def}}{=} \{C_{\boldsymbol{q},\boldsymbol{q}'}\} \tag{4.2.14}$$

with

$$C_{\boldsymbol{q},\boldsymbol{q}'} \stackrel{\text{def}}{=} \frac{1}{D} \sum_{\boldsymbol{r}} \phi_{\boldsymbol{q}+\boldsymbol{q}'}(\boldsymbol{r}) \tag{4.2.15}$$

is symmetric. Assuming that $\det C \neq 0$ and using the Gauß-Jordan method fewer computations are therefore required to calculate the inverse than for a general matrix. Since C does not depend on the specific velocity data contained in $\boldsymbol{b}$, it can be inverted prior to the analysis and reused for several transforms if the data structure is the same.

To capture the most relevant persistent forcing, for the calculation of background expansion coefficients it is important to make sure that fast transient motions on the scale of the tornado prior to tornadogenesis are filtered out. Since the long-term trend of the storm flow can only be determined from time series, for an accurate calculation of the slow expansion coefficients wind velocity data is required at more than one time. Ideally the storm is observed continuously over some period of time during which the data is automatically fed into an analysing system. The slow trend is determined time-averaging or spectral filtering, the expansion coefficients are calculated, and the parameters are evaluated. The trajectory in parameter space is then monitored and a warning is issued if a tornadic region is approached. Today, technologically we are far from this ideal case scenario, but maybe it is the only way to reliably predict tornadoes. In the meantime an important step is to develop a theory on which an interpretation of observations can be based, and a fast prediction model to analyse the available initial wind velocity data obtained from the thunderstorm.

5 Summary and Conclusions

The three-dimensional dynamical systems analysed in the previous chapters were derived in an attempt to minimise the complexity of the full set of equations governing the evolution of a geophysical fluid, and to isolate the kinematical effects of a slowly evolving background velocity field on the formation of an embedded small-scale vortex. Clearly, the simple system is not a complete tornado model. Instead it was designed to take into account the two major complications of tornado forecasting: incomplete thermodynamic data and time constraints. The motivation for this analysis is to obtain a faster prediction model for tornadogenesis and to gain a better understanding of the kinematical processes in a thunderstorm and their connection to the formation of tornadoes. The main results and their implications for the study of tornadogenesis can be summarised as follows.

Helicity, as a combined measure of the intensity and persistence of turbulent eddies, is likely to be the most important kinematical characteristic of tornadolike vortices. Locally and over finite domains helicity, for given values of kinetic energy and enstrophy, is extremised for positively or negatively helical Beltrami flows with a constant ratio of helicity and kinetic energy. These Beltrami flows, together with irrotational gradient flow, are solutions of the curl eigenvector equation. Since the curl operator is Hermitean its (normalised) eigenvectors form a complete orthonormal basis system. To be able to describe helical vortices more easily, the velocity field in Fourier series expansion is therefore decomposed into these curl eigenstates. It is then shown that in simplified form a helical vortex can be described by two entangled waves with the same sign of helicity and a fixed amplitude and phase relationship. To describe vortex formation, the time evolution of these two waves must be coupled. Coupling in wave vector space is through triad interactions. There are only two wave vectors that couple the two vortex waves and it is assumed that their triads represent the most dominant spectral interactions for vortex formation.

Based on current observations parameters characterising the vertical wind profile or the static instability of the large-scale storm environment only weakly separate between tornadic and nontornadic storms. On the other hand, tornadolike vortices tend to occur in the vicinity of strong horizontal gradients of velocity. Prior to tornadogenesis only a limited amount of observational data, particularly of thermodynamic variables, is available. To be able to improve predictions in the near future, kinematical criteria for vortex formation must be derived that only involve the storm velocity field, which can be derived from remote radar observations. For simplicity it is therefore assumed that tornadolike vortices are generated primarily by instabilities of intense shear zones of the storm system. Consequently significant variability of the storm flow is on the scale of the embedded vortex rather than on the scale of the storm circulation itself.

To be able to determine the influence of the storm flow on the formation of the vortex, the two flow phenomena must mathematically be separated. Due to the relevant small-scale variability of the storm system a separation based on the wavenumber of Fourier components is not possible. Instead the velocity field is separated into a slowly evolving part representing the storm flow, and a rapidly evolving part representing the tornadolike vortex. The corresponding equations of motion are derived from the equations for the total flow through scaling arguments and omission of the external forcing for the vortex flow.

A three-dimensional dynamical system is obtained from the equations of motion for the vortex flow by by Fourier transformation and spectral and helical truncation, restricting the fast flow to the two vortex waves and a nonhelical catalyst wave. The two equilibria of the dynamical system are the phase space origin, referred to as the ground state, and a nonvanishing vortex state. The system parameters depend on the expansion coefficients of the slow background flow. The stability of the equilibria can therefore be analysed as a function of the background flow state. Essentially two types of transitions are found: transcritical bifurcations leading to an exchange of stability between the two stationary states, and Hopf bifurcations leading to a change in stability of only one of the equilibria. The mathematical transitions with the most obvious physical interpretation are the transcritical bifurcations. With a stable ground state perturbations of the fast velocity field are damped out. As the ground state loses stability in the transcritical bifurcation the vortex state simultaneously gains stability and weak vortical perturbations are intensified, approaching a steady state as long as the vortex equilibrium is maintained by the background flow.

In the simple model the most relevant changes in the background flow affecting vortex stability are changes in the horizontal shear of horizontal velocity. It is shown that for a given background updraft strength a certain minimum amount of horizontal shear is necessary to spin up an intense vortex. However, as the horizontal shear increases relative to the updraft strength the coherent vortex is destroyed in a Hopf bifurcation.

Due to the slow speed of data acquisition and adequate numerical simulations of the full fluid mechanical equations, a physical interpretation of the storm system prior to tornadogenesis (i.e., science) is necessary. To be able to make predictions an assessment of the storm flow state with respect to the formation of tornadolike vortices must be possible without an explicit determination of the time evolution of the velocity field. Improving tornado forecasts therefore is a quest for new physical concepts and predictive variables of the storm system. In that sense the most important implication of the analysis of the simple model for the study of tornadogenesis is that in principle abstract forecast parameters can be derived from the dynamical equations that, from a strictly empirical point of view, would not be obvious.

Outlook

In this study an attempt was made to reduce the degrees of freedom of the motion of a turbulent fluid to a point where precise numerical criteria can be established for the formation of coherent vortices. The three-dimensional systems studied here represent the maximum simplification of the full set of equations that still produces reasonable results for the particular problem of the formation of tornadolike vortices. The question now is if the simple single-triad-interaction systems themselves are representative of real physical phenomena or if they can systematically be extended to more complex and hopefully more realistic systems. It was briefly indicated already towards the end of Chapter 3 that the effects of single triad interactions are additive for the two complex vortex waves. However, for the forcing of the catalyst waves additional linear terms have to be taken into account. These linear terms represent coupling between perturbation and background flow and help to specify 'tornadic' or 'nontornadic' background flows more completely based on the stability analysis of the vortex state. In addition, to be able to describe travelling vortex perturbations, it is necessary to consider both the real and imaginary parts of the fast expansion coefficients. The investigation of the eight-dimensional real system resulting from a combination of four complex waves with wave vectors $\{\boldsymbol{k}_x, \boldsymbol{k}_y, \boldsymbol{k}_{x,y}, \boldsymbol{k}_{x,-y}\}$ is therefore planned for the near future.

A Derivations

A.1 Schwarz's Inequality

Schwarz's inequality states that for any real numbers a_j and b_j

$$\left(\sum_j a_j b_j\right)^2 \leq \left(\sum_j a_j^2\right)\left(\sum_j b_j^2\right) \ . \tag{A.1.1}$$

From that, with the definition of the scalar product, it immediately follows that

$$\eta^2 \leq \kappa\varepsilon \ , \tag{A.1.2}$$

with η, κ, and ε as defined in Section 2.1. Assuming that the discrete variables a_j and b_j are given on D points of an even lattice over volume V, with gridpoint spacing δx, δy, and δz, and gridpoint values a_{jk} and b_{jk}, after multiplying by $(\delta V/V)^2$, where $\delta V = \delta x \delta y \delta z$, (A.1.1) gives

$$\left(\sum_k \sum_j a_{jk} b_{jk} \frac{\delta V}{V}\right)^2 \leq \left(\sum_k \sum_j a_{jk}^2 \frac{\delta V}{V}\right)\left(\sum_k \sum_j b_{jk}^2 \frac{\delta V}{V}\right) \ . \tag{A.1.3}$$

As the gridpoint spacing becomes infinitesimally small, $\delta V \to dV \to 0$, $D \to \infty$, and the discrete variables become continuous functions of space, $a_{jk} \to a_j(\boldsymbol{x})$, and $b_{jk} \to b_j(\boldsymbol{x})$. The sum over index k is then replaced by an integral over space such that

$$\sum_k (\ ) \frac{\delta V}{V} \to \frac{1}{V} \int (\ )\, dV = \langle (\ ) \rangle \ . \tag{A.1.4}$$

For continuous functions of space (A.1.3) then becomes

$$\left\langle \sum_j a_j b_j \right\rangle^2 \leq \left\langle \sum_j a_j^2 \right\rangle \left\langle \sum_j b_j^2 \right\rangle \ , \tag{A.1.5}$$

from which it follows that

$$\langle \eta \rangle^2 \leq \langle \kappa \rangle \langle \varepsilon \rangle \ , \tag{A.1.6}$$

or

$$H^2 \leq KE \ . \tag{A.1.7}$$

This is Equation 2.1.17 of Section 2.1.3.

A.2 Eigenstates of the Curl Operator

Assuming periodic boundary conditions in a finite domain, solutions to (2.5.19),

$$\boldsymbol{\nabla}\times \boldsymbol{v}_\chi^\lambda = \lambda\chi \boldsymbol{v}_\chi^\lambda \ , \tag{A.2.1}$$

for a particular chirality $\lambda\chi$ with $\chi > 0$ and $\lambda = \pm 1$ are found by expanding the velocity field in a Fourier[1] series,

$$\boldsymbol{v}_\chi^\lambda(t,\boldsymbol{x}) = \sum_{\boldsymbol{k}\in S(1)} \boldsymbol{u}_{\chi\boldsymbol{k}}^\lambda(t) \exp i\chi\boldsymbol{k}\cdot\boldsymbol{x} \ . \tag{A.2.2}$$

The vector amplitudes can be expanded further in the complete set of orthonormal basis vectors[2] $\{\boldsymbol{k}, \boldsymbol{n}\perp\boldsymbol{k}, \boldsymbol{k}\times\boldsymbol{n}\}$ such that

$$\boldsymbol{u}_{\chi\boldsymbol{k}}^\lambda = a_{\chi\boldsymbol{k}}^\lambda \boldsymbol{\eta}_{\boldsymbol{k}}^\lambda \ , \tag{A.2.3}$$

where

$$\boldsymbol{\eta}_{\boldsymbol{k}}^\lambda = \alpha\boldsymbol{k} + \beta\boldsymbol{n} + \gamma\boldsymbol{k}\times\boldsymbol{n} + i\left(a\boldsymbol{k} + b\boldsymbol{n} + c\boldsymbol{k}\times\boldsymbol{n}\right) \ . \tag{A.2.4}$$

The complex amplitudes $a_{\chi\boldsymbol{k}}^\lambda$ may be functions of time, and the $\{\alpha,\ \beta,\ \gamma,\ a,\ b,\ c\}$ are real constants. The unit normal vectors $\boldsymbol{n}$ are defined such that $-\boldsymbol{n}$ corresponds to $-\boldsymbol{k}$. Defining also $\boldsymbol{\eta}_{-\boldsymbol{k}}^\lambda \overset{\text{def}}{=} \boldsymbol{\eta}_{\boldsymbol{k}}^{\lambda *}$ requires that $\alpha = \beta = c \equiv 0$. Since for constant chirality B-flows are nondivergent, $\boldsymbol{k}\cdot\boldsymbol{u}_{\chi\boldsymbol{k}}^\lambda = 0$ for all wave vectors and $a \equiv 0$. The Fourier transforms are therefore given by

$$\boldsymbol{u}_{\chi\boldsymbol{k}}^\lambda = a_{\chi\boldsymbol{k}}^\lambda\left(\gamma\boldsymbol{k}\times\boldsymbol{n} + ib\boldsymbol{n}\right) \ . \tag{A.2.5}$$

Substituting now (A.2.2) into (A.2.1) leads to

$$i\boldsymbol{k}\times\left(\gamma\boldsymbol{k}\times\boldsymbol{n} + ib\boldsymbol{n}\right) = \lambda(\gamma\boldsymbol{k}\times\boldsymbol{n} + ib\boldsymbol{n}) \ . \tag{A.2.6}$$

This requires that $\gamma = -\lambda b$. Since for the definition of the Fourier basis vectors the amplitudes $a_{\chi\boldsymbol{k}}^\lambda$ are arbitrary, $\gamma \equiv 1$ and therefore $b = -\lambda$ can be chosen without loss of generality. Furthermore, a normalisation factor of $2^{-\frac{1}{2}}$ is introduced. Then the helical basis vectors satisfy the curl eigenvector equation in wavenumber space,

$$i\boldsymbol{k}\times\boldsymbol{\eta}_{\boldsymbol{k}}^\lambda = \lambda\boldsymbol{\eta}_{\boldsymbol{k}}^\lambda \ , \tag{A.2.7}$$

and

$$\boldsymbol{v}_\chi^\lambda = \sum_{\boldsymbol{k}\in S(1)} a_{\chi\boldsymbol{k}}^\lambda \frac{1}{\sqrt{2}}(\boldsymbol{k}\times\boldsymbol{n} - i\lambda\boldsymbol{n}) \exp i\chi\boldsymbol{k}\cdot\boldsymbol{x} \ , \tag{A.2.8}$$

---

[1] Assuming cylinder symmetry, vortex solutions to (2.1.20) with a swirling updraft can also be found in terms of Bessel functions [*Dritschel*, 1991].

[2] cf. the discussion in Appendix A.3.

which is equivalent to (2.5.20) with $\lambda = \pm 1$.

For $\lambda = 0$, $\boldsymbol{\nabla} \times \boldsymbol{v}_\chi^0 \equiv \mathbf{0}$, and the nonhelical curl eigenstate $\boldsymbol{v}_\chi^0$ is a gradient flow $-\boldsymbol{\nabla}\Phi_\chi$. The nonhelical basis vectors $\boldsymbol{\eta}_{\boldsymbol{k}}^0$ are derived by expanding the potential function $\Phi_\chi(t, \boldsymbol{x})$ in a Fourier series in space, taking the negative gradient, and by comparing the resulting expression with the definition (2.5.20).

Since helical curl eigenstates extremise helicity for a given kinetic energy distribution, they can also be derived from a variational principle. Considering a general function $L = L(\boldsymbol{v}, \boldsymbol{\omega})$ of velocity and vorticity, $\bar{L} \stackrel{\text{def}}{=} \langle L \rangle_{\mathcal{D}}$ is required to be extreme for a particular velocity field within a fixed domain $\mathcal{D}$ and fixed boundary conditions on velocity. Then the variation $\delta\bar{L}$ of $\bar{L}$ must vanish. Since the expression for the extremising velocity field must hold at all times, L cannot be explicitly time dependent and only variations with respect to the velocity components and their spatial derivatives are taken into account. The *Euler-Lagrange equations* for all three velocity components v_i are then given by [e.g., *Cohen*, 1992; pp. 406–409]

$$\left(\partial_{v_i} - \partial_x \partial_{\partial_x v_i} - \partial_y \partial_{\partial_y v_i} - \partial_z \partial_{\partial_z v_i}\right) L = 0 \; . \tag{A.2.9}$$

If boundary conditions are the only constraints on the velocity field then a function $F = F(\boldsymbol{v}, \boldsymbol{\omega})$ has an extreme spatial average $\bar{F} = \langle F \rangle_{\mathcal{D}}$ if and only if it satisfies (A.2.9). However, if in addition to the boundary conditions the averaged values of N functions $G_i = G_i(\boldsymbol{v}, \boldsymbol{\omega})$, $i = 1, \ldots, N$, are prescribed, $\bar{F}$ is extremised in $\mathcal{D}$ if only if the modified Lagrangian

$$L = F + \sum_{i=1}^{N} \lambda_i G_i \tag{A.2.10}$$

satisfies (A.2.9). Here, the Lagrange multipliers λ_i are real constants that have to satisfy the imposed constraints. Then

$$\begin{aligned} 0 &= \delta\bar{L} \\ &= \delta\bar{F} + \sum_{i=1}^{N} \lambda_i \delta\bar{G}_i \end{aligned} \tag{A.2.11}$$

implies $\delta\bar{F} = 0$ since, by definition $\delta\bar{G}_i \stackrel{\text{def}}{=} \delta\langle G_i \rangle_{\mathcal{D}} \equiv 0$ for all functions G_i, i.e., with $\bar{L}$ also $\bar{F}$ is extremised under the given constraints. However, the set of equations (A.2.9) derived for the Lagrangian (A.2.10) is equivalent to the set of equations derived for the Lagrangian given by any linear combination of the set of functions $\{F, G_i\}$.[3] The optimum velocity field derived from the Euler-Lagrange equations (A.2.9), therefore *simultaneously* extremises all functions $\{F, G_i\}$ of the Lagrangian (A.2.10). The curl eigenstates are then obtained from the Lagrangian

$$L = \lambda\chi^{-1}\eta - \kappa \; , \tag{A.2.12}$$

for which (A.2.9) simultaneously extremises helicity and kinetic energy. This leads to

$$\lambda\chi^{-1}\boldsymbol{\nabla} \times \boldsymbol{v} - \boldsymbol{v} = \mathbf{0} \; , \tag{A.2.13}$$

which is identical with (A.2.1).

[3] The Lagrangian $\lambda_1^{-1} L = G_1 + \lambda_1^{-1}\left(F + \sum_{i=2}^{N} \lambda_i G_i\right)$, for example, is dynamically equivalent to (A.2.10).

A.3 Completeness of Curl Eigenstates

For any vector $\boldsymbol{v}$ in a D-dimensional space

$$\boldsymbol{v} = \sum_{j=1}^{D} v_j \boldsymbol{b}_j \ , \tag{A.3.1}$$

where $v_j \stackrel{\text{def}}{=} \boldsymbol{v} \cdot \boldsymbol{b}_j$ are the components of $\boldsymbol{v}$ into the direction of the real basis vector $\boldsymbol{b}_j$. Since $(\boldsymbol{v} \cdot \boldsymbol{b}_j)\, \boldsymbol{b}_j \equiv \boldsymbol{b}_j \boldsymbol{b}_j^T \boldsymbol{v}$, the decomposition is complete if and only if

$$\sum_{j=1}^{D} \boldsymbol{b}_j \boldsymbol{b}_j^T = E_D \ , \tag{A.3.2}$$

with D-dimensional unit matrix E_D. For complex basis vectors the components are defined by $v_j \stackrel{\text{def}}{=} \boldsymbol{v} \cdot \boldsymbol{b}_j^*$, and the completeness relation becomes

$$\sum_{j=1}^{D} \boldsymbol{b}_j \boldsymbol{b}_j^\dagger = E_D \ . \tag{A.3.3}$$

Since in three dimensions, for any unit vector $\boldsymbol{n}$ normal to unit vector $\boldsymbol{k}$,

$$\boldsymbol{k}\boldsymbol{k}^T + \boldsymbol{n}\boldsymbol{n}^T + (\boldsymbol{k} \times \boldsymbol{n})(\boldsymbol{k} \times \boldsymbol{n})^T = E_3 \ , \tag{A.3.4}$$

any three-dimensional vector can be expanded in the complete orthonormal set of basis vectors $\{\boldsymbol{k}, \boldsymbol{n}, \boldsymbol{k} \times \boldsymbol{n}\}$. With the orthonormal basis vectors $\boldsymbol{\eta}_{\boldsymbol{k}}^{\lambda}$ as defined in Section 2.5 it is easy to verify that

$$\sum_{\lambda=0,\pm1} \boldsymbol{\eta}_{\boldsymbol{k}}^{\lambda} \boldsymbol{\eta}_{\boldsymbol{k}}^{\lambda\dagger} = \boldsymbol{k}\boldsymbol{k}^T + \boldsymbol{n}\boldsymbol{n}^T + (\boldsymbol{k} \times \boldsymbol{n})(\boldsymbol{k} \times \boldsymbol{n})^T \ . \tag{A.3.5}$$

The helical basis vectors therefore also satisfy the completeness relationship (A.3.4).

From the completeness of the helical basis vectors together with the completeness of the spatial Fourier basis functions expressed by (2.5.11) in Section 2.5.1 then follows the completeness of the curl eigenvectors $\boldsymbol{\eta}_{\boldsymbol{k}}^{\lambda} \phi_{\chi \boldsymbol{k}}$,

$$\begin{aligned} E_3 \delta(\boldsymbol{x}' - \boldsymbol{x}) &= \left(\frac{2\pi}{\chi_0}\right)^3 \sum_{\chi \in \Gamma} \sum_{\boldsymbol{k} \in S(1)} \left(\sum_{\lambda=0,\pm1} \boldsymbol{\eta}_{\boldsymbol{k}}^{\lambda} \boldsymbol{\eta}_{\boldsymbol{k}}^{\lambda\dagger} \right) \phi_{\chi \boldsymbol{k}}(\boldsymbol{x}) \phi_{\chi \boldsymbol{k}}^*(\boldsymbol{x}') \\ &= \left(\frac{2\pi}{\chi_0}\right)^3 \sum_{\chi \in \Gamma} \sum_{\boldsymbol{k} \in S(1)} \sum_{\lambda=0,\pm1} \boldsymbol{\eta}_{\boldsymbol{k}}^{\lambda} \phi_{\chi \boldsymbol{k}}(\boldsymbol{x}) \left(\boldsymbol{\eta}_{\boldsymbol{k}}^{\lambda} \phi_{\chi \boldsymbol{k}}(\boldsymbol{x}') \right)^\dagger \ . \end{aligned} \tag{A.3.6}$$

A.4 Rotational Invariance of Curl Eigenstates

Consider a rigid rotation of a vector field $\boldsymbol{a}$ together with the frame of reference and denote the rotated vector field by $\boldsymbol{a}'$. The coordinate basis vectors and field vectors at each point transform under the rotation matrix R such that

$$\boldsymbol{e}' = R\boldsymbol{e} \ . \tag{A.4.1}$$

Then the rotated field vector $R\boldsymbol{a}$ at any point in the rotated frame $\mathcal{O}'$ has the same components as the original field vector $\boldsymbol{a}$ in the original frame $\mathcal{O}$ at the same point. However, in general $\boldsymbol{a}'(\boldsymbol{x}) \neq R\boldsymbol{a}(\boldsymbol{x})$ due to the rotational translation of the vector field from point P with coordinates $\boldsymbol{x}$ to point P' with coordinates $\boldsymbol{x}' = R\boldsymbol{x}$ in addition to the local rotation. The total transformation of the vector field is a superposition of a global and local rotation and, as seen below, is therefore generated by the total angular momentum operator.

Since three-dimensional rotation operators are matrix representations of the *special orthogonal group* SO(3), the rotation matrix is orthogonal, i.e., $R^{-1} = R^T$ and its determinant is equal to one. The inversion of the coordinate transformation is therefore given by $\boldsymbol{x} = R^T\boldsymbol{x}'$.

To discuss rotational invariance of curl eigenstates the *matrix curl operator* $\hat{R}$ is defined such that

$$\hat{R}\boldsymbol{v} \stackrel{\text{def}}{=} \boldsymbol{\nabla}\times\boldsymbol{v}, \tag{A.4.2}$$

where the hat denotes a differential operator quantity. From this definition, $\hat{R}$ is found to be

$$\hat{R} \stackrel{\text{def}}{=} \begin{pmatrix} 0 & -\partial z & \partial y \\ \partial z & 0 & -\partial x \\ -\partial y & \partial x & 0 \end{pmatrix} . \tag{A.4.3}$$

More generally, the cross product between any two three-dimensional column vectors $\boldsymbol{u} = (u_1, u_2, u_3)^T$ and $\boldsymbol{v} = (v_1, v_2, v_3)^T$ in matrix form can be written as

$$\boldsymbol{u}\times\boldsymbol{v} = C_{\boldsymbol{u}}\boldsymbol{v} \ , \tag{A.4.4}$$

where

$$C_{\boldsymbol{u}} \stackrel{\text{def}}{=} \begin{pmatrix} 0 & -u_3 & u_2 \\ u_3 & 0 & -u_1 \\ -u_2 & u_1 & 0 \end{pmatrix} . \tag{A.4.5}$$

Since $C_{\boldsymbol{u}}^T = -C_{\boldsymbol{u}}$ the cross product operator $C_{\boldsymbol{u}}$ is antisymmetric and $\boldsymbol{v}\times\boldsymbol{u} = C_{\boldsymbol{u}}^T\boldsymbol{v}$. Obviously, $C_{\boldsymbol{\nabla}} \equiv \hat{R}$.

An explicit matrix representation for infinitesimally small rotations can then be derived by defining a rotation vector $\delta\boldsymbol{\phi}$ such that changes in the position vector are given by $\delta\boldsymbol{x} = \boldsymbol{x}' - \boldsymbol{x} = \delta\boldsymbol{\phi}\times\boldsymbol{x}$ or $\boldsymbol{x}' = \boldsymbol{x} + \delta\boldsymbol{\phi}\times\boldsymbol{x}$ and therefore $R(\delta\boldsymbol{\phi}) = E_3 + C_\delta$. Similarly $\boldsymbol{x} = \boldsymbol{x}' - \delta\boldsymbol{\phi}\times\boldsymbol{x}$ and therefore $R^T(\delta\boldsymbol{\phi}) = E_3 - C_\delta$ [cf. *Greiner and Müller*, 1994].

A vector of the rotated field at P' is equal to a rotated vector of the original field at P

$$\begin{aligned} \boldsymbol{a}'(\boldsymbol{x}') &= \boldsymbol{a}'(R\boldsymbol{x}) \\ &= R\boldsymbol{a}(\boldsymbol{x}) \ , \end{aligned} \tag{A.4.6}$$

or

$$\boldsymbol{a}'(\boldsymbol{x}) = R\boldsymbol{a}(R^T\boldsymbol{x}) \ . \tag{A.4.7}$$

Then, to first order in $|\delta\boldsymbol{\phi}|$, for infinitesimal rotations

$$\begin{aligned}\boldsymbol{a}'(\boldsymbol{x}) &= \boldsymbol{a}(\boldsymbol{x}-\delta\boldsymbol{\phi}\times\boldsymbol{x}) + \delta\boldsymbol{\phi}\times\boldsymbol{a}(\boldsymbol{x}-\delta\boldsymbol{\phi}\times\boldsymbol{x}) \\ &\overset{\text{Taylor}}{\approx} \boldsymbol{a}(\boldsymbol{x}) - (\delta\boldsymbol{\phi}\times\boldsymbol{x})\cdot\boldsymbol{\nabla}\boldsymbol{a}(\boldsymbol{x}) + \delta\boldsymbol{\phi}\times\boldsymbol{a}(\boldsymbol{x}) + \mathcal{O}(|\delta\boldsymbol{\phi}|^2) \\ &= \left[E_3 - i\hat{J}(\delta\boldsymbol{\phi})\right]\boldsymbol{a}(\boldsymbol{x}) \ ,\end{aligned} \tag{A.4.8}$$

where the total angular momentum operator $\hat{J}$ is defined by

$$\hat{J}(\delta\boldsymbol{\phi}) \overset{\text{def}}{=} \hat{L}(\delta\boldsymbol{\phi}) + S(\delta\boldsymbol{\phi}) \tag{A.4.9}$$

with matrix orbital angular momentum operator

$$\begin{aligned}\hat{L}(\delta\boldsymbol{\phi}) &\overset{\text{def}}{=} -iE_3(\delta\boldsymbol{\phi}\times\boldsymbol{x})\cdot\boldsymbol{\nabla} \\ &= -iE_3\delta\boldsymbol{\phi}\cdot(\boldsymbol{x}\times\boldsymbol{\nabla})\end{aligned} \tag{A.4.10}$$

and intrinsic angular momentum or spin matrix

$$S(\delta\boldsymbol{\phi}) \overset{\text{def}}{=} iC_\delta \quad . \tag{A.4.11}$$

With the vector angular momentum operator

$$\begin{aligned}\hat{\boldsymbol{L}} &\overset{\text{def}}{=} -i\boldsymbol{x}\times\boldsymbol{\nabla} \\ &= \chi\boldsymbol{x}\times\hat{\boldsymbol{k}}_\chi \ ,\end{aligned} \tag{A.4.12}$$

where the wave vector (momentum) operator $\hat{\boldsymbol{k}}_\chi$ is defined as

$$\hat{\boldsymbol{k}}_\chi \overset{\text{def}}{=} -i\chi^{-1}\boldsymbol{\nabla} \ , \tag{A.4.13}$$

the matrix operator can also be written as

$$\hat{L}(\delta\boldsymbol{\phi}) = E_3\delta\boldsymbol{\phi}\cdot\hat{\boldsymbol{L}} \ . \tag{A.4.14}$$

To calculate the transformed vector field under finite rotations, the finite rotation vector $\boldsymbol{\phi}$ is divided into N equal small segments $\delta\boldsymbol{\phi} = \boldsymbol{\phi}/N$. Then, since $\hat{L}(\boldsymbol{\phi}) = N\hat{L}(\delta\boldsymbol{\phi})$ and $S(\boldsymbol{\phi}) = N\,S(\delta\boldsymbol{\phi})$, also $\hat{J}(\boldsymbol{\phi}) = N\hat{J}(\delta\boldsymbol{\phi})$. In the limit $N\to\infty$, the finite rotation can be written as an infinite series of successive infinitesimal rotations

$$\begin{aligned}\boldsymbol{a}'(\boldsymbol{x}) &= \lim_{N\to\infty}\left[E_3 - \frac{i\hat{J}(\boldsymbol{\phi})}{N}\right]^N \boldsymbol{a}(\boldsymbol{x}) \\ &= \hat{U}(\boldsymbol{\phi})\boldsymbol{a}(\boldsymbol{x}) \ ,\end{aligned} \tag{A.4.15}$$

where the unitary matrix rotation operator $\hat{U}$ is defined as

$$\begin{aligned}\hat{U}(\boldsymbol{\phi}) &\overset{\text{def}}{=} \exp(-i\hat{J}(\boldsymbol{\phi})) \\ &= \sum_{j=0}^{\infty}\frac{1}{j!}\left[iE_3\boldsymbol{x}\cdot(\boldsymbol{\phi}\times\hat{\boldsymbol{k}}_\chi) + C\ \right]^j \ .\end{aligned} \tag{A.4.16}$$

For the decomposition of the velocity field into curl eigenstates to be meaningful, the decomposition must be conserved under spatial rotations of the frame of reference, i.e., the rotated curl eigenstates $\boldsymbol{v}'^{\lambda}_{\chi} = \hat{U}\boldsymbol{v}^{\lambda}_{\chi}$ in the rotated frame also have to satisfy the eigenvalue equation $\hat{R}\boldsymbol{v}'^{\lambda}_{\chi} = \lambda\chi\boldsymbol{v}'^{\lambda}_{\chi}$. This is true if and only if the $\boldsymbol{v}^{\lambda}_{\chi}$ are simultaneous eigenstates of the curl and rotation operator, i.e., if and only if the commutator $[\hat{R},\hat{U}] \stackrel{\text{def}}{=} \hat{R}\hat{U} - \hat{U}\hat{R}$ applied to the velocity fields $\boldsymbol{v}^{\lambda}_{\chi}$ vanishes. Since $\left[\hat{A}, \sum_{j=0}^{\infty} \frac{1}{j!}\hat{B}^j\right] = \hat{0}$ if $[\hat{A},\hat{B}] = \hat{0}$ it suffices to show that the curl operator commutes with the total angular momentum operator.

Any operator equation that holds for the individual velocity terms $\boldsymbol{v}^{\lambda}_{\chi\boldsymbol{k}} \stackrel{\text{def}}{=} a^{\lambda}_{\chi\boldsymbol{k}}\boldsymbol{\eta}^{\lambda}_{\boldsymbol{k}}\phi_{\chi\boldsymbol{k}}$ also holds for their linear superposition $\boldsymbol{v}^{\lambda}_{\chi}$. Therefore the curl eigenstates are invariant under spatial rotations if $[\hat{R},\hat{J}] = [\hat{R},\hat{L}] + [\hat{R},S] = \hat{0}$ applied to the $\boldsymbol{v}^{\lambda}_{\chi\boldsymbol{k}}$. With the general vector relationships

$$\boldsymbol{a}\times(\boldsymbol{b}\times\boldsymbol{c}) = (\boldsymbol{a}\cdot\boldsymbol{c})\boldsymbol{b} - (\boldsymbol{a}\cdot\boldsymbol{b})\boldsymbol{c} \ , \tag{A.4.17}$$

$$\hat{R}\,(f\boldsymbol{a}) = f\hat{R}\boldsymbol{a} + \boldsymbol{\nabla} f\times\boldsymbol{a} \ , \tag{A.4.18}$$

and

$$\hat{R}\,(\boldsymbol{c}\times\boldsymbol{a}) = \boldsymbol{c}\,\boldsymbol{\nabla}\cdot\boldsymbol{a} - (\boldsymbol{c}\cdot\boldsymbol{\nabla})\boldsymbol{a} \ , \tag{A.4.19}$$

where $\boldsymbol{c} = const.$, it is straightforward to calculate

$$\begin{aligned} \hat{L}\boldsymbol{v}^{\lambda}_{\chi\boldsymbol{k}} &= -\chi\boldsymbol{x}\cdot(\boldsymbol{\phi}\times\boldsymbol{k})\boldsymbol{v}^{\lambda}_{\chi\boldsymbol{k}} \ , && \text{(A.4.20)}\\ \hat{R}\hat{L}\boldsymbol{v}^{\lambda}_{\chi\boldsymbol{k}} &= -\lambda\chi^2\boldsymbol{x}\cdot(\boldsymbol{\phi}\times\boldsymbol{k})\boldsymbol{v}^{\lambda}_{\chi\boldsymbol{k}} - \chi(\boldsymbol{\phi}\times\boldsymbol{k})\times\boldsymbol{v}^{\lambda}_{\chi\boldsymbol{k}} \ , && \text{(A.4.21)}\\ \hat{L}\hat{R}\boldsymbol{v}^{\lambda}_{\chi\boldsymbol{k}} &= -\lambda\chi^2\boldsymbol{x}\cdot(\boldsymbol{\phi}\times\boldsymbol{k})\boldsymbol{v}^{\lambda}_{\chi\boldsymbol{k}} \ , && \text{(A.4.22)} \end{aligned}$$

and therefore

$$[\hat{R},\hat{L}]\boldsymbol{v}^{\lambda}_{\chi\boldsymbol{k}} = -\chi C_{\ \times\boldsymbol{k}}\boldsymbol{v}^{\lambda}_{\chi\boldsymbol{k}} \ . \tag{A.4.23}$$

Similarly,

$$\begin{aligned} \hat{R}S\boldsymbol{v}^{\lambda}_{\chi\boldsymbol{k}} &= \chi\left[(\boldsymbol{\phi}\cdot\boldsymbol{k})\boldsymbol{v}^{\lambda}_{\chi\boldsymbol{k}} - (\boldsymbol{k}\cdot\boldsymbol{v}^{\lambda}_{\chi\boldsymbol{k}})\boldsymbol{\phi}\right] \ , && \text{(A.4.24)}\\ S\hat{R}\boldsymbol{v}^{\lambda}_{\chi\boldsymbol{k}} &= \chi\left[(\boldsymbol{\phi}\cdot\boldsymbol{k})\boldsymbol{v}^{\lambda}_{\chi\boldsymbol{k}} - (\boldsymbol{\phi}\cdot\boldsymbol{v}^{\lambda}_{\chi\boldsymbol{k}})\boldsymbol{k}\right] \ , && \text{(A.4.25)} \end{aligned}$$

and

$$[\hat{R},S]\boldsymbol{v}^{\lambda}_{\chi\boldsymbol{k}} = \chi C_{\ \times\boldsymbol{k}}\boldsymbol{v}^{\lambda}_{\chi\boldsymbol{k}} \ . \tag{A.4.26}$$

It follows that $[\hat{R},\hat{J}] = \hat{0}$ and consequently the $\boldsymbol{v}'^{\lambda}_{\chi}$ are also eigenstates of the curl operator,

$$\begin{aligned} \hat{R}\boldsymbol{v}'^{\lambda}_{\chi} &= \hat{R}\hat{U}\boldsymbol{v}^{\lambda}_{\chi}\\ &= \hat{U}\hat{R}\boldsymbol{v}^{\lambda}_{\chi}\\ &= \lambda\chi\boldsymbol{v}'^{\lambda}_{\chi} \ , \end{aligned} \tag{A.4.27}$$

where the rotated eigenvectors $\boldsymbol{v}'^{\lambda}_{\chi}$ have the same sign λ of helicity as the original ones.

A.5 Hermiticity of the Curl Operator

An Hermitean or self-adjoint matrix operator $\hat{L}$ by definition satisfies

$$\int_{\mathcal{D}} \psi_1^\dagger \hat{L} \psi_2 \, d^3x = \int_{\mathcal{D}} \left(\hat{L} \psi_2 \right)^\dagger \psi_1 \, d^3x \ , \tag{A.5.1}$$

with arbitrary vector valued functions ψ_1 and ψ_2 that satisfy periodic boundary conditions in a finite domain or tend to zero at infinity. To be Hermitean for bounded fluids, the real curl operator $\hat{R}$ must therefore satisfy

$$\int_{\mathcal{D}} \boldsymbol{u}^T \left(\hat{R} \boldsymbol{v} \right) \, d^3x = \int_{\mathcal{D}} \left(\hat{R} \boldsymbol{v} \right)^T \boldsymbol{u} \, d^3x \ , \tag{A.5.2}$$

where $\boldsymbol{u}$ and $\boldsymbol{v}$ are periodic at the boundary $\partial\mathcal{D}$ of finite domain $\mathcal{D}$. The expression $\boldsymbol{u}\cdot(\boldsymbol{\nabla}\times\boldsymbol{v})$ is a sum of terms $u^j \partial_l \, v^k$. With partial integration it follows that

$$\int_{\mathcal{D}} u^j \partial_l \, v^k \, dx^l = \left[u^j v^k \right]_{\partial\mathcal{D}} - \int_{\mathcal{D}} v^k \partial_l \, u^j \, dx^l \ , \tag{A.5.3}$$

where the first term on the right-hand side vanishes due to the boundary conditions. It is then easy to show that

$$\int_{\mathcal{D}} \boldsymbol{u} \cdot (\boldsymbol{\nabla} \times \boldsymbol{v}) \, d^3x = \int_{\mathcal{D}} \boldsymbol{v} \cdot (\boldsymbol{\nabla} \times \boldsymbol{u}) \, d^3x \ , \tag{A.5.4}$$

and therefore the Hermiticity of the curl operator.

A.6 Parity Transformation and Complex Conjugation

Suppose two observers $\mathcal{O}_R$ and $\mathcal{O}_L$ are describing the same physical phenomenon in a right- and left-handed frame of reference, respectively. By comparing their measurements, a distinction needs to be made between two types of vectors.

A *true vector* (or polar vector) such as velocity is defined such that its direction can be determined without referring to frame dependent conventions by simply connecting two different points in space, possibly at infinitesimally different times. Since the distance between points in spacetime (or the metric) is invariant under a change of handedness of the frame of reference, i.e., a *parity transformation*, both observers see the same vector although its components have different values in the two coordinate systems.

In contrast to true vectors, due to the change of handedness, vector quantities such as cross product and curl (e.g., vorticity) are evaluated differently in the two frames. These vectors are called *pseudo-vectors* (or axial vectors). Since they point in opposite directions in the two frames of reference, a right- and left-handed observer see different pseudo-vectors associated with the same physical process.

The relationship $\boldsymbol{a}\times\boldsymbol{b} = \boldsymbol{c}$ between true vectors $\boldsymbol{a}$, $\boldsymbol{b}$, and $\boldsymbol{c}$ as observed by $\mathcal{O}_R$, using the right-hand rule to evaluate the cross product, is observed as $\boldsymbol{b}\times\boldsymbol{a} = \boldsymbol{c}$ by $\mathcal{O}_L$ using the left-hand rule. Stated differently, the pseudo-vector $\boldsymbol{a}\times\boldsymbol{b}$ as determined by $\mathcal{O}_L$ is equal to

$-\boldsymbol{a} \times \boldsymbol{b}$ in terms of quantities of the right-handed system, i.e., $(\boldsymbol{a} \times \boldsymbol{b})^L = -(\boldsymbol{a} \times \boldsymbol{b})^R$. The same is true for vorticity or any spin vector. Suppose now that $\mathcal{O}_R$ and $\mathcal{O}_L$ observe a spinning solid body, determining the same relationship $\boldsymbol{u} = \boldsymbol{s} \times \boldsymbol{r}$ between the rotational velocity $\boldsymbol{u}$ of a point on the solid body, its position vector $\boldsymbol{r}$ measured from the centre of mass, and the spin vector $\boldsymbol{s}$. Since $\boldsymbol{r}$ and $\boldsymbol{u}$ are objectively measurable in both systems, $\boldsymbol{s}$ cannot be a true vector if the equation $\boldsymbol{u} = \boldsymbol{s} \times \boldsymbol{r}$ is to be preserved under a parity transformation. In fact, there is no objective way for any of the observers of defining $\boldsymbol{s}$ directly without the constraint of the kinematical relationship with the true vectors $\boldsymbol{r}$ and $\boldsymbol{u}$. Given the true vectors of a physical problem, all dynamically relevant pseudo-vectors follow in a consistent way from the requirement that the dynamical equations be invariant under a parity transformation.

In addition to true and pseudo-vectors, a distinction needs to be made between true and pseudo-scalars. While *true scalars* such as kinetic energy and enstrophy are invariant under a change of handedness of the frame of reference, a scalar quantity that changes sign under a parity transformation, such as helicity or chirality, is called a *pseudo-scalar*.

Locally and averaged over limited spatial regions helicity of atmospheric flow is usually non-vanishing. Referring to *parity* as the *symmetry under a parity transformation*, one could argue that parity invariance in these cases is spontaneously broken. *Spontaneous symmetry breaking* generally refers to a situation in which the observable state of a system is not invariant under the full symmetry group of the dynamical equations that govern the given process. Parity conservation, under these circumstances, is a *hidden invariance principle* as opposed to manifest dynamical symmetries associated with conservation laws.

Parity occasionally is referred to as mirror symmetry. Correspondingly, a parity transformation is called mirror transformation, referring to the situation in which either the same physical process is evaluated in frames of reference that are mirror images of each other or the true and mirror image of a process are evaluated in the same frame of reference. Under some circumstances the definition of a parity transformation as the change of handedness of the frame of reference as above is not equivalent with the reflection of the frame of reference. While a reflection of the coordinate system at the origin (full frame inversion) or at one of the coordinate planes inverts an odd number of axes (three or one, respectively) resulting in a frame of reference with switched handedness, the reflection at one of the coordinate axes inverts an even number of axes (two) and the resulting frame of reference has the same handedness as the original frame, in which case true and pseudo-vectors or true and pseudo-scalars transform equally between the two coordinate systems.

The question of whether the mirror image of a process could occur in nature as well is also fundamentally different to the question as to whether right- or left-handed observers are equivalent, or whether the same physical laws are valid in right- and left-handed frames of reference. In classical physics the latter is true because pseudo-quantities are determined that way. However, while the transformation between two different points of view of the same reality necessarily must make them equivalent, different realities seen from the same point of view do not have to follow the same physical equations. A famous example of parity nonconservation is weak interaction and beta-decay.

The velocity field of a fluid has to satisfy two criteria: it has to be real (invariant under complex conjugation) and true (invariant under a parity transformation). Based on the Fourier series representation in helical decomposition these two conditions can be shown to be related.

From the definitions (2.5.21) and (2.5.3) of the curl basis vectors $\boldsymbol{\eta}_{\boldsymbol{k}}^{\lambda}$ and spatial basis functions $\phi_{\chi\boldsymbol{k}}$, respectively, it follows that complex conjugation is equivalent to an inversion of the unit wave vector, $\boldsymbol{k} \mapsto -\boldsymbol{k}$. The set $S(1)$ in the velocity expansion (2.5.20) contains all linearly independent unit vectors $\boldsymbol{q}/q$ plus their negatives. Expanded in terms of only the linearly independent wave vectors in the set $S^{+}(1)$, the helical flows are given by

$$\boldsymbol{v}_{\chi}^{\lambda} = \sum_{\boldsymbol{k}\in S^{+}(1)} a_{\chi\boldsymbol{k}}^{\lambda}\boldsymbol{\eta}_{\boldsymbol{k}}^{\lambda}\phi_{\chi\boldsymbol{k}} + a_{-\chi\boldsymbol{k}}^{\lambda}\boldsymbol{\eta}_{\boldsymbol{k}}^{\lambda *}\phi_{\chi\boldsymbol{k}}^{*} \ . \tag{A.6.1}$$

For the $\boldsymbol{v}_{\chi}^{\lambda}$ to be real, this must be equal to the complex conjugated velocity field,

$$\boldsymbol{v}_{\chi}^{\lambda *} = \sum_{\boldsymbol{k}\in S^{+}(1)} a_{-\chi\boldsymbol{k}}^{\lambda *}\boldsymbol{\eta}_{\boldsymbol{k}}^{\lambda}\phi_{\chi\boldsymbol{k}} + a_{\chi\boldsymbol{k}}^{\lambda *}\boldsymbol{\eta}_{\boldsymbol{k}}^{\lambda *}\phi_{\chi\boldsymbol{k}}^{*} \ . \tag{A.6.2}$$

Therefore

$$a_{-\chi\boldsymbol{k}}^{\lambda} = a_{\chi\boldsymbol{k}}^{\lambda *} \tag{A.6.3}$$

or

$$\mathrm{Re}\left[a_{-\chi\boldsymbol{k}}^{\lambda}\right] = \mathrm{Re}\left[a_{\chi\boldsymbol{k}}^{\lambda}\right] \quad \text{and} \quad \mathrm{Im}\left[a_{-\chi\boldsymbol{k}}^{\lambda}\right] = -\mathrm{Im}\left[a_{\chi\boldsymbol{k}}^{\lambda}\right] \tag{A.6.4}$$

must be satisfied in right- and left-handed frames of reference.

Following the definitions given above, the position vector $\boldsymbol{x}$ is a true vectors and the amount χ of the wave vector is a true scalar.[4] For the phase $\phi_{\chi\boldsymbol{k}}$ of the Fourier components to be a true scalar, the wave vectors $\boldsymbol{k}$ must be true vectors. In fact, their direction is given by the gradient of the phase which can be uniquely determined in right- and left-handed frames of reference if $\phi_{\chi\boldsymbol{k}}$ is a true scalar. If the wave vectors are somehow numbered, $\boldsymbol{k} \to \boldsymbol{k}_i$, then the corresponding normal vectors can systematically be defined by

$$\boldsymbol{n}_i \stackrel{\text{def}}{=} \boldsymbol{k}_i \times \boldsymbol{k}_{i+1} \ . \tag{A.6.5}$$

Then, with the set of true vectors $\{\boldsymbol{k}_i\}$, $\boldsymbol{n}^L = -\boldsymbol{n}^R$ for each $\boldsymbol{n}_i$, since $\mathcal{O}_R$ and $\mathcal{O}_L$ evaluate the cross-product differently. However, $(\boldsymbol{k} \times \boldsymbol{n}^R)^R = (\boldsymbol{k} \times \boldsymbol{n}^L)^L$ and

$$\left(i\boldsymbol{k} \times \left(\left(\boldsymbol{k} \times \boldsymbol{n}^{R/L}\right)^{R/L} \mp i\boldsymbol{n}^{R/L}\right)\right)^{R/L} = \pm\left(\left(\boldsymbol{k} \times \boldsymbol{n}^{R/L}\right)^{R/L} \mp i\boldsymbol{n}^{R/L}\right) \ . \tag{A.6.6}$$

Therefore, $\boldsymbol{k} \times \boldsymbol{n} - i\boldsymbol{n}$ is the positively helical basis vector in both frames of reference and the complex conjugate $\boldsymbol{k} \times \boldsymbol{n} + i\boldsymbol{n}$ is the negatively helical basis vector. As far as the helical basis vectors are concerned, complex conjugation is equivalent to a change of handedness of the coordinate system. Leaving the basis vectors unchanged, the same is true for the basis functions $\phi_{\chi\boldsymbol{k}}$. The complex conjugate phase $\phi_{\chi\boldsymbol{k}}^{*}$ with chirality χ is equal to the phase

[4]For the two helical curl eigenstates $\chi > 0$ is equal to plus or minus chirality where the sign changes under a parity transformation.

$\phi^*_{\chi\boldsymbol{k}} = \phi_{-\chi\boldsymbol{k}}$ with chirality $-\chi$ and the opposite sign of helicity. However, the combined basis vectors $\boldsymbol{\eta}^\lambda_{\boldsymbol{k}}\phi_{\chi\boldsymbol{k}}$ maintain their helicity under complex conjugation, and the sum of a complex velocity field and its complex conjugate,

$$\begin{aligned}\boldsymbol{v}^\lambda_\chi &= \sum_{\boldsymbol{k}\in S^+(1)} a^\lambda_{\chi\boldsymbol{k}}\boldsymbol{\eta}^\lambda_{\boldsymbol{k}}\phi_{\chi\boldsymbol{k}} + \text{c. c.} \\ &= 2\,\mathrm{Re}\left[\sum_{\boldsymbol{k}\in S^+(1)} a^\lambda_{\chi\boldsymbol{k}}\boldsymbol{\eta}^\lambda_{\boldsymbol{k}}\phi_{\chi\boldsymbol{k}}\right]\ ,\end{aligned} \tag{A.6.7}$$

to form a real velocity field, has a unique sign λ of helicity.

To avoid confusion about the sign of helicity, *right-handed flows* $\boldsymbol{v}^R$ and *left-handed flows* $\boldsymbol{v}^L$ can be defined such that they have positive helicity in a right-handed or left-handed frame of reference, respectively. Then, with $\chi > 0$,

$$\boldsymbol{v}^\pm_\chi \stackrel{\text{def}}{=} \boldsymbol{v}^{R/L} = \frac{1}{\sqrt{2}}\sum_{\boldsymbol{k}\in S^(1)} (a^\pm_{\chi\boldsymbol{k}})^R\left(\left(\boldsymbol{k}\times\boldsymbol{n}^R\right)^R \mp i\boldsymbol{n}^R\right)\exp i\chi\boldsymbol{k}\cdot\boldsymbol{x} \tag{A.6.8}$$

in a right-handed system, and

$$\boldsymbol{v}^\mp_\chi \stackrel{\text{def}}{=} \boldsymbol{v}^{R/L} = \frac{1}{\sqrt{2}}\sum_{\boldsymbol{k}\in S^(1)} (a^\mp_{\chi\boldsymbol{k}})^L\left(\left(\boldsymbol{k}\times\boldsymbol{n}^L\right)^L \pm i\boldsymbol{n}^L\right)\exp i\chi\boldsymbol{k}\cdot\boldsymbol{x} \tag{A.6.9}$$

in a left-handed system. For these flows to be invariant under a parity transformation

$$(a^\pm_{\chi\boldsymbol{k}})^R = (a^\mp_{\chi\boldsymbol{k}})^L \tag{A.6.10}$$

must be satisfied. The frame independent concept of right- and left-handed flows is more precise than that of positively and negatively helical flows which is only meaningful with respect to a specific coordinate system. However, for simplicity, throughout the main part of the text a right-handed frame of reference was assumed.

A.7 Beltrami Vortices

The positive curl eigenstate in a right-handed frame of reference was given in Section 2.5.2 as

$$\boldsymbol{v}^+_\chi = \frac{1}{\sqrt{2}}\sum_{\boldsymbol{k}\in S(1)} a^+_{\chi\boldsymbol{k}}(\boldsymbol{k}\times\boldsymbol{n} - i\boldsymbol{n})\exp i\chi\boldsymbol{k}\cdot\boldsymbol{x}\ . \tag{A.7.1}$$

This can be written in explicitly real form as

$$\begin{aligned}\boldsymbol{v}^+_\chi = \sqrt{2}\sum_{\boldsymbol{k}\in S^+(1)} &\left[\alpha^+_{\chi\boldsymbol{k}}(\boldsymbol{k}\times\boldsymbol{n}\cos\chi\boldsymbol{k}\cdot\boldsymbol{x} + \boldsymbol{n}\sin\chi\boldsymbol{k}\cdot\boldsymbol{x})\right. \\ &\left. - \beta^+_{\chi\boldsymbol{k}}(\boldsymbol{k}\times\boldsymbol{n}\sin\chi\boldsymbol{k}\cdot\boldsymbol{x} - \boldsymbol{n}\cos\chi\boldsymbol{k}\cdot\boldsymbol{x})\right]\ ,\end{aligned} \tag{A.7.2}$$

where the sum runs over the set $S^+(1)$ of linearly independent wave vectors in $S(1)$. Choosing the two wave vectors

$$\boldsymbol{k}_x = \begin{pmatrix} 1 \\ 0 \\ 0 \end{pmatrix} \tag{A.7.3}$$

$$\boldsymbol{k}_y = \begin{pmatrix} 0 \\ 1 \\ 0 \end{pmatrix} \tag{A.7.4}$$

with

$$\boldsymbol{n} = \begin{pmatrix} 0 \\ 0 \\ 1 \end{pmatrix} \quad , \tag{A.7.5}$$

and setting

$$\alpha^+_{\chi \boldsymbol{k}_x} = \alpha^+_{\chi \boldsymbol{k}_y} = 0 \tag{A.7.6}$$

and

$$\begin{aligned} A &\stackrel{\text{def}}{=} \sqrt{2}\beta^+_{\chi \boldsymbol{k}_x} \\ B &\stackrel{\text{def}}{=} \sqrt{2}\beta^+_{\chi \boldsymbol{k}_y} \quad , \end{aligned} \tag{A.7.7}$$

this reduces to[5]

$$\boldsymbol{v}^+_\chi = \begin{pmatrix} -B\sin\chi y \\ A\sin\chi x \\ A\cos\chi x + B\cos\chi y \end{pmatrix} \quad . \tag{A.7.8}$$

With $A = B$ the positive curl eigenstate becomes a Beltrami vortex flow with a spatially periodic pattern of counterrotating updrafts and downdrafts, where one of the cyclonic updrafts is centred over the coordinate origin in the horizontal plane. Setting the imaginary parts of the expansion coefficients zero would result in a vortex pattern shifted in the horizontal plane by the vector $(\pi/2\chi, \pi/2\chi)$.

To calculate continuous superpositions of these B-flows the discrete wave vectors $\chi\boldsymbol{k}$ of the Fourier series (A.7.1) are replaced by the continuous wave vector $\boldsymbol{q} = (j, k, l)^T$. As discussed in Appendix A.6, for the $\boldsymbol{v}^\lambda_\chi$ to be real vector functions the set of wave vectors must include the negative of each wave vector. In wavenumber space this means that the wave vectors are distributed mirror symmetrical with respect to the origin. The volumes $V_{\boldsymbol{q}} \stackrel{\text{def}}{=} 8\Delta j\Delta k\Delta l$ of the continuous wave vectors are therefore centred around the positions of

[5] This vector field can be 'completed' by adding the vertically turning (veering for $\chi > 0$) shear flow $(C\sin\chi z, C\cos\chi z, 0)^T$ corresponding to the wave vector $(0, 0, 1)^T$. One then obtains a special case of the famous ABC-flows [e.g., *Galloway and Frisch*, 1987] that, like all B-flows, are analytical, stationary solutions of the Euler equations.

the discrete wave vectors of the Beltrami vortex flow. It simplifies the analysis to relax the constraint of $|\boldsymbol{q}| \equiv 1$ on the discrete wave vector and to replace $\boldsymbol{n}\times\boldsymbol{k}$ in (A.7.1) by $|\boldsymbol{q}_0|^{-1}\boldsymbol{n}\times\boldsymbol{q}$, where $|\boldsymbol{q}_0|$ is equal to j_0 or k_0 depending on whether the spectral volume is centred around the j or k axis. The unit wave vectors $\boldsymbol{k}$ are required for the B-flow property and for the completeness of the velocity decomposition into curl eigenstates. However, the Beltrami property is destroyed anyway by the superposition of B-flows with different chiralities, and completeness is irrelevant since the superposition only defines a special velocity field.

The continuous superposition of Beltrami vortices is then defined as an average over the spectral volume $V_{\boldsymbol{q}}$,

$$
\begin{aligned}
\boldsymbol{v}^+ = \; & V_{\boldsymbol{q}}^{-1} \int_{j_0-\Delta j}^{j_0+\Delta j} \int_{-\Delta k}^{\Delta k} \int_{-\Delta l}^{\Delta l} \left[\frac{1}{j_0} \begin{pmatrix} -k \\ j \\ 0 \end{pmatrix} \sin(jx+ky+lz) \right. \\
& \qquad \left. + \begin{pmatrix} 0 \\ 0 \\ 1 \end{pmatrix} \cos(jx+ky+lz) \right] dl\, dk\, dj \\
& + V_{\boldsymbol{q}}^{-1} \int_{-\Delta j}^{\Delta j} \int_{k_0-\Delta k}^{k_0+\Delta k} \int_{-\Delta l}^{\Delta l} \left[\frac{1}{k_0} \begin{pmatrix} -k \\ j \\ 0 \end{pmatrix} \sin(jx+ky+lz) \right. \\
& \qquad \left. + \begin{pmatrix} 0 \\ 0 \\ 1 \end{pmatrix} \cos(jx+ky+lz) \right] dl\, dk\, dj \;.
\end{aligned}
\tag{A.7.9}
$$

Using the formula

$$
\begin{aligned}
& \int_{x_1}^{x_2} x \sin(ax+b)\, dx \\
& \quad = \frac{1}{a^2} \left[\sin(ax_2+b) - \sin(ax_1+b) - ax_2 \cos(ax_2+b) + ax_1 \cos(ax_1+b) \right]
\end{aligned}
\tag{A.7.10}
$$

the six integrals of (A.7.9) are found to be

$$
\begin{aligned}
I_1 &= -(j_0 V_{\boldsymbol{q}})^{-1} \int_{j_0-\Delta j}^{j_0+\Delta j} \int_{-\Delta k}^{\Delta k} \int_{-\Delta l}^{\Delta l} k \sin(jx+ky+lz) dl\, dk\, dj \\
&= j_0^{-1} \frac{\cos j_0 x \sin \Delta j\, x}{\Delta j\, x} \times \frac{\Delta k\, y \cos \Delta k\, y - \sin \Delta k\, y}{\Delta k\, y^2} \times \frac{\sin \Delta l\, z}{\Delta l\, z} \;,
\end{aligned}
\tag{A.7.11}
$$

$$
\begin{aligned}
I_2 &= (k_0 V_{\boldsymbol{q}})^{-1} \int_{-\Delta j}^{\Delta j} \int_{k_0-\Delta k}^{k_0+\Delta k} \int_{-\Delta l}^{\Delta l} j \sin(jx+ky+lz) dl\, dk\, dj \\
&= k_0^{-1} \frac{\sin \Delta j\, x - \Delta j\, x \cos \Delta j\, x}{\Delta j\, x^2} \times \frac{\cos k_0 y \sin \Delta k\, y}{\Delta k\, y} \times \frac{\sin \Delta l\, z}{\Delta l\, z} \;,
\end{aligned}
\tag{A.7.12}
$$

$$
\begin{aligned}
I_3 &= -(k_0 V_{\boldsymbol{q}})^{-1} \int_{-\Delta j}^{\Delta j} \int_{k_0-\Delta k}^{k_0+\Delta k} \int_{-\Delta l}^{\Delta l} k \sin(jx+ky+lz) dl\, dk\, dj \\
&= k_0^{-1} \frac{\sin \Delta j\, x}{\Delta j\, x} \times \frac{1}{\Delta k\, y^2} \left[\cos k_0 y (\Delta k\, y \cos \Delta k\, y - \sin \Delta k\, y) - k_0 y \sin k_0 y \sin \Delta k\, y \right] \\
&\quad \times \frac{\sin \Delta l\, z}{\Delta l\, z} \ ,
\end{aligned}
\tag{A.7.13}
$$

$$
\begin{aligned}
I_4 &= (j_0 V_{\boldsymbol{q}})^{-1} \int_{j_0-\Delta j}^{j_0+\Delta j} \int_{-\Delta k}^{\Delta k} \int_{-\Delta l}^{\Delta l} j \sin(jx+ky+lz) dl\, dk\, dj \\
&= j_0^{-1} \frac{1}{\Delta j\, x^2} \left[\cos j_0 x (\sin \Delta j\, x - \Delta j\, x \cos \Delta j\, x) + j_0 x \sin j_0 x \sin \Delta j\, x \right] \\
&\quad \times \frac{\sin \Delta k\, y}{\Delta k\, y} \times \frac{\sin \Delta l\, z}{\Delta l\, z} \ ,
\end{aligned}
\tag{A.7.14}
$$

$$
\begin{aligned}
I_5 &= V_{\boldsymbol{q}}^{-1} \int_{j_0-\Delta j}^{j_0+\Delta j} \int_{-\Delta k}^{\Delta k} \int_{-\Delta l}^{\Delta l} \cos(jx+ky+lz) dl\, dk\, dj \\
&= \cos j_0 x \, \frac{\sin \Delta j\, x}{\Delta j\, x} \times \frac{\sin \Delta k\, y}{\Delta k\, y} \times \frac{\sin \Delta l\, z}{\Delta l\, z} \ ,
\end{aligned}
\tag{A.7.15}
$$

and

$$
\begin{aligned}
I_6 &= V_{\boldsymbol{q}}^{-1} \int_{-\Delta j}^{\Delta j} \int_{k_0-\Delta k}^{k_0+\Delta k} \int_{-\Delta l}^{\Delta l} \cos(jx+ky+lz) dl\, dk\, dj \\
&= \cos k_0 y \, \frac{\sin \Delta j\, x}{\Delta j\, x} \times \frac{\sin \Delta k\, y}{\Delta k\, y} \times \frac{\sin \Delta l\, z}{\Delta l\, z} \ .
\end{aligned}
\tag{A.7.16}
$$

The superimposed vortex flows discussed in Section 2.6 are then given by

$$
\boldsymbol{v}^+ = \begin{pmatrix} I_1 + I_3 \\ I_2 + I_4 \\ I_5 + I_6 \end{pmatrix} \ .
\tag{A.7.17}
$$

Defining the approximate Beltrami vortex flows

$$
\boldsymbol{v}_{\boldsymbol{q}}^+ \stackrel{\text{def}}{=} \frac{1}{|\boldsymbol{q}_0|} \begin{pmatrix} -k \\ j \\ 0 \end{pmatrix} \sin(jx+ky+lz) + \begin{pmatrix} 0 \\ 0 \\ 1 \end{pmatrix} \cos(jx+ky+lz) \ ,
\tag{A.7.18}
$$

their spectral average (A.7.9) can be written in short form as

$$
\boldsymbol{v}^+ = \frac{1}{V_{\boldsymbol{q}}} \int \boldsymbol{v}_{\boldsymbol{q}}^+ \, d^3 q \ .
\tag{A.7.19}
$$

The mean spectral kinetic energy referred to in Section 2.6 is then defined as

$$
\begin{aligned}
K_{\text{mean}}^+(\boldsymbol{x}) &\stackrel{\text{def}}{=} \boldsymbol{v}^+ \cdot \boldsymbol{v}^+ \\
&= \frac{1}{V_{\boldsymbol{q}}^2} \int \int \boldsymbol{v}_{\boldsymbol{q}}^+ \cdot \boldsymbol{v}_{\boldsymbol{q}'}^+ \, d^3 q \, d^3 q' \ ,
\end{aligned}
\tag{A.7.20}
$$

rather than

$$\frac{1}{V_{\boldsymbol{q}}} \int \boldsymbol{v}^+_{\boldsymbol{q}} \cdot \boldsymbol{v}^+_{\boldsymbol{q}} \, d^3q \ , \tag{A.7.21}$$

and the mean kinetic energy is defined as the spatial average of the spectral mean kinetic energy,

$$K^+_{\text{mean}} \stackrel{\text{def}}{=} \left\langle K^+_{\text{mean}}(\boldsymbol{x}) \right\rangle \ . \tag{A.7.22}$$

A.8 Time-Averaging

If the slow and fast dependence of the velocity fields $\boldsymbol{u}$ and $\boldsymbol{v}$ is *symbolically* expressed by writing

$$\begin{aligned} \boldsymbol{u} &= \boldsymbol{u}(\tau, \boldsymbol{x}) \\ \boldsymbol{v} &= \boldsymbol{v}(t, \boldsymbol{x}) \end{aligned} \tag{A.8.1}$$

with slow and fast time variables τ and t, respectively, the time-derivative in the equations of motion is replaced by

$$\partial_{\tilde{t}} \tilde{\boldsymbol{v}}(\tilde{t}, \boldsymbol{x}) \longrightarrow \partial_\tau \boldsymbol{u} + \partial_t \boldsymbol{v} \ . \tag{A.8.2}$$

Formally one might try to introduce the variable transformation $\tilde{t} = \tau + t$. Then, however, for any function $f = f(\tilde{t}) = f(\tau + t)$, $\partial_\tau f = \partial_{\tilde{t}} f \partial_\tau \tilde{t} = \partial_{\tilde{t}} f \partial_t \tilde{t} = \partial_t f$, which would be wrong. Instead the formal transformation of the differential operator $\partial_{\tilde{t}} \to \partial_\tau + \partial_t$ must be introduced. Together with $\tilde{\boldsymbol{v}}(\tilde{t}, \boldsymbol{x}) \to \boldsymbol{u}(\tau, \boldsymbol{x}) + \boldsymbol{v}(t, \boldsymbol{x})$ this leads to (A.8.2).

A particular case is where $\boldsymbol{u}$, at each time τ, is the time-average of $\tilde{\boldsymbol{v}}$ over the previous period T,

$$\begin{aligned} \boldsymbol{u}(\tau, \boldsymbol{x}) &\stackrel{\text{def}}{=} \overline{\tilde{\boldsymbol{v}}(\tilde{t}, \boldsymbol{x})}(\tau) \\ &\stackrel{\text{def}}{=} \frac{1}{T} \int_{\tau - T}^{\tau} \tilde{\boldsymbol{v}}(\tilde{t}, \boldsymbol{x}) d\tilde{t} \ . \end{aligned} \tag{A.8.3}$$

By the Leibniz rule

$$\partial_\tau \int_{g(\tau)}^{h(\tau)} f(\tau, t) dt = \int_{g(\tau)}^{h(\tau)} \partial_\tau f(\tau, t) dt + f(\tau, h(\tau)) \partial_\tau h(\tau) - f(\tau, g(\tau)) \partial_\tau g(\tau) \ , \tag{A.8.4}$$

and the time-derivative of the time-average, with $\partial_\tau \tilde{\boldsymbol{v}}(\tilde{t}, \boldsymbol{x}) = \boldsymbol{0}$,

$$\partial_\tau \overline{\tilde{\boldsymbol{v}}}(\tau, \boldsymbol{x}) = \frac{1}{T} \left(\tilde{\boldsymbol{v}}(\tau, \boldsymbol{x}) - \tilde{\boldsymbol{v}}(\tau - T, \boldsymbol{x}) \right) \tag{A.8.5}$$

is equal to the time-average of the time-derivative

$$\overline{\partial_{\tilde{t}} \tilde{\boldsymbol{v}}}(\tau, \boldsymbol{x}) = \frac{1}{T} \int_{\tau - T}^{\tau} \partial_{\tilde{t}} \tilde{\boldsymbol{v}}(\tilde{t}, \boldsymbol{x}) d\tilde{t} \ . \tag{A.8.6}$$

The equations of motion for the slowly evolving velocity field $\boldsymbol{u}$ are then derived from the equations of motion

$$\partial_{\tilde{t}}\tilde{\boldsymbol{v}} + \partial_{\tilde{\boldsymbol{v}}}\tilde{\boldsymbol{v}} = \tilde{\boldsymbol{f}} \tag{A.8.7}$$

for the total velocity field $\tilde{\boldsymbol{v}}$ through time (Reynolds) averaging, and are given by

$$\partial_\tau \boldsymbol{u} + (\boldsymbol{u}\cdot\boldsymbol{\nabla})\boldsymbol{u} + \overline{(\boldsymbol{v}\cdot\boldsymbol{\nabla})\boldsymbol{v}} = \boldsymbol{f} \ . \tag{A.8.8}$$

Subtracting (A.8.8) from (A.8.7) then gives the equations of motion for the velocity perturbations $\boldsymbol{v} \stackrel{\text{def}}{=} \tilde{\boldsymbol{v}} - \boldsymbol{u}$,

$$\partial_t \boldsymbol{v} + (\boldsymbol{u}\cdot\boldsymbol{\nabla})\boldsymbol{v} + (\boldsymbol{v}\cdot\boldsymbol{\nabla})\boldsymbol{u} + (\boldsymbol{v}\cdot\boldsymbol{\nabla})\boldsymbol{v} - \overline{(\boldsymbol{v}\cdot\boldsymbol{\nabla})\boldsymbol{v}} = \boldsymbol{f}' \ . \tag{A.8.9}$$

Often in turbulence and boundary layer theory it is assumed that the fast velocity perturbations, and in fact the total velocity field, are incompressible.[6] Assuming as in Section 2.7 that thermodynamic forcing varies on the slow timescale, the time-perturbations $\boldsymbol{f}'$ of the forcing term in the Navier-Stokes, Boussinesq, or Euler equations vanishes. Also, since

$$\boldsymbol{\nabla}^T \left(\boldsymbol{a}\boldsymbol{a}^T\right) = (\boldsymbol{a}\cdot\boldsymbol{\nabla})\boldsymbol{a} + (\boldsymbol{\nabla}\cdot\boldsymbol{a})\boldsymbol{a} \tag{A.8.10}$$

for any column vector $\boldsymbol{a}$, the term $(\boldsymbol{v}\cdot\boldsymbol{\nabla})\boldsymbol{v}$ is equal to the divergence of the symmetrical stress tensor $\boldsymbol{v}\boldsymbol{v}^T = (\boldsymbol{v}\boldsymbol{v}^T)^T$,

$$(\boldsymbol{v}\cdot\boldsymbol{\nabla})\boldsymbol{v} = \boldsymbol{\nabla}^T \left(\boldsymbol{v}\boldsymbol{v}^T\right) \ . \tag{A.8.11}$$

Defining the time-averaged stress tensor $R \stackrel{\text{def}}{=} \overline{\boldsymbol{v}\boldsymbol{v}^T}$ and introducing the notation

$$\boldsymbol{\nabla}\cdot R \stackrel{\text{def}}{=} \boldsymbol{\nabla}^T\overline{\boldsymbol{v}\boldsymbol{v}^T} \ , \tag{A.8.12}$$

the 'fast' equations of motion (A.8.9) become

$$\partial_t \boldsymbol{v} + (\boldsymbol{u}\cdot\boldsymbol{\nabla})\boldsymbol{v} + (\boldsymbol{v}\cdot\boldsymbol{\nabla})\boldsymbol{u} + (\boldsymbol{v}\cdot\boldsymbol{\nabla})\boldsymbol{v} = \boldsymbol{\nabla}\cdot R \ . \tag{A.8.13}$$

The Fourier transformations of (A.8.8) and (A.8.9) or (A.8.13) are equivalent with (2.7.10) and (2.7.11) of Section 2.7 if $\overline{(\boldsymbol{v}\cdot\boldsymbol{\nabla})\boldsymbol{v}} \equiv \boldsymbol{0}$. This is consistent with the fact that in Section 2.7 the expansion coefficients of the fast flow were assumed to be small perturbations of the corresponding expansion coefficients of the total flow.

Technically, (A.8.8) and (A.8.9) or (A.8.13), with a prognostic equation for the forcing term $\tilde{\boldsymbol{f}}$, constitute a closed system of equations. However, due to the time-averaged nonlinear quantities in $\boldsymbol{v}$ the system cannot be integrated without a closure assumption expressing the time-averaged quantities in terms of the time-averaged velocity field $\boldsymbol{u}$. If instead of some parameterisation of the stress tensor divergence it can be assumed that the quadratic terms in the time-perturbations can be neglected, the analysis simplifies significantly. For the description of space filling, continuously generated turbulent eddies, i.e., for the general

[6] Under the Boussinesq approximation density fluctuations are still taken into account in the buoyancy term.

description of turbulence, this is not a good assumption. Away from solid boundaries (above the planetary boundary layer) or strong gradients (fronts) the divergence of the time-averaged stress tensor is generally small. However, in the vicinity of jets and in regions of strong convection, even in the free atmosphere, this term can become large. For the description of general turbulent motion in the storm cloud, (2.7.10) and (2.7.11), derived for the study of a particular flow instability, are not valid.

A.9 Centre-Manifold Reduction

Similarly to the helical decomposition of the flow in physical space into curl eigenstates the flow in phase space can be projected onto any orthonormal system of basis vectors. Initially the most obvious choice of phase space coordinates are the Fourier expansion coefficients directly. However, after a linear stability analysis the dynamics in phase space in a small neighbourhood of the fixed points can often be simplified by projecting the dynamical system onto their linear eigenspaces. At criticality the significant dynamics takes place on the centre-manifold.

To study the centre-manifold dynamics by standard normal forms the system (3.4.6) must be reduced to a one-parameter problem. This is achieved by setting $p \equiv r$ and by keeping all parameters fixed except for q, which therefore becomes the bifurcation parameter with critical value $q_c = \sigma/2$. At criticality (3.4.6) is then given by

$$\begin{aligned} \dot{X} &= -p(Y+Z) \\ \dot{Y} &= p(X+Z) \\ \dot{Z} &= XY - \frac{\sigma}{2}(X+Y+2Z)\ . \end{aligned} \tag{A.9.1}$$

For the transcritical, steady-state bifurcation one real eigenvalue vanishes at criticality. The centre-manifold is therefore one-dimensional. The eigenvector corresponding to that eigenvalue, at criticality, is proportional to

$$\boldsymbol{c} \stackrel{\text{def}}{=} \frac{1}{\sqrt{3}} \begin{pmatrix} 1 \\ 1 \\ -1 \end{pmatrix}\ , \tag{A.9.2}$$

i.e., it is pointing along the line on which lie the vortex equilibria as a function of q (see Figure 3.14). If this centre-direction is taken as one of the new coordinate axes, the normal vector $\boldsymbol{n}$ can be defined as

$$\boldsymbol{n} \stackrel{\text{def}}{=} \frac{1}{\sqrt{2}} \begin{pmatrix} 1 \\ -1 \\ 0 \end{pmatrix}\ , \tag{A.9.3}$$

and the binormal vector $\boldsymbol{b}$ as

$$\boldsymbol{b} \stackrel{\text{def}}{=} \frac{1}{\sqrt{6}} \begin{pmatrix} 1 \\ 1 \\ 2 \end{pmatrix}\ . \tag{A.9.4}$$

The new phase space coordinates in terms of the old ones are then given by

$$c \stackrel{\text{def}}{=} \boldsymbol{c} \cdot \boldsymbol{X} = \frac{1}{\sqrt{3}}(X + Y - Z) \tag{A.9.5}$$

$$n \stackrel{\text{def}}{=} \boldsymbol{n} \cdot \boldsymbol{X} = \frac{1}{\sqrt{2}}(X - Y) \tag{A.9.6}$$

$$b \stackrel{\text{def}}{=} \boldsymbol{b} \cdot \boldsymbol{X} = \frac{1}{\sqrt{6}}(X + Y + 2Z) \ , \tag{A.9.7}$$

or vice versa

$$X = \frac{1}{\sqrt{3}}c + \frac{1}{\sqrt{2}}n + \frac{1}{\sqrt{6}}b \tag{A.9.8}$$

$$Y = \frac{1}{\sqrt{3}}c - \frac{1}{\sqrt{2}}n + \frac{1}{\sqrt{6}}b \tag{A.9.9}$$

$$Z = -\frac{1}{\sqrt{3}}c + \frac{2}{\sqrt{6}}b \ . \tag{A.9.10}$$

Since the basis vectors $\boldsymbol{c}$, $\boldsymbol{n}$, and $\boldsymbol{b}$ are constant, the dynamical system for the new phase space coordinates c, n, and b is given by

$$\begin{aligned} \dot{c} &= \boldsymbol{c} \cdot \dot{\boldsymbol{X}} \\ &= \sqrt{\frac{2}{3}}pn + \frac{1}{\sqrt{2}}\sigma b - XY \end{aligned} \tag{A.9.11}$$

$$\begin{aligned} \dot{n} &= \boldsymbol{n} \cdot \dot{\boldsymbol{X}} \\ &= -\sqrt{3}pb \end{aligned} \tag{A.9.12}$$

$$\begin{aligned} \dot{b} &= \boldsymbol{b} \cdot \dot{\boldsymbol{X}} \\ &= \frac{1}{\sqrt{3}}pn - \sigma b + 2XY \ , \end{aligned} \tag{A.9.13}$$

where the product XY can also be expressed in terms of the new variables. Since at the equilibrium the linear eigenspaces are tangent to the corresponding nonlinear manifolds, near an equilibrium points on the nonlinear centre-manifold can be described by writing the variables n and b as functions of the centre coordinate c,

$$n = n(c) \tag{A.9.14}$$

$$b = b(c) \ , \tag{A.9.15}$$

where due to the tangency $\partial_c n = \partial_c b = 0$ at the equilibrium. Then

$$\dot{n} = (\partial_c n)\, \dot{c} \tag{A.9.16}$$

$$\dot{b} = (\partial_c b)\, \dot{c} \tag{A.9.17}$$

with (A.9.11). Comparing these two equations with (A.9.12) and (A.9.13), respectively, gives an equation for $n = n(c)$ and $b = b(c)$, which can be solved by power series expansion to any order in c. Substituting these expression into (A.9.11) then gives an uncoupled equation for the dynamics on the centre-manifold near the equilibrium.[7]

Due to the nonlinearity of the centre-manifold an exact analytical representation is generally not possible. However, near an equilibrium at criticality an approximate description of the dynamics can often be derived. In this particular case, since the stable vortex equilibria lie on a straight line from the origin parallel to the centre-direction at the origin, the centre-manifold dynamics at the transcritical bifurcation is in fact an accurate dynamical description for the origin to vortex transition for supercritical values of q as well, i.e., for noncoinciding equilibria.

[7] For an introduction to normal-form dynamics and centre-manifold reduction see *Crawford* [1991].

B Glossary

alignment measure of the correlation between velocity and vorticity vectors; alignment density is the cosine of the angle between velocity and vorticity vectors. [→ Section 2.1.3]

asymptotic stability state of an equilibrium of a phase space flow or map without unstable and neutral directions, i.e., with empty unstable and centre subspaces. [→ Section 3.3]

B-flow Beltrami flow with constant chirality; spatially periodic solutions are given by monochromatic Fourier series expansions where the single wavenumber is equal to the amount of chirality. [→ Section 2.1.3]

Beltrami flow flow for which velocity and vorticity are parallel or antiparallel everywhere in a specified domain; alignment is constant and equal to plus or minus one. [→ Section 2.1.3]

bifurcation significant change in the qualitative behaviour of a dynamical system due to small changes in the system parameters; more specifically the change in linear stability of certain equilibria upon small parameter changes. [→ Section 3.4]

chirality ratio of helicity density to kinetic energy density; wavenumber of a B-flow. [→ Section 2.1.3]

curl eigenstates solutions of the curl eigenvector equation with constant chirality; positively and negatively helical B-flows and irrotational gradient flows; in Fourier series representation pure helical and spectral states. [→ Section 2.5.2, Appendix A.2]

curl eigenvectors combined spectral and helical basis vectors of curl eigenstates. [→ Section 2.5.2, Appendix A.2]

eddy spatially limited positive perturbation of kinetic energy from normal flow state; intense eddies are associated with localised, positively correlated positive perturbations in kinetic energy and enstrophy, and helical eddies with positively correlated positive perturbations in intensity and alignment. [→ Section 2.1.4 and 2.6.1]

enstrophy measure of the rotational energy of small fluid elements; enstrophy density is the square of the vorticity vector. [→ Section 2.1.2]

flow structures intense and persistent eddies that preserve their qualitative kinematical properties over sufficiently long periods of time to be able to interact with each other. [→ Section 2.3.2 and 2.6.1]

fluid element infinitesimal volume containing the same molecules at all times; infinitesimal Lagrangian volume. [→ Section 2.1.1]

fundamental law of algebra states that the polynomial $x^n + a_{n-1}x^{n-1} + \cdots + a_1 x + a_0 = 0$ with $a_j \in \mathbb{C}$ has n roots in $\mathbb{C}$. For $a_j \in \mathbb{R}$ the roots are real or come in complex conjugate pairs.

helical property of eddies or flow structures, referring to positively correlated positive perturbations of intensity and alignment. [→ Section 2.1.4]

helical basis vectors three eigenvectors of the curl operator in wavenumber space; orthonormal vector basis for Fourier transform of velocity. [→ Section 2.5.2, Appendix A.2]

helicity combined measure of intensity and persistence of flow perturbations; helicity density is the scalar product between velocity and vorticity. [→ Section 2.1.3]

hyperbolic fixed point equilibrium of a dynamical system without centre (neutral) directions. [→ Section 3]

intensity combined measure of kinetic energy and enstrophy. [→ Section 2.1.2]

kinetic energy of fluid elements is a measure of their kinetic energy in the usual mechanical definition for solid particles; kinetic energy density is the square of velocity. [→ Section 2.1.2]

Lagrangian surface surface of a Lagrangian volume. [→ Section 2.1.1]

Lagrangian volume volume of fluid containing the same molecules at all times; mass is constant and all fluxes across the bounding surface vanish. [→ Section 2.1.1]

left-handed property of a frame of reference whose ordered coordinate axes are arranged according to the left-hand rule. [→ Appendix A.6]

parity invariance (symmetry) of the physical laws under a change of handedness of the frame of reference. [→ Appendix A.6]

parity transformation transformation between right- and left-handed frames of reference. [→ Appendix A.6]

pseudo-scalar scalar that changes sign under a parity transformation. [→ Appendix A.6]

pseudo-vector vector that points in opposite directions in a right- and left-handed frame of reference. [→ Appendix A.6]

right-handed property of frame of reference whose ordered coordinate axes are arranged according to the right-hand rule. [→ Appendix A.6]

supercell thunderstorm a particular type of thunderstorm characterised by a persistent, quasi-stationary, strongly rotating updraft (a mesocyclone), which promotes storm organisation and maintenance. The majority of supercell thunderstorms is severe. The environmental mean flow is generally veering over the lowest 3 km, and, given sufficient instability for initial updraft formation, the flow structure of the storm cloud is determined by this large-scale vertical wind profile. The storm usually moves to the right of the mean wind.

thunderstorm (or electrical storm) a cumulonimbus cloud that, in addition to precipitation, is associated with gusty winds, and thunder and lightning. Ordinary thunderstorms generally do not last for more than one hour. They do not have organised rotating updrafts and are usually nonsevere. Since the environmental mean flow does not have a consistent wind shear over the depth of the storm cloud, buoyancy is the dominant factor for storm formation. The storm usually moves with the mean wind.

topology branch of geometry where distance is not relevant. Since no metric is defined, topology investigates geometrical properties without measurements of length. Knot theory and the investigation of the structure of streamlines and vortex-lines have become an important part of topology. [→ Section 2.2]

true scalar scalar that does not change sign under a parity transformation. [→ Appendix A.6]

true vector vector that points in the same direction in right- and left-handed frames of reference. [→ Appendix A.6]

C Abbreviations and Plot Annotations

CAD	Convergent anticyclonically rotating downdraft
CCU	Convergent cyclonically rotating updraft
DAD	Divergent anticyclonically rotating downdraft
DCU	Divergent cyclonically rotating updraft
NTU	Nondimensional time unit
T1	Vortex triad $\boldsymbol{k}_x + \boldsymbol{k}_y = \sqrt{2}\boldsymbol{k}_{x,y}$
T2	Vortex triad $\boldsymbol{k}_x - \boldsymbol{k}_y = \sqrt{2}\boldsymbol{k}_{x,-y}$
VORTEX	Verification of the Origins of Rotation in Tornadoes Experiment

D List of Symbols and Notation

Symbols

a	real constant; scale factor of continuous spectral function, Section 2.6.1
$a_k,\ a_{jkl},\ a_{\chi\boldsymbol{k}}$	expansion coefficients of Fourier series
$a^{\lambda}_{\chi\boldsymbol{k}}$	helical expansion coefficients of $\boldsymbol{v}$
$\boldsymbol{a_q}$	$= (a_{\boldsymbol{q}}, b_{\boldsymbol{q}}, c_{\boldsymbol{q}})^T$, imaginary part of $\boldsymbol{u_q}$
$\boldsymbol{a}_{j,k}$	$= (a_{j,k}, b_{j,k}, c_{j,k})^T$, index notation for $\boldsymbol{u_q}$ with $\boldsymbol{q} = (j, k, 0)^T$
$a(k)$	continuous isotropic kinetic energy spectral function
$a_{\text{hor}}(k_h)$	continuous horizontal kinetic energy spectral function
$a^{\lambda}_{\text{hor}}(k_h)$	continuous horizontal kinetic energy spectral function in helical decomposition
$\lvert a_\chi\rvert^2$	discrete isotropic kinetic energy spectrum
$\lvert a_{\chi\text{hor}}\rvert^2$	horizontal discrete isotropic kinetic energy spectrum
$\lvert a^{\lambda}_{\chi\text{hor}}\rvert^2$	horizontal discrete isotropic kinetic energy spectrum in helical decomposition
A	real amplitude function of Beltrami vortex; complex factor of spatial and spectral kinetic energy distribution functions, Section 2.6.1
$A(\bar{\boldsymbol{X}})$	attractor strength of equilibrium $\bar{\boldsymbol{X}}$
$A_{\boldsymbol{q}}$	real expansion coefficients of Fourier series
b	real constant;
B	real amplitude function of Beltrami vortex; complex factor of spatial and spectral kinetic energy distribution functions, Section 2.6.1
$\mathcal{B}$	domain in which the flow satisfies the Beltrami condition
c	real constant
C	real amplitude function of Beltrami vortex
D	number of data points
$\mathcal{D}$	three-dimensional spatial domain
$\boldsymbol{e}_x$	unit vector in the direction given by coordinate x
E	$\stackrel{\text{def}}{=} \langle\varepsilon\rangle$, averaged enstrophy
f	arbitrary analytic scalar function
$\boldsymbol{f}$	sum of all acceleration terms in fluid dynamical equations; slow forcing term of storm system
$\tilde{\boldsymbol{f}}$	forcing term for $\tilde{\boldsymbol{v}}$
$\boldsymbol{f}'$	fast forcing term for $\boldsymbol{v}$
$\boldsymbol{f_q}$	expansion coefficients of $\boldsymbol{f}$
$\boldsymbol{f}'_{\boldsymbol{q}}$	expansion coefficients of $\boldsymbol{f}'$

F	Fourier transform of f
F_f	undetermined integral of f
H	$\stackrel{\text{def}}{=} \langle \eta \rangle$, averaged helicity
i	$\stackrel{\text{def}}{=} \sqrt{-1}$, imaginary unit; index
I	Lagrange invariant, $d_t I \equiv 0$, Section 2.2; ensemble average of spatial helicity correlation, Section 2.6.1
j	continuous wavenumber component in x-direction; index of summation
j_0	central wavenumber of wave packet
$J(\boldsymbol{X})$	Jacobian matrix of dynamical system evaluated at point $\boldsymbol{X}$
$\boldsymbol{J}$	frozen-in vector field
k	wavenumber; continuous wavenumber component in y-direction; index of summation
k_0	central wavenumber of wave packet
$\boldsymbol{k}$	discrete unit wave vector in Fourier series
$k_{\max}$	wavenumber of maximum of $\lvert a(k) \rvert^2$
k_h	$\stackrel{\text{def}}{=} \sqrt{k_x^2 + k_y^2}$, horizontal wave vector
$k_{h\max}$	wavenumber of maximum of $\lvert a_{\text{hor}}(k_h) \rvert^2$
k_x	component of wave vector $\boldsymbol{k}$ corresponding to coordinate x
$\boldsymbol{k}_x$	wave vector $(1, 0, 0)^T$
$\boldsymbol{k}_y$	wave vector $(0, 1, 0)^T$
$\boldsymbol{k}_{x,y}$	wave vector $(1, 1, 0)^T/\sqrt{2}$
$\boldsymbol{k}_{x,-y}$	wave vector $(1, -1, 0)^T/\sqrt{2}$
$\hat{\boldsymbol{k}}_\chi$	vector operator corresponding to $\boldsymbol{k}$, $\hat{\boldsymbol{k}}_\chi \phi_{\chi \boldsymbol{k}} = \boldsymbol{k} \phi_{\chi \boldsymbol{k}}$
K	$\stackrel{\text{def}}{=} \langle \kappa \rangle$, averaged kinetic energy
$\bar{K}$	total integrated kinetic energy
l	continuous wavenumber component in z-direction; index of summation
L	length scale; length of spatial domain, Section 2.6.1
m	mass of Lagrangian volume
n	positive integer
$\boldsymbol{n}$	unit normal vector to $\boldsymbol{k}$; outward unit normal on a closed surface
$\mathcal{M}$	spatial domain of the mesocyclone
$\mathbb{N}$	set of natural numbers including zero
$\mathcal{O}(\varepsilon)$	term of order ε
p	air pressure, Chapter 2; parameter in dynamical system, Chapter 3
$\mathcal{P}^3$	domain in which $\phi_{\chi \boldsymbol{k}}$ satisfies periodic boundary conditions

q	amount of wave vector $\boldsymbol{q}$, Chapter 2; parameter in dynamical system, Chapter 3
$\boldsymbol{q}$	continuous wave vector in Fourier transformation; discrete wave vector with integer components in Fourier series
q_c	critical value of parameter q
$r,\ r_j$	parameters in dynamical system
r_h	$\stackrel{\text{def}}{=} \sqrt{x^2+y^2}$, horizontal radial coordinate
$R(\bar{\boldsymbol{X}})$	repellor strength of equilibrium $\bar{\boldsymbol{X}}$
$\hat{R}$	matrix curl operator, $\hat{R}\boldsymbol{v} \equiv \boldsymbol{\nabla}\times\boldsymbol{v}$
$\mathbb{R}$	set of all real numbers
s	supercriticality q/q_c
$\boldsymbol{s}$	spin vector of fluid element; rotation vector of solid body vortex
S	size of any surface
$\mathcal{S}(\mathcal{D})$	closed bounding surface of $\mathcal{D}$
$S(1)$	set of all unit wave vectors $\boldsymbol{k}$
$S(k)$	spherical shell in continuous wave vector space with radius k
$S_{xy}(1)$	set of horizontal unit wave vectors
$S_z(1)$	set of vertical unit wave vectors
$\boldsymbol{S}$	nonhelical vector field for which planes $\boldsymbol{S}\cdot d\boldsymbol{x}=0$ are frozen in
S_f	Fourier series of f
t	(fast) time parameter
T	timescale; time interval
u	eastward velocity component
$\boldsymbol{u}$	velocity of centre of mass of fluid element, Section 2.1.2; slowly evolving velocity field
$\boldsymbol{u}_{\boldsymbol{q}}$	expansion coefficients of $\boldsymbol{u}$
v	northward velocity component
$\boldsymbol{v}$	$=(u,v,w)^T$, general velocity field; rapidly evolving vortex flow field
$\tilde{\boldsymbol{v}}$	total velocity field
$\boldsymbol{v}_{\boldsymbol{q}}$	expansion coefficients of $\boldsymbol{v}$
$\tilde{\boldsymbol{v}}_{\boldsymbol{q}}$	expansion coefficients of $\tilde{\boldsymbol{v}}$
$v(k)$	amount of Fourier transform of velocity
$\boldsymbol{v}_h$	$\stackrel{\text{def}}{=} (u,v,0)^T$, horizontal velocity vector
$\boldsymbol{v}_L$	pointwise average of $\boldsymbol{v}_S$
$\boldsymbol{v}_S$	velocity field on smallest resolvable scale
$\boldsymbol{v}_\chi$	monochromatic periodic velocity field with wavenumber χ
$\boldsymbol{v}_\chi^\lambda$	curl eigenstates, $\hat{R}\boldsymbol{v}_\chi^\lambda = \lambda\chi\boldsymbol{v}_\chi^\lambda$
V	size of any volume
$V(\mathcal{D})$	size of volume $\mathcal{D}$
$\mathcal{V}$	spatial domain of tornado vortex

$\mathcal{V}_L$	any Lagrangian volume
w	upward velocity component
x	(eastward) Cartesian coordinate
x^j	$= \{x, y, z\}$, Cartesian coordinates in 3D tensor notation
$\boldsymbol{x}$	$= (x, y, z)^T$, 3D position vector
$\boldsymbol{x}_0$	constant position in space
X	phase space variable
$\bar{X}$	position coordinate of vortex equilibrium in phase space
$\boldsymbol{X}$	$= (X, Y, Z)^T$, position vector in phase space
$\boldsymbol{X}_0$	$= (0, 0, 0)^T$, origin in phase space, ground state
$\bar{\boldsymbol{X}}$	$= (\bar{X}, \bar{Y}, \bar{Z})^T$, position vector of equilibrium in phase space; position vector of vortex equilibrium
y	(northward) Cartesian coordinate
Y	phase space variable
$\bar{Y}$	position coordinate of vortex equilibrium in phase space
z	(vertical) Cartesian coordinate
Z	phase space variable
$\bar{Z}$	position coordinate of vortex equilibrium in phase space
$\mathbb{Z}$	set of all integers
α	$\stackrel{\text{def}}{=} \cos\phi$, local alignment
$\alpha^\lambda_{\chi\boldsymbol{k}}$	real part of $a^\lambda_{\chi\boldsymbol{k}}$
$\boldsymbol{\alpha}_{\boldsymbol{q}}$	$= (\alpha_{\boldsymbol{q}}, \beta_{\boldsymbol{q}}, \gamma_{\boldsymbol{q}})^T$, real part of $\boldsymbol{u}_{\boldsymbol{q}}$
$\beta^\lambda_{\chi\boldsymbol{k}}$	imaginary part of $a^\lambda_{\chi\boldsymbol{k}}$
Γ	set of discrete wavenumbers in Fourier series
δ	$\stackrel{\text{def}}{=} \Delta k/k_0$, measure of spectral width of wave packet
$\delta(\boldsymbol{x}' - \boldsymbol{x})$	$\stackrel{\text{def}}{=} \delta(x' - x)\delta(y' - y)\delta(z' - z)$, 3D Dirac distribution
$\delta_{\boldsymbol{k}',\boldsymbol{k}}$	$\stackrel{\text{def}}{=} \delta_{k'_x,k_x}\delta_{k'_y,k_y}\delta_{k'_z,k_z}$, 3D Kronecker symbol
Δk	width of spectral kinetic energy distribution
Δx	width of spatial kinetic energy distribution
ε	$\stackrel{\text{def}}{=} \boldsymbol{\omega}\cdot\boldsymbol{\omega}$, enstrophy density; small positive number
ζ	vertical vorticity component
η	$\stackrel{\text{def}}{=} \boldsymbol{v}\cdot\boldsymbol{\omega}$, helicity density
$\boldsymbol{\eta}^\lambda_{\boldsymbol{k}}$	helical basis vector
θ	potential temperature
κ	$\stackrel{\text{def}}{=} \boldsymbol{v}\cdot\boldsymbol{v}$, kinetic energy density
κ'	perturbation of κ from K
κ^λ	kinetic energy of $\boldsymbol{v}^\lambda_\chi$
λ	$= 0, \pm 1$, index denoting helical state of Fourier wave, Chapter 2; eigenvalue of Jacobian matrix of dynamical system, Chapter 3
$\boldsymbol{\xi}$	position vector along vortex line
$\boldsymbol{\xi}_0$	position of $\boldsymbol{\xi}$at $t = 0$
ρ	mass density;

	any conserved density
ρ_0	constant mass density
σ	$\stackrel{\text{def}}{=} \sqrt{\kappa\varepsilon}$, intensity, Chapter 2;
	parameter in dynamical system, Chapter 3
τ	slow timescale variable
ϕ	locally shortest planar angle between velocity and vorticity vectors
ϕ_{jkl}	$\stackrel{\text{def}}{=} \exp i\chi_0(jx + ky + lz)$, Fourier series basis function
$\phi_{\chi\boldsymbol{k}}$	$\stackrel{\text{def}}{=} \exp i\chi\boldsymbol{k} \cdot \boldsymbol{x}$, identical to ϕ_{jkl}
$\phi(\boldsymbol{x}, \boldsymbol{q})$	$\stackrel{\text{def}}{=} \exp i\boldsymbol{q} \cdot \boldsymbol{x}$, Fourier transformation basis function
Φ	effective gravitational potential
χ	wavenumber of Fourier series; for B-flows chirality $= \eta\kappa^{-1} = const.$
$\bar{\chi}$	$\stackrel{\text{def}}{=} \langle\chi\rangle$, averaged chirality
χ'	perturbation of χ from $\bar{\chi}$
χ_0	smallest nonzero wavenumber in Γ
$\psi(x)$	Fourier transform of $a(k)$
$\psi_{\text{hor}}(x_h)$	Fourier transform of $a_{\text{hor}}(k_h)$
$\psi^{\lambda}_{\text{hor}}(x_h)$	Fourier transform of $a^{\lambda}_{\text{hor}}(k_h)$
$\boldsymbol{\omega}$	$\stackrel{\text{def}}{=} \boldsymbol{\nabla} \times \boldsymbol{v}$, 3D vorticity field
$\boldsymbol{\omega}_h$	horizontal vorticity vector
$\boldsymbol{\omega}_p$	$\stackrel{\text{def}}{=} \frac{\boldsymbol{\omega}}{\rho}$, potential vorticity
$\boldsymbol{\omega}_\chi$	vorticity of $\boldsymbol{v}_\chi$
$\boldsymbol{\Omega}$	Earth's spin vector

Notation

$\boldsymbol{A}$	a boldface symbol denotes a vector quantity
$\lvert A\rvert$	absolute value of real number A, magnitude of complex number A
$\lvert\boldsymbol{A}\rvert$	amount of vector $\boldsymbol{A}$
A^*	complex conjugate of quantity A
A^T	transpose of matrix A
$A^\dagger$	$= (A^*)^T = (A^T)^*$, Hermitean transpose of matrix A
$\text{Re}\,[A]$	real part of A
$\text{Im}\,[A]$	imaginary part of A
$\hat{A}$	(differential) operator quantity
$\dot{A}$	total time derivative of A
$\langle A\rangle$	spatial mean of A over an unspecified volume;
	ensemble average of A
$\langle A\rangle_{\mathcal{D}}$	spatial mean of A over domain $\mathcal{D}$
A'	deviations of A from $\langle A\rangle$
$\lambda',\ \lambda''$	equivalent indices to λ in multiple sum
A_j	covariant components of vector A
A^j	contravariant components of vector A

A_{jk}	covariant components of matrix A
$\{A_j\}$	set of all functions or parameters A_j
∂_j	$\stackrel{\text{def}}{=} \partial/\partial x^j$, used in tensor notation
∂_f	$\stackrel{\text{def}}{=} \partial/\partial f$, for a scalar f
$\partial_{\boldsymbol{v}}$	$\stackrel{\text{def}}{=} \boldsymbol{v} \cdot \boldsymbol{\nabla}$, spatial derivative in the direction of vector $\boldsymbol{v}$
$\mathcal{L}_{\boldsymbol{v}}\boldsymbol{J}$	$\stackrel{\text{def}}{=} \partial_{\boldsymbol{v}}\boldsymbol{J} - \partial_{\boldsymbol{J}}\boldsymbol{v}$, Lie derivative of $\boldsymbol{J}$ along $\boldsymbol{v}$ in Cartesian coordinates
$\boldsymbol{\nabla}$	$\stackrel{\text{def}}{=} \boldsymbol{e}_x\partial_x + \boldsymbol{e}_y\partial_y + \boldsymbol{e}_z\partial_z$, nabla operator
$\boldsymbol{\nabla}^2$	$\stackrel{\text{def}}{=} \partial_x^2 + \partial_y^2 + \partial_z^2$, Laplacian operator
d_t	$\stackrel{\text{def}}{=} \partial_t + \partial_{\boldsymbol{v}}$, total or Lagrangian derivative
d^3x	$\stackrel{\text{def}}{=} dx\,dy\,dz$, infinitesimal 3D volume element
δx	finite difference in variable x
$\mathrm{TP}\big[\bar{\boldsymbol{X}}_1 \to \bar{\boldsymbol{X}}_2\big]$	$\stackrel{\text{def}}{=} R(\bar{\boldsymbol{X}}_1)A(\bar{\boldsymbol{X}}_2)$, transition probability from $\bar{\boldsymbol{X}}_1$ to $\bar{\boldsymbol{X}}_1$

References

Barcilon, A., and P. Drazin, *Dust devil formation*, Geophys. Fluid Dyn., **4**, 147–159, 1972.

Batchelor, G. K., *An Introduction to Fluid Dynamics*, second paperback edition, Cambridge University Press, Cambridge, England, 1999.

Belian, A., O. Chkhetiani, E. Golbraikh, and S. Moiseev, *Helical turbulence: turbulent viscosity and instability of the second moments*, Physica A, **258**, 55–68, 1998.

Bluestein, H. B., and A. L. Pazmany, *Observations of tornadoes and other convective phenomena with a mobile, 3-mm wavelength, Doppler radar: The Spring 1999 field experiment*, Bull. Am. Met. Soc., **81**(12), 2939–2951, 2000.

Chen, Q., S. Chen, and G. L. Eyink, *The joint cascade of energy and helicity in three-dimensional turbulence*, Phys. Fluids, **15**(2), 361–374, 2003.

Chorin, A. J., *Vorticity and Turbulence*, Springer-Verlag, New York, USA, 1994.

Cohen, H., *Mathematics for Scientists and Engineers*, Prentice Hall, Englewood Cliffs, New Jersey, USA, 1992.

Crawford, J. D., *Introduction to bifurcation theory*, Rev. Mod. Phys., **63**(4), 990–1037, 1991.

Davies-Jones, R. P., *Streamwise vorticity: The origin of updraft rotation in supercell storms*, J. Atmos. Sci., **41**, 2991–3006, 1984.

Davies-Jones, R. P., and H. Brooks, *Mesocyclogenesis from a theoretical perspective*, in *The Tornado: Its Structure, Dynamics, Prediction, and Hazards*, edited by C. Church, D. Burgess, C. Doswell, and R. Davies-Jones, pp. 105–114, American Geophysical Union, Washington, D.C., USA, 1993.

Ditlevsen, P. D., and P. Giuliani, *Dissipation in helical turbulence*, Phys. Fluids, **13**(11), 3508–3509, 2001.

Dritschel, D. G., *Generalized helical Beltrami flows in hydrodynamics and magnetohydrodynamics*, J. Fluid. Mech., **222**, 525–541, 1991.

Dutton, J. A., *Dynamics of Atmospheric Motion*, Dover, Mineola, New York, USA, 1995.

Galloway, D., and U. Frisch, *A note on the stability of a family of space-periodic Beltrami flows*, J. Fluid Mech., **180**, 557–564, 1987.

Greiner, W., *Quantum Mechanics - An Introduction*, fourth edition, Springer-Verlag, Berlin, Germany, 2001.

Greiner, W., and B. Müller, *Quantum Mechanics - Symmetries*, Springer-Verlag, Berlin, Germany, 1994.

Heisenberg, W., *Über Stabilität und Turbulenz von Flüssigkeitsströmen*, Annalen der Physik, **4** (74), 577–627, 1924.

Heisenberg, W., *Zur statistischen Theorie der Turbulenz*, Zeitschrift für Physik, **124**, 628–657, 1948.

Kármán, T. von, *The fundamentals of the statistical theory of turbulence*, J. Aeronaut. Sci., **4**(4), 131–138, 1937.

Klemp, J. B., and R. Rotunno, *A study of the tornadic region within a supercell thunderstorm*, J. Atmos. Sci., **40**, 359–377, 1983.

Kolmogorov, A. N., *Local structure of turbulence in an incompressible viscous fluid at very large Reynolds numbers*, Dokl. Akad. Nauk SSSR, **30**(4), 299-301, 1941a.

Kolmogorov, A. N., *On the degeneration of isotropic turbulence in an incompressible viscous fluid*, Dokl. Akad. Nauk SSSR, **31**(6), 538–541, 1941b.

Kraichnan, R. H., *Helical turbulence and absolute equilibrium*, 1973.

Levich, E., and A. Tsinober, *On the role of helical structures in three-dimensional turbulent flow*, Phys. Lett. A, **93**(6), 293–297, 1983a.

Levich, E., and A. Tsinober, *Helical structures, fractal dimensions and renormalization-group approach in homogeneous turbulence*, Phys. Lett. A, **96** (6), 292–298, 1983b.

Levich, E., and E. Tzvetkov, *Helical cyclogenesis*, Phys. Lett. A, **100** (1), 53–56, 1984.

Levich, E., and E. Tzvetkov, *Helical inverse cascade in three-dimensional turbulence as a fundamental dominant mechanism in mesoscale atmospheric phenomena*, Phys. Reports, **128** (1), 2–37, 1985.

Lilly, D. K., *The structure, energetics and propagation of rotating convective storms. Part II: Helicity and storm stabilization*, J. Atmos. Sci., **43**(2), 126–140, 1986.

Moffatt, H. K., *The degree of knottedness of tangled vortex lines*, J. Fluid Mech., **35**, 117–129, 1969.

Moffat, H. K., and A. Tsinober, *Helicity in laminar and turbulent flow*, Ann. Rev. Fluid Mech., **24**, 281, 1992.

Moses, H. E., *Eigenfunctions of the curl operator, rotationally invariant Helmholtz theorem, and applications to electromagnetic theory and fluid mechanics*, SIAM J. Appl. Math., **21**(2), 114–144, 1971.

Onsager, L., *The distribution of energy in turbulence*, Phys. Rev., *68*, 286, 1945.

Rasmussen, E. N., J. M. Straka, R. Davies-Jones, C. A. Doswell III, F. H. Carr, M. D. Eilts, and D. R. MacGorman, *Verification of the Origins of Rotation in Tornadoes Experiment: VORTEX*, Bull. Am. Met. Soc., **75**(6), 995–1006, 1994.

Rasmussen, E. N., and D. O. Blanchard, *A baseline climatology of sounding-derived supercell and tornado forecast parameters*, Wea. Forecasting, **13**, 1148–1164, 1998.

Straka, J. M., E. N. Rasmussen, and S. E. Fredrickson, *A mobile mesonet for finescale meteorological observations*, J. Atmos. Ocean. Technol., **13**(5), 921–936, 1996.

Taylor, G. I., *Statistical Theory of Turbulence I-IV*, Proc. Roy. Soc. London, **151A**, 421–478, 1935.

Taylor, G. I., *Statistical Theory of Turbulence V - Effect of turbulence on the boundary layer. Theoretical discussion of the relationship between the scale of turbulence and the critical resistance of a sphere.*, Proc. Roy. Soc. London, **156A**, 307–317, 1936.

Taylor, G. I., *The spectrum of Turbulence*, Proc. Roy. Soc. London, **164A**, 476–490, 1938.

Tur, A. V., and V. V. Yanovsky, *Invariants in dissipationless hydrodynamic media*, J. Fluid Mech., textbf248, 67–106, 1993.

Wakimoto, R. M., and N. T. Atkins, *Observations on the origins of rotation: the Newcastle tornado during VORTEX-94*, Mon. Wea. Rev., **124**, 384–407, 1996.

Wakimoto, R. M., and J. W. Wilson, *Nonsupercell tornadoes*, Mon. Wea. Rev., **117**, 1113–1140, 1989.

Waleffe, F., *The nature of triad interactions in homogeneous turbulence*, Phys. Fluids A, **4**(2), 350–363, 1992.

Walker, J. S., Fast Fourier Transforms, second edition, CRC Press, Boca Raton, Florida, USA, 1996.

Walko, R. L., Tornado spin-up beneath a convective cell: required basic structure of the near-field boundary layer winds, in *The Tornado: Its Structure, Dynamics, Prediction, and Hazards*, edited by C. Church, D. Burgess, C. Doswell, and R. Davies-Jones, pp. 89–95, American Geophysical Union, Washington, D.C., USA, 1993.

Wallace, J. M., and J.-L. Balint, An experimental study of helicity and related properties in turbulent flow, in *Topological Fluid Mechanics: Proceedings of the IUTAM Symposium, Cambridge, August 13–18, 1989*, edited by H. K. Moffatt and A. Tsinober, pp. 585-597, Cambridge University Press, Cambridge, UK, 1990.

Index